Distribution Agreement

In presenting this thesis or dissertation as a partial fulfillment of the requirements for an advanced degree from Emory University, I hereby grant to Emory University and its agents the non-exclusive license to archive, make accessible, and display my thesis or dissertation in whole or in part in all forms of media, now or hereafter known, including display on the world wide web. I understand that I may select some access restrictions as part of the online submission of this thesis or dissertation. I retain all ownership rights to the copyright of the thesis or dissertation. I also retain the right to use in future works (such as articles or books) all or part of this thesis or dissertation.

Signature:

_____ _____

Christopher D. Poff Date

Design, Synthesis, and Utility of Group IX Metal Catalysts for C–H Functionalization

By

Christopher D. Poff
Doctor of Philosophy

Chemistry

Simon B. Blakey, Ph.D.
Advisor

Frank E. McDonald, Ph.D.
Committee Member

Huw M. L. Davies, Ph.D.
Committee Member

Accepted:

Kimberly Jacob Arriola, Ph.D, MPH
Dean of the James T. Laney School of Graduate Studies

Date

Design, Synthesis, and Utility of Group IX Metal Catalysts for C–H Functionalization

By

Christopher D. Poff

B.Sc., University of Richmond, 2017

Advisor: Simon B. Blakey, Ph.D.

An abstract of
A dissertation submitted to the Faculty of the James T. Laney School of Graduate Studies of Emory University
in partial fulfillment of the requirements for the degree of
Doctor of Philosophy
in Chemistry
2022

Abstract

Design, Synthesis, and Utility of Group IX Metal Catalysts for C–H Functionalization

By Christopher D. Poff

The field of group IX transition metal catalyzed enantioselective reaction development has been dominated by complexes bearing C_2-symmetric chiral cyclopentadienyl ligand platforms. Key design elements within this ligand scaffold allow for logical modification and effectively eliminate the need for catalyst resolution strategies once complexed. However, the lengthy syntheses required for the best performing catalysts can limit overall utility. Alternatively, the ligands used in catalysts featuring planar chirality are often much simpler to synthesize but do require resolution strategies to access enantioenriched pre-catalysts. Herein, we will describe our efforts towards the design and synthesis of a planar chiral indenyl ligand scaffold, as well as the use of a simplified ligand platform for enantioselective catalysis. Additionally, we will detail our efforts in the development of new reaction methodology for natural product synthesis. This new methodology uses a cobalt catalyst as we have endeavored to move into base metal catalysis for more environmentally sustainable chemistry.

Design, Synthesis, and Utility of Group IX Metal Catalysts for C–H Functionalization

By

Christopher D. Poff

B.Sc., University of Richmond, 2017

Advisor: Simon B. Blakey, Ph.D.

A dissertation submitted to the Faculty of the James T. Laney School of Graduate Studies of Emory University
in partial fulfillment of the requirements for the degree of
Doctor of Philosophy
in Chemistry
2022

Acknowledgments

The completion of a Ph.D. is an incredible roller coaster of an experience as you navigate your development as an independent scientist. You are put through the gauntlet and are constantly tested as you determine why you enjoy chemistry and figure out what you plan to do after receiving the degree. Reaching the end of the journey, however, there is a sense of euphoria as you think back on how much the friendship and support of others has helped you succeed along the way. To that end, there are people that I need to thank personally for their role in helping me to achieve this accomplishment.

First off, I need to thank my advisor, Professor Simon Blakey, for allowing me to join the Blakey group and work towards this degree. You always push me to think critically about the reactions I perform and how I present information in a scientific setting. Through this, I feel truly prepared to step into my new career and succeed as I continue to develop as a chemist.

As well, I need to thank all the past and present members of the Blakey group that I have had the pleasure to work alongside throughout grad school. To Amaan Kazerouni, Jacob Burman, Caitlin Farr, and Taylor Nelson, the group was quite small when I started but y'all made it feel like a family and made me feel at home. To Patrick Gross, cheer up and be positive. To Sophia Xu, it has been a pleasure mentoring you as you have developed your skills at the bench. I know you will do well in grad school and wish you the best of luck! To Chris Poff… I mean… Michael Hollerbach, there aren't enough words to describe the bond we have formed over the past few years. From finding crazy videos and songs to bother Patrick with, to discussing the existence of God and starting #AGSB, I never know what any day has in store. While others may not see your wisdom like I do, I will always hold your friendship dear, and I hope you get into Nature at some point with all 10 fingers.

Next, I must thank my family for all their love and support throughout the years. Mom and Dad, you have helped me immensely by being there for me no matter what. The last two years especially have been difficult for the family, but I can always count on you to help in any way possible, teach me new ways to fix things, and be ready to try out new breweries and distilleries any time I am around to visit. To Benjamin, you are always there to rant with (or to) me. I am so thankful to have you as a brother and have such a great relationship with you. To Amanda, Shay, and Asher, I can always look forward to seeing y'all and making new memories. I can't wait to have more of a chance to be more involved in your lives after we move to Mass.

Finally, and most importantly, thank you to my loving and beautiful wife, Maddie Dekarske. We have been through so much together already, the thick and thin of grad school, a pandemic, and starting a life together with our precious little bean, Vera. You always love and support me, even if I am being ridiculous. You are always there to drink a beer with me and try out new things. I have become a better man because of you, and I am looking forward to the future as we both finish our Ph.D.'s and start our dream jobs in a dream location.

"Now, bring me that horizon!" – Captain Jack Sparrow

Table of Contents

Chapter 1: Design and Synthesis of C_2-Symmetric Chiral Cyclopentadienyl Ligands and their Associated Late-Transition Metal Complexes 1

1.1 Overview of C_2-Symmetric Chiral Cyclopentadienyl Ligand Platforms 1

1.2 Synthetic Routes to Access Transition Metal Complexes Bearing C_2-Symmetric Cp Ligand Frameworks 3

1.2.1 Synthesis of Established C_2-Symmetric Cp Ligands 3

1.2.2 Complexation of C_2-Symmetric Ligands to Late-Transition Metals 8

1.3 Selected Catalytic Studies Using C_2-Symmetric Chiral Ligand Scaffolds 11

1.3.1 Group VIII Transition Metal Catalyzed Enantioselective Transformations 11

1.3.2 Group IX Transition Metal Catalyzed Enantioselective Transformations 11

1.4 Conclusion 15

1.5 References 16

Chapter 2. Planar Chiral π-Complexes: Assigning Planar Chirality, Synthesis of Selected Ligands and their Associated Late-Transition Metal Complexes, and Selected Catalytic Examples 20

2.1 Definition of Planar Chirality and Methods for Stereochemical Assignment 20

2.1.1 Defining Planar Chirality 20

2.1.2 Assigning Planar Chirality of Transition Metal π-Complexes 21

2.2 Planar Chiral π-Complexes of Late Transition Metals 25

2.2.1 Synthesis of Ligands and the Associated Late-Transition Metal π-Complexes for Selected Compounds 25

2.2.2 Selected Examples of Planar Chiral π-Complexes in Enantioselective Catalysis 29

2.3 Conclusion 31

2.4 References 32

Chapter 3. Development of a Convergent Synthetic Route to Improve Access to an Axial and Planar Chiral Indenyl Ligand Scaffold 38

3.1 Introduction to the Baker-Type Ligand Scaffold 38

3.1.1 Examining the Reactivity Trends of Indenyl *vs*. Cyclopentadienyl Ligands 38

3.1.2 Indene Ring Slip as a Key Facet of Asymmetric Induction 39

3.2 Development of a Modular Synthesis Towards a Baker-Type Ligand Scaffold 40

3.2.1 Analysis of the Previously Disclosed Synthetic Route 40

3.2.2 New Modular Synthetic Route Development 43

3.3 Conclusion 46

3.4 References 48

3.5 Supporting Information 52

3.5.1 General Information 52

3.5.2 Experimental Section 53

3.5.3 Supplemental References 64

3.5.4 Spectra and HPLC Data 65

Chapter 4. Designing a Planar Chiral Rhodium Indenyl Catalyst for Regio- and Enantioselective Allylic C–H Amidation 83

4.1 Introduction to Blakey Group Allylic C–H Functionalization 83

4.1.1 First Generation Racemic Allylic Amination and Etherification 83

4.1.2 Second Generation Oxidative Allylic C–H Functionalization 85

4.2 Design of a Planar Chiral Rhodium Indenyl Ligand Platform for Enantioselective C–H Functionalization 86

4.2.1 From Model System to Active Catalyst 86

4.2.2 Stereochemical Determination of the Catalyst and Allylic Amide Products 88

4.2.3 Reaction Scope 90

4.2.4 Mechanistic and Computational Studies 92

4.3 Conclusion 95

4.4 References 96

4.5 Supplementary Information 100

4.5.1 General Information 100

4.5.2 Experimental Section 101

4.5.3 Supplementary References 139

4.5.4 Spectra 140

Chapter 5. Towards a Peptide Macrocyclization Strategy *via* the Cobalt-Catalyzed 1,2-Carboamidation of Acrylamides 166

5.1 Introduction to Ribosomally-Synthesized and Post-Translationally Modified Peptides 166

5.1.1 Overview of Several Key Peptides Under Investigation by the Blakey Group 166

5.1.2 Key Synthetic Strategies to Access RiPPs 167

5.2 Blakey Group Strategy to Access the Key ß-Amino Aryl-Alkyl Disconnection 171

5.2.1 Application of Previous Methodology and New Synthetic Plan 171

5.2.2 Development and Optimization of the Cobalt-Catalyzed 1,2-Carboamidation of Acrylamides 173

5.2.3 Tyrosine Hydroxamate Studies and Linear Peptide Design/Synthesis 176

5.3 Conclusion 180

5.4 References 181

5.5 Supplementary Information 185

5.5.1 General Information 185

5.5.2 Experimental Section 186

5.5.3 Supplementary References 197

5.5.4 Spectra 199

List of Figures

Figure 1.1: Key cyclopentadiene and cyclopentadienyl structure definitions 1

Figure 1.2: Previous C_2-symmetric Ligands and structural approach for new chiral ligand scaffolds 2

Figure 1.3: Ruthenium catalyzed enantioselective cyclization to form dihydrobenzoindoles 11

Figure 1.4: Spiro-annulation with various rhodium based Cp^X-bearing catalysts 13

Figure 2.1: Defining planar chirality in cyclophanes and transition metal π-complexes 21

Figure 2.2: Two methods for assigning planar chirality of π-complexes 22

Figure 2.3: Limitation of simplified method for stereochemical assignment 23

Figure 2.4: Overview of disclosed planar chiral late transition metal π-complexes 25

Figure 3.1: General depiction of indenes and the indenyl ligand platform 38

Figure 3.2: Indenyl migratory insertion studies and ring slip mechanistic rationale 39

Figure 3.3: Baker's tethered indenyl π-allyl complex analysis 40

Figure 4.1: First generation oxidative allylic C–H functionalization: Previous work, precedent, and Blakey group publications 83

Figure 4.2: Proposed mechanism for the Blakey group's first generation oxidative allylic C–H functionalization 84

Figure 4.3: Allylic C–H amidation with dioxazolones and azides 85

Figure 4.4: Planar chiral indenyl catalyst redesign 86

Figure 4.5: Enantioselective allylic C–H amidation dioxazolone and olefin reaction scope 91

Figure 4.6: DFT calculated reaction coordinate diagram for the amidation of allyl benzene 93

Figure 4.7: Proposed catalytic cycle for the allylic C–H amidation of allyl benzene with *tert*-butyl dioxazolone 94

Figure 5.1: Selection of RiPP natural products featuring a ß-amino aryl-alkyl crosslink 166

Fifure 5.2: Structural Analysis of celogentin C 167

Figure 5.3: Proposed catalytic intermediate in the 8-aminoquinoline directed ß-C–H arylation 171

Figure 5.4: RiPP natural product targeted by the Blakey group for total synthesis 171

Figure 5.5: Synthetic design and plan of the linear peptide sequence for cyclization *via* 1,2-carboamidation 178

Figure 5.6: Tyrosine hydroxamate reactivity leading to linear peptide synthesis redesign 179

List of Schemes

Scheme 1.1: Synthesis of the Mannitol-Cp scaffold 3

Scheme 1.2: Synthesis of the BINOL-Cp scaffold 4

Scheme 1.3: Modification of the BINOL-Cp scaffold 4

Scheme 1.4: Further exploration of side wall, back wall, and Cp-ring modifications of BINOL-Cp 5

Scheme 1.5: Synthesis of cPent-Cp 5

Scheme 1.6: Synthesis of the SCp ligand scaffold 6

Scheme 1.7: Synthesis of FcCp and its derivatives 7

Scheme 1.8: General methods for the complexation of pre-ligands to transition metals 8

Scheme 1.9: Cp^XH complexation with ruthenium 8

Scheme 1.10: Complexation of Cp^XH pre-ligand with cobalt 9

Scheme 1.11: Synthesis of rhodium and iridium Cp^X pre-catalysts 9

Scheme 1.12: Use of a Mannitol-Cp bearing catalyst for enantioselectivity 12

Scheme 1.13: BINOL-Cp bearing rhodium catalyst for spiro-annulation 12

Scheme 1.14: Iridium and cobalt C_2-symmetric chiral catalysts used in enantioselective reactions 14

Scheme 2.1: General synthesis of several planar chiral iron π-complexes 26

Scheme 2.2: Synthesis of tethered ruthenium complex **2.15** 26

Scheme 2.3: Synthesis of 1-menthylindenyl cobalt COD **2.24** 27

Scheme 2.4: Synthesis of the rhodium JasCp platform 27

Scheme 3.1: Stoichiometric studies towards enantioselective allylic alkylation 39

Scheme 3.2: Baker's racemic synthesis of sulfide tethered planar chiral rhodium indenyl complexes 41

Scheme 3.3: Racemic oxidation to access sulfoxide-tethered rhodium complexes 41

Scheme 3.4: Stereoselective synthesis of enantioenriched ligands 42

Scheme 3.5: Identification of a key retrosynthetic disconnection 43

Scheme 3.6: Retrosynthetic analysis of cross-coupling fragments 43

Scheme 3.7: Forward synthesis to access aryl iodide coupling partners 44

Scheme 3.8: Alternative route to access chiral aryl-alkyl sulfoxides 45

Scheme 3.9: Synthetic route to access functionalized indene boronic acids 45

Scheme 3.10: Atroposelective cross-coupling to access completed Baker-type ligand scaffold derivatives 46

Scheme 4.1: Racemic indenyl catalyst synthesis and proof-of-concept allylic C–H amidation 87

Scheme 4.2: Catalyst chiral resolution, enantioselective proof-of-concept, and optimized conditions 87

Scheme 4.3: Catalyst stereochemical determination by isolation of a π-allyl complex 88

Scheme 4.4: Stereochemical determination of allylic amide products 89

Scheme 5.1: Bentley *et al.* synthesis of stephanotic acid methyl ester 168

Scheme 5.2: Multi-step diastereoselective tryptophan-leucine crosslink syntheses 169

Scheme 5.3: Directed asymmetric C–H arylation to access the troptophan-leucine crosslink 170

Scheme 5.4: Proposed route to the eastern ring of darobactin A utilizing the Blakey group's enantioselective allylic C–H amidation reaction for key bond disconnections 172

Scheme 5.5: Previous group IX transition metal catalyzed 1,2-carboamination methodologies and the strategic plan for application to the total synthesis of RiPPs including darobactin A 173

Scheme 5.6: Proof-of-concept 1,2-carboamidation of acrylamides 174

Scheme 5.7: Intermolecular model system for dipepetide formation *via* 1,2-carboamidation 176

Scheme 5.8: Published route to access phenol-derived hydroxamate functionality 176

Scheme 5.9: Chan-Evans-Lam coupling to access functionalized hydroxamates 177

List of Tables

Table 2.1: Planar chiral ruthenium π-complex catalyzed allylic oxidation 29

Table 2.2: Rhodium JasCp catalyzed directed C–H functionalization 30

Table 5.1: Optimization of 1,2-carboamidation of acrylamides with amino acid derived hydroxamates 175

Table of Abbreviations

Ac	Acetyl
Ar	Aryl
BINAP	2,2'-Bis(diphenylphosphino)-1,1'-binaphthalene
BINOL	1,1'-Bi-2-naphthol
BINOL-Cp	BINOL-derived cyclopentadienyl
Bn	Benzyl
Boc	*tert*-Butoxycarbonyl
BPE	1,2-Bis(dimethylphospholano)ethane
Bu	Butyl
Bz	Benzoyl
Cbz	Carboxybenzyl
CIP	Cahn-Ingold-Prelog
COD	1,5-Cyclooctadiene
Cp	Cyclopentadienyl
Cp*	1,2,3,4,5-Pentamethylcyclopentadienyl
cPent-Cp	Cyclopentyl-bearing cyclopentadienyl
CpH	Cyclopentadiene
CpNa	Sodium cyclopentadienide
Cp^X	Functionalized cyclopentadienyl
Cp^XH	Functionalized cyclopentadiene
Cy	Cyclohexyl
DCE	1,2-Dichloroethane

DCM	Dichloromethane
de	Diastereomeric excess
DET	Diethyltartarate
DFT	Density functional theory
DIPEA	Diisopropylamine (Hunig's base)
DMF	Dimethylformamide
Dppf	1,1'-Bis(diphenylphosphino)ferrocene
dr	Diastereomeric ratio
EDC	1-Ethyl-3-(3-dimethylaminopropyl)carbodiimide
EDCI	See EDC
ee	Enantiomeric excess
er	Enantiomeric ratio
Et	Ethyl
EWG	Electron-withdrawing group
FcCp	Ferrocene-derived cyclopenadienyl
Fmoc	Fluorenylmethyloxycarbonyl
G3	3rd Generation
HFIP	1,1,1,3,3,3-Hexafluoro-2-propanol
HOBt	Hydroxybenzotriazole
HPLC	High-Performance Liquid Chromatography
^{i}Bu	*iso*-Butyl
Ind	Indenyl
IndH	Indene

^{i}Pr	*iso*-Propyl
KAIST	Korea Advanced Institute of Science and Technology
L	Ligand
LAH	Lithium aluminum hydride
M	Metal
Mannitol-Cp	Mannitol-derived cyclopentadienyl
*m*CPBA	*meta*-Chloroperbenzoic acid
Me	Methyl
MOM	Methoxy methyl
Ms	Mesyl
MS	Molecular sieves
^{n}Bu	*n*-Butyl
NMM	*N*-methylmorpholine
^{n}Pr	*n*-Propyl
Nu	Nucleophile
OTf	Trifluoromethanesulfonate (triflate)
PG	Protecting group
Ph	Phenyl
Phen	1,10-Phenanthroline
Phth	Phthalimide
Pin	Pinacol
Piv	Pivaloyl
R	Carbon group

RiPP	Ribosomally-synthesized and post-translationally modified peptide
R_L	Large R group
R_S	Small R group
^{s}Bu	*sec*-Butyl
SCp	Spiro-cyclopentadienyl
SPhos	2-Dicyclohexylphosphino-2',6'-dimethoxybiphenyl
TBDPS	*tert*-Butyldiphenylsilyl
TBS	*tert*-Butyldimethylsilyl
^{t}Bu	*tert*-Butyl
TEA	Triethylamine
TES	Triethylsilyl
Tf	Triflyl
TFA	Trifluoroacetic acid
TFE	2,2,2-Trifluoroethan-1-ol
THF	Tetrahydrofuran
TIPS	Triisopropylsilyl
TMP	2,2,6,6-Tetramethylpiperidinyl
TMS	Trimethylsilyl
Ts	Tosyl
TS	Transition state
X	Halide (generally): also, carbon or heteroatom

Chapter 1. Design and Synthesis of C_2-Symmetric Chiral Cyclopentadienyl Ligands and their Associated Late-Transition Metal Complexes

In this chapter, we will discuss the importance of C_2-symmetric chiral cyclopentadienyl ligands. Specifically, we will investigate the design and synthesis of these ligands and their associated complexes with group VIII and group IX transition metals. Additionally, we will present a limited sample of the use of the chiral complexes as catalysts for enantioselective transformations. This chapter will solely focus on C_2-symmetric platforms, whereas those bearing additional planar chirality will be detailed in subsequent chapters.

1.1 Overview of C_2-Symmetric Chiral Cyclopentadienyl Ligand Platforms

Cyclopentadienyl (Cp) compounds have been extensively studied as ligands within the context of late-transition metal catalysis since the discovery of ferrocene (**1.1**) in 1951 (**Figure 1.1a**).[1–5] These compounds offer many benefits when utilized as ligands including high complex stability, tunable electronic properties, and an η^5-coordination mode that favors the preservation of open coordination sites for productive reactivity to occur (**Figure 1.1b**).[4] Therefore, with the ever-increasing need for the development of enantioselective reactions, the scope of Cp ligands available has been expanded to chiral variations in response this call.

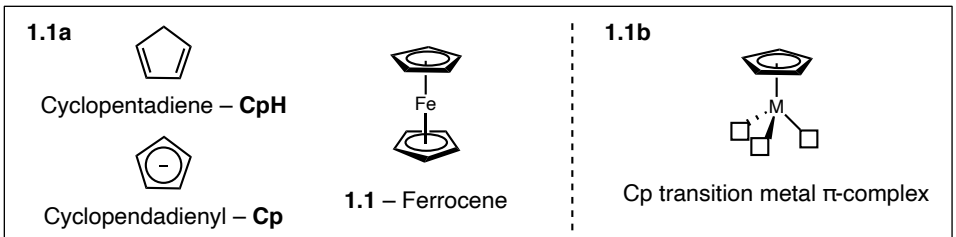

Figure 1.1: Key cyclopentadiene and cyclopentadienyl structure definitions

The first chiral Cp ligands, and their associated transition metal complexes, were disclosed in the late 1970's-80's and often bore natural product-derived substituents to induce chirality (**Figure 1.2a**).[6–9] Due to limited success with enantioinduction, the platform ultimately stalled

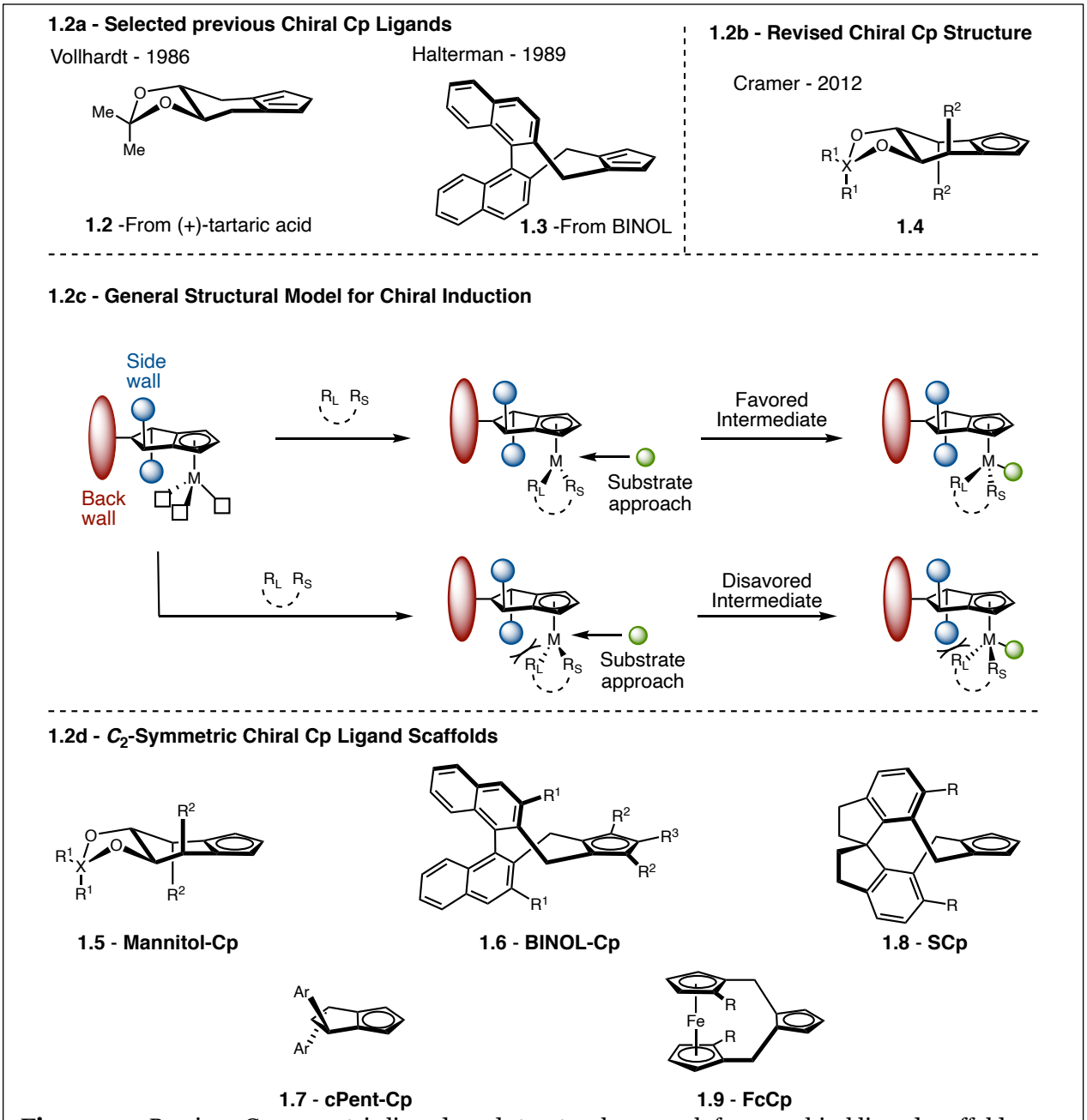

Figure 1.2: Previous C_2-symmetric ligands and structural approach for new chiral ligand scaffolds

until 2012 when Cramer *et al.* disclosed the first example of a modified platform (**1.4**) that built upon the initial benefits of the natural product-derived ligands (**Figure 1.2b**).[4,10] The initially disclosed ligands, and the subsequent ligands that will be the focus of this chapter, have relied on several common features: a sterically large "back wall" to prevent the approach of substrates from one face of the complex, "side walls" to guide the coordination of initial substrate binding, and a C_2-symmetric nature to eliminate facial selectivity during complexation and the need for chiral

resolution of the final transition metal complex (**Figure 1.2c**).[10] Under this synthetic plan, the groups of Cramer (**1.5 - Mannitol-Cp**, **1.6 - BINOL-Cp**, **1.7 - cPent-Cp**),[10–12] You (**1.8 - SCp**),[13] and Wang (**1.9 - FcCp**)[14] have each presented novel scaffolds to this class of chiral Cp ligands/complexes (**Figure 1.2d**).

1.2 Synthetic Routes to Access Transition Metal Complexes Bearing C_2-Symmetric Cp Ligand Frameworks

1.2.1 Synthesis of Established C_2-Symmetric Cp Ligands

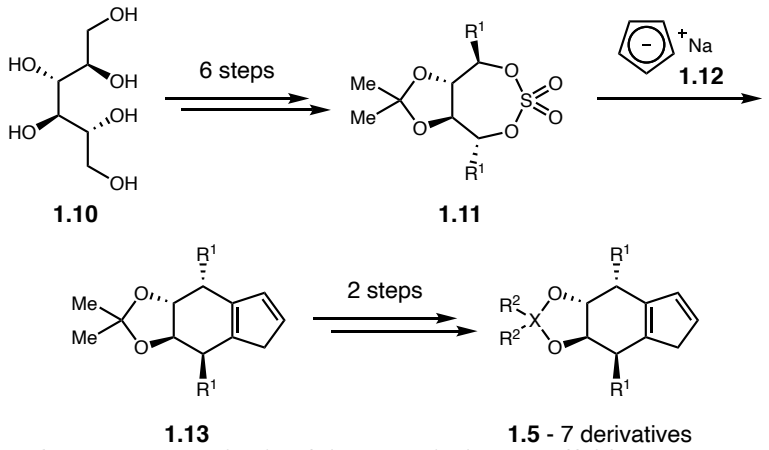

Scheme 1.1: Synthesis of the Mannitol-Cp Scaffold

Mannitol-Cp (**1.5**) is the earliest C_2-symmetric Cp compound to be disclosed under this paradigm of ligand design. Closely resembling the (+)-tartaric acid-derived Cp reported by Vollhardt *et al.* (**1.2**), the Cramer group begins their synthesis with D-mannitol (**1.10**, **Scheme 1.1**).[7,10] Through two different synthetic pathways, the side walls can be installed to cyclic sulfate **1.11** in 6 steps from D-mannitol. The cyclopentadiene (CpH) ring can then be installed *via* alkylation with sodium cyclopentadienide (CpNa, **1.12**) to form pre-ligand **1.13**, and, if desired, the back wall modified further. Following this route, the Cramer group reported 7 different variations on the Mannitol-Cp platform.

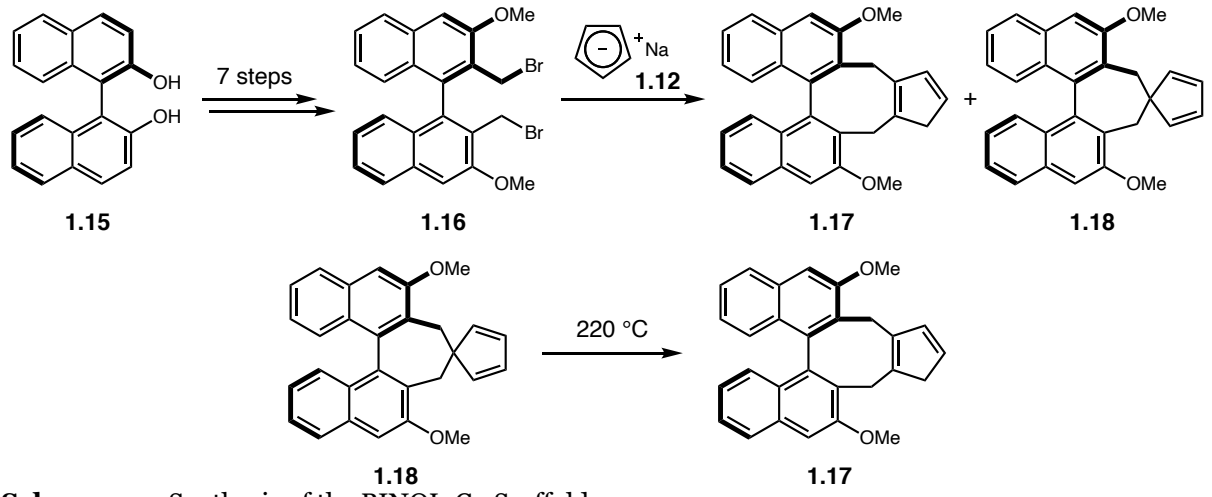

Scheme 1.2: Synthesis of the BINOL-Cp Scaffold

The next disclosed ligand, BINOL-Cp **1.6**, is perhaps the most thoroughly studied ligand within this design paradigm. Initially disclosed in 2013, this ligand is a functionalized variation of the simple BINOL-derived Cp originally reported by Halterman *et al.* (**1.3**).[9,11] The Cramer group's ligand design uses the BINOL functionality as the back wall and makes use of additional 3 and 3' substituents to create the side walls of the overall model. Construction and modification of the 3,3' side wall substituents represent the largest synthetic challenges. Starting from BINOL (**1.14**), 3,3'-dimethoxy **1.15** can be accessed in 7 steps before alkylation with CpNa to form a mixture of CpH adducts **1.16** and **1.17** (**Scheme 1.2**). Spirocyclic **1.18** can be thermally isomerized to BINOL-CpH (**1.16**) prior to complexation to metal to utilize all the product formed.

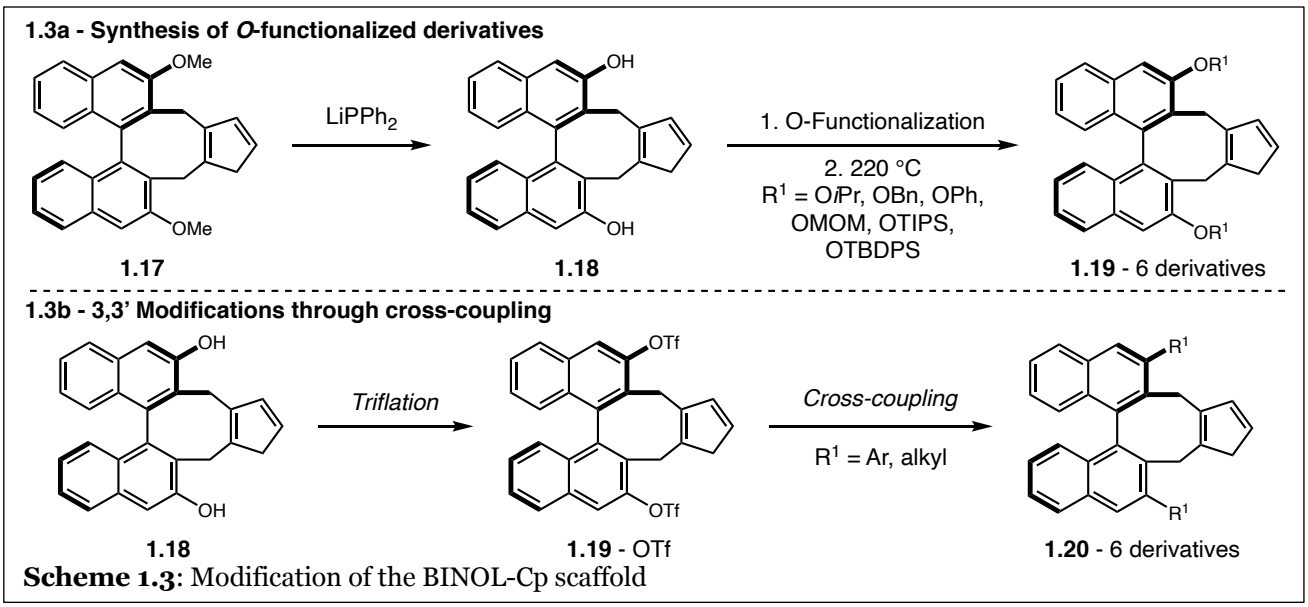

Scheme 1.3: Modification of the BINOL-Cp scaffold

Ethereal side wall modification of **1.17** can be accomplished by reducing the 3 and 3' substituents to the phenol derivative **1.18** and functionalizing with a variety of alkyl or silyl groups (**Scheme 1.3a**).[15] Installation of a triflate (**1.19** - OTf) generates a cross-coupling handle for the incorporation of various aryl or alkyl groups (**1.20**, **Scheme 1.3b**).[11,16,17] Halide or silyl 3,3' substituents have been explored; however, these modifications require *de novo* ligand synthesis in 5 steps from BINOL ester **1.21** (**Scheme 1.4a**).[18] Back wall modification has been explored through the study of biphenyl **1.23**. Unlike the BINOL-derived variations, biphenyl **1.23** relies on chiral preparative HPLC for separation of the ligand enantiomers (**1.24**, **Scheme 1.4b**).[18] Finally, modification of the Cp ring can be accomplished *via* functionalization with ketones to access 1,2,4-

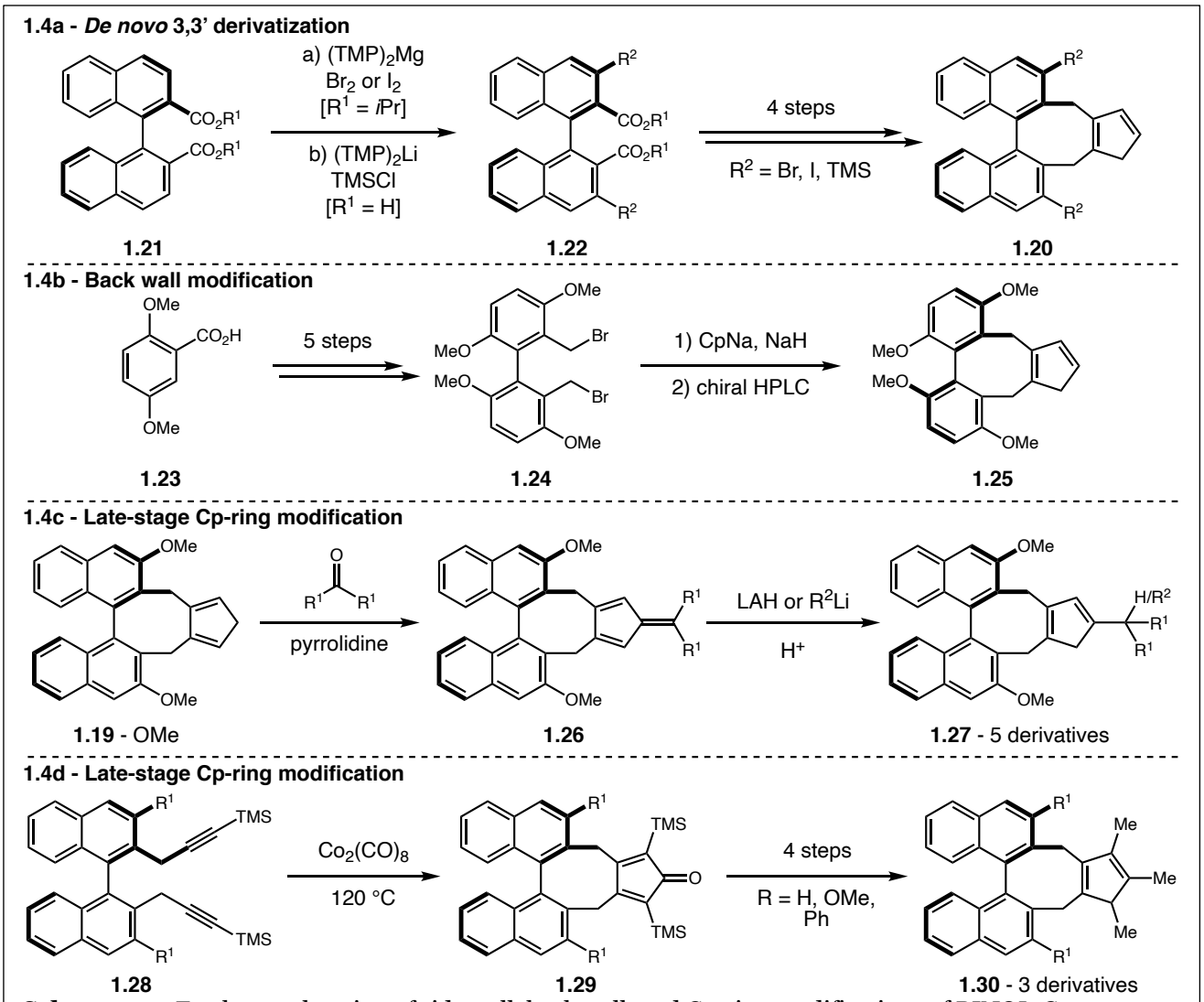

Scheme 1.4: Further exploration of side wall, back wall, and Cp-ring modifications of BINOL-Cp

substituted BINOL-CpH **1.27** (**Scheme 1.4c**).[19] A fully substituted alternative, **1.30**, was also recently disclosed through diversification of intermediate **1.16** to form bis-alkyne **1.28** (**Scheme 1.4d**).[20] After carbonylative cyclization, methyl groups can be installed through Grignard addition and cross-coupling chemistry.

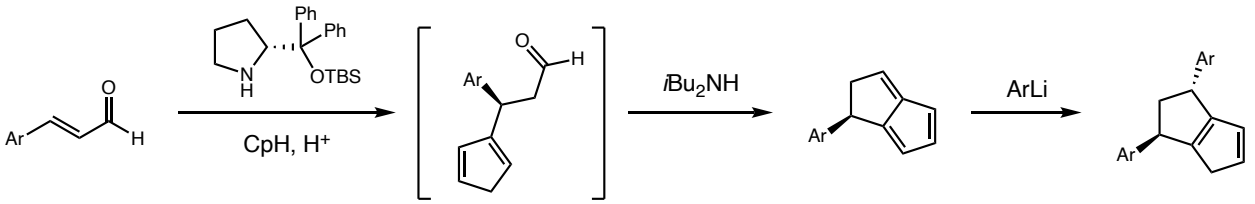

Scheme 1.5: Synthesis of cPent-Cp

In addition to Mannitol-Cp and BINOL-Cp, Cramer and coworkers have also disclosed the bicyclic scaffold cPent-Cp **1.7** (**Figure 1.2d**).[12] This ligand scaffold benefits from the shortest ligand synthesis of all the C_2-symmetric Cp ligands. The 2-step process begins with an organo-catalyzed ene-type reaction between cinnamaldehyde **1.31** and cyclopendadiene, which, after an *in-situ* condensation of **1.32**, affords chiral fulvene **1.33** (**Scheme 1.5**). The second aryl ring can be installed stereoselectively by addition of an aryl-lithium reagent to the least sterically hindered face of the fulvene intermediate providing cPent-CpH (**1.34**) in moderate yields but excellent enantioselectivities. However, despite the rapid route to access the cPent-CpH scaffold, the linear nature of the synthesis requires *de novo* ligand synthesis for each desired derivative.

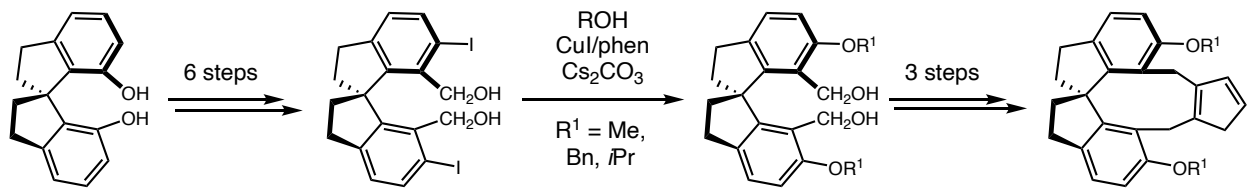

Scheme 1.6: Synthesis of the SCp ligand scaffold

In the exploration of a back wall alternative, You *et al.* disclosed the SPINOL-derived SCp **1.8**.[21] The natural product **1.35** can be transformed to diiodide **1.36** in 6 steps (**Scheme 1.6**). Diiodide **1.36** is the common intermediate to which various ethereal side walls have been installed (**1.37**). Chlorination of primary alcohol then allows for dialkylation of CpNa and thermal

racemization is once again utilized to convert all available product to the desired diene compound **1.38** in 3 additional steps.

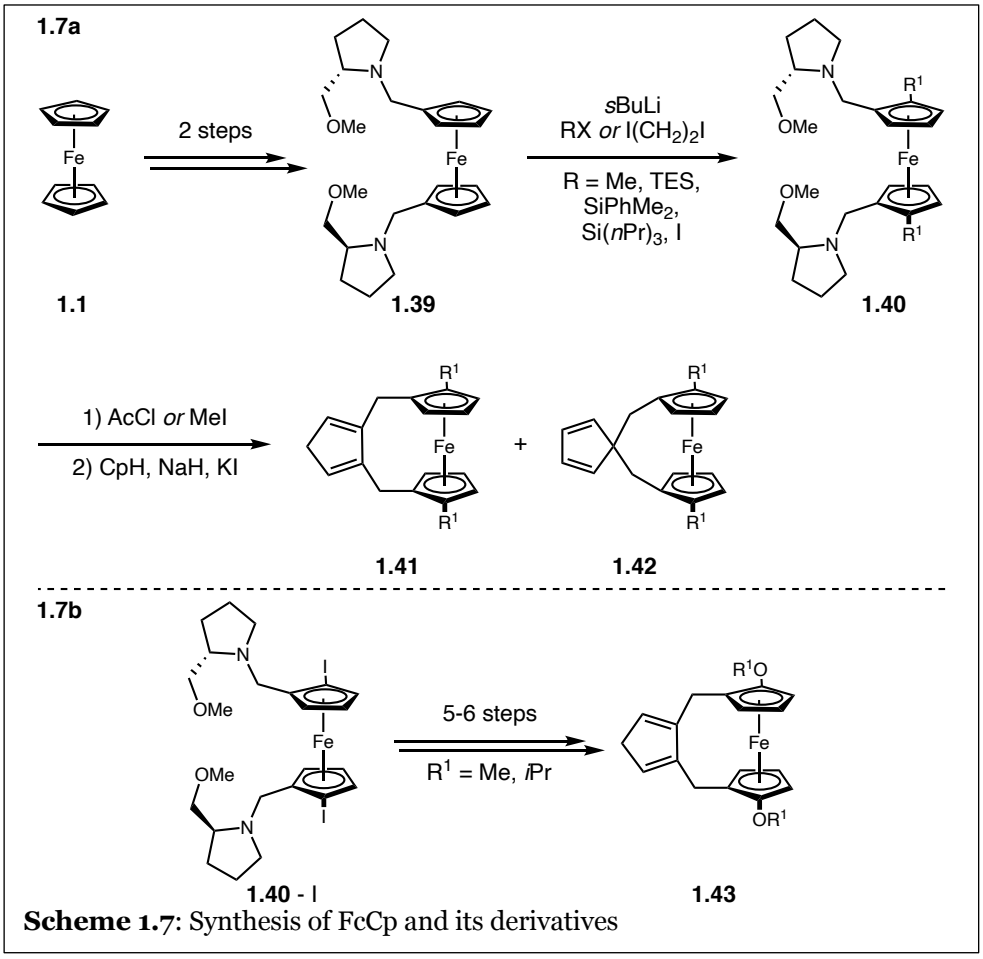

Scheme 1.7: Synthesis of FcCp and its derivatives

The most recently disclosed C_2-symmetric chiral Cp scaffold is the ferrocene-derived FcCp **1.9** from Liang *et al.* originally reported in 2020.[14] The synthesis of FcCp begins from ferrocene (**1.1**) and installs a proline-derived pyrrolidine to access chiral diamine **1.39** (**Scheme 1.7a**). From here, the compound can be diasterioselectively functionalized to install the synthetic handles that will ultimately become the side walls of the Cp ligand (**1.40**). Alkyl groups, silyl groups, or halides can be installed before addition to CpNa affords an inseparable mixture of 1,2-disubstituted CpH **1.41** and spirocyclic **1.42**, akin to the routes to access BINOL-Cp and SCp. Thermal isomerization to the desired 1,2-difunctionalized CpH ring (**1.41**) and, if necessary, installation of ethereal linkages provide the completed ligand scaffold (**1.43**) in 6-8 steps (**Scheme 1.7b**).

1.2.2 Complexation of C_2-Symmetric Ligands to Late Transition Metals

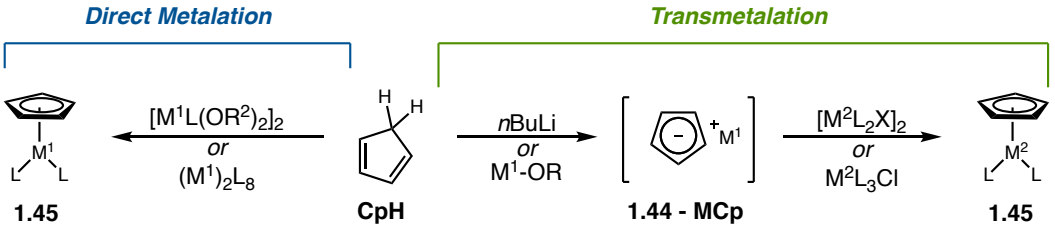

Scheme 1.8: General methods for the complexation of pre-ligands to transition metals

Having discussed the routes to access C_2-symmetric CpH compounds in the previous section, the next integral step to create a functional pre-catalyst is to complex the molecules as ligands to transition metals. The methods examined will focus specifically on complexation with group VIII and group IX transition metals for the purpose of this dissertation.

Fundamentally, the various sets of conditions that have been utilized to complex these functionalized Cp ligands (Cp^X) to metals can be classified into two distinct groups: transmetalation and direct metalation (**Scheme 1.8**).[4] Transmetalation requires deprotonation of the CpH pre-ligand to form the Cp anion which is then stabilized by the specific metal (M) used for the reaction (**1.44**). These often utilize hard organometallic bases to provide a strong base sufficient to form the Cp anion while simultaneously providing the metal to stabilize the resultant charge. Direct metalation simply requires the addition of the desired transition metal and is typically conducted under reflux or microwave reaction conditions. The choice of method for complexation of ligands (L) to metals can be tuned according to the choice of transition metal and the identity of the desired additional supporting ligands on the metal.

Within the specific context of late transition metals, the elements that have been explored with C_2-symmetric ligands include ruthenium (Ru), cobalt (Co), rhodium (Rh), and iridium (Ir).[4] Beginning with group VIII, ruthenium complexes (**1.46**) have mostly relied on transmetalation initiated complexation, making use of thallium ethoxide (TlOEt) as the organometallic base in the

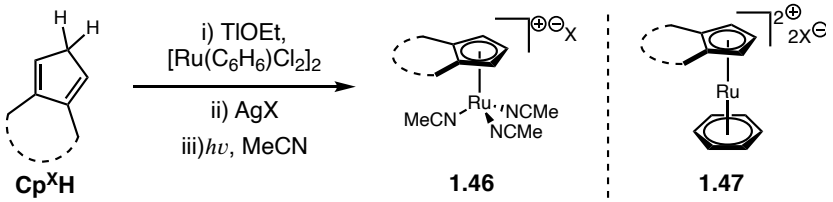

Scheme 1.9: Cp^XH complexation with ruthenium

reaction (**Scheme 1.9**).[17] This metal/base combination works to disfavor the formation of a ruthenocene complex **1.47** and allows for further tuning of the supporting ligands.

Moving to group IX metals, both transmetalation and direct metalation have been studied through various methods.[4] Cobalt complexes have stand-alone methods while rhodium and iridium tend to rely on similar chemistry to one another. Cobalt complexes bearing a 1,5-cyclooctadiene (COD) ligand (**1.49**) can be formed *via* transmetalation initiated complexation with *n*-butyllithium (*n*-BuLi) as the base to form stabilized intermediate **1.48** (**Scheme 1.10a**).[22,23] Further reaction of **1.48** with a cobalt precursor and exogenous COD can provide $Cp^XCo(COD)$ complex **1.50**. Direct metalation can be attained by reaction between the desired Cp^XH ligand and dicobalt octacarbonyl [$Co_2(CO_2)_8$] (**Scheme 1.10b**). Oxidation with iodine then provides the desired $Cp^XCo(CO)I_2$ pre-catalyst **1.50**.[24]

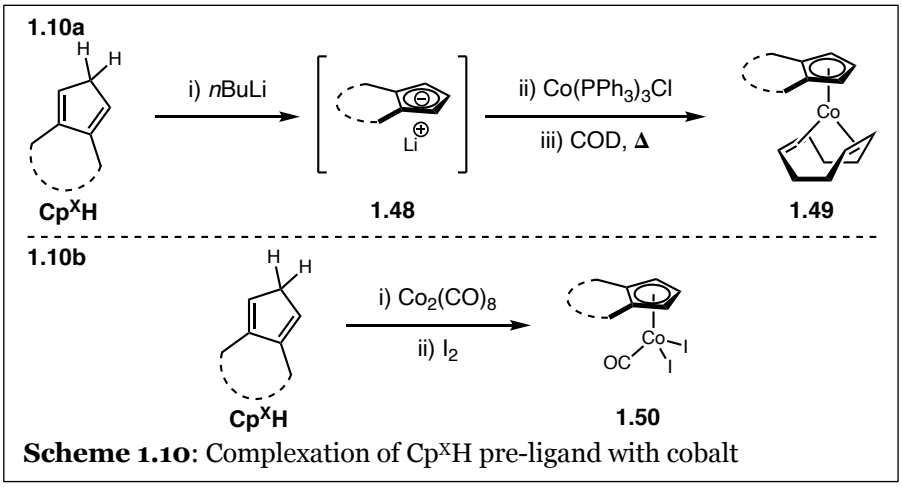

Scheme 1.10: Complexation of Cp^XH pre-ligand with cobalt

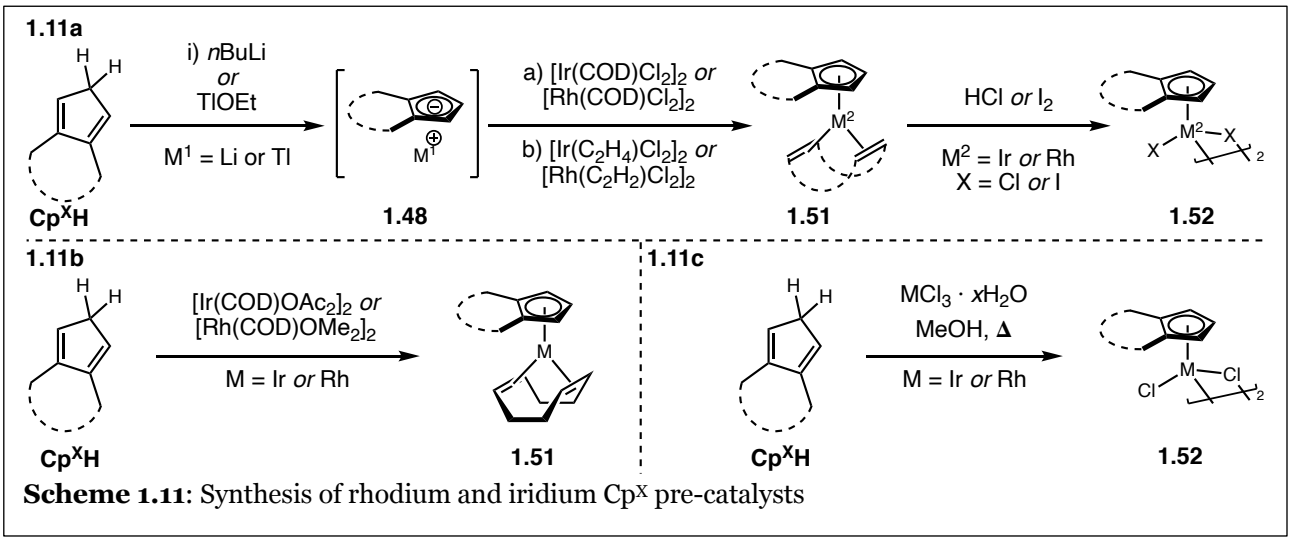

Scheme 1.11: Synthesis of rhodium and iridium Cp^X pre-catalysts

As mentioned above, both rhodium and iridium complexes have made use of similar chemical transformations to complex Cp^XH ligands. Like cobalt, rhodium and iridium complexes (**1.51**) have been formed with *n*-BuLi as the base and the associated COD or bis ethylene starting dimeric species (**Scheme 1.11a**).[10,11,25] However, the use TlOEt has also been detailed to access identical rhodium(I) or iridium(I) species **1.51** that can then be oxidized to the desired dihalide dimer **1.52** with either hydrochloric acid (HCl) or molecular iodine (I_2, **Scheme 1.11a**). Direct metalation can occur through two separate pathways. Reaction of Cp^XH pre-ligand with $[Rh(COD)OAc]_2$ or $[Ir(COD)OMe]_2$ provides access to the rhodium(I) or iridium(I) COD adducts **1.51** in a single step (**Scheme 1.11b**).[26] The success of this method relies on the presence of a reactive methoxide (OMe) or acetate (OAc) coordinating ligand that can act as an endogenous base, allowing for deprotonation of the Cp^XH ligand during complexation. Access to dihalide dimers directly can be accomplished through reaction between a Cp^XH pre-ligand and $RhCl_3$- or $IrCl_3$-hydrates (**Scheme 1.11c**).[20,27] This direct metalation route operates at high temperatures and goes through a C–H activation pathway to afford the desired dihalide dimer complex.

1.3 Selected Catalytic Studies Using C_2-Symmetric Chiral Ligand Scaffolds

1.3.1 Group VIII Transition Metal Catalyzed Enantioselective Transformations

In the study of enantioselective transformations utilizing group VIII metals bearing C_2-symmetric chiral ligand scaffolds as catalysts, ruthenium is the primary metal that has been explored.[4] Complexes of BINOL-Cp and cPent-Cp derivatives, in particular, have been utilized for several different annulation reactions, a common theme for C_2-symmetric ligands in enantioselective catalysis.

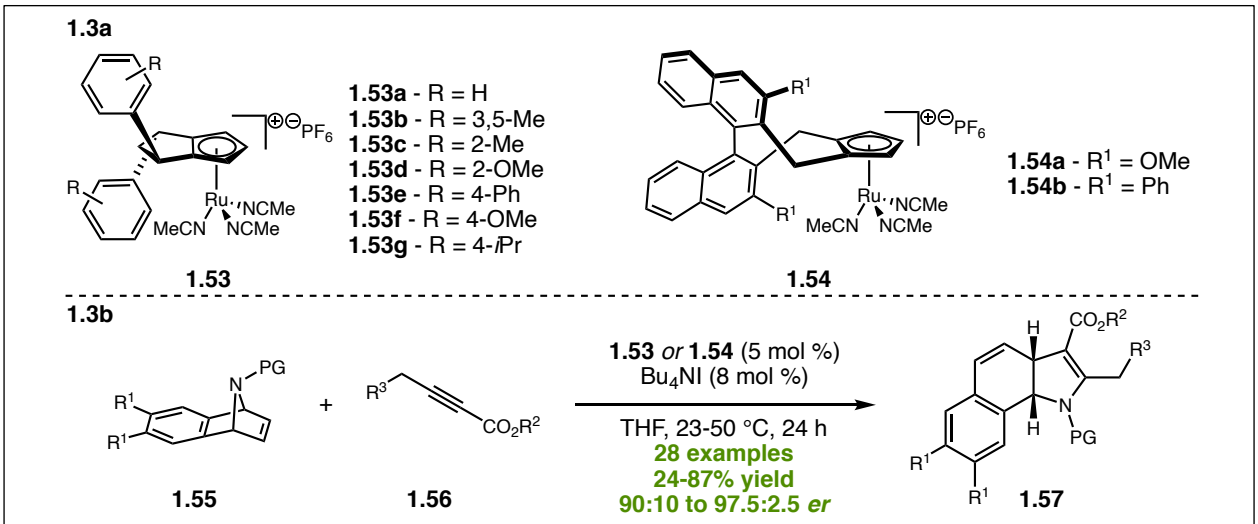

Figure 1.3: Ruthenium catalyzed enantioselective cyclization to form dihydrobenzoindoles

To highlight one such example, in the initial disclosure of the cPent-Cp ligand scaffold, Wang *et. al.* utilized the ruthenium catalyst **1.53** (**Figure 1.3a**) to carry out the enantioselective cyclization of **1.55** and **1.56** to form dihydrobenzoindole derivatives **1.57** (**Figure 1.3b**).[12] When using the cPent-Cp derivatives under optimized reaction conditions, enantiomeric ratios from 90:10 to 97.5:2.5 were observed. BINOL-Cp derivatives **1.54a** and **1.54b** were able to achieve ratios of 60:40 and 93:7, respectively. The range of selectivity's observed demonstrates the sensitivity of the reaction conditions to the identity of the side wall in the Cp^X ligand.

1.3.2 Group XI Transition Metal Catalyzed Enantioselective transformations

In contrast to the limited studies of group VIII transition metal catalyzed transformations utilizing C_2-symmetric Cp ligands as the source of enantioinduction, group IX metals have been studied much more extensively.[4,28] While a range of reactivity has been explored, this section will

focus on some of the directed C–H functionalization reactions that have become a benchmark for assessing the reactivity of new catalyst derivatives.

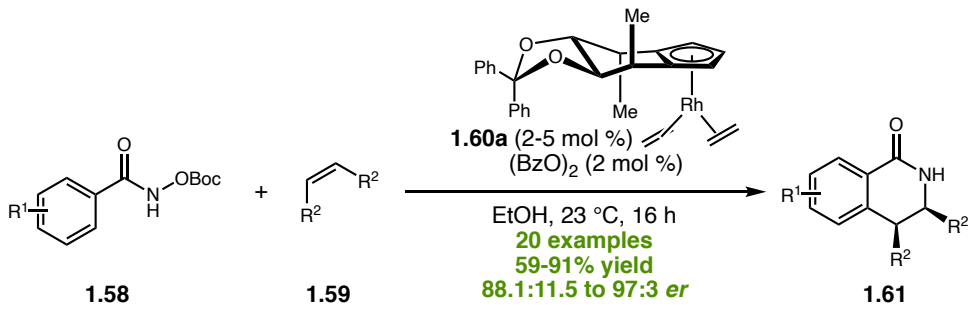

Scheme 1.12: Use of a Mannitol-Cp bearing catalyst for enantioselectivity

Early work with Mannitol-Cp explored the use of **1.60a** for the enantioselective C–H activation annulation of **1.58** with various olefins **1.59** to form heterocyclic **1.61** (**Scheme 1.12**).[10] This early work showed that this catalyst was extremely effective at providing enantioenriched products. While yields ranged from 59 to 91%, the selectivity was primarily greater than a 95:5 enantiomeric ratio, barring a few exceptions.

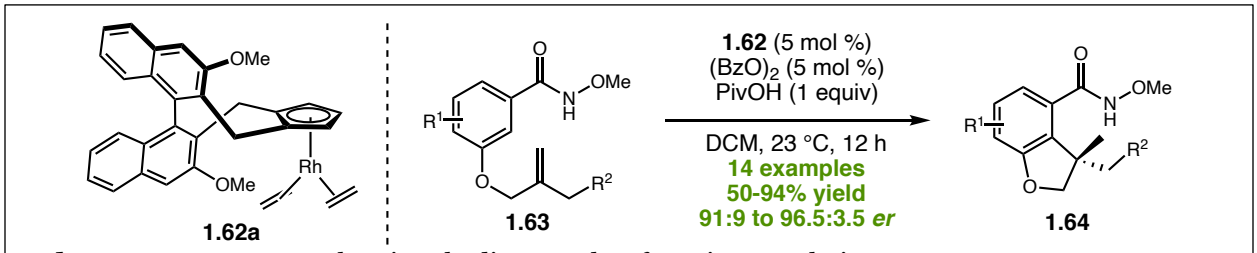

Scheme 1.13: BINOL-Cp bearing rhodium catalyst for spiro-annulation

BINOL-Cp based catalysts are the most extensively studied, with more than 35 current applications in enantioselective catalysis.[4] Often, new catalysts will seek to compare the yield and selectivity to BINOL-Cp derivatives. Taking note of an early example, however, **1.65a** was used in the cyclization of **1.63** to form dihydrobenzofuran derivatives **1.64** (**Scheme 1.13**).[29] The use of

BINOL-Cp bearing **1.62a**, akin to Mannitol-Cp from the previously discussed work, provided yields ranging from 50% to 94% with enantiomeric ratios greater than 91:9.

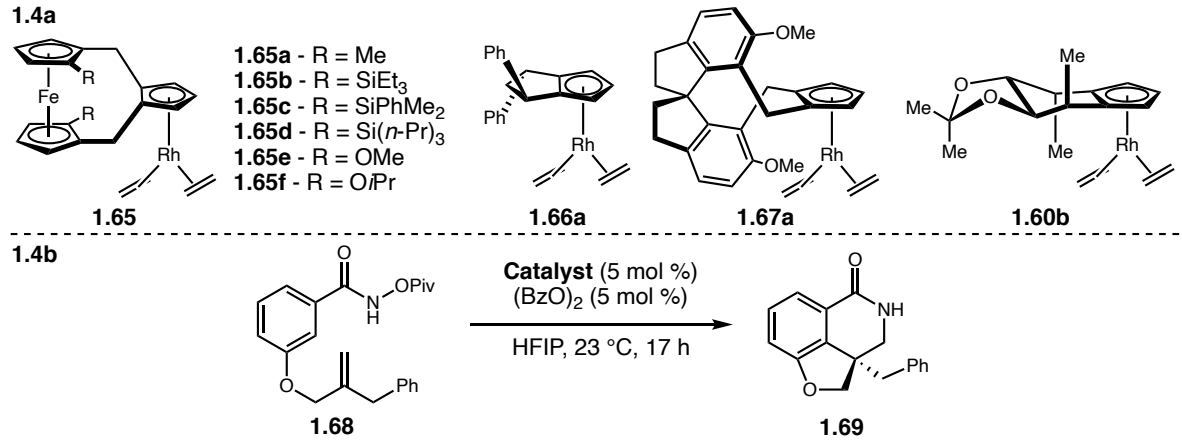

Figure 1.4: Spiro-annulation with various rhodium based Cp^X-bearing catalysts

In general, newer catalyst systems have not existed long enough to be utilized extensively in enantioselective transformation. One reason for this is whether an individual catalyst system performs well during initial testing. The initial disclosure of FeCp from Liang *et. al.* demonstrates this thorough investigation during their catalyst optimization (**Figure 1.4**).[14] Unsurprisingly, their catalyst system provides the optimal balance of yield and selectivity for the spiro-annulation of **1.68** to **1.69**, the focus of this report. However, in addition to FeCp **1.65**, BINOL-Cp **1.62a**, cPent-Cp **1.66a**, SCp **1.67a**, and Mannitol-Cp **1.60b** are tested (**Figure 1.4a**). As is common, the yield varies widely in the reaction. The optimal catalyst for this reaction (**1.35d**) affords dihydrobenzofuran **1.69** in 76% yield and 66% *ee*. BINOL-Cp **1.62a** outperforms the selectivity with 70% *ee* but suffers in yield. cPent-Cp **1.66a** maintains an excellent >99% yield but only provides 14% *ee*. SCp **1.67a** is the least effective catalyst with respect to yield (4%) and falls in the middle of the road with selectivity (57% *ee*). Finally, Mannitol-Cp **1.60b** affords high yield (82%) but suffers from low selectivity (37% *ee*).

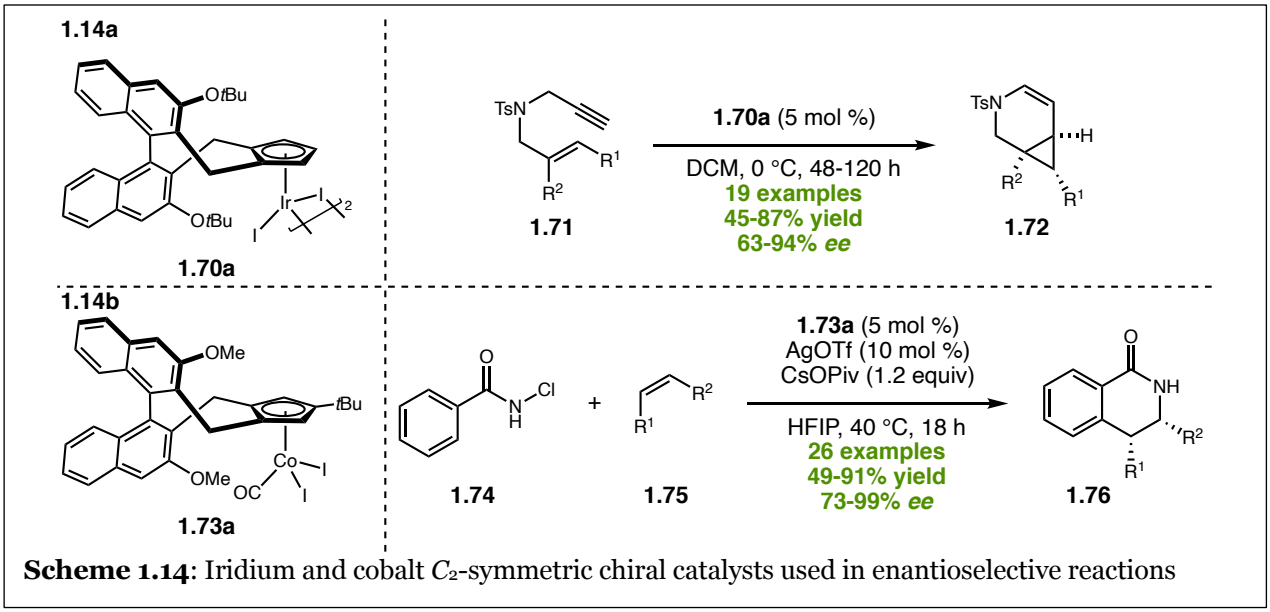

Scheme 1.14: Iridium and cobalt C_2-symmetric chiral catalysts used in enantioselective reactions

In contrast to rhodium, iridium and cobalt have relatively few examples in enantioselective catalysis.[4] Furthermore, the examples disclosed rely on ligands within the BINOL-Cp scaffold, primarily. One such iridium-catalyzed example uses catalyst **1.70a** for the synthesis of fused cyclopropanes **1.72** in up to 87% yield with up to 94% *ee* (**Scheme 1.14a**).[25] With respect to cobalt, **1.73a** was recently explored in the cyclization of **1.74** with olefins **1.75** to form dihydroixoquinolinones **1.76** with up to 91% yield and up to 99% *ee* (**Scheme 1.14b**).[24]

1.4 Conclusion

The synthesis and development of C_2-symmetric Cp ligands, and their associated late transition metal complexes, has been explored extensively over the past few decades. The C_2-symmetric nature of the pre-ligand is a clever route to eliminate facial selectivity concerns during metal complexation and any need for chiral resolution of the final catalyst. The general concept for ligand design to include a back wall to direct coordination of reactants and modular side walls to orient initial substrate binding has been exploited to develop various scaffolds. The BINOL-Cp platform, owing to its versatility and ever-growing collection of derivatives, has served as the "gold standard" for new catalysts and reactions to be compared against. Overall, this chapter serves to provide a foundation for some of the considerations examined during the development of new chiral Cp catalysts and to set the stage for the field of study. Further considerations more directly applicable to the design of the catalyst system detailed in this dissertation will be discussed in the next section.

1.5 References

(1) Kealy, T. J.; Pauson, P. L. A New Type of Organo-Iron Compound. *Nature*. **1951**, *168*, 1039–1040.

(2) Jutzi, P.; Burford, N. Structurally Diverse π-Cyclopentadienyl Complexes of the Main Group Elements. *Chem. Rev.* **1999**, *99*, 969–990.

(3) Newton, C. G.; Kossler, D.; Cramer, N. Asymmetric Catalysis Powered by Chiral Cyclopentadienyl Ligands. *J. Am. Chem. Soc.* **2016**, *138*, 3935-3941.

(4) Mas-Roselló, J.; Herraiz, A. G.; Audic, B.; Laverny, A.; Cramer, N. Chiral Cyclopentadienyl Ligands: Design, Syntheses, and Applications in Asymmetric Catalysis. *Angew. Chem. Int. Ed.* **2021**, *60*, 13198-13224.

(5) Arndt, S.; Okuda, J. Mono(Cyclopentadienyl) Complexes of the Rare-Earth Metals. *Chem. Rev.* **2002**, *102*, 1953–1976.

(6) Cesarotti, E.; Kagan, H. B.; Goddard, R.; Krager, C. Synthesis of New Ligands for Transition Metal Complexes: Menthyl- and Neomenthyl- Cyclopentadienes. *J. Organomet. Chem.* **1978**, *162*, 297–309.

(7) Halterman, R. L.; Vollhardt, K. P. C. Practical Synthesis of Two Annelated Optically Active Cyclopentadienes from the Chiral Pool and Their Transition Metal Complexes. *Tet. Lett.* **1986**, *27*, 1461–1464.

(8) Halterman, R. L.; Vollhardt, K. P. Synthesis and Asymmetric Reactivity of Enantiomerically Pure Cyclopentadienylmetal Complexes Derived from the Chiral Pool. *Organometallics* **1988**, *7*, 883–892.

(9) Colletti, S. L.; Halterman, R. L. Binaphthylcyclopentadiene: A C2-Symmetric Annulated Cyclopentadienyl Ligand with Axial Chirality. *Tet. Lett.* **1989**, *30*, 3513–3516.

(10) Ye, B.; Cramer, N. Chiral Cyclopentadienyl Ligands as Stereocontrolling Element in Asymmetric C–H Functionalization. *Science (80-.).* **2012**, *338* (6106), 504.

(11) Ye, B. H.; Cramer, N. A Tunable Class of Chiral Cp Ligands for Enantioselective

Rhodium(III)-Catalyzed C-H Allylations of Benzamides. *J. Am. Chem. Soc.* **2013**, *135*, 636–639.

(12) Wang, S.-G.; Park, S. H.; Cramer, N. A Readily Accessible Class of Chiral Cp Ligands and Their Application in Ru ^{II} -Catalyzed Enantioselective Syntheses of Dihydrobenzoindoles. *Angew. Chem. Int. Ed.* **2018**, *57*, 5459–5462.

(13) Zheng, J.; Cui, W. J.; Zheng, C.; You, S. L. Synthesis and Application of Chiral Spiro Cp Ligands in Rhodium-Catalyzed Asymmetric Oxidative Coupling of Biaryl Compounds with Alkenes. *J. Am. Chem. Soc.* **2016**, *138*, 5242–5245.

(14) Liang, H.; Vasamsetty, L.; Li, T.; Jiang, J.; Pang, X.; Wang, J. A New Class of C2-Symmetric Chiral Cyclopentadienyl Ligand Derived from Ferrocene Scaffold: Design, Synthesis and Application. *Chem. Eur. J.* **2020**, *26*, 14546–14550.

(15) Reddy Chidipudi, S.; Burns, D. J.; Khan, I.; Lam, H. W. Enantioselective Synthesis of Spiroindenes by Enol-Directed Rhodium(III)-Catalyzed C-H Functionalization and Spiroannulation. *Angew. Chem. Int. Ed.* **2015**, *54*, 13975–13979.

(16) Ye, B. H.; Cramer, N. Chiral Cyclopentadienyl Ligands Enable a Rhodium(III)-Catalyzed Enantioselective Access to Hydroxychromanes and Phthalides. *Synlett* **2015**, *26*, 1490–1495.

(17) Kossler, D.; Cramer, N. Chiral Cationic CpxRu(II) Complexes for Enantioselective Yne-Enone Cyclizations. *J. Am. Chem. Soc.* **2015**, *137*, 12478–12481.

(18) Duchemin, C.; Smits, G.; Cramer, N. Rh I , Ir III ,and Co III Complexes with Atropchiral Biaryl Cyclopentadienyl Ligands: Syntheses, Structures, and Catalytic Activities. *Organometallics*. **2019**, *38*, 3939-3947.

(19) Sun, Y.; Cramer, N. Tailored Trisubstituted Chiral CpxRhIII Catalysts for Kinetic Resolutions of Phosphinic Amides. *Chem. Sci.* **2018**, *9,* 2981–2985.

(20) Cui, W. J.; Wu, Z. J.; Gu, Q.; You, S. L. Divergent Synthesis of Tunable Cyclopentadienyl Ligands and Their Application in Rh-Catalyzed Enantioselective Synthesis of

Isoindolinone. *J. Am. Chem. Soc.* **2020**, *142*, 7379–7385.

(21) Zheng, J.; Cui, W. J.; Zheng, C.; You, S. L. Synthesis and Application of Chiral Spiro Cp Ligands in Rhodium-Catalyzed Asymmetric Oxidative Coupling of Biaryl Compounds with Alkenes. *J. Am. Chem. Soc.* **2016**, *138* , 5242–5245.

(22) Gutnov, A.; Heller, B.; Fischer, C.; Drexler, H. J.; Spannenberg, A.; Sundermann, B.; Sundermann, C. Cobalt(I)-Catalyzed Asymmetric [2+2+2] Cycloaddition of Alkynes and Nitriles: Synthesis of Enantiomerically Enriched Atropoisomers of 2-Arylpyridines. *Angew. Chem. Int. Ed.* **2004**, *43*, 3795–3797.

(23) Jungk, P.; Täufer, T.; Thiel, I.; Hapke, M. Synthesis of Chiral Indenylcobalt(I) Complexes and Their Evaluation in Asymmetric [2+2+2] Cycloaddition Reactions. *Synthesis*. **2016**, *48*, 2026–2035.

(24) Ozols, K.; Jang, Y.-S.; Cramer, N. Chiral Cyclopentadienyl Cobalt(III) Complexes Enable Highly Enantioselective 3d-Metal-Catalyzed C–H Functionalizations. *J. Am. Chem. Soc.* **2019**, *141*, 5675-5680.

(25) Dieckmann, M.; Jang, Y.-S.; Cramer, N. Chiral Cyclopentadienyl Iridium(III) Complexes Promote Enantioselective Cycloisomerizations Giving Fused Cyclopropanes. *Angew. Chem. Int. Ed.* **2015**, *54*, 12149-12152.

(26) Audic, B.; Wodrich, M. D.; Cramer, N. Mild Complexation Protocol for Chiral CpxRh and Ir Complexes Suitable for: In Situ Catalysis. *Chem. Sci.* **2019**, *10* 781–787.

(27) Brauns, M.; Cramer, N. Efficient Kinetic Resolution of Sulfur-Stereogenic Sulfoximines by Exploiting Cp X Rh III -Catalyzed C–H Functionalization . *Angew. Chem. Int. Ed.* **2019**, *58,* 8902-8906.

(28) Newton, C. G.; Kossler, D.; Cramer, N. Asymmetric Catalysis Powered by Chiral Cyclopentadienyl Ligands. *J. Am. Chem. Soc.* **2016**, *138*, 3935–3941.

(29) Ye, B. H.; Donets, P. A.; Cramer, N. Chiral Cp-Rhodium(III)-Catalyzed Asymmetric Hydroarylations of 1,1-Disubstituted Alkenes. *Angew. Chem. Int. Ed.* **2014**, *53*, 507–511.

Chapter 2. Planar Chiral π-Complexes: Assigning Planar Chirality, Synthesis of Selected Ligands and their Associated Late-Transition Metal Complexes, and Selected Catalytic Examples

In this chapter, we will move away from C_2-symmetric ligands and discuss those that exhibit planar chirality when complexed to transition metals. This discussion will first require an understanding of how to define and assign planar chirality. Once again, within the context of this dissertation, this section will focus specifically on group VIII and group IX transition metal complexes. The synthesis of notable ligand and catalyst systems will be examined along with selected catalytic uses of the late-transition metal complexes. At the time of writing this dissertation, a manuscript of this overview is being prepared for submission as a tutorial review to Chemical Society Reviews.

2.1 Definition of Planar Chirality and Methods for Stereochemical Assignment

2.1.1 Defining Planar Chirality

Conventional point chirality was originally described by Cahn and Ingold in 1951 and further expanded upon with Prelog during the 1950's and 1960's.[1–4] In naming conventions, point chirality bears the highest priority and so it garners the most attention when looking at new molecules.[2] However, other forms of chirality have arisen to meet the needs of describing various kinds of molecules that cannot be assigned through the original conventions for assigning the "handedness" of a compound including axial and helical chirality.[1–4] While not studied as frequently, planar chirality is one of the methods currently gaining more relevance in modern chemistry.

Planar chirality was originally employed to describe cyclophanes in 1956.[2] A plane of symmetry in a molecule such as **2.1** can be disrupted simply by changing the identity of the R

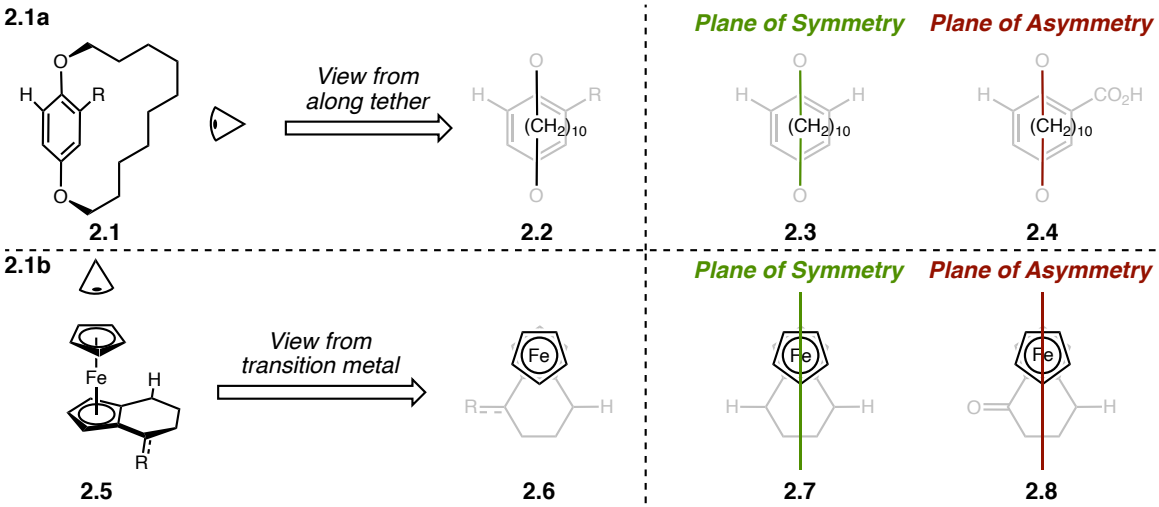

Figure 2.1: Defining planar chirality in cyclophanes and transition metal π-complexes

group without the addition of a chiral center (**Figure 2.1a**). When viewed from the direction of the ethereal tether (**2.2**), this change becomes more visible. A plane of symmetry exists when the R group is a hydrogen (**2.3**), however, this becomes a plane of asymmetry when R is a different functional group such as a carboxylic acid (**2.4**). With this observation, new rules had to be developed to describe this molecule, and as such, planar chirality was defined.

Transition metal π-complexes (**2.5**), however, introduce several complications when compared to cyclophanes (**Figure 2.1b**). Where the cyclic tether of cyclophane **2.1** orients the structure for planar chiral assignment, the complexed transition metal now serves to orient the structure (**2.5** to **2.6**).[2] Here, a plane of symmetry now can exist in the molecule, depending on the identity of the R group. If the R group is a proton (**2.7**), a plane of symmetry exists dividing the molecule into identical eastern and western halves. This plane, however, becomes a plane of asymmetry if R is a carbonyl (**2.8**).

2.1.2 Assigning Planar Chirality of Transition Metal π-Complexes

Two primary methods for assigning planar chirality to transition metal π-complexes will be described in this section. The first method involves reducing planar chirality to point chirality.[2,5] This conversion will always unambiguously provide the correct stereochemical assignment but requires more changes to the orientation of the molecule to determine the assignment. The second

method is a simplified method that allows for more flexibility in assigning chirality from transition metal complexes drawn in different orientations.[6] Despite its ease, the second method does have inherent limitations that must be considered when they arise.

In order to demonstrate these two methods, we will examine ferrocene **2.6**, the compound that Schlögl and Falk characterized, in conjunction with Cahn, Ingold, and Prelog (CIP), to determine the rules for assigning planar chirality to π-complexes (**Figure 2.2**).[7] First, the transition metal coordinated to the ligand that serves to orient the stereochemical assignment will be referred to as the pilot atom.[5,8] Next, when assigning planar chirality, it is important to always only do so for the most substituted ligand in the complex, if multiple ligands are present.[9] In ferrocene **2.6**, this is the bicyclic Cp with the ketone bearing ring. Finally, chirality will be determined specifically when considering the highest priority atom of the π-complex. To determine the highest priority atom, which will be referred to as the centroid, it is important to consider each atom of the π-complex to be bound to the transition metal, in addition to any other substituents.[5] One of the simplest ways to do this is to consider the pilot atom to have a single bond to each atom of the π-complex (**2.7**).[5]

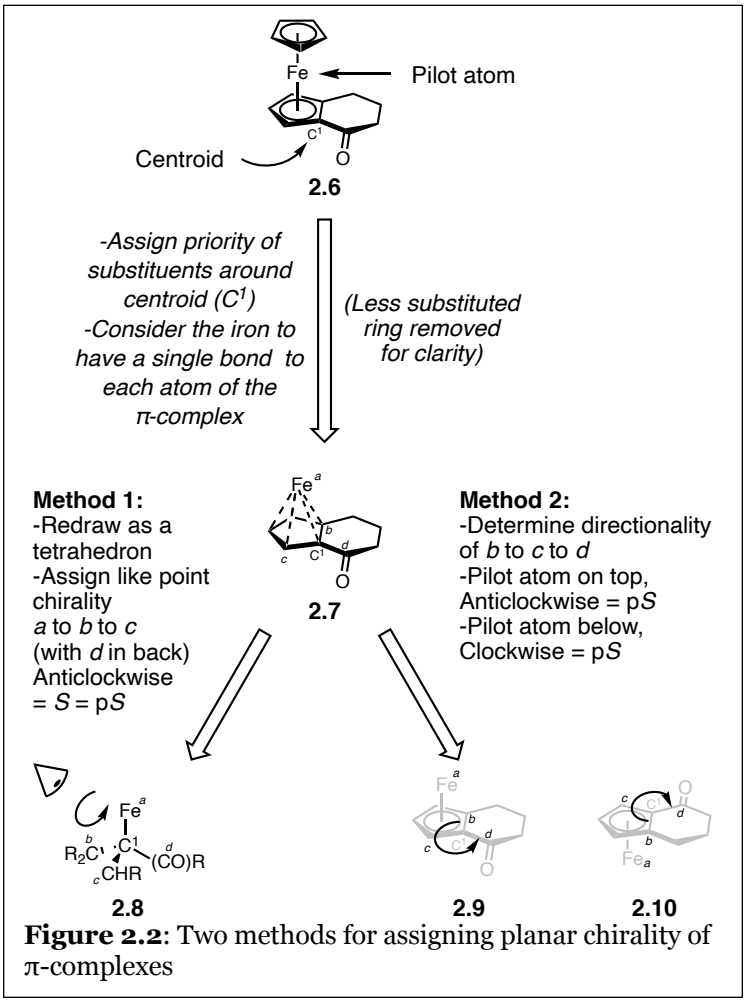

Figure 2.2: Two methods for assigning planar chirality of π-complexes

First, to assign chirality of **2.6** through reduction of planar chirality to point chirality, follow the conventions previously detailed to determine the pilot atom and the centroid (C^1,

Figure 2.2).[1–4] Assign priority to the substituents (*a*, *b*, *c*, and *d*; where *a* > *b* > *c* > *d*) of the centroid according to CIP rules, remembering to consider any atoms of the π-complex to have a single bond to the pilot atom (**2.7**).[8] Finally, redraw the centroid in a tetrahedral configuration and determine chirality of the centroid by traditional CIP naming conventions (**2.8**). This chirality, *R* or *S*, is equivalent to the planar *R* (p*R*) or planar *S* (p*S*) configuration of the π-complex.[1,2]

For the second method, the centroid of the highest priority π-coordinated ligand is determined in the same fashion (**2.6**, **Figure 2.2**).[5,9] From here, as before, assign the priority of each substituent of the centroid (*a*, *b*, *c*, and *d*; where *a* > *b* > *c* > *d*, **2.7**).[1,2] In this method, instead of redrawing the centroid in a tetrahedral configuration, determine the directionality of the ligand substituents around the centroid, ignoring the pilot atom initially (**2.9**, and **2.10**).[6] Once the directionality (clockwise or anticlockwise) is determined for the priority of the substituents around the centroid, the position of the pilot atom becomes important. If the pilot atom is above the plane of the ligand (**2.9**), the chiral assignment is the same for point chirality if the highest priority substituent is in front and the lowest is in back: clockwise is p*R* and anticlockwise is p*S*.[1,2,6] Similarly, if the pilot atom is below the plane (**2.10**), the assignments are flipped as if, in tetrahedral point chirality, the lowest priority atom is in front: clockwise is p*S* and anticlockwise is p*R*.[1,2,6]

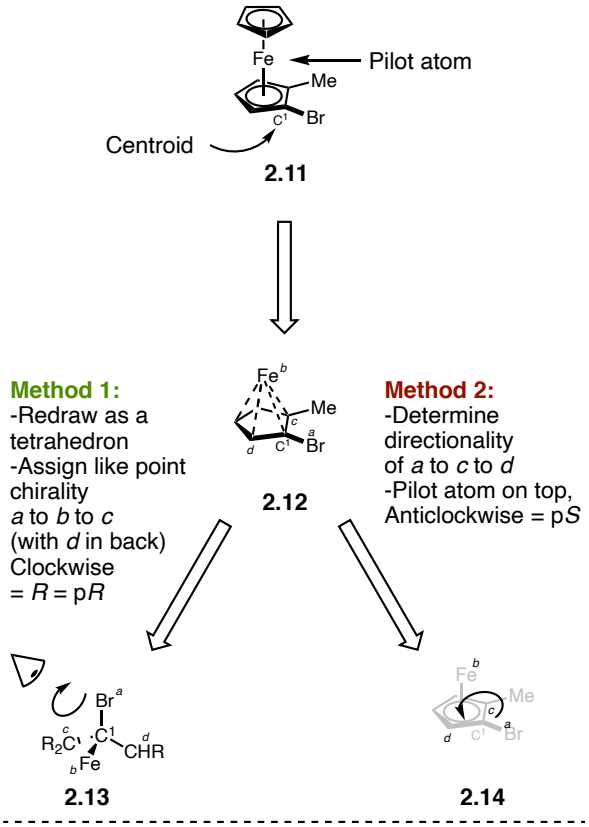

Figure 2.3: Limitation of simplified method for stereochemical assignment

In most cases, both methods will afford the same stereochemical assignment. A limitation of the second method, however, arises when one of the substituents on the π-system has a higher CIP priority than the transition metal pilot atom. One of the most likely scenarios for this to occur is with a halogen substituent such as the case in **2.11** (**Figure 2.3**). For **2.11**, the reduction to point chirality affords an assignment of p*R* (**2.13**), while the simplified second method affords p*S* (**2.14**). If this exception occurs, the reduction to point chirality is the method that provides the correct stereochemical assignment.[2] This is due, once again, to the fact that point chirality has priority over central chirality.

In addition to these two primary methods, a third method exists that describes the direct application of cyclophane chirality to π-complexes.[5,8] An in-depth analysis of this method will be available in the tutorial review when published.

2.2 Planar Chiral π-Complexes of Late Transition Metals

2.2.1 Synthesis of Ligands and the Associated Late Transition Metal π-Complexes for Selected Compounds

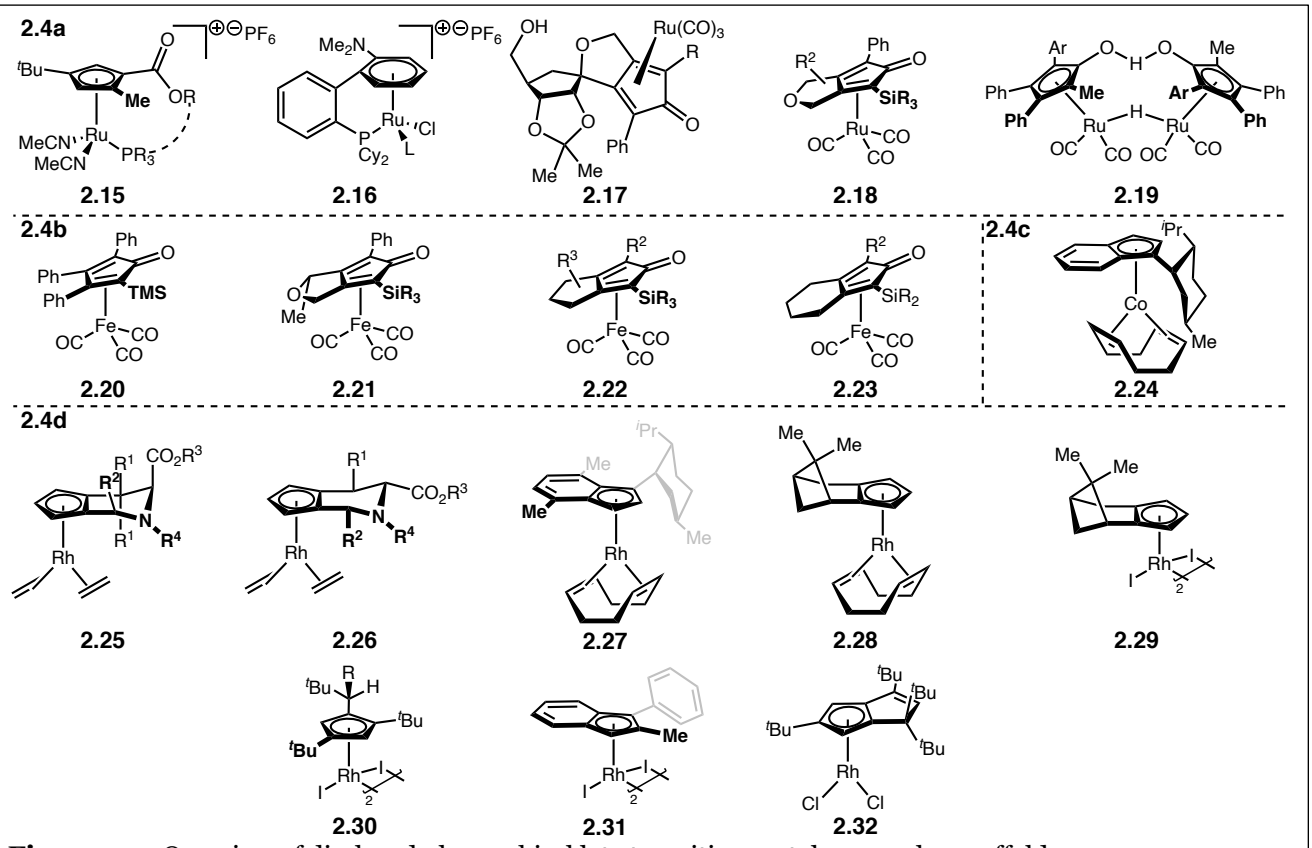

Figure 2.4: Overview of disclosed planar chiral late transition metal π-complex scaffolds

While there has been a large body of work on planar chiral π-complexes with early transition metals, the focus of this dissertation is specifically on late transition metal complexes. Further, for the purposes of the discussion on the synthesis of ligands and the associated π-complexes, this discussion will only include complexes that have been utilized as enantioselective catalysts. In total, there are 15 unique scaffolds within this paradigm: five with ruthenium (**Figure 2.4a**),[10–17] four with iron (**Figure 2.4b**),[16,18–20] one with cobalt (**Figure 2.4c**),[21,22] and eight with rhodium (**Figure 2.4d**).[23–28] The tutorial review will contain an exhaustive overview on the synthesis of these scaffolds; however, this dissertation will focus on a select few complexes to highlight some of the synthetic challenges that arise when utilizing planar chirality.

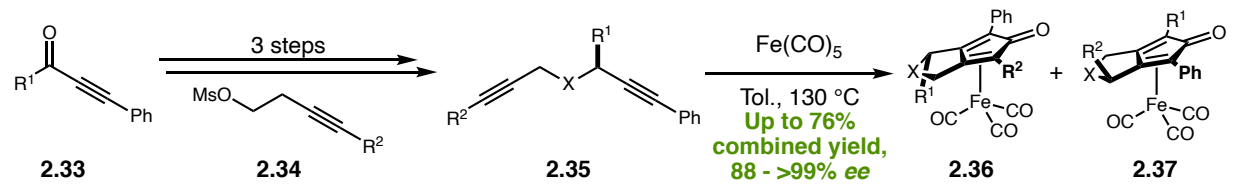

Scheme 2.1: General synthesis of several planar chiral iron π-complexes

A significant portion of the complexes that have been explored with iron as the transition metal follow the same general synthetic scheme (**Scheme 2.1**).[16,18–20] Following this scheme, a tethered diyne compound (**2.35**) is reacted with iron(0) pentacarbonyl [$Fe(CO)_5$] in toluene at high temperature.[16,18,19] The net result of this reaction is the [2 + 1] cyclization of the diyne and a molecule of carbon monoxide to form the cyclopentadienone and metalate in a single step, affording **2.36**, and **2.37**. The tethered diyne contains all the information for the substituents around the cyclopentadienone, including any chiral centers that will allow for the synthesis of diastereomers rather than solely planar chiral enantiomers, or heteroatoms in the bicyclic scaffold. Products that are made of diastereomeric mixtures have successfully been resolved on silica gel chromatography. However, if only planar chiral enantiomers are formed, resolution on preparatory chiral HPLC has been necessary to afford enantioenriched catalysts.[20]

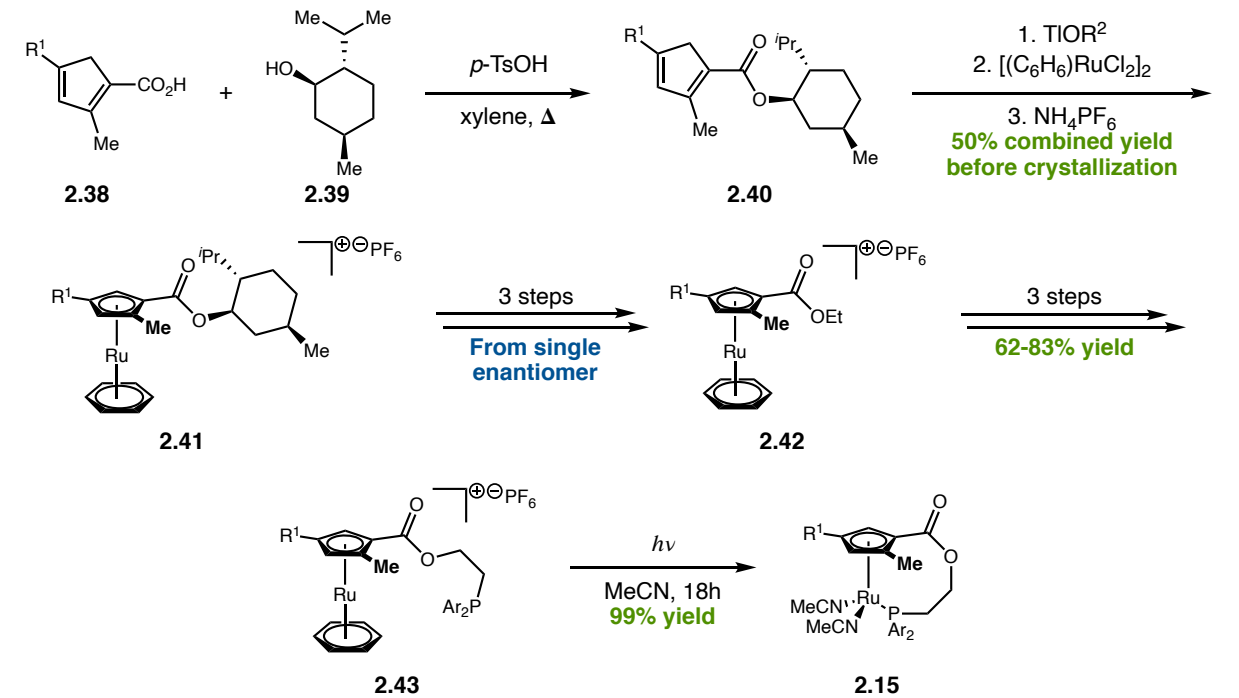

Scheme 2.2: Synthesis of tethered ruthenium complex **2.15**

For ruthenium-based complexes, perhaps the most thoroughly explored scaffold is the phosphine tethered Cp^X-bearing **2.15** (**Scheme 2.2**).[10] The synthesis of these complexes begins with the installation of menthol **2.39** to trisubstituted CpH **2.38**.[29] Following a transmetalation complexation protocol with thallium (discussed previously in Chapter 1), ruthenium sandwich complex **2.41** is accessed in 50% overall yield as a mixture of diastereomers.[30] Fractional crystallization and removal of the menthol auxiliary affords enantiomerically pure **2.42**. From a single enantiomer of the sandwich complex **2.42**, a 3-step transesterification process allows for installation of the phosphine tether to the ester moiety (**2.43**).[30] Finally, irradiation of **2.43** in the presence of acetonitrile affords the tethered ruthenium piano-stool complex **2.15**.[10]

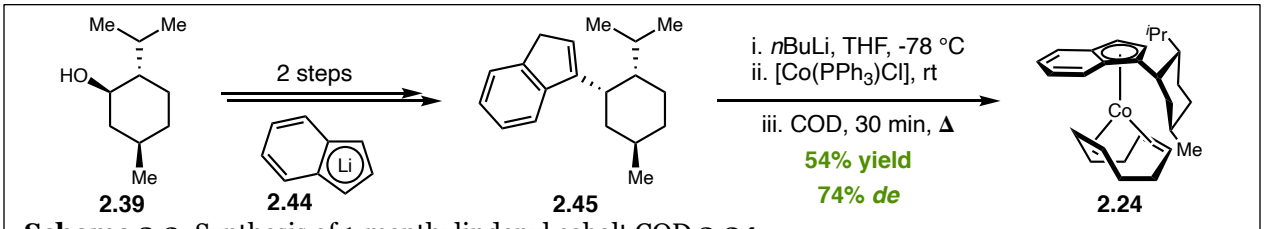

Scheme 2.3: Synthesis of 1-menthylindenyl cobalt COD **2.24**

Currently, the only planar chiral complex that has successfully been utilized for enantioselective catalysis with cobalt is 1-menthyl/1-neomenthylindenyl cobalt complex **2.24** (**Figure 2.4c**).[21,22] The synthesis of this scaffold begins with the natural product menthol **2.39** (**Scheme 2.3**). Tosylation of the alcohol and S_N2 addition of indenyllithium **2.44** affords the indenyl pre-ligand **2.45**.[31] The menthyl substituent directs metalation during a transmetalation

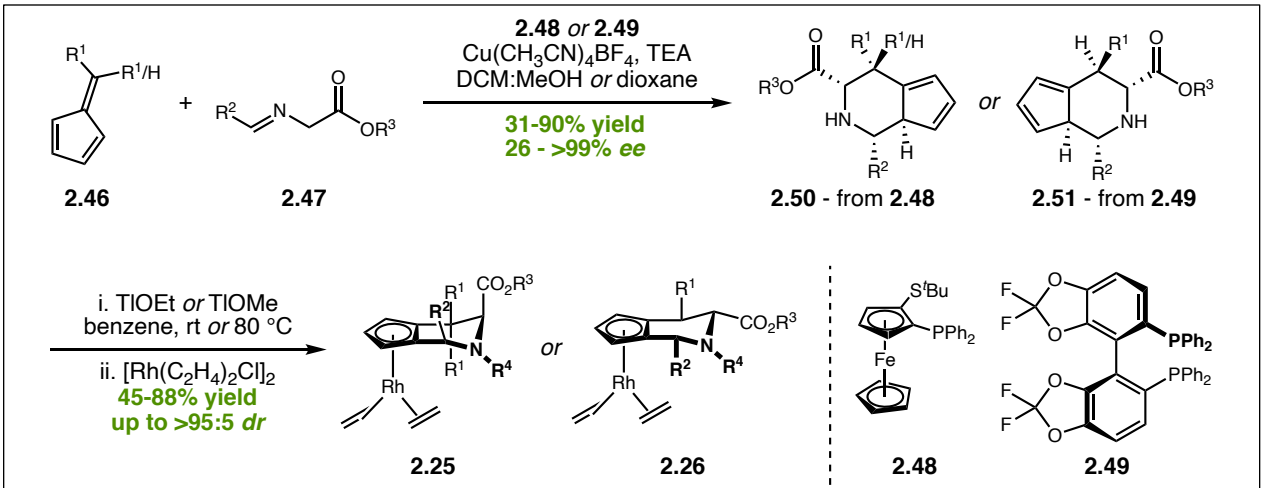

Scheme 2.4: Synthesis of the rhodium JasCp platform

complexation protocol with BuLI and the cobalt source to afford diasteriomerically enriched **2.24** after silica gel chromatography.[21]

The JasCp platform (**2.25**, and **2.26**) disclosed by Antonchick and Waldmann is one of the most diverse chiral Cp-based platforms available, with more than 30 derivatives currently reported (**Figure 2.4a**).[23,32] Beginning from achiral building blocks, enantioselective cycloaddition of fulvenes **2.46** with imines **2.47** affords enantiomerically enriched **2.50** or **2.51**, depending on the chiral ligand used (**2.48**, or **2.49**, **Scheme 2.4**).[23] While a reasonable to good level of enantiocontrol is exerted over the reaction, fractional crystallization or chiral preparative HPLC have been necessary to access highly enantioenriched ligands. Alkylation of the nitrogen, if desired, followed by transmetalation complexation with thallium ethoxide or methoxide and $[Rh(C_2H_4)_2Cl]_2$ provides the final catalysts **2.25** or **2.26**.[23]

One common theme of these planar chiral complexes is the difficulty in the resolution of the final complexes. Often, the synthesis of either the ligand, or the final transition metal π-complex, relies on chiral preparative HPLC to access enantiopure pre-catalysts.[20,23,28] Some of the ligand systems rely on enantiopure starting materials to generate diastereomeric π-complexes which may be able to be separated via normal silica gel chromatography.[15,16,18,19,21,22] Perekalin has explored complexation with amino acid-derived chiral ligands, such as proline, either through discrete or transient intermediates; however, these methods are unique to the ligand scaffolds they are used on and not ubiquitously applicable.[25–27]

2.2.2 Selected Examples of Planar Chiral π-Complexes in Enantioselective Catalysis

Within the context of enantioselective transformations catalyzed by planar chiral late transition metal π-complexes, the first row group VIII and group IX transition metals have received the least attention. The iron compounds **2.20-2.23** specifically have only been used as catalysts for asymmetric hydrogenation and asymmetric transfer hydrogenation reactions.[16,18,19] Functioning similarly to the C_2-symmetric catalysts with the sterically different R^1 and R^2 groups of the ligand serving to orient the substrate, the planar chiral Shvo-type catalysts **2.21a-c** were able to carry out the transfer hydrogenation of acetophenone **2.52** in up to 91% yield with modest selectivities up to 25% *ee*.[17] Cobalt complexes, on the other hand, have been explored most notably in the context of [2 + 2 + 2] cyclotrimerizations of alkynes (**Figure 2.5a**).[33–36] One key example is the cyclotrimerization of phosphines **2.54** with acetylene using menthol-derived indenyl cobalt

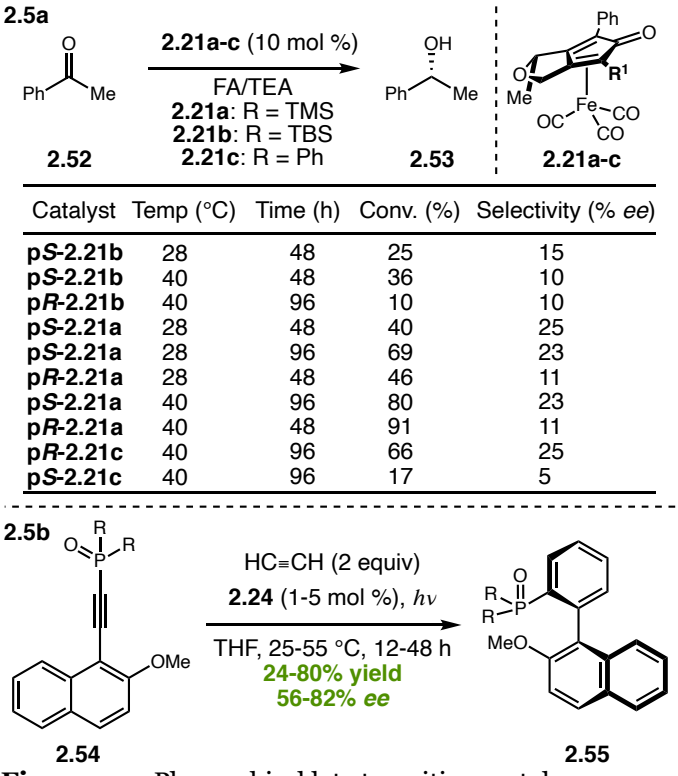

Catalyst	Temp (°C)	Time (h)	Conv. (%)	Selectivity (% *ee*)
p*S*-**2.21b**	28	48	25	15
p*S*-**2.21b**	40	48	36	10
p*R*-**2.21b**	40	96	10	10
p*S*-**2.21a**	28	48	40	25
p*S*-**2.21a**	28	96	69	23
p*R*-**2.21a**	28	48	46	11
p*S*-**2.21a**	40	96	80	23
p*R*-**2.21a**	40	48	91	11
p*R*-**2.21c**	40	96	66	25
p*S*-**2.21c**	40	96	17	5

Figure 2.5: Planar chiral late transition metal π-complexes of first row transition metals used in enantioselective catalysis

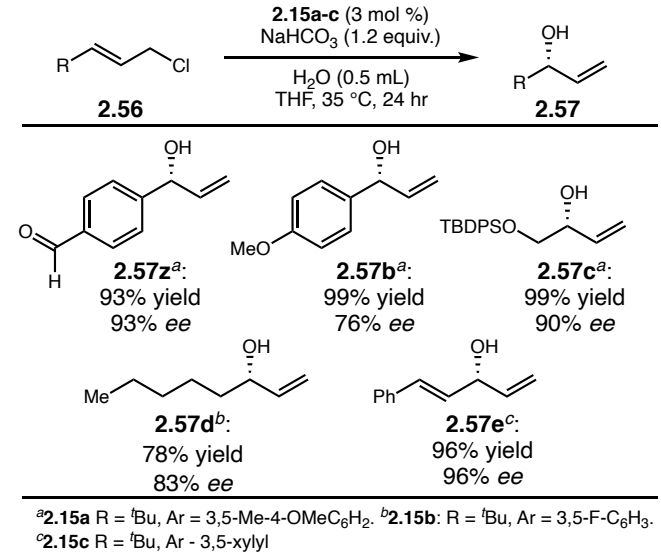

[a]**2.15a** R = ^{t}Bu, Ar = 3,5-Me-4-OMeC$_6$H$_2$. [b]**2.15b**: R = ^{t}Bu, Ar = 3,5-F-C$_6$H$_3$. [c]**2.15c** R = ^{t}Bu, Ar - 3,5-xylyl

Table 2.1: Planar chiral ruthenium π-complex catalyzed allylic oxidation

catalysts **2.24** (**Figure 2.5b**).[34] The enantioselective transformations afforded axially chiral phosphines **2.55** in 24-60% yield with 56-82% *ee*. These chiral phosphines could then be further transformed into functional chiral ligands for use in enantioselective catalysis.

Ruthenium planar chiral π-complexes have been used extensively in the realm of allylic substitution chemistry. Specifically, Kanbayashi and coworkers have utilized **2.15** (**Scheme 2.2**) for reactions ranging from simple small molecule substitution reactions to polymer synthesis.[37–46] One key example is the allylic alcohol formation *via* substitution of **2.56** with water as the nucleophile (**Table 2.1**).[40] With catalyst **2.15a-c**, allylic alcohols **2.57** were accessed in up to 99% yield and 96% *ee*.

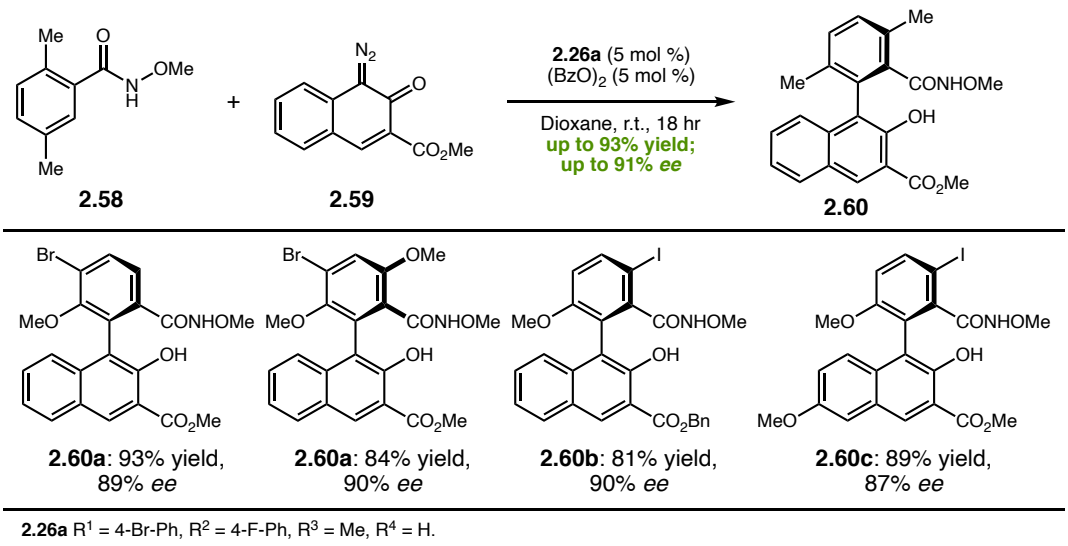

Table 2.2: Rhodium JasCp catalyzed directed C–H functionalization

Finally, the JasCp platform on rhodium (**2.25**-**2.26**) has had great success with directed C–H activation reactions (**Table 2.2**).[23,32] Like the 1-menthylindenylcobalt **2.24** previously noted for the synthesis of axially chiral biaryls, one such directed C–H functionalization reaction explored is the addition of diazo **2.59** to hydroxamate **2.58**.[23] Furnishing a different variety of these axially chiral biaryls **2.60**, the yield and enantiocontrol for this transformation were excellent, with up to 93% yield and 91% *ee*.

2.3 Conclusion

Through a deeper understanding of planar chirality and the methods available to assign this form of stereochemistry, the tools are becoming more present to incorporate planar chirality into catalyst design for transition metal π-complexes. Ligand synthesis within the context of these complexes is often quite simple, however, problems arise related to facial selectivity in the complexation with transition metals leading the need for more difficult chiral resolution strategies to access enantiopure pre-catalysts. The need for chiral preparative HPLC in some of the simplest ligand systems is a major limitation, and strategies around chiral ligand coordination to allow for diastereomeric separation through silica gel chromatography are not yet ubiquitous across ligand scaffolds. Ultimately, this chapter serves to introduce the concept of planar chirality and to discuss, generally, the current landscape of disclosed catalysts for enantioselective reactions that utilize this form of chirality. Much of the work in the rest of this dissertation will incorporate the application of these concepts into new complex synthesis and design.

2.4 References

(1) Cahn, R. S.; Ingold, C. K. 131. Specification of Configuration about Quadricovalent Asymmetric Atoms. *J. Chem. Soc.* **1951**, 612–622.

(2) Cahn, R. S.; Ingold, C. K.; Prelog, V. The Specification of Asymmetric Configuration in Organic Chemistry. *Experientia. 1956 123* **1956**, *12*, 81–94.

(3) Cahn, R. S.; Ingold, C.; Prelog, V. Specification of Molecular Chirality. *Angew. Chem. Int. Ed.* **1966**, *5*, 385–415.

(4) Prelog, V.; Helmchen, G. Basic Principles of the CIP-System and Proposals for a Revision. *Angew. Chem. Int. Ed.* **1982**, *21*, 567–583.

(5) SCHLÖGL, K. Configurational and Conformational Studies in the Metallocene Field. *Organomet. Chem.* **1970**, 413–432.

(6) Marquarding, D.; Klusacek, H.; Gokel, G.; Hoffmann, P.; Ugi, I. Stereoselective Syntheses. VI. Correlation of Central and Planar Chirality in Ferrocene Derivatives. *J. Am. Chem. Soc.* **2002**, *92*, 5389–5393.

(7) Schögl, K.; Falk, H. The Absolute Configuration of 1,2-(α-Oxotetramethylene)Ferrocene. *Angew. Chem. Int. Ed.* **1964**, *3*, 512–512.

(8) Schlögl, K. Stereochemistry of Metallocenes: 20 Years of Progress and Recent Advances. *J. Organomet. Chem.* **1986**, *300*, 219–248.

(9) Schlögl, K. Stereochemistry of Metallocenes. In *Topics in Stereochemistry*; Allinger, N. L., Eliel, E. L., Eds.; Interscience Publishers: New York, 1967; pp 39–92.

(10) Dodo, N.; Matsushima, Y.; Uno, M.; Onitsuka, K.; Takahashi, S. Synthesis of Ruthenium Complexes with Planar-Chiral Cyclopentadienyl-Pyridine or -Phosphine Bidentate Ligands. *J. Chem. Soc. Dalt. Trans.* **2000**, No. 1, 35–41.

(11) Matsushima, Y.; Onitsuka, K.; Kondo, T.; Mitsudo, T. A.; Takahashi, S. Asymmetric Catalysis of Planar-Chiral Cyclopentadienylruthenium Complexes in Allylic Amination and Alkylation [10]. *J. Am. Chem. Soc.* **2001**, *123*, 10405–10406.

(12) Faller, J. W.; D'Alliessi, D. G. Planar Chirality in Tethered H6:H1-(Phosphinophenylenearene-P)Ruthenium(II) Complexes and Their Potential Use as Asymmetric Catalysts. *Organometallics* **2003**, *22*, 2749–2757.

(13) Faller, J. W.; Fontaine, P. P. Resolution and Diels - Alder Catalysis with Planar Chiral Arene-Tethered Ruthenium Complexes. *Organometallics* **2005**, *24*, 4132–4138.

(14) Faller, J. W.; Fontaine, P. P. Synthesis and Characterization of a Planar Chiral and Chiral-at-Metal Ruthenium N-Heterocyclic Carbene Complex. *J. Organomet. Chem.* **2006**, *691*,

(15) Yamamoto, Y.; Yamashita, K.; Nakamura, M. Synthesis of Organometallic Analogues of Spirocyclic C-Arylribosides. *Organometallics* **2010**, *29*, 1472–1478.

(16) Hopewell, J. P.; Martins, J. E. D.; Johnson, T. C.; Godfrey, J.; Wills, M. Developing Asymmetric Iron and Ruthenium-Based Cyclone Complexes; Complex Factors Influence the Asymmetric Induction in the Transfer Hydrogenation of Ketones. *Org. Biomol. Chem.* **2012**, *10*, 134–145.

(17) Dou, X.; Hayashi, T. Synthesis of Planar Chiral Shvo Catalysts for Asymmetric Transfer Hydrogenation. *Adv. Synth. Catal.* **2016**, *358*, 1054–1058.

(18) Johnson, T. C.; Clarkson, G. J.; Wills, M. (Cyclopentadienone)Iron Shvo Complexes: Synthesis and Applications to Hydrogen Transfer Reactions. *Organometallics* **2011**, *30*, 1859–1868.

(19) Del Grosso, A.; Chamberlain, A. E.; Clarkson, G. J.; Wills, M. Synthesis and Applications to Catalysis of Novel Cyclopentadienone Iron Tricarbonyl Complexes. *Dalton Trans.* **2018**, *47*, 1451–1470.

(20) Bai, X.; Cettolin, M.; Mazzoccanti, G.; Pierini, M.; Piarulli, U.; Colombo, V.; Dal Corso, A.; Pignataro, L.; Gennari, C. Chiral (Cyclopentadienone)Iron Complexes with a Stereogenic Plane as Pre-Catalysts for the Asymmetric Hydrogenation of Polar Double Bonds. *Tetrahedron* **2019**, *75*, 1415–1424.

(21) Gutnov, A.; Drexler, H. J.; Spannenberg, A.; Oehme, G.; Heller, B. Syntheses of Chiral

Nonracemic Half-Sandwich Cobalt Complexes with Menthyl-Derived Cyclopentadienyl, Indenyl, and Fluorenyl Ligands. *Organometallics* **2004**, *23*, 1002–1009.

(22) Jungk, P.; Täufer, T.; Thiel, I.; Hapke, M. Synthesis of Chiral Indenylcobalt(I) Complexes and Their Evaluation in Asymmetric [2+2+2] Cycloaddition Reactions. *Synthesis (Stuttg)*. **2016**, *48*, 2026–2035.

(23) Jia, Z.-J.; Merten, C.; Gontla, R.; Daniliuc, C. G.; Antonchick, A. P.; Waldmann, H. General Enantioselective C–H Activation with Efficiently Tunable Cyclopentadienyl Ligands. *Angew. Chem. Int. Ed.* **2017**, *56*, 2429-2434.

(24) Schumann, H.; Stenzel, O.; Dechert, S.; Girgsdies, F.; Halterman, R. L. Menthyl-Functionalized Chiral Nonracemic Monoindenyl Complexes of Rhodium, Iridium, Cobalt, and Molybdenum. *Organometallics* **2001**, *20*, 2215–2225.

(25) Trifonova, E. A.; Ankudinov, N. M.; Mikhaylov, A. A.; Chusov, D. A.; Nelyubina, Y. V.; Perekalin, D. S. A Planar-Chiral Rhodium(III) Catalyst with a Sterically Demanding Cyclopentadienyl Ligand and Its Application in the Enantioselective Synthesis of Dihydroisoquinolones. *Angew. Chemie Int. Ed.* **2018**, *57*, 7714–7718.

(26) Pototskiy, R. A.; Kolos, A. V.; Nelyubina, Y. V.; Perekalin, D. S. Rhodium Catalysts with a Chiral Cyclopentadienyl Ligand Derived from Natural R-Myrtenal. *Eur. J. Org. Chem.* **2020**, 37, 6019–6025.

(27) Kolos, A. V.; Nelyubina, Y. V.; Sundararaju, B.; Perekalin, D. S. Synthesis of Overloaded Cyclopentadienyl Rhodium(III) Complexes via Cyclotetramerization of Tert-Butylacetylene. *Organometallics* **2021**, *40*, 3712–3719.

(28) Farr, C. M. B.; Kazerouni, A. M.; Park, B.; Poff, C. D.; Won, J.; Sharp, K. R.; Baik, M. H.; Blakey, S. B. Designing a Planar Chiral Rhodium Indenyl Catalyst for Regio- And Enantioselective Allylic C-H Amidation. *J. Am. Chem. Soc.* **2020**, *142*, 13996–14004.

(29) Uno, M.; Ando, K.; Komatsuzdci, N.; Takahashi, S. A New Route to Planar-Chiral Cyclopentadienyl-Lron(Ii) and-Rhodium([) Complexes. *J. Chem. Soc., Chem. Commun*

1992, 964-965.

(30) Komatsuzaki, N.; Uno, M.; Kikuchi, H.; Takahashi, S. Synthesis and Property of Planar-Chiral Cyclopentadienyl-Ruthenium Complexes. *Chem. Lett.* **1996**, No. 8, 677–678.

(31) Erker, G.; Aulbach, M.; Knickmeier, M.; Wingbermühle, D.; Krüger, C.; Nolte, M.; Werner, S. The Role of Torsional Isomers of Planarly Chiral Nonbridged Bis(Indenyl)Metal Type Complexes in Stereoselective Propene Polymerization. *J. Am. Chem. Soc.* **1993**, *115*, 4590–4601.

(32) Mas-Roselló, J.; Herraiz, A. G.; Audic, B.; Laverny, A.; Cramer, N. Chiral Cyclopentadienyl Ligands: Design, Syntheses, and Applications in Asymmetric Catalysis. *Angew. Chem. Int. Ed.* **2021**, *60*, 13198-13224.

(33) Gutnov, A.; Heller, B.; Fischer, C.; Drexler, H. J.; Spannenberg, A.; Sundermann, B.; Sundermann, C. Cobalt(I)-Catalyzed Asymmetric [2+2+2] Cycloaddition of Alkynes and Nitriles: Synthesis of Enantiomerically Enriched Atropoisomers of 2-Arylpyridines. *Angew. Chem. Int. Ed.* **2004**, *43*, 3795–3797.

(34) Heller, B.; Gutnov, A.; Fischer, C.; Drexler, H. J.; Spannenberg, A.; Redkin, D.; Sundermann, C.; Sundermann, B. Phosphorus-Bearing Axially Chiral Biaryls by Catalytic Asymmetric Cross-Cyclotrimerization and a First Application in Asymmetric Hydrosilylation. *Chem. Eur. J.* **2007**, *13*, 1117–1128.

(35) Heller, B.; Hapke, M.; Fischer, C.; Andronova, A.; Starý, I.; Stará, I. G. Chiral Cobalt(I) and Nickel(0) Complexes in the Synthesis of Nonracemic Helicenes through the Enantioselective [2 + 2 + 2] Cyclotrimerisation of Alkynes. *J. Organomet. Chem.* **2013**, *723*, 98–102.

(36) Fischer, F.; Siegle, A. F.; Checinski, M.; Fischer, C.; Kral, K.; Thede, R.; Trapp, O.; Hapke, M. Synthesis of Naphthylpyridines from Unsymmetrical Naphthylheptadiynes and the Configurational Stability of the Biaryl Axis. *J. Org. Chem.* **2016**, *81*, 3087–3102.

(37) Onitsuka, K.; Matsushima, Y.; Takahashi, S. Kinetic Resolution of Allyl Carbonates in

Asymmetric Allylic Alkylation Catalyzed by Planar-Chiral Cyclopentadienyl-Ruthenium Complexes. *Organometallics* **2005**, *24*, 6472–6474.

(38) Onitsuka, K.; Okuda, H.; Sasai, H. Regio- and Enantioselective O-Allylation of Phenol and Alcohol Catalyzed by a Planar-Chiral Cyclopentadienyl Ruthenium Complex. *Angew. Chem. Int. Ed.* **2008**, *47* 1454–1457.

(39) Onitsuka, K.; Kameyama, C.; Sasai, H. Regio- and Enantioselective Allylation of Indole Catalyzed by a Planar-Chiral Cyclopentadienyl–Ruthenium Complex. *Chem. Lett.* **2009**, *38*, 444–445.

(40) Kanbayashi, N.; Onitsuka, K. Ruthenium-Catalyzed Regio- and Enantioselective Allylic Substitution with Water: Direct Synthesis of Chiral Allylic Alcohols. *Angew. Chem. Int. Ed.* **2011**, *50*, 5197–5199.

(41) Kanbayashi, N.; Takenaka, K.; Okamura, T.; Onitsuka, K.; Kanbayashi, N.; Okamura, T.; Onitsuka, K.; Takenaka, K. Asymmetric Auto-Tandem Catalysis with a Planar-Chiral Ruthenium Complex: Sequential Allylic Amidation and Atom-Transfer Radical Cyclization. *Angew. Chem. Int. Ed.* **2013**, *52*, 4897–4901.

(42) Kanbayashi, N.; Okamura, T. A.; Onitsuka, K. New Method for Asymmetric Polymerization: Asymmetric Allylic Substitution Catalyzed by a Planar-Chiral Ruthenium Complex. *Macromolecules* **2014**, *47*, 4178–4185.

(43) Kanbayashi, N.; Hosoda, K.; Kato, M.; Takii, K.; Okamura, T. A.; Onitsuka, K. Enantio- and Diastereoselective Asymmetric Allylic Alkylation Catalyzed by a Planar-Chiral Cyclopentadienyl Ruthenium Complex. *Chem. Commun.* **2015**, *51*, 10895–10898.

(44) Kanbayashi, N.; Yamazawa, A.; Takii, K.; Okamura, T. A.; Onitsuka, K. Planar-Chiral Cyclopentadienyl-Ruthenium-Catalyzed Regio- and Enantioselective Asymmetric Allylic Alkylation of Silyl Enolates under Unusually Mild Conditions. *Adv. Synth. Catal.* **2016**, *358*, 555–560.

(45) Kanbayashi, N.; Hosoda, K.; Okamura, T. A.; Aoshima, S.; Onitsuka, K. Enantio- and

Diastereoselective Polymerization: Asymmetric Allylic Alkylation Catalyzed by a Planar-Chiral Cp′Ru Complex. *Polym. Chem.* **2016**, *7*, 3691–3699.

(46) Kanbayashi, N. Synthetic Approach for Optically Active Polymers through the Combination of Asymmetric Chirogenic Polymerization and Postpolymerization Modification. *Polym. J. 2019 5112* **2019**, *51*, 1235–1247.

Chapter 3. Development of a Convergent Synthetic Route to Improve Access to an Axial and Planar Chiral Indenyl Ligand Scaffold

In this chapter, we will discuss the development of an improved synthetic route to access a class of axial and planar chiral indenes for use as ligands with late transition metals. Through this route, a variety of derivatives can be accessed more rapidly than in similar previously disclosed scaffolds. This work will lay the intellectual and experimental groundwork for the development of a simplified ligand scaffold in the next chapter.

3.1 Introduction to the Baker-Type Ligand Scaffold

3.1.1 Examining the Reactivity Trends of Indenyl *vs.* Cyclopentadienyl Ligands

Most of the transition metal π-complexes discussed in the previous chapters have featured variations on the cyclopentadienyl (Cp) ligand platform.[1] Only with the introduction to planar chiral compounds did we begin to see the introduction of an indene (**3.1**) based platform, the indenyl (Ind) ligand (**3.2**, **Figure 1**).[2,3] On a structural level, the indenyl ligand platform resembles the cyclopentadienyl platform in several ways: the ligand, as has been drawn, is coordinated with an η^5 hapticity to the metal center (**3.3**), is a negatively charged 6 π-electron donor ligand (**3,2**), and is often featured in half-sandwich complexes allowing for the coordination of additional ligands and/or reactive species (**3.3**).[2] From a reactivity perspective, however, notable discrepancies begin to emerge.[4–6]

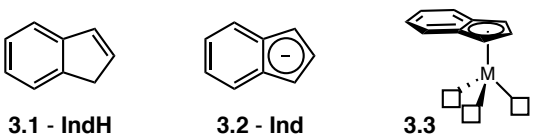

3.1 - IndH 3.2 - Ind 3.3

Figure 3.1: General depiction of indenes and the indenyl ligand platform

The effect on reactivity when switching from a Cp to an Ind ligand was first seen in the study of ligand-induced migratory insertion reactions by Hart-Davis and Mawby in 1969 (**Figure 3.2a**).[4] The relative rate of insertion was an order of magnitude faster when an Ind ligand was

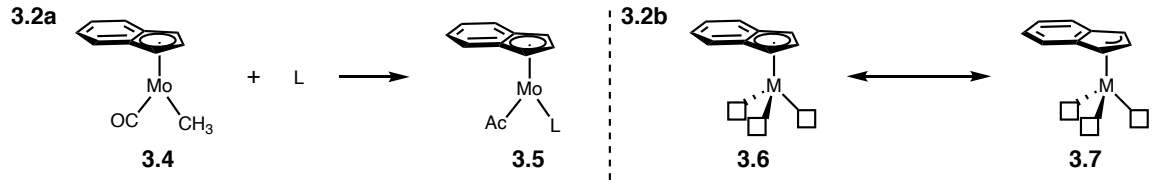

Figure 3.2: Indenyl migratory insertion studies and ring slip mechanistic rationale

used over the more common Cp ligands. The mechanistic rationale for this, which has been further supported throughout more recent studies, is that the Ind ligand can ring slip between an η^5 (**3.6**) and an η^3-like (**3.7**) coordination mode (**Figure 3.2b**).[4–6] One of the primary drivers for this ring slip is the ligands' ability to increase the aromaticity of the 6-membered ring while localizing the allylic moiety for metal coordination.[5] This ring slip alters the total *d*-electron count of the complex and can open a coordination site on the metal center, which is believed to have been the basis for the rate acceleration first observed.[4]

3.1.2 Indene Ring Slip as a Key Facet of Asymmetric Induction

In the context of late transition metal catalyzed asymmetric reactions, Baker and coworkers have been working towards the development of an indenyl rhodium complex that relies largely on asymmetric induction *via* the indenyl effect for enantioinduction.[3,7,8] To achieve this, Baker focused on an allylic functionalization platform for his initial studies, following work from Shibata, Tanaka, and coworkers.[9]

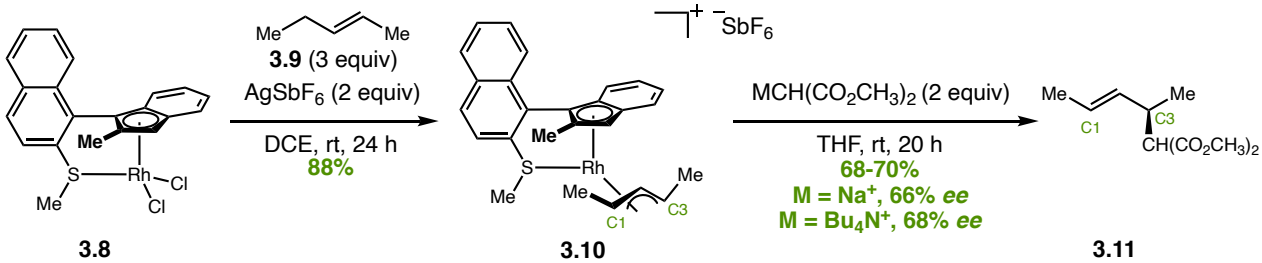

Scheme 3.1: Stoichiometric studies towards enantioselective allylic alkylation

To study the influence of the indenyl effect on this reaction, Baker began by synthesizing rhodium π-allyl complex **3.10** from planar chiral **3.8** (**Scheme 3.1**, the synthesis of which will be discussed further in the next section).[7,8] After isolation, π-allyl complex **3.10** was exposed to malonate nucleophiles with various counter ions and enantioselective allylic alkylation was observed (**3.11**). Mechanistically, this reaction is believed to proceed through the outer-sphere

nucleophilic attack of the malonate to one of the allylic termini. Thus, the enantioselectivity observed is ultimately a result of the regioselectivity between addition to C1 or C3 of **3.10**. To fully ascertain the source of this regioselectivity, computational and spectral analysis of the reaction and key starting materials were conducted.

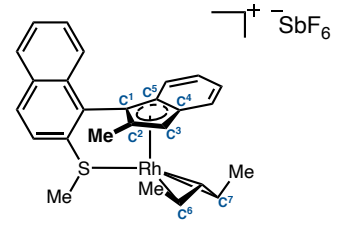

3.12

Figure 3.3: Baker's tethered indenyl π-allyl complex analysis

First, spectral analysis of **3.12** revealed the same sort of distortion previously observed to indicate the partial ring slip of the η^5 indenyl coordination towards an η^3-like conformation (**Figure 3.3**).[7,8] When this ring slip occurs, there is a lengthening of the Rh-C4, and Rh-C5 bonds coordinated to the sites of the benzene moiety within the indene. As a result, there is a shortening of the Rh-C6 bond *trans* to the benzene moiety. Computation analysis of reaction intermediates also reveals a similar trend and further suggests that the site of nucleophilic addition is *syn* to the benzene moiety at the lengthened Rh-C7 termini of the π-allyl fragment.

Overall, the net transformation conducted was the asymmetric allylic alkylation of (*E*)-2-pentene (**3.9** to **3.11**, **Scheme 3.1**). While a catalytic system has yet to be fully realized with the complex studied, the structural and computational work completed provided much insight into the source of asymmetric induction in the reaction.

3.2 Development of a Modular Synthesis Towards a Baker-Type Ligand Scaffold

3.2.1 Analysis of the Previously Disclosed Synthetic Route

Having developed a strong presence in the field of rhodium-catalyzed allylic C–H functionalization, we in the Blakey lab became aware of the work by Baker as we sought to develop an enantioselective platform for our chemistry.[10–16] We endeavored to build on the planar chiral indenyl scaffold and utilize our expertise to develop a catalytic system with this platform. With this goal in mind, we began with an analysis of the previously disclosed synthetic route to access this scaffold to assess the feasibility of modularity in the platform.[7]

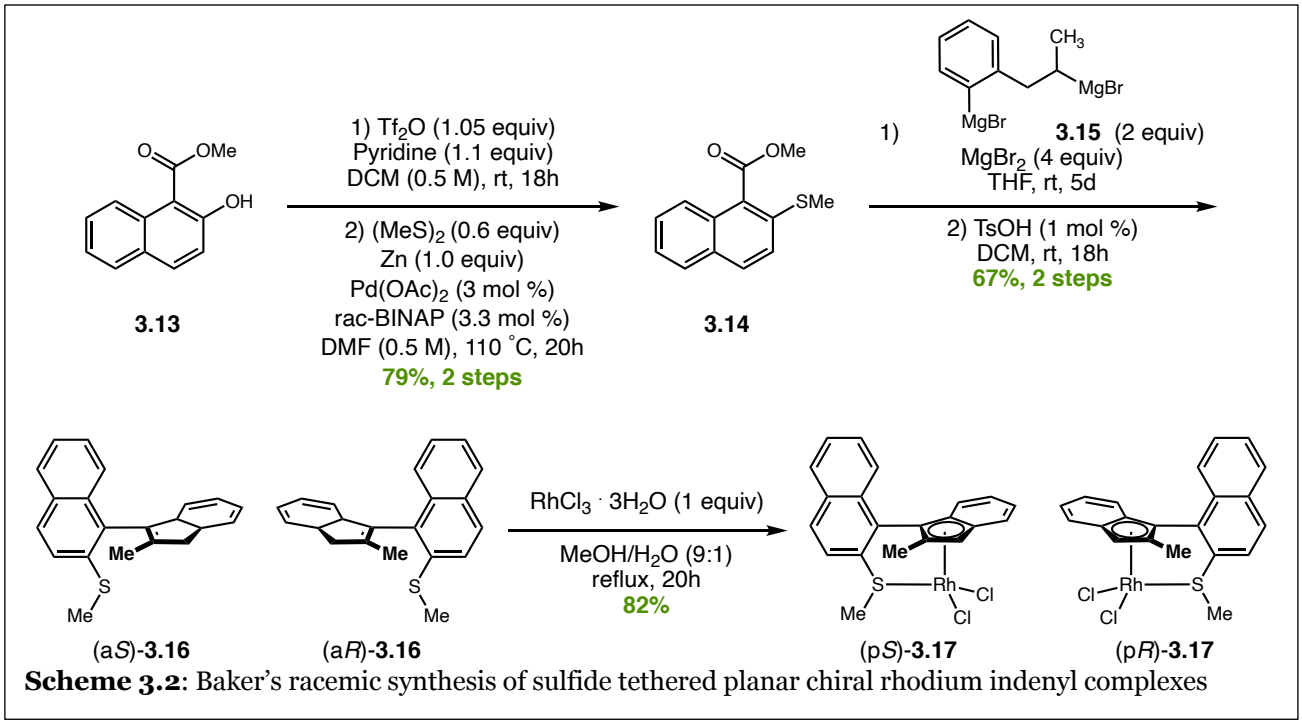

Scheme 3.2: Baker's racemic synthesis of sulfide tethered planar chiral rhodium indenyl complexes

The synthesis began with installation of a thioether to naphthol ester **3.13** in two steps (**3.14**, **Scheme 3.2**).[7] From here, di-Grignard addition of designer reagent **3.15** to ester **3.14** followed by elimination of the resultant alcohol furnished naphthylindene **3.16** as a racemic mixture of two planar chiral enantiomers. Direct metalation with a rhodium precursor afforded racemic **3.17** in good yield. Complexation of rhodium at this step served to detail how the presence of the sulfur tether directs facial selectivity during the metalation step.

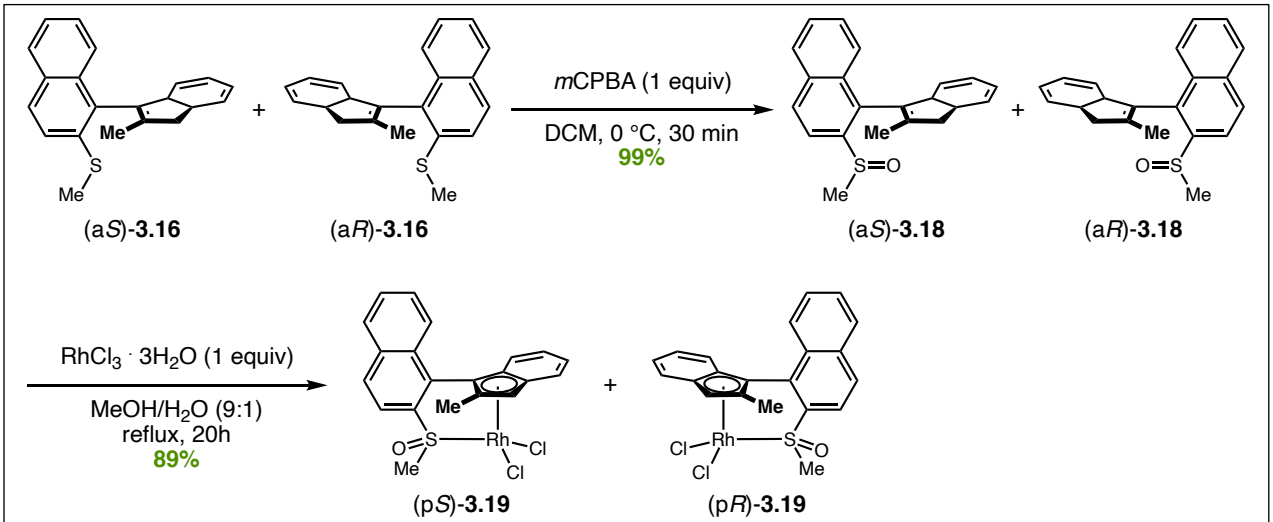

Scheme 3.3: Racemic oxidation to access sulfoxide-tethered rhodium complexes

To selectively synthesize and isolate single enantiomers of rhodium complexes, a further elaborated sulfoxide structure **3.19** was targeted (**Scheme 3.3**).[7] Racemic **3.16** can be oxidized with *meta*-chloroperbenzoic acid (*m*CPBA) prior to metalation with rhodium to afford compelexes **3.18** as mixtures of enantiomers. Access to the enantioenriched ligands **3.18** required a series of enantioselective Kagan oxidations and recrystallizations prior to metal complexation

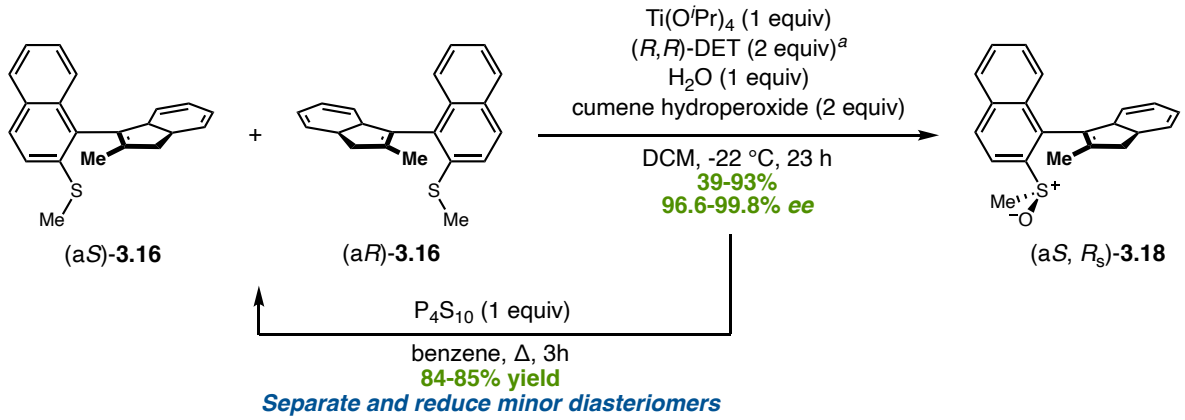

[a](*R*,*R*)-DET or (*S*,*S*)-DET used during oxidation of recovered diastereomer to access the opposite ligand

Scheme 3.4: Stereoselective synthesis of enantioenriched ligands

(**Scheme 3.4**). The recovered, undesired diastereomers from each oxidation were reduced back to the sulfide and purified prior to enantioselective oxidation with the opposite chiral ligand.

This synthetic route successfully afforded access to each individual diastereomer of both sulfide bearing **3.17** and sulfoxide bearing **3.19**.[7] However, we identified several key limitations when attempting to develop this platform for a catalytic system that may require diversification of the ligand structure. First, the linear nature of the synthetic route dictates that any modulation of the naphthyl backbone to change steric or electronic properties would require *de novo* ligand synthesis. Next, the construction of the indene fragment is limited by the di-Grignard chemistry utilized.[17] The reaction in and of itself takes five days to reach completion and any change to the periphery of the indene must be tolerant of these reaction conditions. Finally, with no internal stereo-directing elements until the enantioselective oxidation sequence, the multi-step method required to access completed complexes from racemic **3.16** is limiting and requires effective reactivity and handling of precious late-stage materials.

3.2.2 New Modular Synthetic Route Development

To address these limitations and build a modular synthetic route that would improve access to derivatization within this ligand framework, my original project in the group was formed. In the development of this revised route, we first identified that the primary disconnection would be to build the indene-naphthyl cross-link as the final step of the synthesis (**3.20**, **Scheme 3.5**). This would split the molecule into two fragments (**3.21**, and **3.22**) that would, ideally, be of similar complexity in their synthesis. Using an atroposelective cross-coupling reaction in the presence of a chiral sulfoxide on one of the coupling partners, a level of diastereocontrol can be exerted on this final step, allowing for a more simplified separation of enantioenriched ligands prior to metalation.[18] The sulfoxide-bearing fragment **3.21** was chosen as the electrophilic coupling partner as the electron-withdrawing nature of the sulfoxide could aid in oxidative addition to this fragment. In turn, the indenyl fragment **3.22** was chosen as the nucleophilic coupling partner.

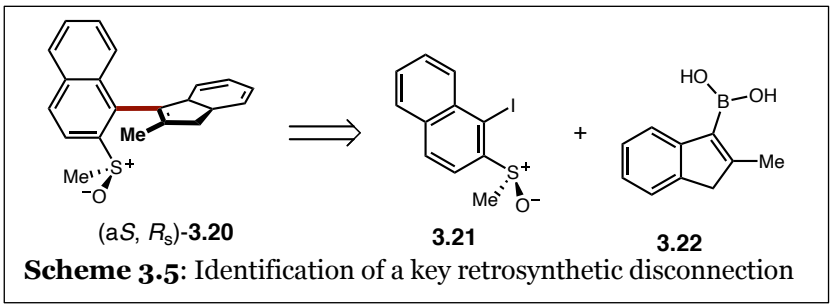

Scheme 3.5: Identification of a key retrosynthetic disconnection

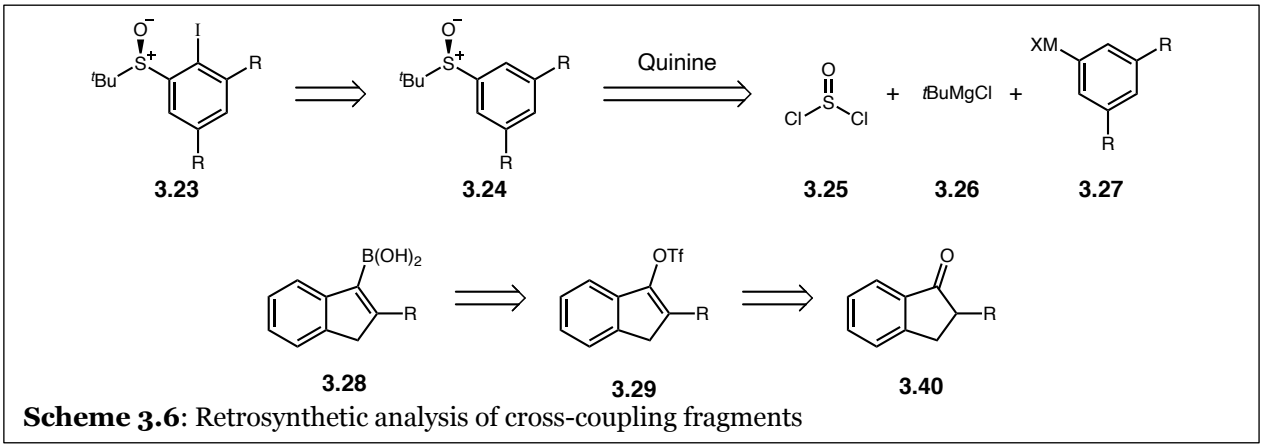

Scheme 3.6: Retrosynthetic analysis of cross-coupling fragments

Further retrosynthetic analysis of the coupling partners led to a redesign of the sulfoxide fragment (**3.23**, **Scheme 3.6**). Aryl iodide **3.23** can be synthesized through a sulfoxide-directed *ortho* lithiation/iodination sequence of **3.24**.[18,19] Here, simplification of the naphthyl aryl group

of **3.21** to a symmetrical 3,5-dialkyl aryl group was chosen to eliminate any potential regioselectivity issues that may arise during this step. Additionally, the second, non-tethered aryl ring of the naphthyl moiety largely serves as a steric block to hinder rotation of the indene.[7] Maintaining a substituent *ortho* to the indenyl fragment in the final ligand accomplishes this same goal. Simplification of the aryl backbone also improves access to aryl-alkyl sulfoxide **3.24**, which could be built stereoselectively through the quinine-mediated addition of two Grignard reagents to thionyl chloride (**3.25**).[20] Access to indenyl boron fragment **3.28** was identified as arising from borylation of indene triflate **3.29**.[21,22] Finally, the triflate could be synthesized from enolizing and trapping an indanone similar to **3.30**.[22]

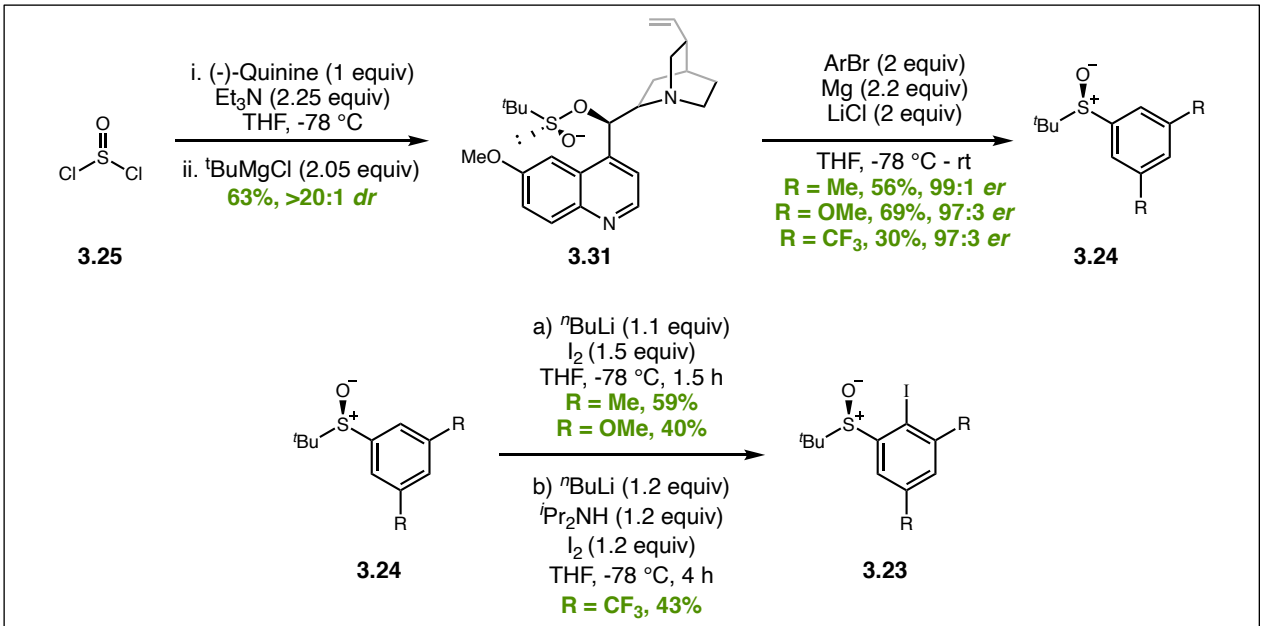

Scheme 3.7: Forward synthesis to access aryl iodide coupling partners

With a full synthetic plan in hand, forward synthesis of the ligand was underway (**Scheme 3.7**). Construction of the aryl iodide coupling partner **3.23**, as described, began with the stereoselective synthesis of sulfinate **3.24**.[20] The first step in this sequence is to add quinine to thionyl chloride followed by the addition of *tert*-butyl Grignard. Quinine-adduct **3.31** was synthesized with excellent diastereoselectivity, and the diastereomers formed can be separated by normal phase flash chromatography on silica. From this common intermediate, Grignard addition of 3,5-difunctionalized aryl groups allowed for the construction of several aryl-alkyl sulfoxides

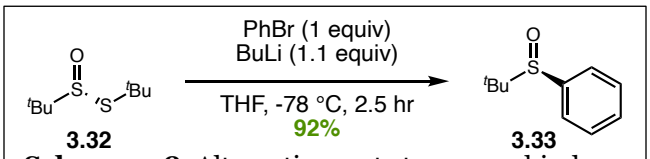

Scheme 3.8: Alternative route to access chiral aryl-alkyl sulfoxides

3.24.[20] While similar chemistry has been disclosed starting from **3.32**, these chiral compounds require special handling considerations and are prone to stereochemical erosion under ambient conditions (**Scheme 3.8**).[23–25] Quinine-adduct **3.21**, however, is conformationally bench stable and available from much more cost-effective starting materials. Lastly, the iodine can be installed to **3.24** through the sulfoxide-directed *ortho* lithiation sequence to complete the synthesis of coupling partner **3.23**.[18,19] Some tuning of the lithium base was required in this final step depending on the identity of the R groups *meta* to the sulfoxide.

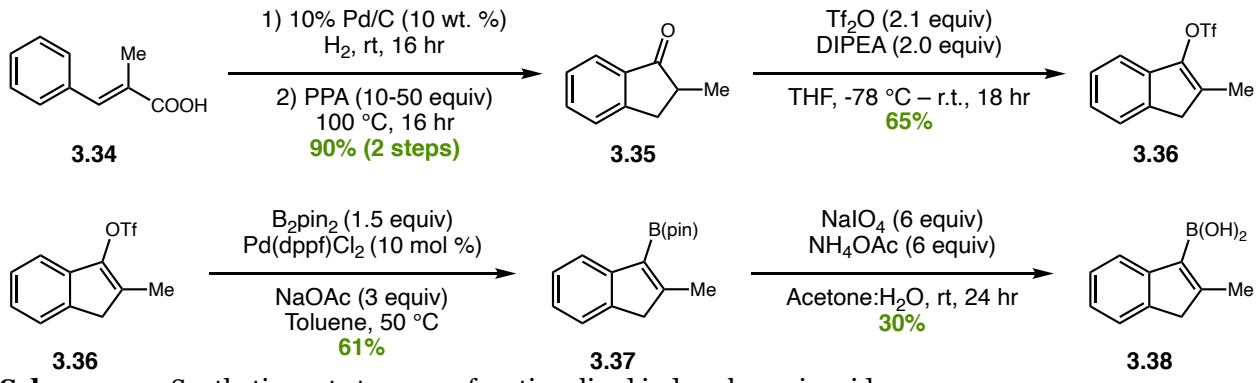

Scheme 3.9: Synthetic route to access functionalized indene boronic acids

While an unfunctionalized indenyl boronic acid was commercially available, 2-methylindenyl boronic acid (**3.38**) synthesis began from *alpha*-methylcinnamic acid **3.34** (**Scheme 3.9**). Hydrogenation of the olefin followed by polyphosphoric acid-mediated cyclization afforded indanone **3.35** in excellent yields with no purification beyond simple reaction work-up required.[26,27] Formation of indene triflate **3.36** required some optimization.[22] Initial attempts using a hard base (sodium hydride or BuLi) with a milder triflating reagent (phenyl triflimide or Comin's reagent) were successful at providing the indene triflate, but always in low yields.[28,29] Mechanistically, the rapid formation of a lithium or sodium enolate formed in the presence of a relatively acidic benzylic proton could allow the intermediate to react with another molecule of the indene triflate and, ultimately, return starting material. Therefore, switching to a harsher

triflating reagent (triflic anhydride) and an amine base (Hunig's base) allowed for isolation of the triflate product in more synthetically useful yields.[22] Palladium catalyzed borylation of triflate **3.36** with bis(pinacolato)diboron installed the boronic ester (**3.37**) which could then be cleaved under oxidative conditions to afford the boronic acid coupling partner **3.38**.[21,22,30]

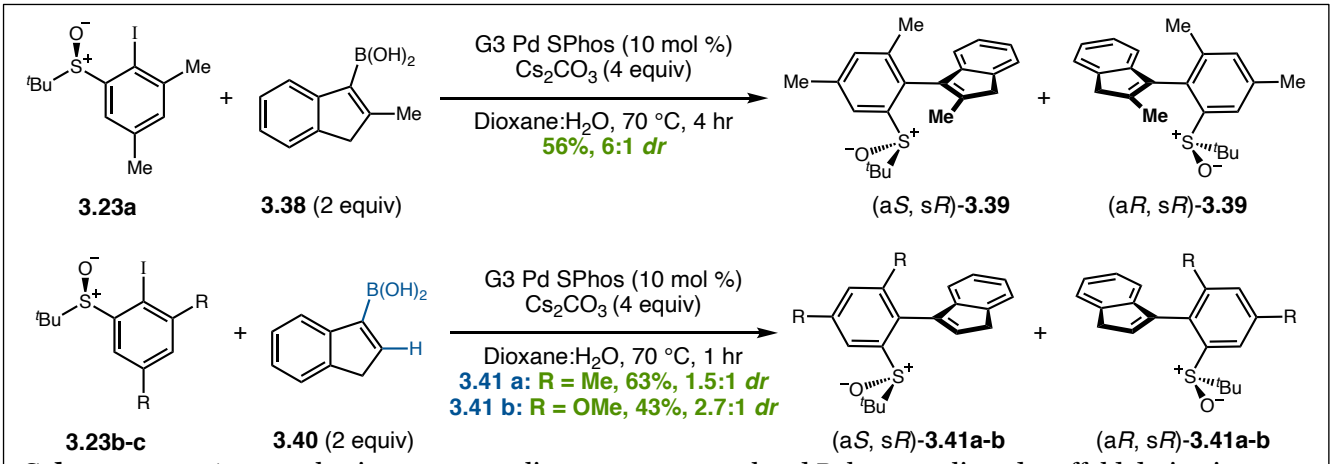

Scheme 3.10: Atroposelective cross-coupling to access completed Baker-type ligand scaffold derivatives

Having successfully synthesized both the electrophilic aryl iodide coupling partner **3.23** and the nucleophilic indene boronic acid coupling partner **3.38**, attention was turned to the atroposelective cross-coupling. Following conditions like those reported by Colobert for chiral sulfoxide directed atroposelective aryl-aryl cross-coupling reactions, several aryl iodides were successfully coupled with indene boronic acids to form completed ligands **3.39** and **3.41a-b**, albeit with modest selectivity.[18] The increased steric bulk of the 2-methyl in **3.38** helped to improve the selectivity in the cross-coupling over the less hindered, commercially available indene boronic acid **3.40**.

3.3 Conclusion

Through the development and completion of this work, we have successfully identified a modular and convergent synthetic route to allow improved access to a variety of analogues within this Baker-type axial and planar chiral ligand framework. The use of a quinine-mediated stereoselective sulfoxide synthesis allows for early and highly enantioselective installation of a chiral sulfoxide from a common intermediate to allow for diversification. Having installed a chiral

sulfur in the molecule, the atroposelective cross coupling affords diastereomeric mixtures of products that can be separated more simply than enantiomeric mixtures. Several ligands have successfully been synthesized using this route, and ongoing work is being conducted by Ethan Heyboer, currently a second-year graduate student in the Blakey lab, to address the synthesis of additional derivatives, complex the completed ligand frameworks onto group IX metals, and begin to assess the potential catalytic activity of these complexes. Additionally, preliminary model studies conducted during the completion of this work led to the identification of a simplified ligand system capable of effecting enantioselective catalysis.[27] Those results will be the focus of the upcoming chapter.

3.4 References

(1) Mas-Roselló, J.; Herraiz, A. G.; Audic, B.; Laverny, A.; Cramer, N. Chiral Cyclopentadienyl Ligands: Design, Syntheses, and Applications in Asymmetric Catalysis. *Angew. Chem. Int.l Ed.* **2021**, *60*, 13198-13224.

(2) Trost, B. M.; Ryan, M. C. Indenylmetal Catalysis in Organic Synthesis. *Angew. Chem. Int. Ed.* **2017**, *56*, 2862–2879.

(3) Kharitonov, V. B.; Muratov, D. V.; Loginov, D. A. Indenyl Complexes of Group 9 Metals: Synthetic and Catalytic Chemistry. *Coord. Chem. Rev.* **2019**, *399*, 213027.

(4) Hart-Davis, A. J.; Mawby, R. J. Reactions of π-Indenyl Complexes of Transition Metals. Part I. Kinetics and Mechanisms of Reactions of Tricarbonyl-π-Indenylmethylmolybdenum with Phosphorus(III) Ligands. *J. Chem. Soc. A Inorganic, Phys. Theor.* **1969**, No. 0, 2403–2407.

(5) Westcott, S. A.; Kakkar, A. K.; Stringer, G.; Taylor, N. J.; Marder, T. B. Flexible Coordination of Indenyl Ligands in Sandwich Complexes of Transition Metals. Molecular Structures of [(η-C9R7)2M] (M = Fe, R = H, Me; M = Co, Ni, R = H): Direct Measurement of the Degree of Slip-Fold Distortion as a Function of d-Electron Count. *J. Organomet. Chem.* **1990**, *394*, 777–794.

(6) Marder, T. B.; Calabrese, J. C.; Roe, D. C.; Tulip, T. H. The Slip-Fold Distortion of η-Bound Indenyl Ligands. Dynamic NMR and X-Ray Crystallographic Studies of (η-Indenyl)RhL2 Complexes. *Organometallics* **1987**, *6*, 2012–2014.

(7) Baker, R. W.; Radzey, H.; Lucas, N. T.; Turner, P. Stereospecific Syntheses and Structures of Planar Chiral Bidentate H5:KS-Indenyl-Sulfanyl and -Sulfinyl Complexes of Rhodium(III). *Organometallics* **2012**, *31*, 5622–5633.

(8) Baker, R. W. Asymmetric Induction via the Structural Indenyl Effect. *Organometallics* **2018**, *37*, 433-440.

(9) Shibata, Y.; Kudo, E.; Sugiyama, H.; Uekusa, H.; Tanaka, K. Facile Generation and

Isolation of Pi-Allyl Complexes from Aliphatic Alkenes and an Electron-Deficient Rh(III) Complex: Key Intermediates of Allylic C-H Functionalization. *Organometallics* **2016**, *35*, 1547–1552.

(10) Burman, J. S.; Blakey, S. B. Regioselective Intermolecular Allylic C–H Amination of Disubstituted Olefins via Rhodium/π-Allyl Intermediates. *Angew. Che.e Int. Ed.* **2017**, *56*, 13666–13669.

(11) Nelson, T.; Blakey, S. B. Intermolecular Allylic C–H Etherification of Internal Olefins. *Angew. Chem. Int. Ed.* **2018**, *57*, 14911-14915.

(12) Harris, R. J.; Park, J.; Nelson, T. A. F.; Iqbal, N.; Salgueiro, D. C.; Bacsa, J.; Macbeth, C. E.; Baik, M. H.; Blakey, S. B. The Mechanism of Rhodium-Catalyzed Allylic C-H Amination. *J. Am. Chem. Soc.* **2020**, *142*, 5842–5851.

(13) Burman, J. S.; Harris, R. J.; Farr, C. M. B.; Bacsa, J.; Blakey, S. B. Rh(III) and Ir(III)Cp* Complexes Provide Complementary Regioselectivity Profiles in Intermolecular Allylic C–H Amidation Reactions. *ACS Catal.* **2019**, *9*, 5474-5479.

(14) Kazerouni, A. M.; McKoy, Q. A.; Blakey, S. B. Recent Advances in Oxidative Allylic C–H Functionalization via Group IX-Metal Catalysis. *Chem. Commun.* **2020**, *56*, 13287–13300.

(15) Nelson, T. A. F.; Hollerbach, M. R.; Blakey, S. B. Allylic C–H Functionalization via Group 9 π-Allyl Intermediates. *Dalton Trans.* **2020**, *49*, 13928–13935.

(16) Kazerouni, A. M.; Nelson, T. A. F.; Chen, S. W.; Sharp, K. R.; Blakey, S. B. Regioselective Cp*Ir(III)-Catalyzed Allylic C-H Sulfamidation of Allylbenzene Derivatives. *J. Org. Chem.* **2019**, *84*, 13179–13185.

(17) Baker, R. W.; Foulkes, M. A.; Griggs, M.; Nguyen, B. N. A New Synthesis of 3-Substituted-1H-Indenes through Reaction of o-(Beta-Magnesioalkyl)Phenylmagnesium Dihalides with Carboxylate Esters. *Tetrahedron Lett.* **2002**, *43*, 9319–9322.

(18) Colobert, F.; Valdivia, V.; Choppin, S.; Leroux, F. R.; Fernández, I.; Álvarez, E.; Khiar, N.

Axial Chirality Control During Suzuki–Miyaura Cross-Coupling Reactions: The Tert-Butylsulfinyl Group as an Efficient Chiral Auxiliary. *Org. Lett.* **2009**, *11*, 5130–5133.

(19) Wesch, T.; Leroux, F. R.; Colobert, F. Atropodiastereoselective C-H Olefination of Biphenyl p-Tolyl Sulfoxides with Acrylates. *Adv. Synth. Catal.* **2013**, *355*, 2139–2144.

(20) Lu, B. Z.; Jin, F.; Zhang, Y.; Wu, X.; Wald, S. A.; Senanayake, C. H. New General Sulfinylating Process for Asymmetric Synthesis of Enantiopure Sulfinates and Sulfoxides. *Org. Lett.* **2005**, *7*, 1465–1468.

(21) Bifu, T; Biju, P.; Blizzard, T. A.; Chen, Z.; Clements, M. J.; Cui, M.; Frie, J. L.; Hagmann, W. K.; Hu, B.; Josien, H.; Nair, A. G.; Plummer, C. W.; Zhu, C. Adiabatetic Tricyclic Compounds. WO 2015/176640 A1, November 26, 2015.

(22) Witzig, R. M.; Fäseke, V. C.; Häussinger, D.; Sparr, C. Atroposelective Synthesis of Tetra-Ortho-Substituted Biaryls by Catalyst-Controlled Non-Canonical Polyketide Cyclizations. *Nat. Catal.* **2019**, *2*, 925–930.

(23) Wojaczyńska, E.; Wojaczyński, J. Modern Stereoselective Synthesis of Chiral Sulfinyl Compounds. *Chem. Rev.* **2020**, *120*, 4578-4611.

(24) Weix, D. J.; Ellman, J. A. Improved Synthesis of Tert-Butanesulfinamide Suitable for Large-Scale Production. *Org. Lett.* **2003**, *5*, 1317–1320.

(25) Wang, P.; Chen, J.; Cun, L.; Deng, J.; Zhu, J.; Liao, J. Aryl Tert-Butyl Sulfoxide-Promoted Highly Enantioselective Addition of Allyltrichlorosilane to Aldehydes. *Org. Biomol. Chem.* **2009**, *7*, 3741–3747.

(26) Monguchi, Y.; Fujita, Y.; Hashimoto, S.; Ina, M.; Takahashi, T.; Ito, R.; Nozaki, K.; Maegawa, T.; Sajiki, H. Palladium on Carbon-Catalyzed Solvent-Free and Solid-Phase Hydrogenation and Suzuki–Miyaura Reaction. *Tetrahedron* **2011**, *67*, 8628–8634.

(27) Farr, C. M. B.; Kazerouni, A. M.; Park, B.; Poff, C. D.; Won, J.; Sharp, K. R.; Baik, M. H.; Blakey, S. B. Designing a Planar Chiral Rhodium Indenyl Catalyst for Regio- And Enantioselective Allylic C-H Amidation. *J. Am. Chem. Soc.* **2020**, *142*, 13996–14004.

(28) Hu, J. T.; Zheng, B.; Chen, Y. C.; Xiao, Q. Expedient Synthesis of 9,10-Phenanthrenes via LiOPiv-Promoted and Palladium-Catalysed Aryne Annulation by Vinyl Triflates. *Org. Chem. Front.* **2018**, *5*, 2045–2050.

(29) Wu, D. P.; He, Q.; Chen, D. H.; Ye, J. L.; Huang, P. Q. A Stepwise Annulation for the Transformation of Cyclic Ketones to Fused 6 and 7-Membered Cyclic Enimines and Enones. *Chinese J. Chem.* **2019**, *37*, 315–322.

(30) Feng, Z.; Min, Q. Q.; Xiao, Y. L.; Zhang, B.; Zhang, X. Palladium-Catalyzed Difluoroalkylation of Aryl Boronic Acids: A New Method for the Synthesis of Aryldifluoromethylated Phosphonates and Carboxylic Acid Derivatives. *Angew. Chem. Int. Ed.* **2014**, *53*, 1669–1673.

3.5 Supporting Information

3.5.1 General Information

All reactions were carried out under nitrogen atmosphere with anhydrous solvents in oven- or flame-dried glassware using standard Schlenk technique, unless otherwise stated. Anhydrous dichloromethane (DCM), diethyl ether (Et2O), tetrahydrofuran (THF), and toluene were obtained by passage through activated alumina using a Glass Contours solvent purification system. Solvents for workup, extraction, and column chromatography were used as received from commercial suppliers without further purification. All other chemicals were purchased from Millipore Sigma, Strem Chemicals, Oakwood Chemicals, Alfa Aesar, or Combi-Blocks and used as received without further purification, unless otherwise stated.

^{1}H and 13C nuclear magnetic resonance (NMR) spectra were recorded on a Varian Inova 600 spectrometer (600 MHz 1 H, 151 MHz 13C), a Bruker 600 spectrometer (600 MHz 1 H, 151 MHz 13C), a Varian Inova 500 spectrometer (500 MHz 1 H, 126 MHz 13C), and a Bruker 400 spectrometer (400 MHz 1 H, 126 MHz 13C) at room temperature in CDCl3 (dried over activated molecular sieves) with internal CHCl3 as the reference (7.26 ppm for 1 H, 77.16 ppm for 13C), unless otherwise stated. Chemical shifts (δ values) were reported in parts per million (ppm) and coupling constants (J values) in Hz. Multiplicity was indicated using the following abbreviations: s = singlet, d = doublet, t = triplet, q = quartet, qn = quintet, m = multiplet, br = broad. High resolution mass spectra (HRMS) were obtained using a Thermo Electron Corporation Finigan LTQFTMS (at the Mass Spectrometry Facility, Emory University). High Pressure Liquid Chromatography (HPLC) was performed on an Agilent 1100 series HPLC utilizing CHIRALPAK AD-H, AS-H, OD-H and OJ-H 4.6 x 150 mm analytical columns. Analytical thin layer chromatography (TLC) was performed on precoated glass-backed Silicycle SiliaPure® 0.25 mm silica gel 60 plates and visualized with UV light, ethanolic p-anisaldehyde, ethanolic bromocresol green, or aqueous potassium permanganate (KMnO4). Flash column chromatography was performed using Silicycle SiliaFlash® F60 silica gel (40- 63 μm) on a Biotage Isolera One system.

Preparatory TLC was performed on precoated glass-backed Silicycle SiliaPure® 1.0 mm silica gel 60 plates. We acknowledge the use of shared instrumentation provided by grants from the NIH and the NSF.

3.5.2 Experimental Section

3.5.2.1 General Procedures

General Procedure 1 (Synthesis of chiral *tert*-butyl-arylsulfinates): To a 7 mL oven-dried vial equipped with a vial, added Mg (2.2 equiv) and LiCl (1.0 equiv). The vial was then sealed, the atmosphere exchanged with N_2, and THF (1.5 mL) was added with vigorous stirring. To a flame dried 20 mL scintillation vial, added ArBr (2.0 equiv) before sealing, exchanging the atmosphere with nitrogen, and dissolving in THF (3.5 equiv). Slowly added ArBr solution to the vial containing Mg and LiCl and allowed to stir vigorously at room temperature for 30 minutes. To an oven-dried 15 mL vial equipped with a stir bar, added quinine-*R*-*tert*-butylsulfinate[1] (1.0 equiv), sealed, exchanged the atmosphere with nitrogen, and dissolved in THF (5.0 mL). Cooled to -78 °C in a dry ice/acetone bath before the slow addition of the freshly prepared ArMgBr solution. Upon complete addition of the Grignard reagent, removed the ice bath and allowed to warm to room temp while stirring under N_2. After 24 hours, quenched with a saturated solution of NH_4Cl (1.0 mL). Transferred to a separatory funnel with DI H_2O (10 mL) and EtOAc (10 mL). Separated layers and extracted the aqueous layer with EtOAc (2 x 15 mL). Combined organic layers were dried with Na_2SO_4, filtered, and concentrated *in vacuo*. Purified on silica afforded *(R)*-*tert*-butyl-arylsulfinates **3.24**.

General Procedure 2 (Synthesis of racemic *tert*-butyl-arylsulfinates): To a 7 mL oven-dried vial equipped with a stir, added ArBr (3.0 equiv). The vial was then sealed, the atmosphere exchanged with N_2, and the ArBr dissolved in THF (2.0 mL) before cooling to -78 °C in a dry ice/acetone bath. *n*BuLi was added (3.05 equiv) and the reaction continued to stir at -78 °C for 30

minutes. To a separate oven-dried 15 mL vial equipped with a stir bar was added *tert*-butylthiosulfinate ***rac*-3.32**[2] (1.0 equiv). The vial was sealed, the atmosphere exchanged with N_2, and the *tert*-butylthiosulfinate dissolved in THF (6.0 mL) before cooling to -78 °C in a dry ice/acetone bath. The freshly prepared ArLi solution was then added to the 15 mL reaction vial and the reaction allowed to stir for 1 hour at -78 °C under N_2. After complete conversion, as determined by TLC, the reaction was quenched with saturated NH_4Cl (1.0 mL). The reaction was then poured into a separatory funnel and excess DI H_2O (~10 mL) and EtOAc (~10 mL) were used to transfer all the contents of the vial to the separatory funnel. The layers were separated, and the aqueous layer extracted with EtOAc (2x20 mL). The combined organic layers were dried over Na_2SO_4, filtered, concentrated *in vacuo*, and purified on silica to afford *rac*-*tert*-butyl-arylsulfinates ***rac*-3.24**.

General Procedure 3a (*Ortho*-iodination of *tert*-butyl-arylsulfinates): To a 4 mL oven-dried reaction vial equipped with a stir bar under a N_2 atmosphere, added THF (0.75 mL). Cooled to -78 °C in a dry ice/acetone bath before the addition of *n*-BuLi (1.1 equiv). Dissolved *tert*-butyl-arylsulfinate (1.0 equiv) in THF (0.75 mL) and added the solution to the cooled BuLi solution. The reaction was allowed to stir at -78 °C for 1 hour. In a separate vial, I_2 (1.5 equiv) was dissolved in THF (1.0 mL). The ice bath was removed from the reaction vial and the I_2 solution added quickly. The reaction warmed to room temperature and continued to stir for 2 hours. The reaction was diluted with $Na_2S_2O_3$ (1.0 mL) and transferred to a separatory funnel. The layers were separated, and the aqueous layer extracted with Et_2O (15 mL). The combined organic layers were washed with brine (20 mL), dried over Na_2SO_4, filtered, and concentrated *in vacuo*. Purification on silica afforded the *ortho*-iodinated *tert*-butyl-arylsulfinate coupling partner **3.23**.

General Procedure 3b (*Ortho*-iodination of *tert*-butyl-arylsulfinates): To a 4 mL oven-dried reaction vial equipped with a stir bar under a N_2 atmosphere, added THF (0.75 mL) and

*i*PrNH (1.2 equiv). Cooled to -78 °C in a dry ice/acetone bath before the addition of *n*-BuLi (1.2 equiv). After 30 minutes, dissolved *tert*-butyl-arylsulfinate (1.0 equiv) in THF (0.75 mL) and added the solution to the cooled LDA solution. The reaction was allowed to stir at -78 °C for 2 hours. In a separate vial, I_2 (1.2 equiv) was dissolved in THF (1.0 mL). The ice bath was removed from the reaction vial and the I_2 solution added quickly. The reaction warmed to room temperature and continued to stir for 10 minutes. The reaction was diluted with $Na_2S_2O_3$ (1.0 mL) and transferred to a separatory funnel. The layers were separated, and the aqueous layer extracted with Et_2O (15 mL). The combined organic layers were washed with brine (20 mL), dried over Na_2SO_4, filtered, and concentrated *in vacuo*. Purification on silica afforded the *ortho*-iodinated *tert*-butyl-arylsulfinate coupling partner **3.23**.

General Procedure 4 (Atroposelective cross-coupling): To a 4 mL oven-dried reaction vial equipped with a stir bar in a N_2-filled glove box, added SPhos Pd G3 (10 mol %), Cs_2CO_3 (4.0 equiv), and indene boronic acid coupling partner (2.0 equiv), sealed, and removed from the glove box. Dissolved aryl iodide (1.0 equiv) in 1,4-dioxane (1 mL, 0.1 M) and added the solution to the reaction vial followed by DI H_2O (0.5 mL). Placed the reaction vial into a pre-heated 70 °C heating block and allowed to stir under a positive pressure of N_2 until reaction was complete by TLC. Upon complete conversion of starting material, quenched with excess DI H_2O. Transferred the reaction to a separatory funnel, extracted the aqueous layer with EtOAc (3 x 10 mL). Dried the combined organic layers over Na_2SO_4, filtered off the drying agent, and concentrated *in vacuo*. Purification on silica afforded the completed axial and planar chiral indene ligands **3.39** or **3.41**.

3.5.2.2 Tabulated Data for Compounds

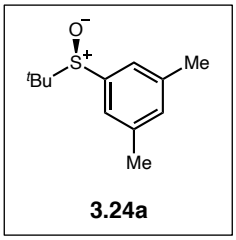

3.24a

(R)-1-(tert-butylsulfinyl)-3,5-dimethylbenzene (**3.24a**) – Prepared according to **General Procedure 1** from Mg (0.0535 mg, 2.20 mmol), LiCl (0.0848 g, 2.00 mmol), 1-bromo-3,5-dimethylbenzene (0.3701 g, 2.00 mmol), and **3.31** (0.4286 g, 1.00 mmol). Purification by flash chromatography on silica (15% EtOAc in hexane) afforded **3.24a** (0.1180 g, 56% yield, 99:1 *er*) as a white solid. **^{1}H NMR** ($CDCl_3$, 400 MHz) δ 7.18 – 7.17 (m, 2H), 7.11 – 7.09 (m, 1H), 2.37 (d, *J* = 0.7 Hz, 6H), 1.17 (s, 9H). **^{13}C NMR** ($CDCl_3$ 101 MHz) δ 139.82, 138.32, 133.01, 123.97, 55.67, 23.01, 21.46. **HRMS** (+APCI) calculated for $C_{12}H_{19}OS$ $[M+H]^+$ 211.1151, found 211.1152. **HPLC** (AS-H column, 10% 2-propanol in hexanes, 1 mL/min) t_M = 14.8 min, t_m = 6.9 min, 99:1 e.r.

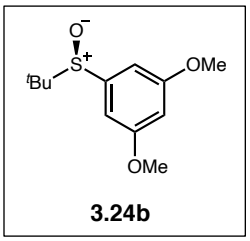

3.24b

(R)-1-(tert-butylsulfinyl)-3,5-dimethoxybenzene (**3.24b**) – Prepared according to **General Procedure 1** from Mg (0.0535 mg, 2.20 mmol), LiCl (0.0848 g, 2.00 mmol), 1-bromo-3,5-dimethoxybenzene (0.4341 g, 2.00 mmol), and **3.31** (0.4286 g, 1.00 mmol). Purification by flash chromatography on silica (35% EtOAc in hexane) afforded **3.24b** (0.1681 g, 69% yield, 97:3 *er*) as a white solid. **^{1}H NMR** ($CDCl_3$, 400 MHz) δ 6.72 (d, *J* = 2.3 Hz, 2H), 6.54 (t, *J* = 2.3 Hz, 1H), 3.82 (s, 6H), 1.19 (s, 9H). **^{13}C NMR** ($CDCl_3$ 101 MHz) δ 160.74, 142.47, 104.01, 103.55, 56.23, 55.80, 23.11. **HRMS** (+APCI) calculated for $C_{12}H_{19}O_3S$ $[M+H]^+$ 243.1049, found 243.1051. **HPLC** (OD-H column, 20% 2-propanol in hexanes, 1 mL/min) t_M = 7.6 min, t_m = 5.4 min, 98:2 e.r.

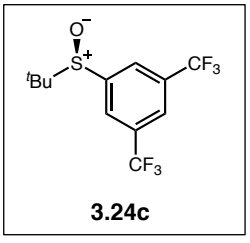

3.24c

(R)-1-(tert-butylsulfinyl)-3,5-bis(trifluoromethyl)benzene (**3.24c**) – Prepared according to **General Procedure 1** from Mg (0.0919 mg, 3.78 mmol), LiCl (0.1457 g, 3.44 mmol), 1-bromo-3,5-bis(trifluoromethyl)benzene (1.007 g, 3.44 mmol), and **3.31** (0.7367 g, 1.72 mmol). Purification by flash chromatography on silica (10% EtOAc in hexane) afforded **3.24c**

(0.1618 g, 30% yield, 97:3 *er*) as a yellow oil. **^{1}H NMR** ($CDCl_3$, 400 MHz) δ 8.06 – 8.03 (m, 2H), 8.02 – 8.00 (m, 1H), 1.20 (s, 9H). **^{13}C NMR** ($CDCl_3$ 101 MHz) δ 144.16, 132.26 (q, J = 34.2 Hz), 126.63, 124.25, 121.53, 57.154, 22.78. **HRMS** (+APCI) calculated for $C_{12}H_{13}OF_6S$ $[M+H]^+$ 319.0586, found 319.0586. **HPLC** (AS-H column, 5% 2-propanol in hexanes, 1 mL/min) t_M = 8.0 min, t_m = 5.2 min, 97:3 e.r.

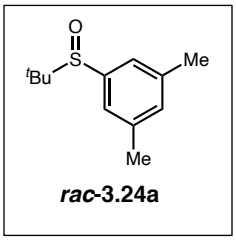

***rac*-3.24a**

1-(tert-butylsulfinyl)-3,5-dimethylbenzene (***rac*-3.24a**) – Prepared according to **General Procedure 2** from 1-bromo-3,5-dimethylbenzene (0.5552 g, 3.00 mmol), BuLi (0.1954 g, 1.22 mL, 2.5 M, 3.05 mmol), and ***rac*-3.32** (0.1944 g, 1.00 mmol). Purification by flash chromatography on silica (15% EtOAc in hexanes) afforded ***rac*-3.24a** (0.1293 g, 61% yield) as an off-white solid. **^{1}H NMR** (CDCl3, 400 MHz) δ 7.18 – 7.17 (m, 2H), 7.11 – 7.09 (m, 1H), 2.37 (d, J = 0.7 Hz, 6H), 1.17 (s, 9H). **HPLC** (AS-H column, 10% 2-propanol in hexanes, 1 mL/min) t_1 = 7.0 min, t_2 = 15.5 min.

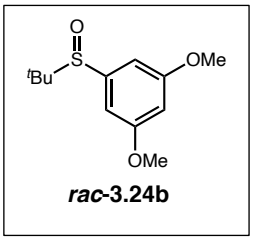

***rac*-3.24b**

1-(tert-butylsulfinyl)-3,5-dimethoxybenzene (***rac*-3.24b**) – Prepared according to **General Procedure 2** from 1-bromo-3,5-dimethoxybenzene (0.6512 g, 3.00 mmol), BuLi (0.1954 g, 1.22 mL, 2.5 M, 3.05 mmol), and ***rac*-3.32** (0.1944 g, 1.00 mmol). Purification by flash chromatography on silica (35% EtOAc in hexanes) afforded ***rac*-3.24b** (0.1758 g, 73% yield) as an off-white solid. **^{1}H NMR** ($CDCl_3$, 400 MHz) δ 6.72 (d, J = 2.3 Hz, 2H), 6.54 (t, J = 2.3 Hz, 1H), 3.82 (s, 6H), 1.19 (s, 9H). **HPLC** (OD-H column, 20% 2-propanol in hexanes, 1 mL/min) t_1 = 5.6 min, t_2 = 7.9 min.

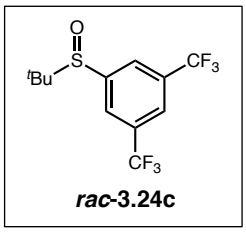

***rac*-3.24c**

1-(tert-butylsulfinyl)-3,5-bis(trifluoromethyl)benzene (***rac*-3.24c**) – Prepared according to **General Procedure 1** from 1-bromo-3,5-bis(trifluoromethyl)benzene (1.239 g, 4.23 mmol), Mg (0.1130 g, 4.65

mmol), LiCl (0.1792 g, 4.23 mmol) and ***rac*-3.32** (0.4108 g, 2.11 mmol). Purification by flash chromatography on silica (10% EtOAc in hexanes) afforded ***rac*-3.24c** (0.1858 g, 28% yield) as a yellow oil. **^{1}H NMR** ($CDCl_3$, 400 MHz) δ 8.06 – 8.03 (m, 2H), 8.02 – 8.00 (m, 1H), 1.20 (s, 9H). **HPLC** (AS-H column, 5% 2-propanol in hexanes, 1 mL/min) t_1 = 5.2 min, t_2 = 8.0 min.

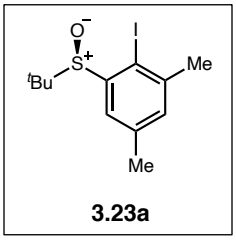

3.23a

(R)-1-(tert-butylsulfinyl)-2-iodo-3,5-dimethylbenzene (**3.23a**) – Prepared according to **General Procedure 3a** from **3.24a** (0.1110 g, 0.528 mmol), BuLi (0.0372 g, 0.30 mL, 1.95 M, 0.581 mmol), and I_2 (0.2009 g, 0.792 mmol). Purification by flash chromatography on silica (12% EtOAc in hexanes) afforded **3.23a** (0.1045 g, 59% yield) as an off-white solid. **^{1}H NMR** (CDCl3, 400 MHz) δ 7.33 – 7.32 (m, 1H), 7.21 – 7.20 (m, 1H), 2.46 (s, 3H), 2.35 (s, 3H), 1.29 (s, 9H). **^{13}C NMR** ($CDCl_3$ 101 MHz) δ 144.48, 142.48, 138.64, 134.02, 126.94, 99.84, 59.58, 28.82, 23.85, 21.04. **HRMS** (+APCI) calculated for $C_{12}H_{18}OIS$ $[M+H]^+$ 337.0118, found 337.0117.

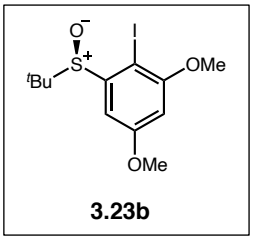

3.23b

(R)-1-(tert-butylsulfinyl)-2-iodo-3,5-dimethoxybenzene (**3.23b**) – Prepared according to **General Procedure 3a** from **3.24b** (0.1640 g, 0.677 mmol), BuLi (0.077 g, 0.39 mL, 1.95 M, 0.744 mmol), and I_2 (0.2577 g, 1.02 mmol). Purification by flash chromatography on silica (15% Et_2O in toluene) afforded **3.23b** (0.0997 g, 40% yield) as a yellow solid. **^{1}H NMR** (CDCl3, 400 MHz) δ 6.95 (d, *J* = 2.7 Hz, 1H), 6.53 (d, *J* = 2.7 Hz, 1H), 3.88 (s, 3H), 3.86 (s, 3H), 1.31 (s, 9H). **^{13}C NMR** ($CDCl_3$ 101 MHz) δ 161.51, 158.66, 146.33, 104.49, 102.38, 78.41, 60.12, 56.83, 56.03, 23.98. **HRMS** (+APCI) calculated for $C_{12}H_{18}O_3IS$ $[M+H]^+$ 369.0015, found 369.0010.

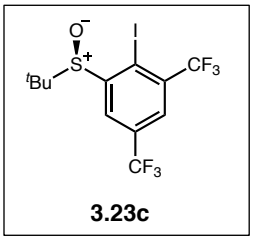

3.23c

(R)-1-(tert-butylsulfinyl)-2-iodo-3,5-bis(trifluoromethyl)benzene (**3.23c**) – Prepared according to **General Procedure 3b** from **3.24c** (0.2940 g, 0.924 mmol), BuLi (0.0710

g, 0.57 mL, 1.95 M, 1.011 mmol), *i*Pr_2NH (0.1122 g, 0.16 mL, 1.11 mmol), and I_2 (0.2813 g, 1.11 mmol). Purification by flash chromatography on silica (5% EtOAc in toluene) afforded **3.23c** (0.1753 g, 43% yield) as a yellow solid **^{1}H NMR** ($CDCl_3$, 500 MHz) δ 8.12 (d, *J* = 2.2 Hz, 1H), 8.00 (d, *J* = 2.2 Hz, 1H), 1.33 (s, 8H). **HRMS** (+APCI) calculated for $C_{12}H_{12}OF_6IS$ $[M+H]^+$ 444.9552, found 444.9558.

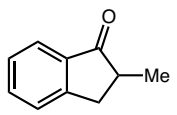

3.35

2-methyl-2,3-dihydro-1H-inden-1-one (**3.35**) - To a flame-dried 50 mL RBF equipped with a stir bar, added alpha-methylcinnamic acid (15.0260 g, 92.644 mmol, 1.0 equiv) and 10 wt. % Pd/C (1.6240 g, 1.526 mmol, 10 wt. %). The flask was sealed, the atmosphere exchanged with H_2, and the reaction allowed to stir at room temperature overnight under a balloon of H_2. After 24 hours, the reaction was diluted with Et_2O, filtered through a pad of celite, and concentrated *in vacuo* to afford crude alpha-methylhydrocinnamic acid which was used directly without further purification. To a flame-dried 250 mL RBF equipped with a stir bar was added crude alpha-methylhydrocinnamic acid (15.21 g, 92.63 mmol, 1.0 equiv), and polyphosphoric acid (115% H_3PO_4, ~125 mL). The flask was sealed, the atmosphere exchanged with N_2, and allowed to stir overnight at 100 °C under a balloon of nitrogen. After 16 hours, the reaction was poured hot into a 2L Erlenmeyer flask equipped with ~500 mL of ice. DI H_2O and heat were used to ensure complete transfer of the reaction to the Erlenmeyer flask. The crude material was then quenched with K_2CO_3 portion wise while manually agitating until the evolution of CO_2 ceased. The quenched reaction was transferred to a 1L separatory funnel, and the aqueous layer extracted with EtOAc (4 x 100 mL). The combined organic layers were washed with 3N NaOH (3 x 100 mL), dried over $MgSO_4$, filtered, and concentrated *in vacuo* to afford **3.35** (12.234 g, 90% yield) as a red oil. **^{1}H NMR** ($CDCl_3$, 400 MHz) δ 7.76 (d, *J* = 7.7 Hz, 1H), 7.59 (td, *J* = 7.5, 1.3 Hz, 1H), 7.45 (dt, *J* = 7.7, 0.9 Hz, 1H), 7.40 – 7.35 (m, 1H), 3.41 (dd, *J* = 18.1, 8.9 Hz, 1H), 2.78 – 2.66 (m, 2H), 1.32 (d, *J* = 7.3 Hz, 3H).[3]

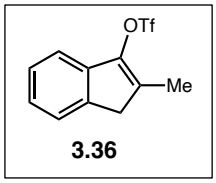

3.36

2-methyl-1H-inden-3-yl trifluoromethanesulfonate (**3.36**) – To a flame-dried 100 mL RBF equipped with a stir bar, added 2-methylindanone (1.0110 g, 6.92 mmol, 1.0 equiv). The flask was sealed with a rubber septum and the atmosphere exchanged with N_2 before the addition of DCM (30 mL, 0.25 M), Hunig's base (1.0726 g, 8.27 mmol, 1.2 equiv), and TF_2O (2.4389 g, 8.64 mmol, 1.25 equiv). The reaction was allowed to stir at room temperature for 5 hours and then transferred to a separatory funnel. The organic layer was washed with DI H_2O (30 mL). The aqueous layer was extracted with DCM (2 x 20 mL) and the combined organic extracts dried over Na_2SO_4, filtering off the drying agent, and concentrating *in vacuo*. Purification by flash chromatography (5% EtOAc in pentane) afforded **3.36** (1.1613 g, 60% yield) as a red oil. **^{1}H NMR** (CDCl3, 400 MHz) δ 7.39 (dt, *J* = 7.4, 1.0 Hz, 1H), 7.33 (dd, *J* = 4.0, 1.6 Hz, 2H), 7.28 – 7.21 (m, 1H), 3.40 (s, 2H), 2.17 (s, 3H). **^{13}C NMR** ($CDCl_3$ 101 MHz) δ 142.71, 139.35, 137.76, 132.76, 127.01, 125.90, 124.13, 118.74 (q, *J* = 320.2 Hz), 117.59, 39.43, 12.75. **HRMS** (+APCI) calculated for $C_{11}H_{10}O_3F_3S$ $[M+H]^+$ 279.0297, found 279.0294.

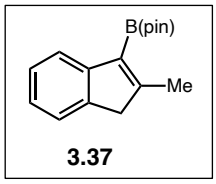

3.37

4,4,5,5-tetramethyl-2-(2-methyl-1H-inden-3-yl)-1,3,2-dioxaborolane (**3.37**) – To an oven-dried 4 mL reaction vial equipped with a stir bar, added 2-methylindene triflate **3.36** (0.0613 g, 0.22 mmol, 1.0 equiv), $Pd(dppf)Cl_2$ (16.5 mg, 0.022 mmol, 10 mol %), bis(pinacolato)diboron (83.9 mg, 0.33 mmol, 1.5 equiv), and KOAc (64.5 mg, 0.66 mmol, 3.0 equiv). Exchanged atmosphere with N_2 and added 1,4-dioxane (1.1 mL, 0.2 M). Heated to 100 °C and allowed to stir for 3 hours under positive pressure of nitrogen. After 3 hours, quenched with excess DI H_2O and transferred to a separatory funnel. Extracted the aqueous layer with EtOAc (3 x 10 mL). Washed the combined organic layers with brine (20 mL), dried over $MgSO_4$, filtered off the drying agent, and concentrated *in vacuo*. Purification by flash chromatography on silica (5% EtOAc in pentane) afforded **3.37** (34.1 mg, 61% yield) as an off-white solid. **^{1}H NMR** (CDCl3, 400 MHz) δ 7.75 (d, *J* = 7.6 Hz, 1H), 7.34 (dt, *J* = 7.3, 1.0 Hz, 1H), 7.23 (td, *J* = 7.6, 1.1 Hz, 1H), 7.08 (td, *J* = 7.4, 1.2 Hz, 1H), 3.39 (s, 2H), 2.39

(s, 3H), 1.36 (s, 12H). **^{13}C NMR** ($CDCl_3$ 101 MHz) δ 162.42, 148.76, 142.77, 126.32, 123.58, 122.92, 121.99, 83.00, 45.63, 25.13, 17.42. **HRMS** (+APCI) calculated for $C_{16}H_{21}O_2B$ $[M+H]^+$ 255.1665, found 255.1666.

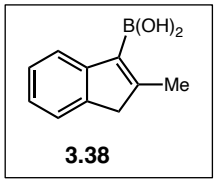

3.38

(2-methyl-1H-inden-3-yl)boronic acid (**3.38**) – To a 20 mL scintillation vial containing indene boronic ester **3.37** (0.1100 g, 0.429 mmol, 1 equiv), added NH_4OAc (0.5511 g, 2.58 mmol, 6 equiv), $NaIO_4$ (0.1986 g, 2.58 mmol, 6 equiv), and a stir bar. Sealed with a rubber septum and exchanged the atmosphere with N_2. Added 2:1 acetone:DI H_2O (2.9 mL acetone, 1.45 mL DI H_2O, 0.1 M) and allowed to stir vigorously at room temperature under a balloon of N_2. After 22 hours, the reaction was diluted with Et_2O (10.0 mL), filtered over a pad of celite, and concentrated *in vacuo*. Purification by flash chromatography on silica (60% EtOAc in hexanes) afforded **3.38** (22.5 mg, 30% yield) as a white solid. **^{1}H NMR** (CDCl3, 400 MHz) δ 8.05 (d, *J* = 7.4 Hz, 1H), 7.44 (d, *J* = 7.3 Hz, 1H), 7.30 – 7.24 (m, 1H), 7.16 (td, *J* = 7.4, 1.1 Hz, 1H), 3.56 (s, 2H), 2.62 (s, 3H). **^{13}C NMR** ($CDCl_3$ 101 MHz) δ 166.08, 148.25, 142.58, 126.46, 123.94, 123.17, 122.53, 46.48, 17.95. **HRMS** (+APCI) calculated for $C_{10}H_{12}O_2B$ $[M+H]^+$ 174.0961, found 174.0965.

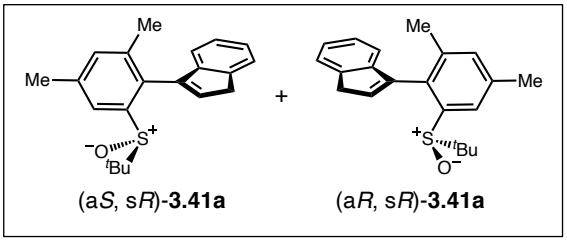

(R)-3-(2-(tert-butylsulfinyl)-4,6-dimethylphenyl)-1H-indene (**3.41a**) – Prepared according to **General Procedure 4** from **3.23a** (0.0210 g, 0.0625 mmol), **3.40** (0.0200 g, 0.125 mmol), SPhos Pd G3 (0.0050 g, 0.00625 mmol), and Cs_2CO_3 (0.0814 g, 0.0250 mmol). Purification by flash chromatography on silica (25% EtOAc in hexanes) afforded **3.14a** (0.0128 g, 63% yield, 1.5:1 *dr*) as a white solid. **Major Diastereomer: ^{1}H NMR** (CDCl3, 600 MHz) δ 7.66 (dd, *J* = 1.2, 0.6 Hz, 1H), 7.55 – 7.48 (m, 1H), 7.25 – 7.22 (m, 3H), 7.04 – 6.98 (m, 1H), 6.36 (t, *J* = 2.1 Hz, 1H), 3.57 (d, *J* = 2.1 Hz, 2H), 2.45 (s, 3H), 2.13 (s, 3H), 1.12 (s, 9H). **^{13}C**

NMR ($CDCl_3$ 151 MHz) δ 145.04, 142.98, 141.40, 140.26, 137.90, 137.43, 135.49, 134.26, 132.69, 126.87, 125.26, 124.66, 123.72, 120.48, 57.26, 38.70, 23.62, 21.45, 20.23. **Minor Diastereomer:** **^{1}H NMR** (CDCl3, 600 MHz) δ 7.66 – 7.63 (m, 1H), 7.55 – 7.48 (m, 1H), 7.24 – 7.18 (m, 3H), 6.99 – 6.92 (m, 1H), 6.58 (t, *J* = 2.1 Hz, 1H), 3.57 (d, *J* = 2.1 Hz, 2H), 2.44 (s, 3H), 2.10 (s, 3H), 0.91 (s, 9H). **^{13}C NMR** ($CDCl_3$ 151 MHz) δ 144.94, 143.92, 140.64, 140.27, 137.94, 137.65, 134.91, 133.81, 133.33, 126.08, 124.89, 124.82, 124.22, 120.97, 55.67, 38.54, 23.33, 21.44, 20.37. **HRMS** (+APCI) calculated for $C_{21}H_{25}OS$ $[M+H]^+$ 325.1621, found 325.1623.

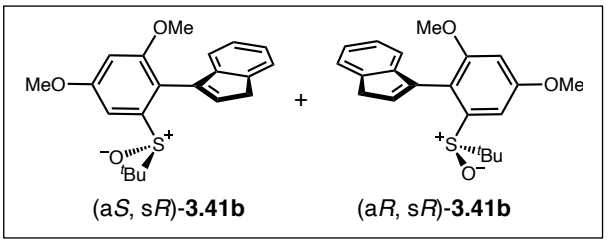

(R)-3-(2-(tert-butylsulfinyl)-4,6-dimethoxyphenyl)-1H-indene (**3.41b**) – Prepared according to **General Procedure 4** from **3.23b** (0.0812 g, 0.221 mmol), **3.40** (0.0706 g, 0.441 mmol), SPhos Pd G3 (0.0193 g, 0.0221 mmol), and Cs_2CO_3 (0.2870 g, 0.882 mmol). Purification by flash chromatography on silica (35% EtOAc in toluene) afforded **3.14b** (0.0335 g, 43% yield, 2.7:1 *dr* as an inseparable mixture of diasteriomers, major diastereomer denoted with a #, minor diastereomer with an *) as a yellow oil. **^{1}H NMR** (CDCl3, 600 MHz) δ 7.52 – 7.46 (m, 1.4H), 7.25 – 7.14 (m, 4.3H), 7.11 – 7.07 (m, 0.4H*), 7.03 – 6.98 (m, 1H#), 6.64 (ddd, *J* = 6.1, 3.7, 2.3 Hz, 2.4H), 6.44 (t, *J* = 2.1 Hz, 0.4H*), 3.92 (d, *J* = 0.8 Hz, 4.3H), 3.71 (s, 3H#), 3.69 (s, 1.3H*), 3.61 – 3.46 (m, 3H), 1.11 (s, 3.6H*), 0.90 (s, 9H#). **^{13}C NMR** ($CDCl_3$ 151 MHz) δ 160.53, 160.33, 158.50, 158.35, 145.37, 145.27, 143.51, 142.96, 142.58, 142.38, 138.18, 137.23, 137.07, 135.40, 126.65, 125.85, 124.93, 124.49, 123.83, 123.72, 121.24, 120.31, 118.48, 117.97, 102.47, 101.76, 101.67, 101.23, 57.84, 56.70, 56.19, 55.93, 55.90, 55.88, 38.81, 38.48, 31.09, 23.69, 23.35. **HRMS** (+APCI) calculated for $C_{21}H_{25}O_3S$ $[M+H]^+$ 357.1519, found 357.1520.

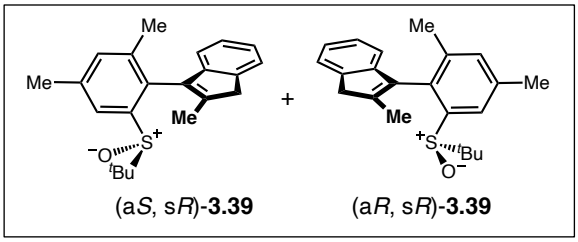

(a*S*, s*R*)-**3.39** (a*R*, s*R*)-**3.39**

(R)-3-(2-(tert-butylsulfinyl)-4,6-dimethylphenyl)-2-methyl-1H-indene (**3.39**) – Prepared according to **General Procedure 4** from **3.23a** (0.0193 g, 0.0575 mmol), **3.38** (0.0200 g, 0.115 mmol), SPhos Pd G3 (0.0050 g, 0.00575 mmol), and Cs_2CO_3 (0.0749 g, 0.230 mmol). Purification by preparative TLC (60% EtOAc in toluene) afforded **3.39** (0.0109 g, 56% yield, 6:1 *dr*) as a off-white solid (as an inseparable mixture of diasteriomers, major diastereomer denoted with a #, minor diastereomer with an *). **^{1}H NMR** ($CDCl_3$, 600 MHz) δ 7.68 (dd, *J* = 1.3, 0.7 Hz, 1H#), 7.64 – 7.63 (m, 0.2H*), 7.43 – 7.40 (m, 1.2H), 7.26 – 7.24 (m, 1H#), 7.24 – 7.09 (m, 3.5H), 6.93 (dt, *J* = 7.6, 1.0 Hz, 1H#), 6.80 – 6.78 (m, 0.2H*), 3.48 (s, 0.4H*), 3.46 (s, 2H#), 2.45 (s, 3.5H), 2.08 (s, 3H#), 2.07 – 2.04 (m, 1.3H), 1.93 (s, 3H#), 1.07 (s, 9H#), 0.93 (s, 1.6H*). **Major Diastereomer ^{13}C NMR** ($CDCl_3$ 151 MHz) δ 145.96, 143.51, 141.49, 141.00, 137.74, 137.65, 135.76, 134.19, 131.64, 126.77, 124.90, 124.26, 123.03, 119.76, 56.26, 42.71, 23.16, 19.56, 16.23. **Minor Diastereomer ^{13}C NMR** ($CDCl_3$ 151 MHz) δ 146.04, 142.81, 142.17, 140.46, 137.91, 137.82, 135.06, 133.92, 132.13, 125.87, 124.81, 123.80, 123.45, 120.00, 60.41, 55.73, 23.30, 20.08, 15.60. **HRMS** (+APCI) calculated for $C_{22}H_{27}OS$ $[M+H]^+$ 339.1777, found 339.1779.

3.5.3 Supplemental References

1) Baker, R. W.; Radzey, H.; Lucas, N. T.; Turner, P. Stereospecific Syntehses and Structures of Planar Chiral Bidentate η^5:κS-Indenyl-Sulfanyl and-Sulfinyl Complexes of Rhodium(III). *Organometallics* **2012**, *31*, 5622-5633.

2) Savile, C. K.; Magloire, V. P.; Kazlauskas, R. J. Subtilisin-Catalyzed Resolution of *N*-Acyl Arylsulfinamides. *J. Am. Chem. Soc.* **2005**, *127*, 2104-2113.

3) Farr, C. M. B.; Kazerouni, A. M.; Park, B.; Poff, C. D.; Won, J.; Sharp, K. R.; Baik. M.-H.; Blakey, S. B. Designing a Planar Chiral Rhodium Indenyl Catalyst for Regio- and Enantioselective Allylic C–H Amidation. *J. Am. Chem. Soc.* **2020**, *142*, 13996-14004.

3.5.4 Spectra and HPLC Data

***(R)-1-(tert-butylsulfinyl)-3,5-dimethylbenzene* (3.24a)**

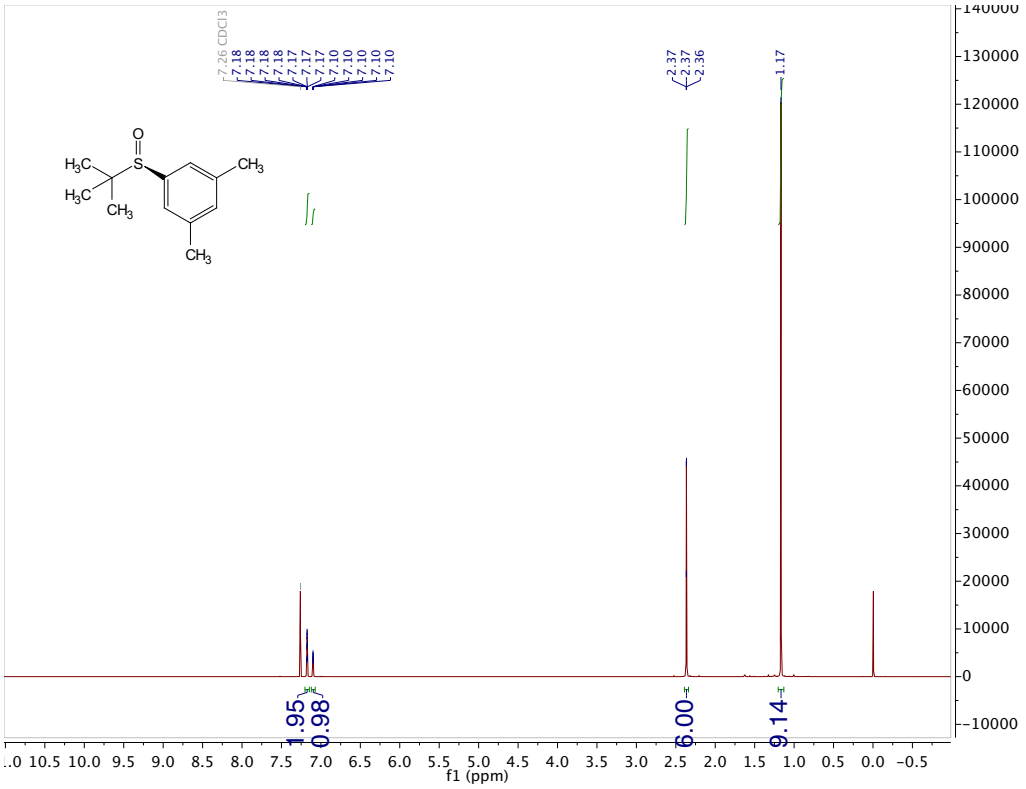

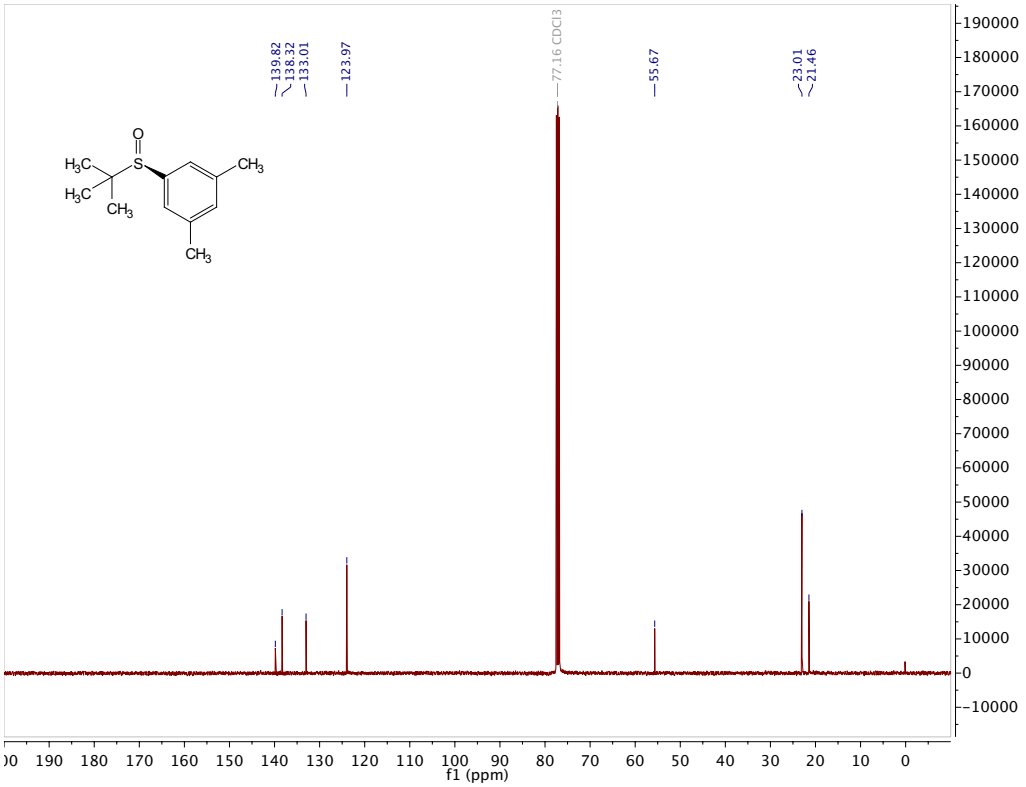

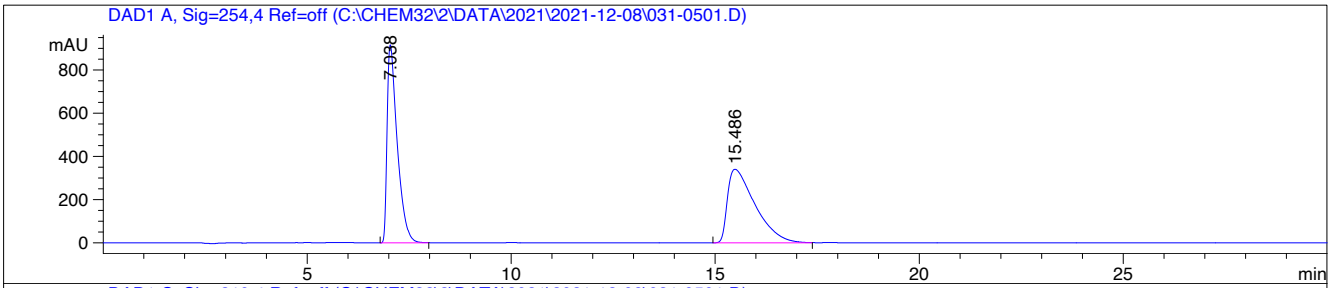

Signal 1: DAD1 A, Sig=254,4 Ref=off

Peak #	RetTime [min]	Type	Width [min]	Area [mAU*s]	Height [mAU]	Area %
1	7.038	BB	0.2588	1.59235e4	916.24915	49.9004
2	15.486	BB	0.7119	1.59871e4	340.39127	50.0996

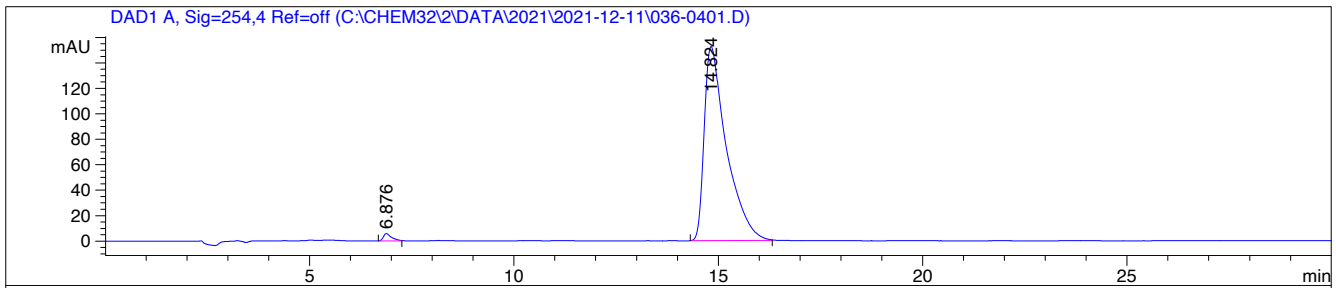

Signal 1: DAD1 A, Sig=254,4 Ref=off

Peak #	RetTime [min]	Type	Width [min]	Area [mAU*s]	Height [mAU]	Area %
1	6.876	BB	0.2013	79.69378	5.76299	1.3698
2	14.824	BB	0.5449	5738.18701	152.53801	98.6302

(R)-1-(tert-butylsulfinyl)-3,5-dimethoxybenzene (3.24b)

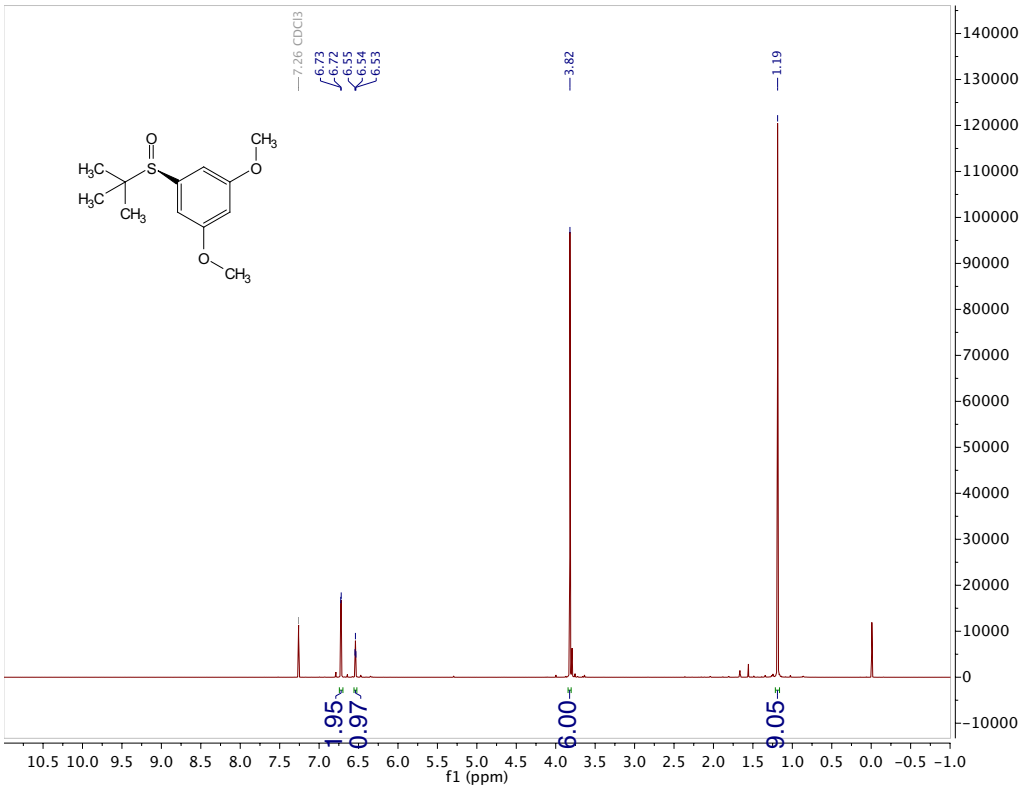

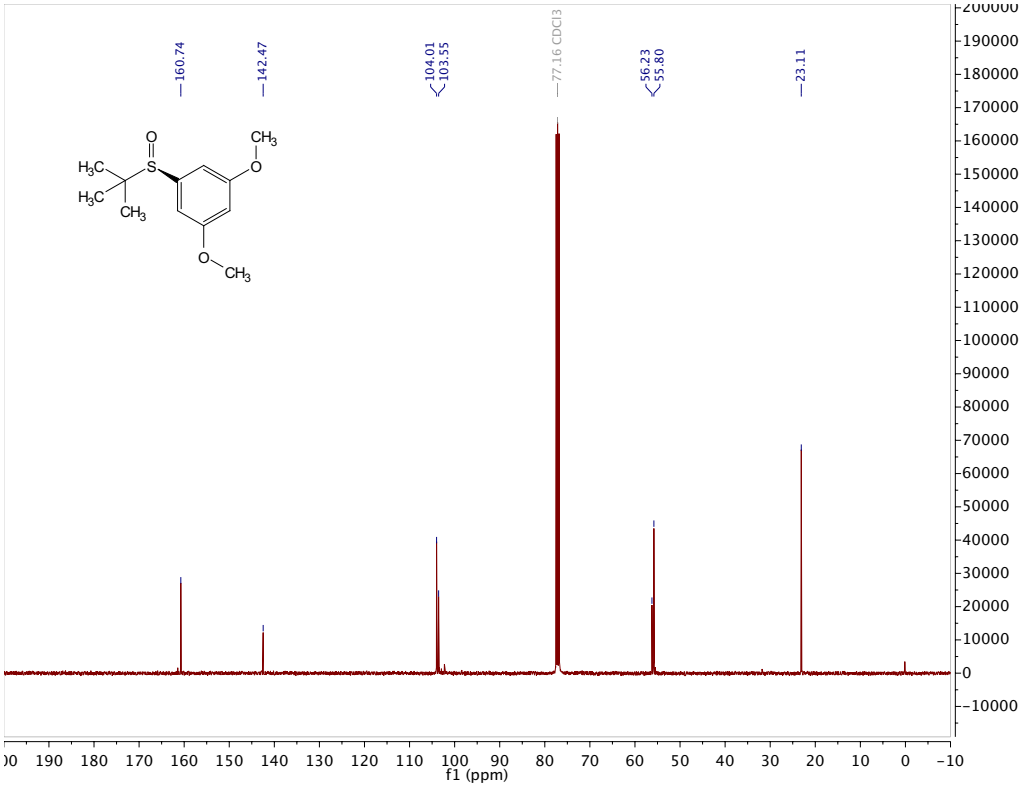

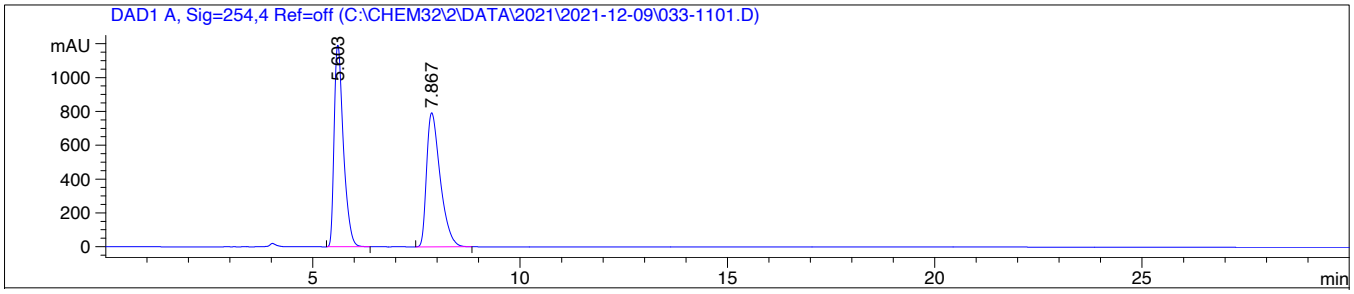

Signal 1: DAD1 A, Sig=254,4 Ref=off

Peak #	RetTime [min]	Type	Width [min]	Area [mAU*s]	Height [mAU]	Area %
1	5.603	BB	0.2291	1.80838e4	1191.04871	49.8541
2	7.867	BB	0.3497	1.81896e4	792.62616	50.1459

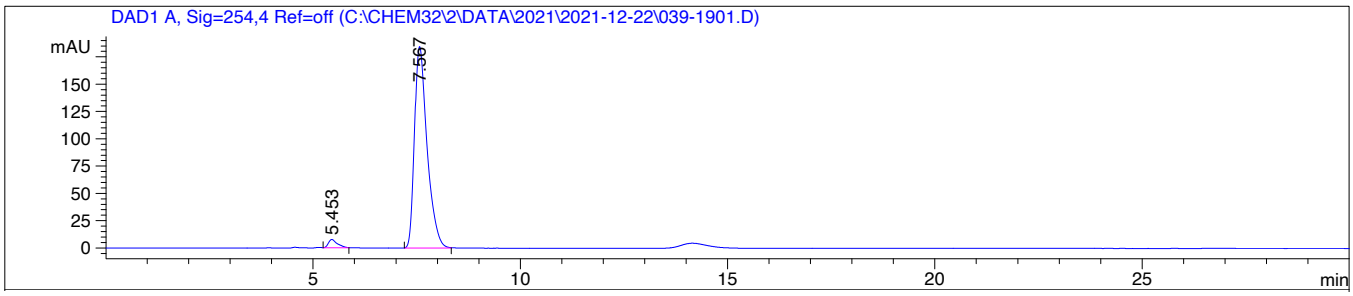

Signal 1: DAD1 A, Sig=254,4 Ref=off

Peak #	RetTime [min]	Type	Width [min]	Area [mAU*s]	Height [mAU]	Area %
1	5.453	BB	0.2208	114.73515	7.65816	2.8747
2	7.567	BB	0.3153	3876.50171	184.40038	97.1253

(R)-1-(tert-butylsulfinyl)-3,5-bis(trifluoromethyl)benzene (3.24c)

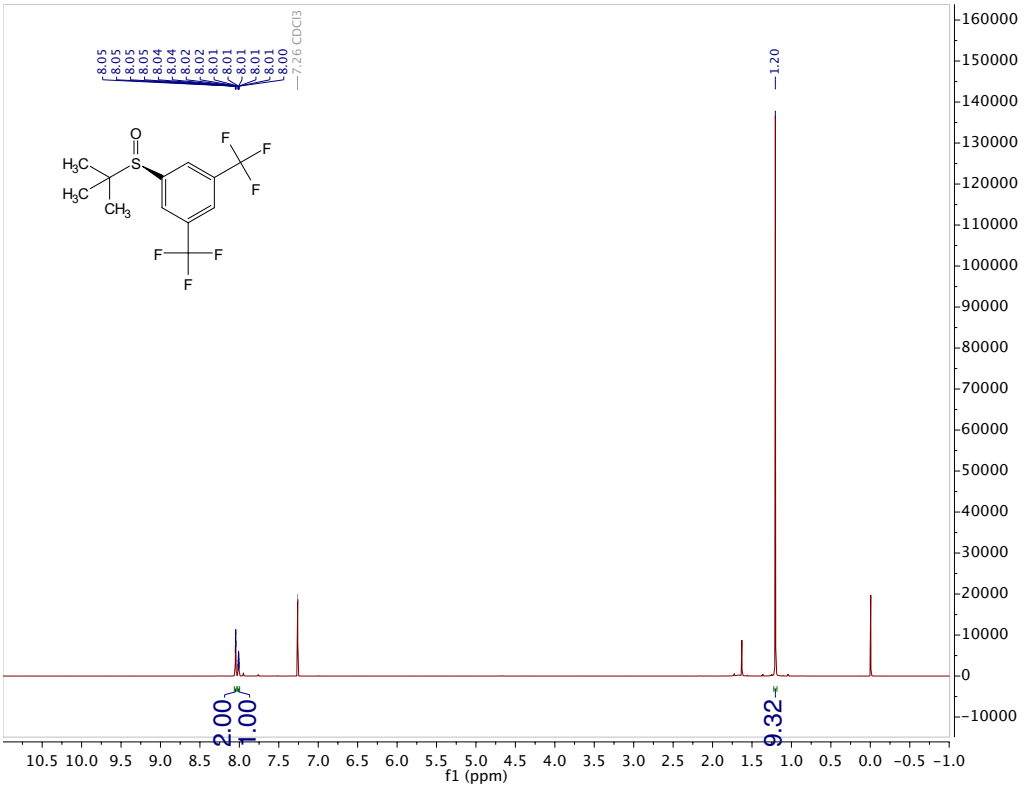

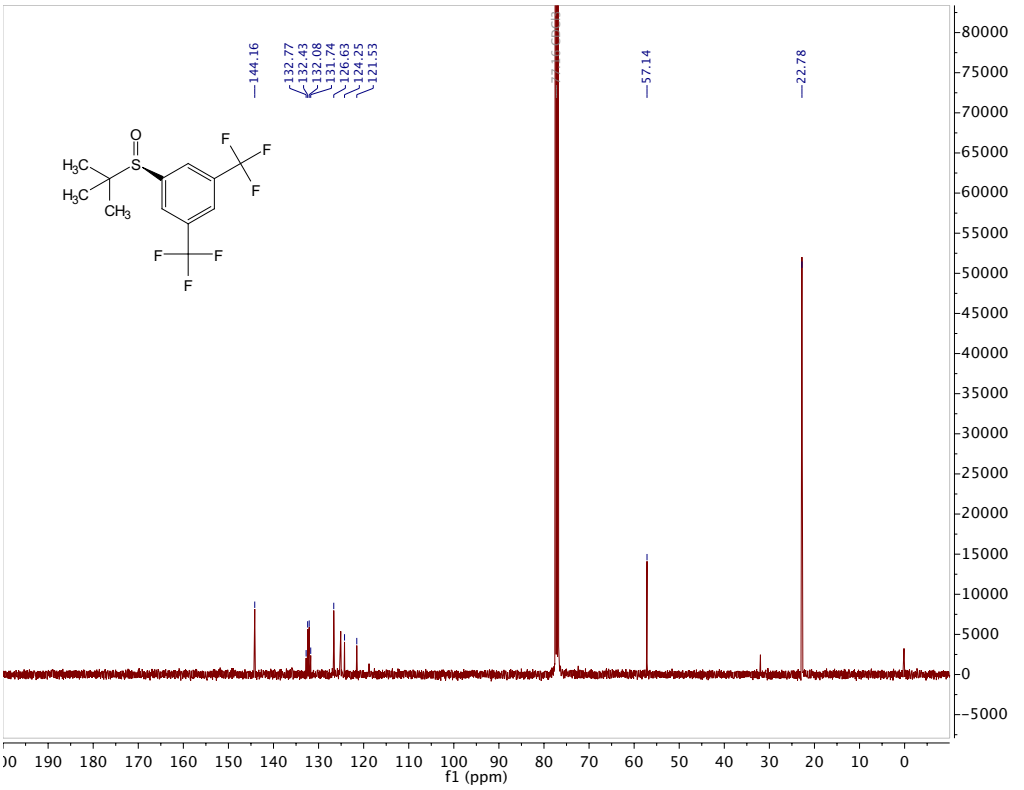

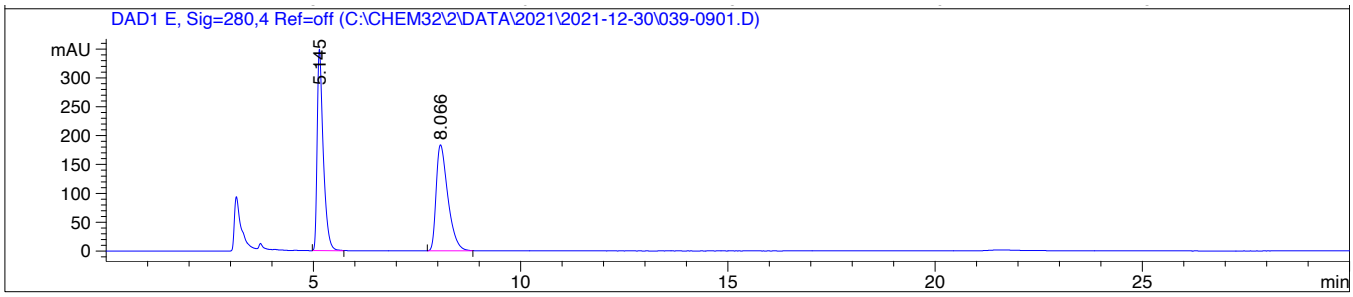

Signal 4: DAD1 E, Sig=280,4 Ref=off

Peak #	RetTime [min]	Type	Width [min]	Area [mAU*s]	Height [mAU]	Area %
1	5.145	BB	0.1520	3594.46216	349.53094	49.7755
2	8.066	BB	0.2980	3626.88965	184.00929	50.2245

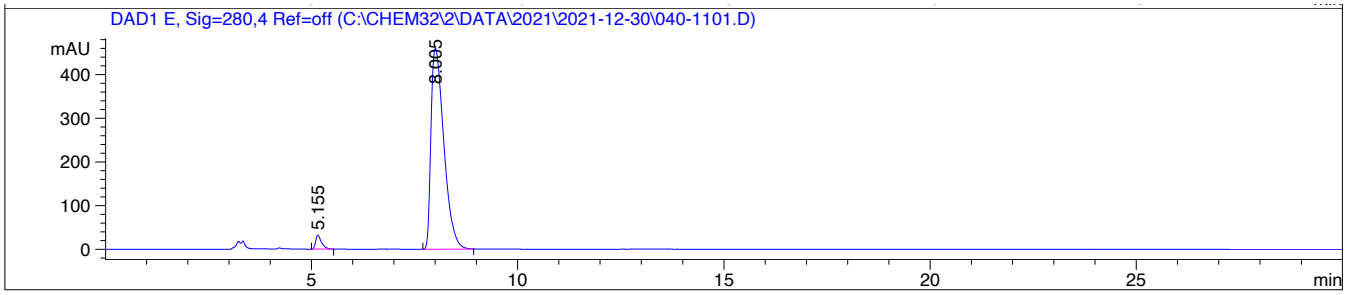

Signal 4: DAD1 E, Sig=280,4 Ref=off

Peak #	RetTime [min]	Type	Width [min]	Area [mAU*s]	Height [mAU]	Area %
1	5.155	BB	0.1460	320.12659	32.19831	3.1028
2	8.005	BB	0.3397	9997.37988	459.76239	96.8972

1-(tert-butylsulfinyl)-3,5-dimethylbenzene (*rac*-3.24a)

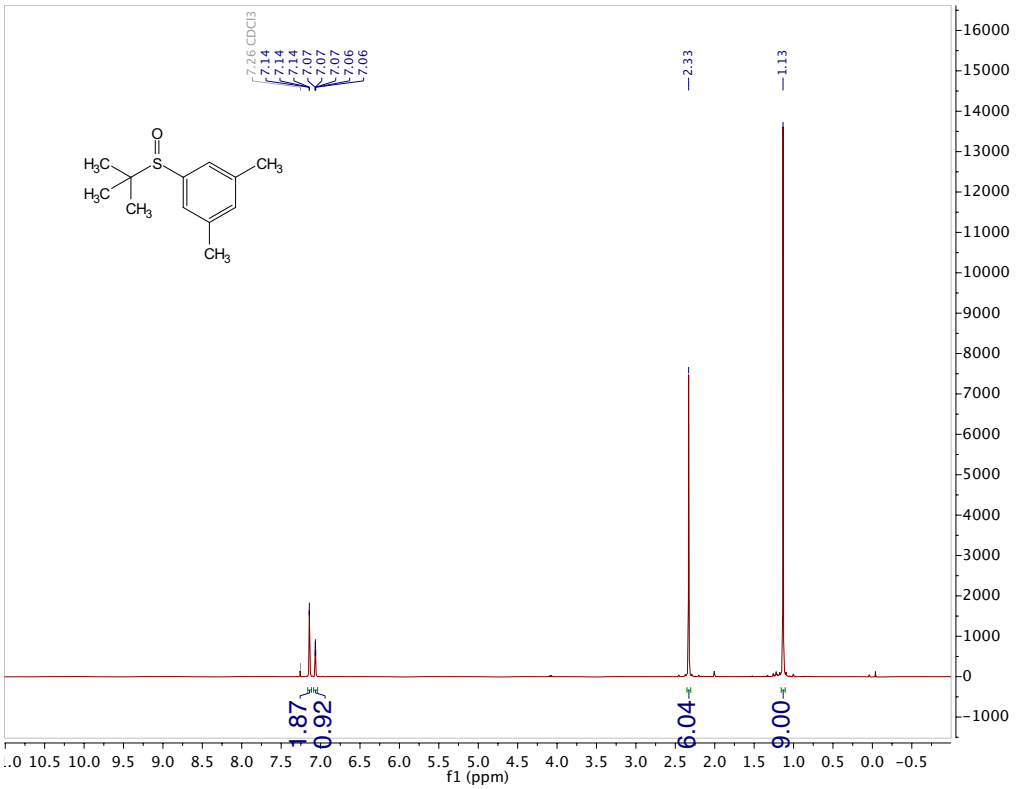

1-(tert-butylsulfinyl)-3,5-dimethoxybenzene (*rac*-3.24b)

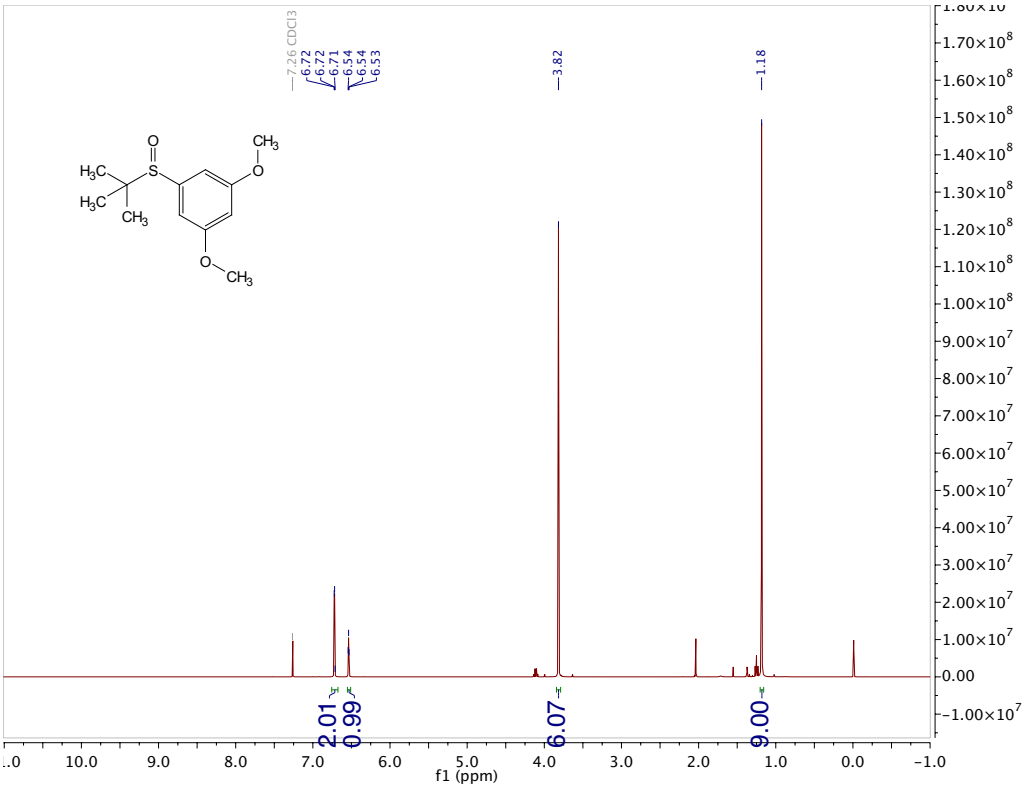

***1-(tert-butylsulfinyl)-3,5-bis(trifluoromethyl)benzene* (*rac*-3.24c)**

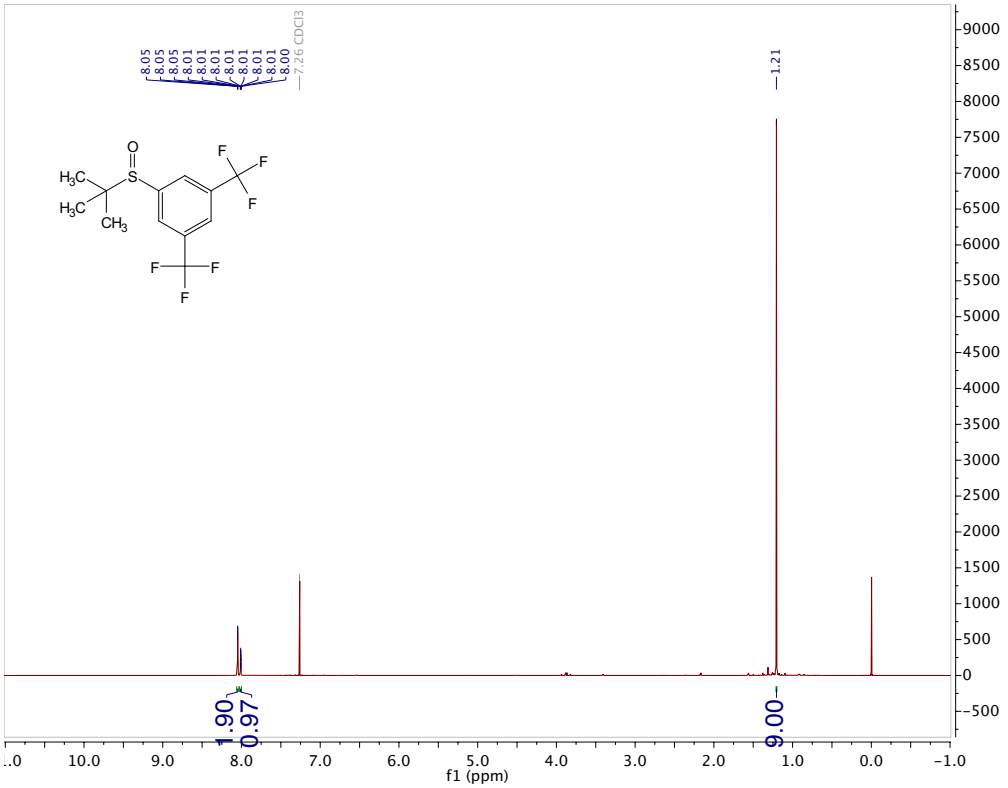

(R)-1-(tert-butylsulfinyl)-2-iodo-3,5-dimethylbenzene (3.23a)

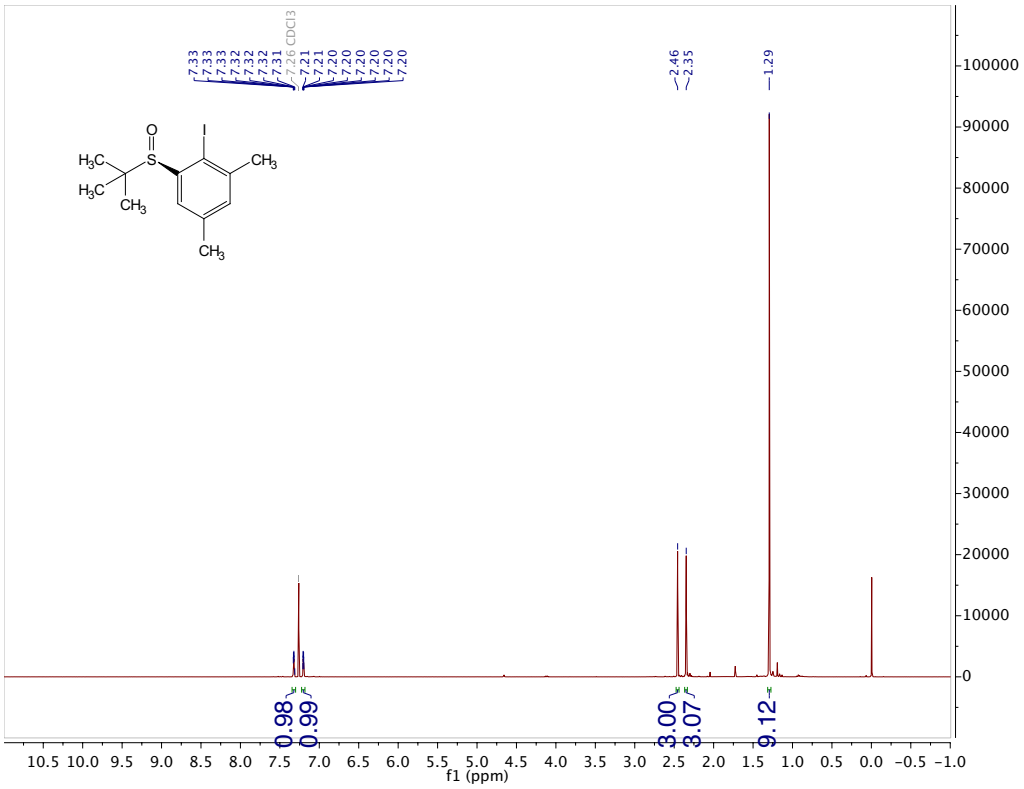

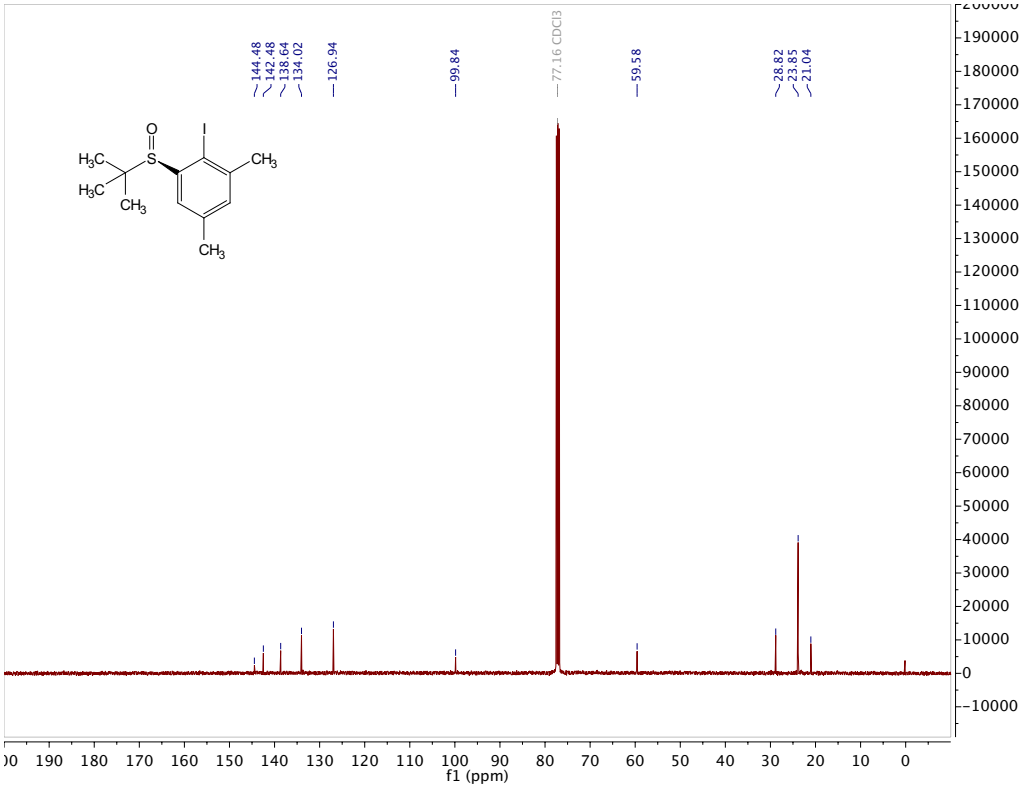

***(R)-1-(tert-butylsulfinyl)-2-iodo-3,5-dimethoxybenzene* (3.23b)**

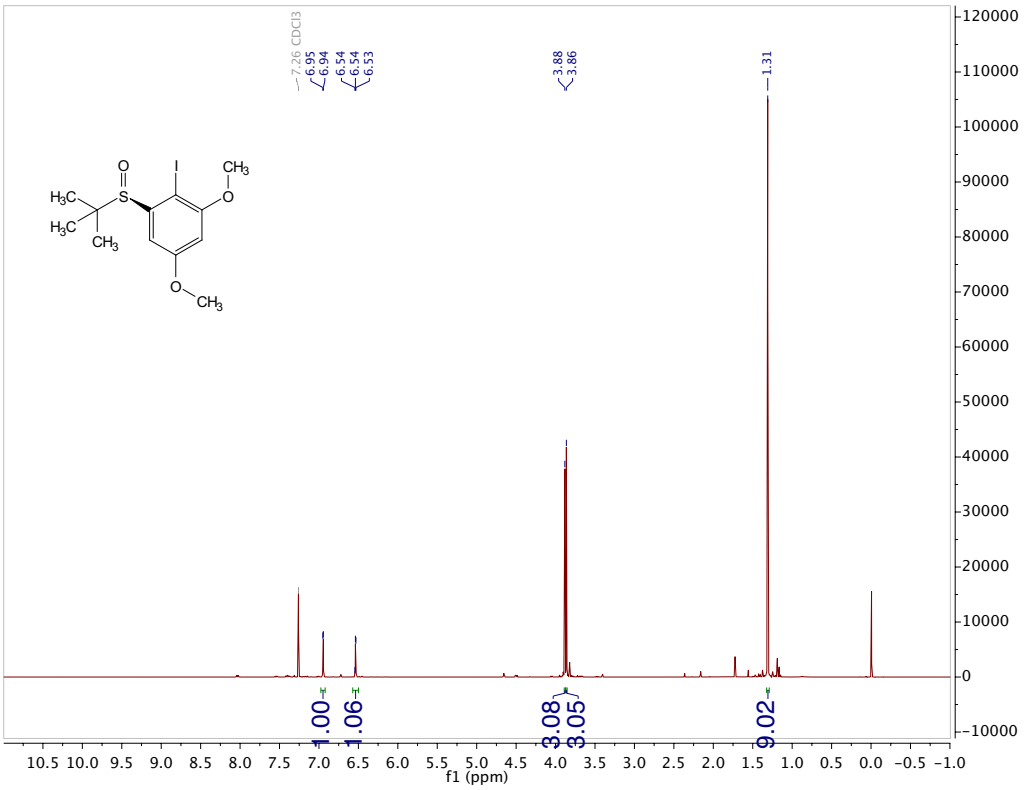

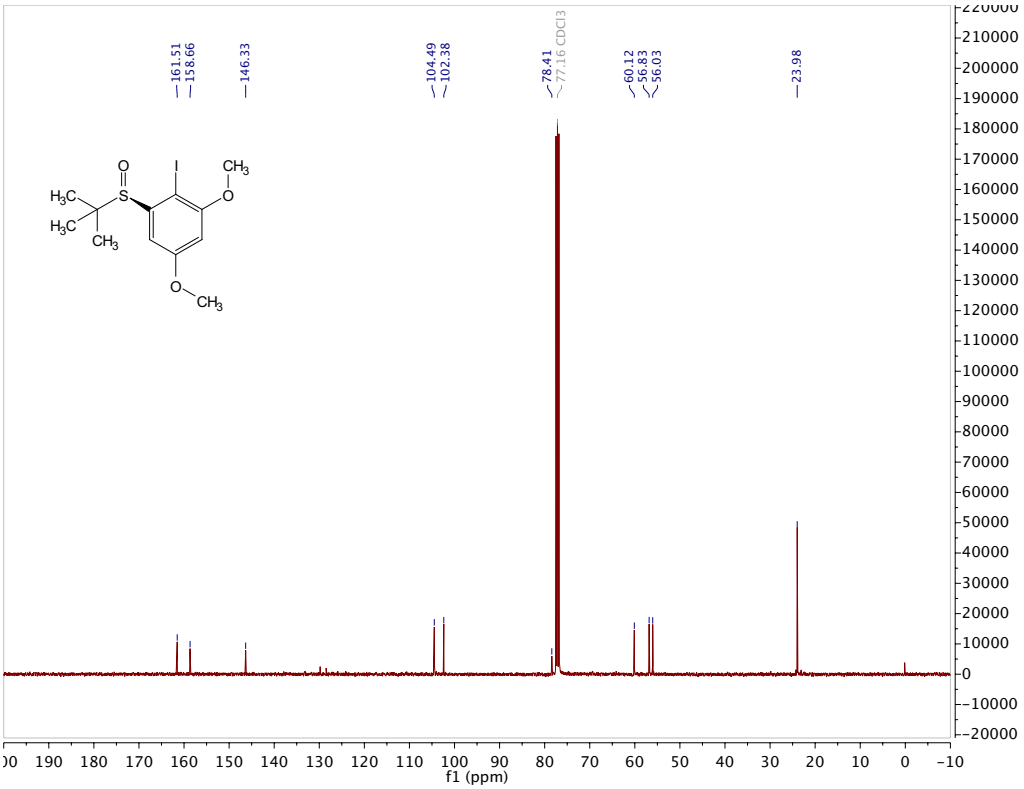

***(R)-1-(tert-butylsulfinyl)-2-iodo-3,5-bis(trifluoromethyl)benzene* (3.23c)**

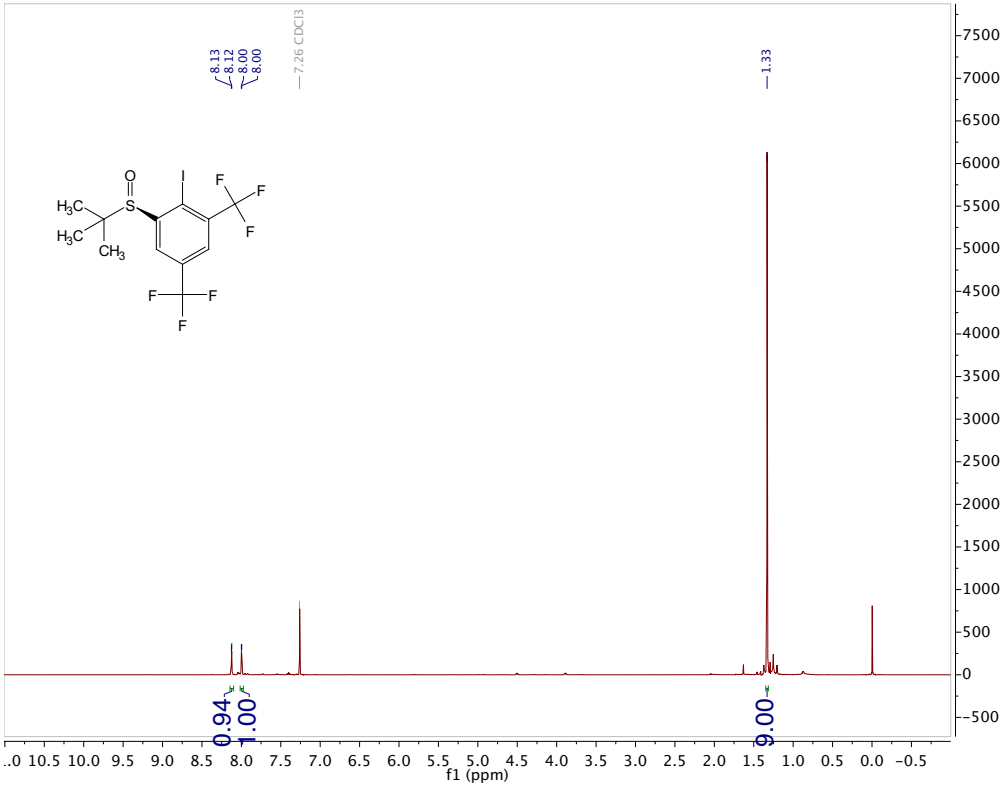

***2-methyl-2,3-dihydro-1H-inden-1-one* (3.35)**

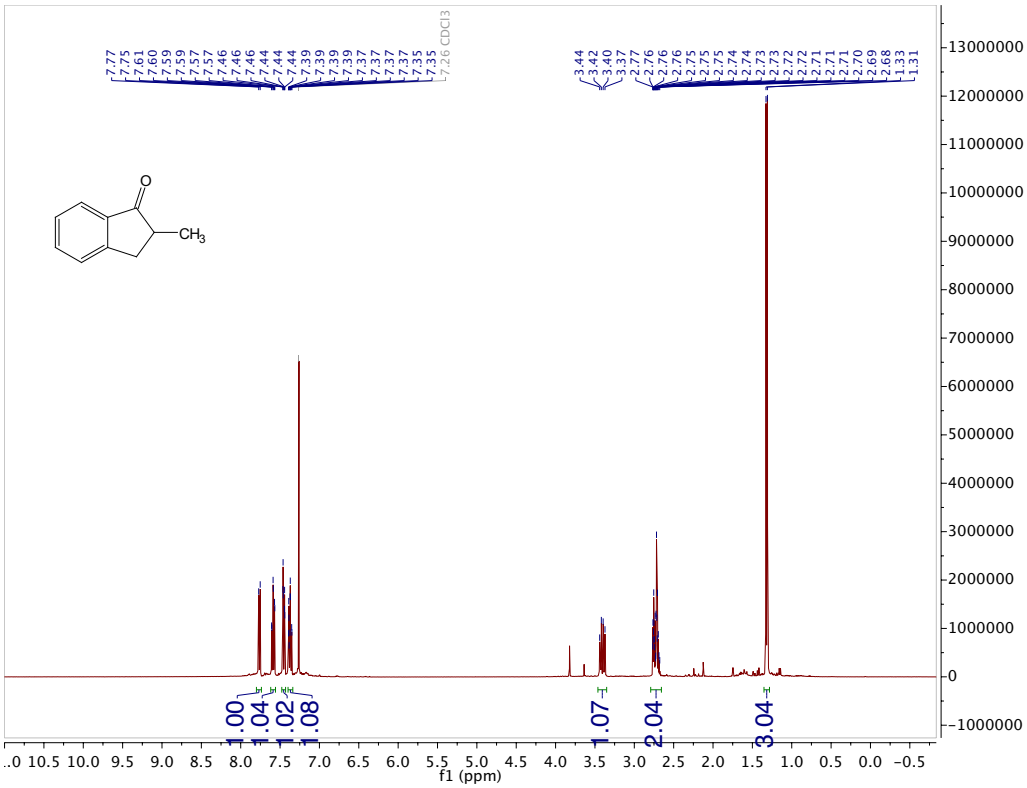

2-methyl-1H-inden-3-yl trifluoromethanesulfonate (3.36)

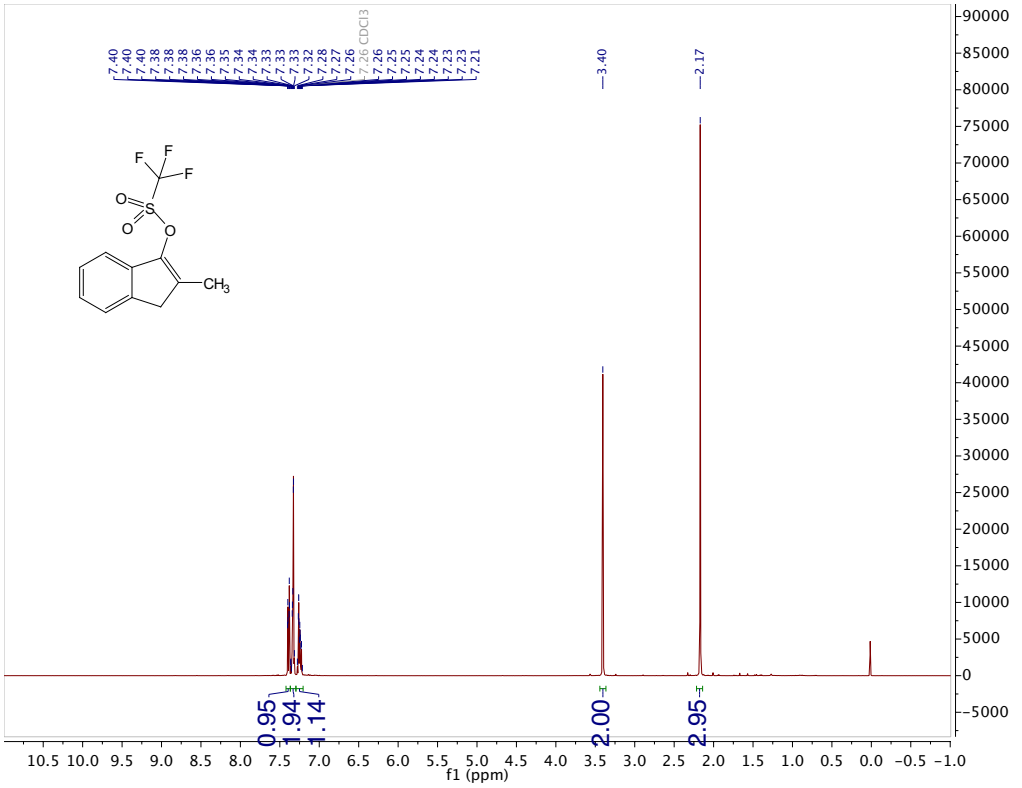

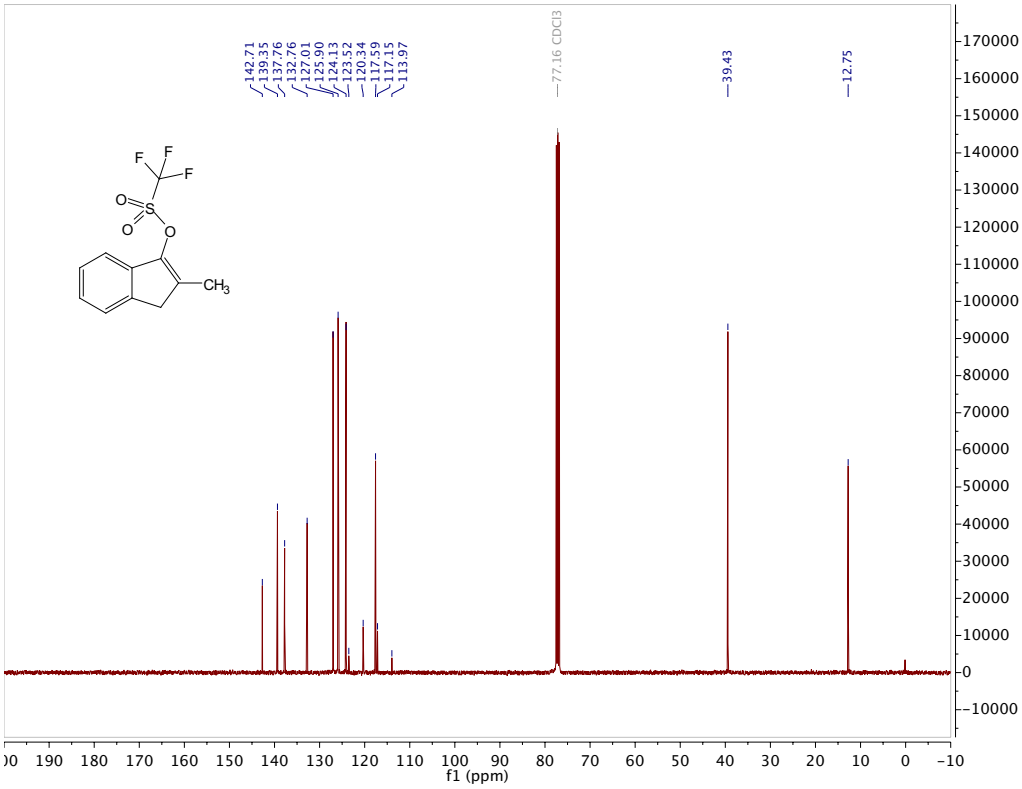

4,4,5,5-tetramethyl-2-(2-methyl-1H-inden-3-yl)-1,3,2-dioxaborolane (3.37)

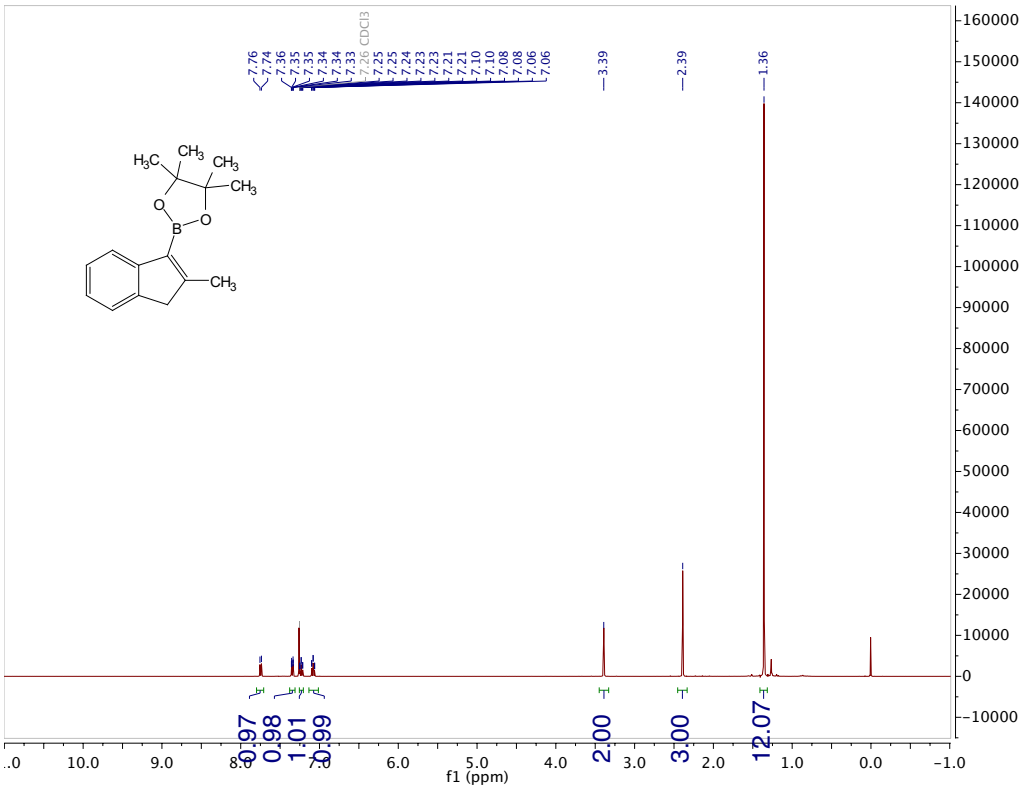

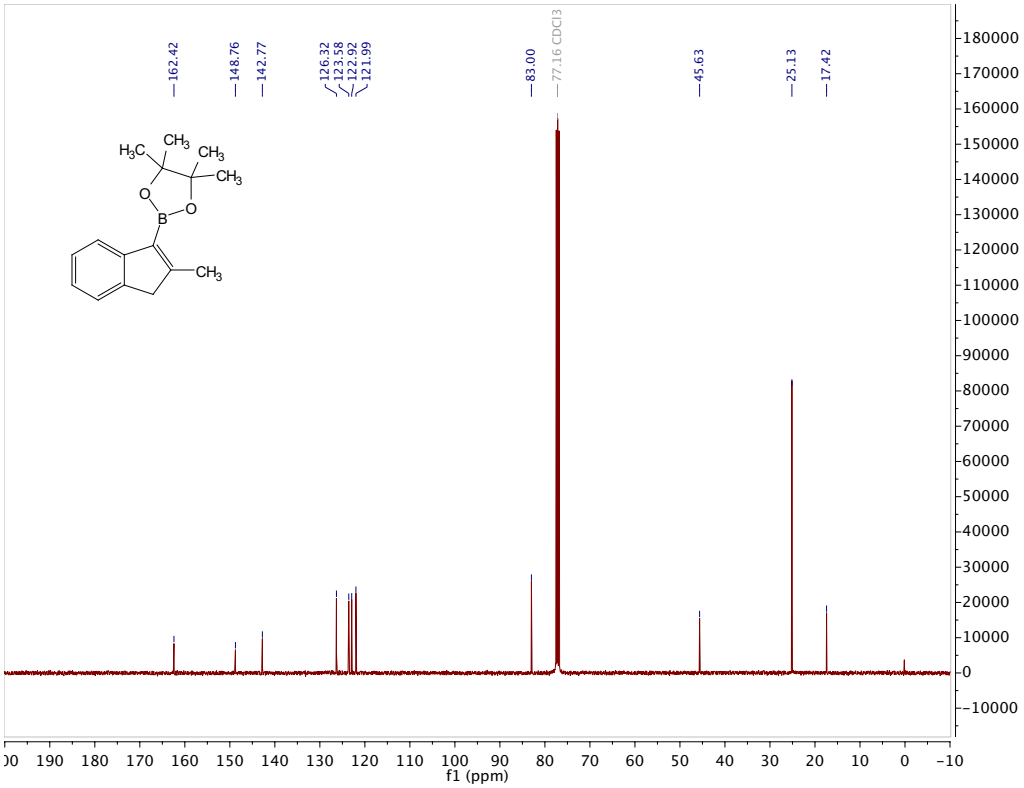

(2-methyl-1H-inden-3-yl)boronic acid (3.38)

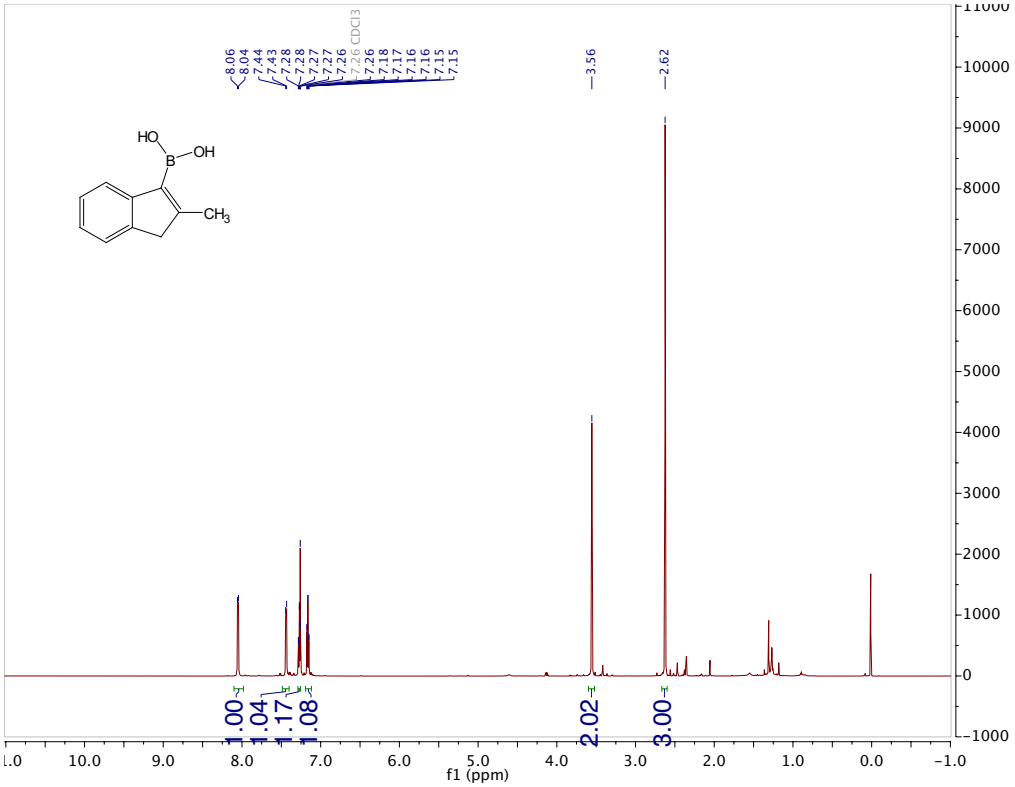

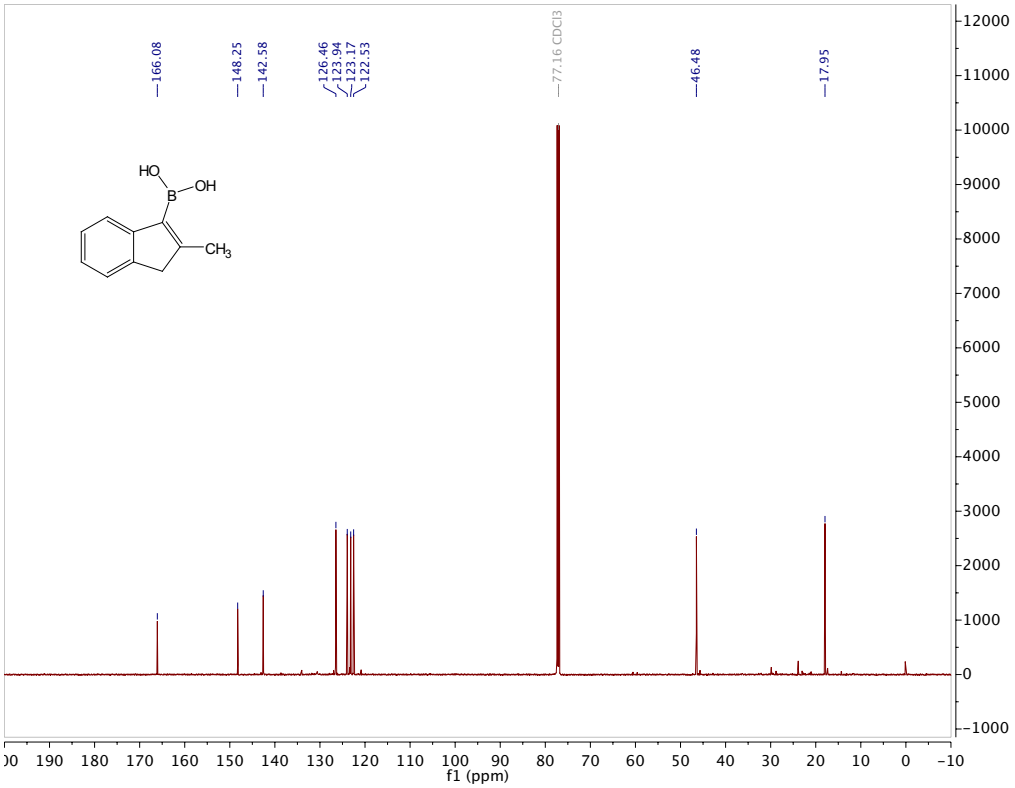

(R)-3-(2-(tert-butylsulfinyl)-4,6-dimethylphenyl)-1H-indene (**3.41a**) – Major Ligand

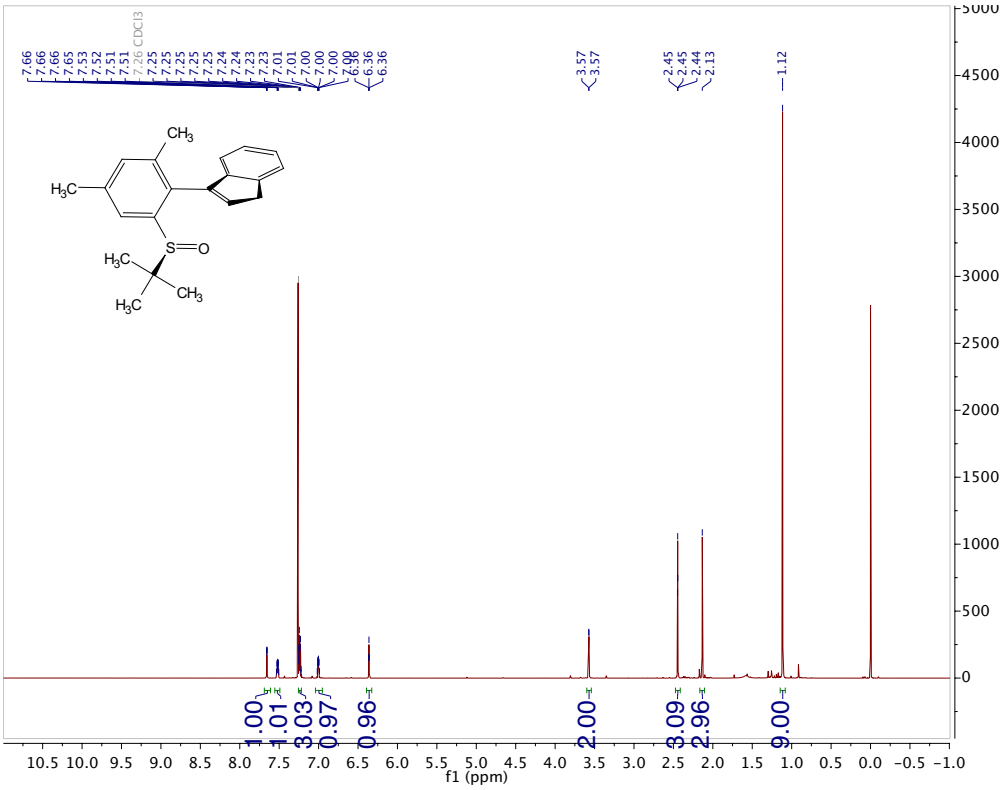

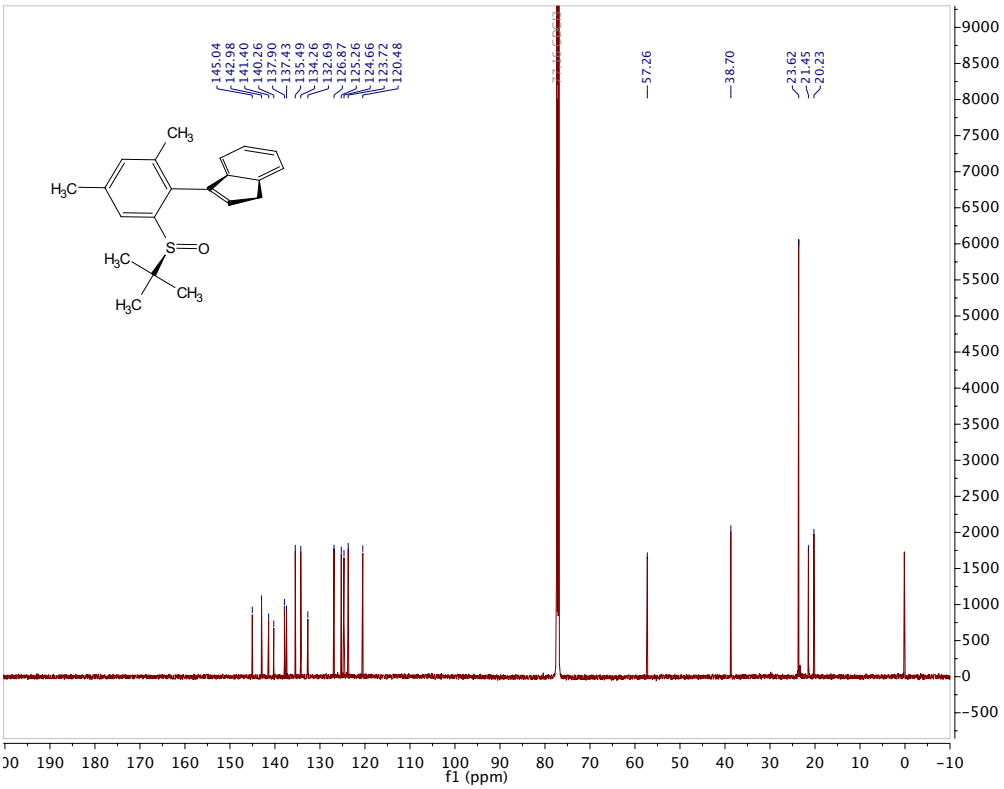

(R)-3-(2-(tert-butylsulfinyl)-4,6-dimethylphenyl)-1H-indene (**3.41a**) – Minor Ligand

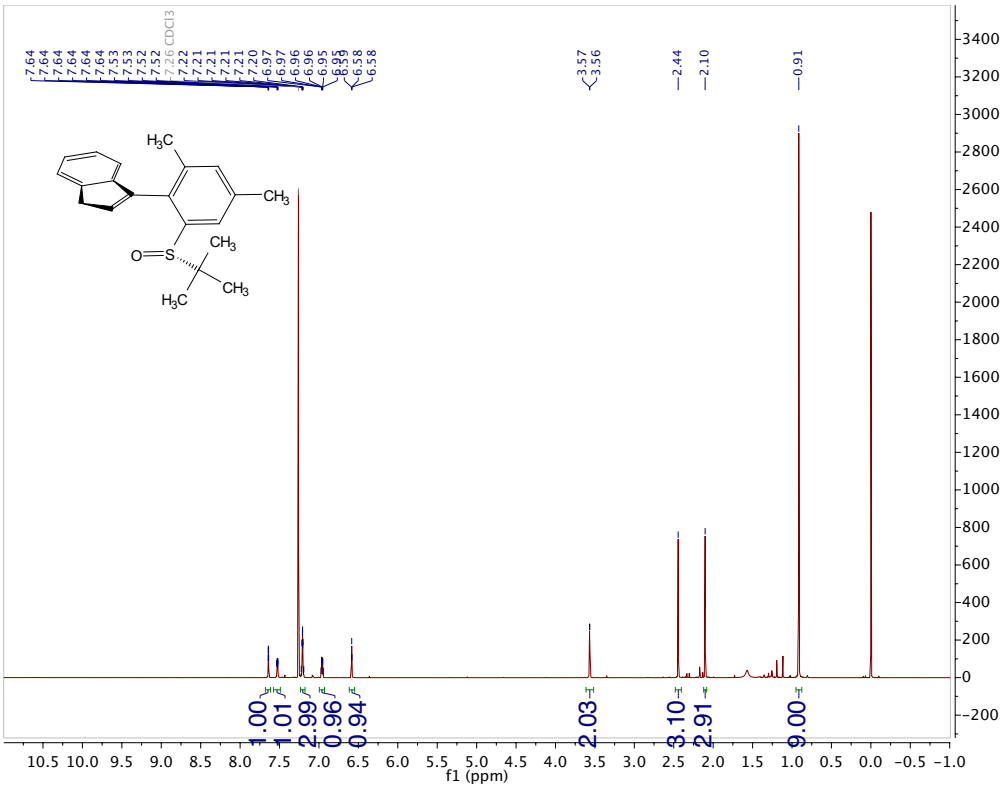

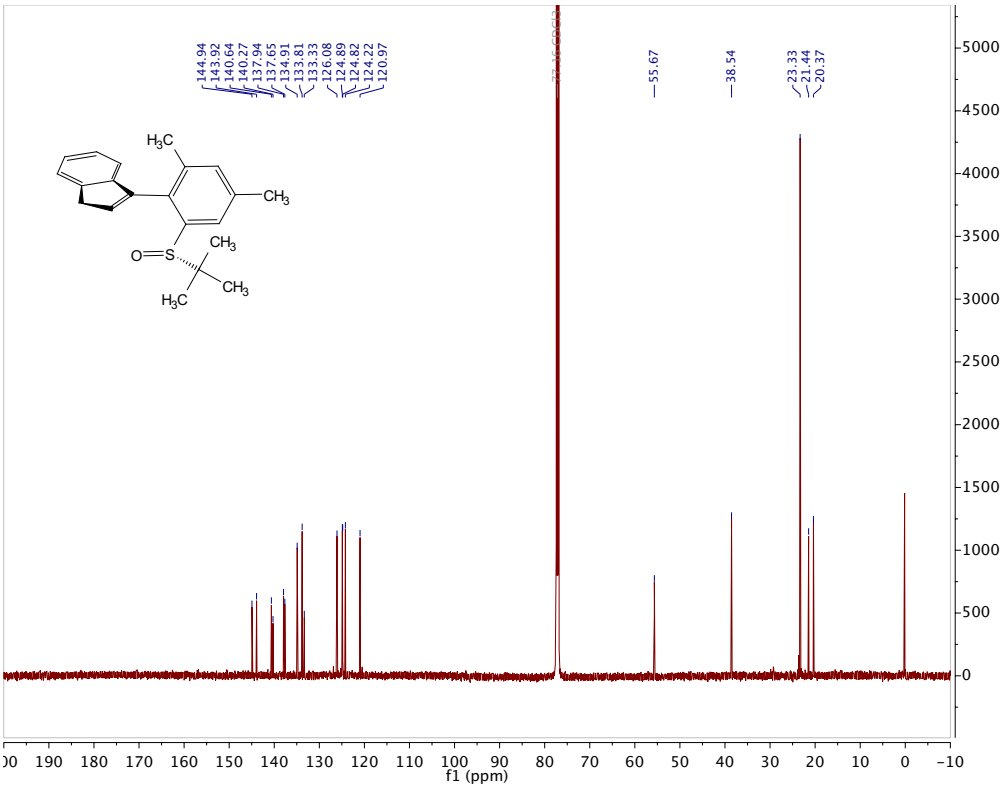

(R)-3-(2-(tert-butylsulfinyl)-4,6-dimethoxyphenyl)-1H-indene (3.41b)

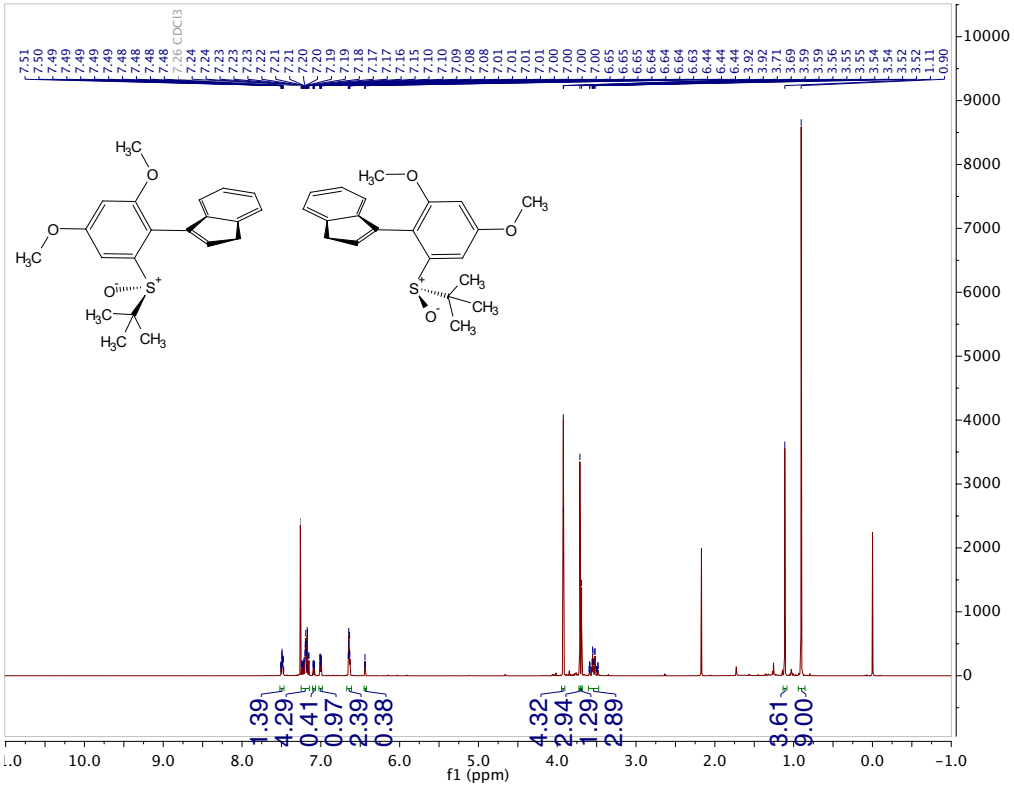

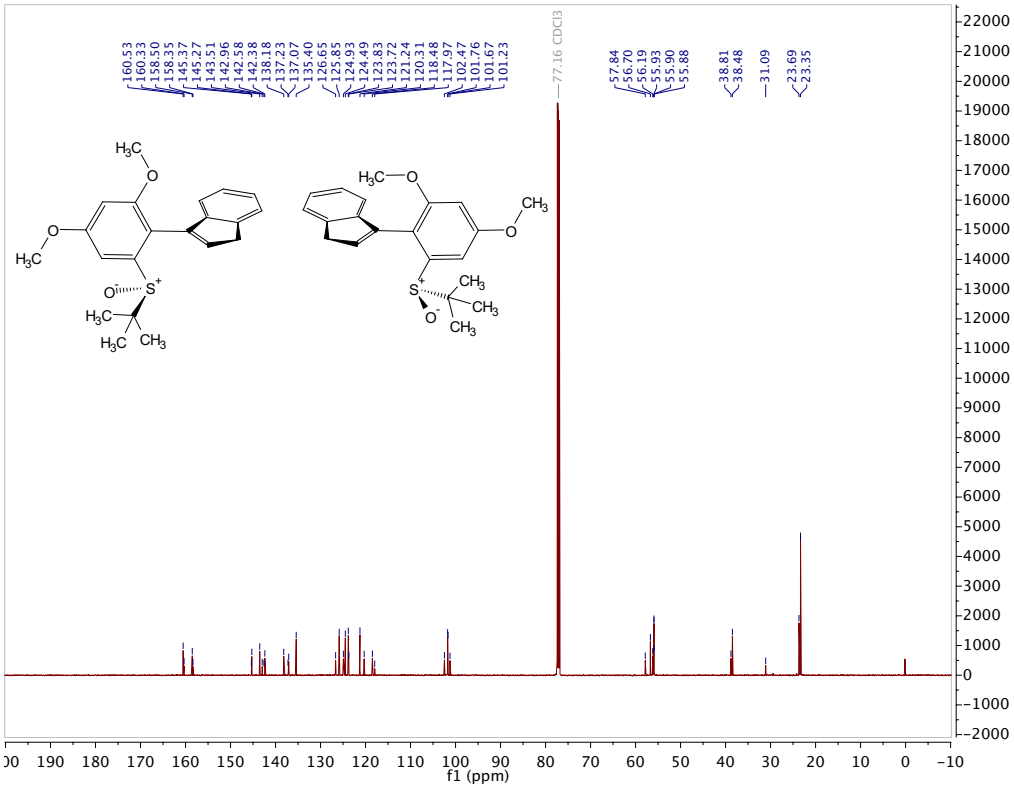

(R)-3-(2-(tert-butylsulfinyl)-4,6-dimethylphenyl)-2-methyl-1H-indene (**3.39**)

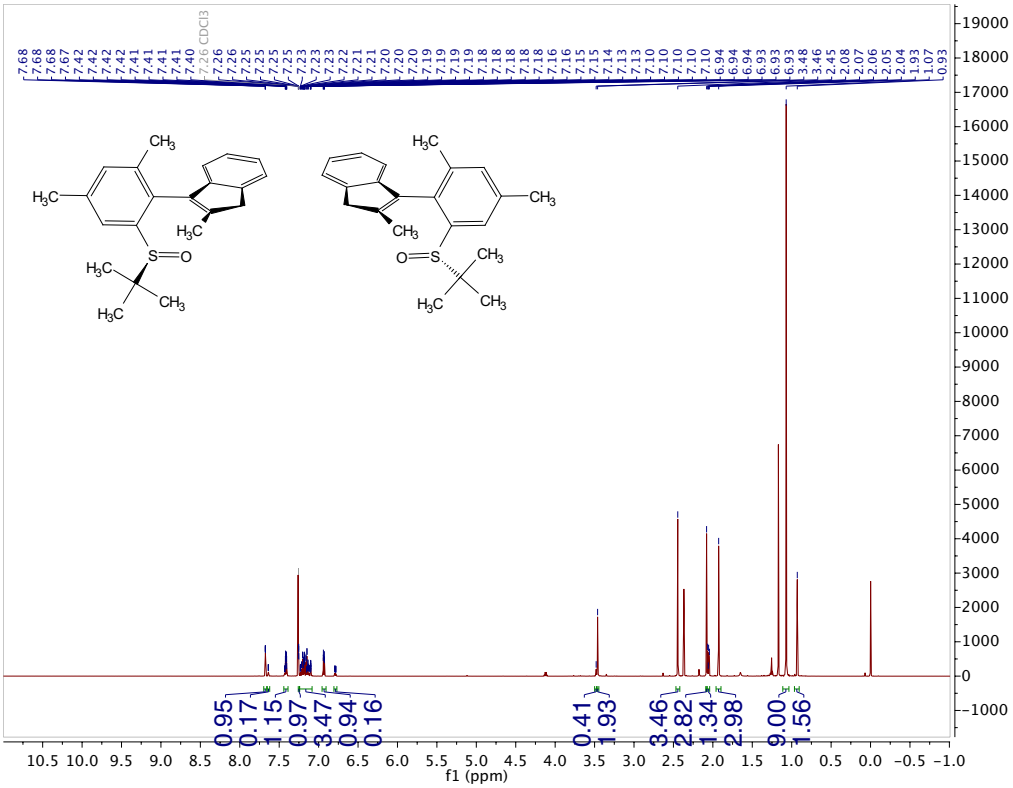

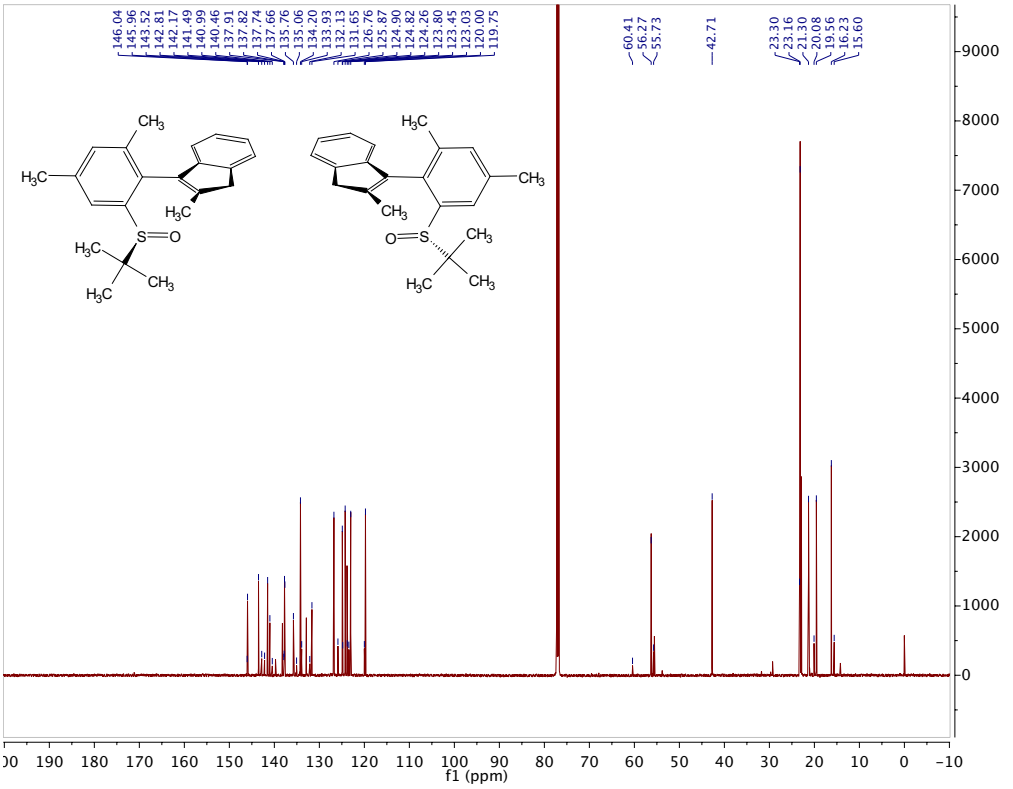

Chapter 4. Designing a Planar Chiral Rhodium Indenyl Catalyst for Regio- and Enantioselective Allylic C–H Amidation[1]

In this chapter, we will discuss the design of a simplified planar chiral rhodium indenyl catalyst platform for enantioselective allylic C–H functionalization. This work was published as a co-first author paper in JACS in 2020. Adapted with permission from Farr, C. M. B.; Kazerouni, A. M.; Park, B.; Poff, C. D.; Won, J.; Sharp, K. R.; Baik, M.-H.; Blakey, S. B. *J. Am. Chem. Soc.* **2020**, *142*, 13996-14004. Copyright 2020 American Chemical Society.

4.1 Introduction to Blakey Group Allylic C–H Functionalization

4.1.1 First Generation Racemic Allylic Amination and Etherification

In 2017, the Blakey group disclosed its first foray into the field of oxidative allylic C–H functionalization.[2] At the time, the field of oxidative allylic C–H functionalization was dominated by examples of palladium catalyzed functionalization of terminal olefins (**4.2**, **Figure 4.1a**).[3–10] While alkylation, oxidation, and amination reactions had been explored, the scope of olefins was limited to terminal systems. However, reports from the Cossy and Tanaka groups detailed the ability of rhodium to

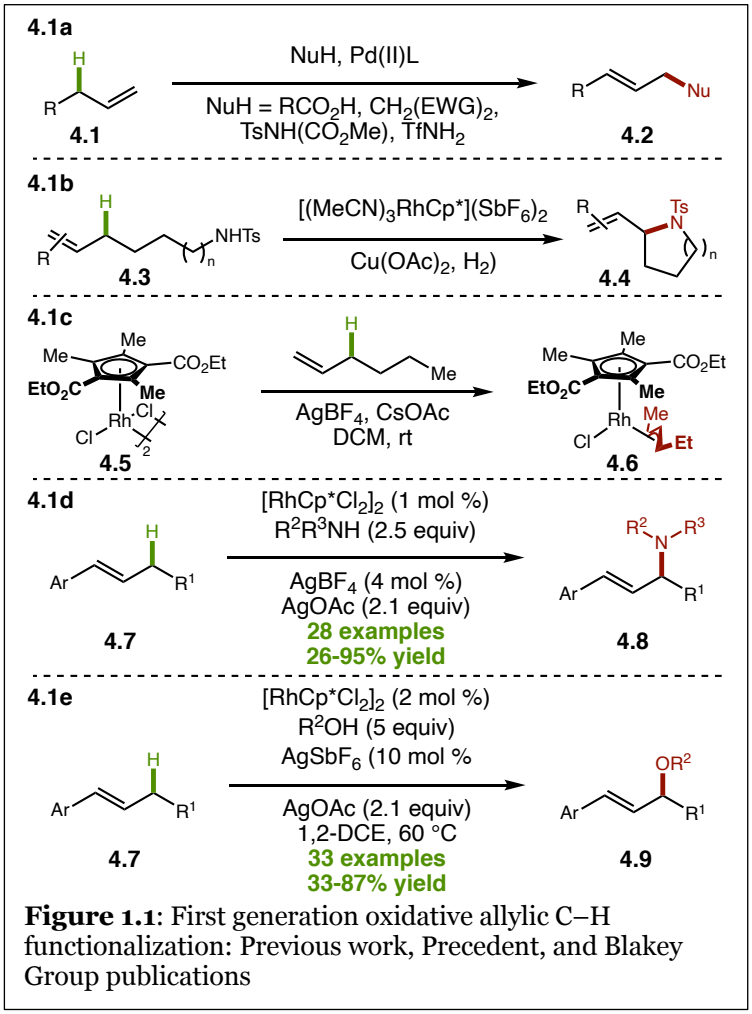

Figure 1.1: First generation oxidative allylic C–H functionalization: Previous work, Precedent, and Blakey Group publications

carry out oxidative allylic C–H functionalization (**4.3** to **4.4**, **Figure 4.1b**)[11] and the isolation of rhodium π-allyl complexes (**4.6**) that had originated from the C–H activation of a 1,2-disubstituted olefin (**Figure 4.1c**).[12] These reports provided the basis for Burman *et al.* to investigate the rhodium catalyzed oxidative allylic C–H amination of internal olefins (**Figure 4.1d**).[2] This work was followed shortly thereafter with a report on oxidative allylic C–H etherification by Nelson *et al.* in 2018 (**Figure 4.1e**).[13]

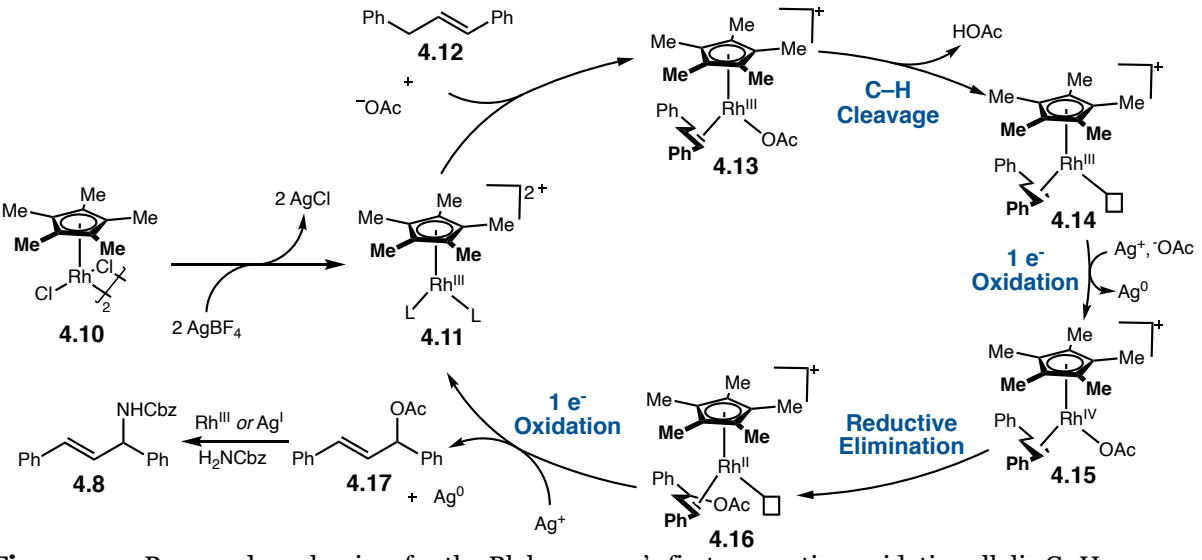

Figure 4.2: Proposed mechanism for the Blakey group's first generation oxidative allylic C–H functionalization

During these investigations, and in collaboration with the Cramer group, preliminary attempts at developing an enantioselective reaction by switching from an achiral Cp* to a chiral Cp were unsuccessful, and thus a detailed mechanistic investigation was performed.[14] Reports from Evans[15] and Miura[16] suggested a Rh(III)-Rh(I) pathway would be in operation for this system, while the Glorious group proposed a Rh(III)-Rh(V) mechanism instead.[17] Careful isolation and mechanistic experiments conducted from key potential reaction intermediates, however, led to the proposal of a Rh(III)-Rh(IV)-Rh(II)-Rh(III) pathway (**Figure 4.2**).[14] One key aspect of this pathway within the context of allylic amination is that the catalytic product is an allylic acetate (**4.17**), and not the allylic amine isolated. Further studies showed that the allylic amine is likely formed through a S_N1-type pathway that can be catalyzed by either the RhCp* catalyst, or silver halide scavenger. The formation of the allylic amine under this mechanistic

paradigm explains the lack of enantioinduction when chiral catalysts were explored in place of the achiral Cp* platform.

4.1.2 Second Generation Oxidative Allylic C–H Functionalization

In a quest to expand the scope of competent nucleophiles to include amide precursors, Dr. Jacob Burman, a graduate student in the Blakey group at the time, began exploring the use of dioxazolones (**4.20**, **Figure 4.3a**) under similar reaction conditions.[18] Observing a change in regioselectivity from previous reactions, the allylic amidation with dioxazolones was believed to be operating under a new mechanistic paradigm. A Rh(III)-Rh(V) pathway was proposed as work from the Chang lab has popularized the use of dioxazolones **4.20** as nitrene precursors.[21–26] Concurrent reports from the Rovis, Glorius, and Blakey groups detailed the rhodium and iridium Cp* catalyzed allylic amidation reactions from these dioxazolones (**Figure 4.3a**).[19,20] This mechanism would use the cleavable N-O bond of the dioxazolone to aid in the formation of a Rh(V) nitrenoid intermediate (see **4.24**, **Figure 4.3b** for a representative example). Facile reductive elimination from this intermediate would afford the observed C–N bond formation.

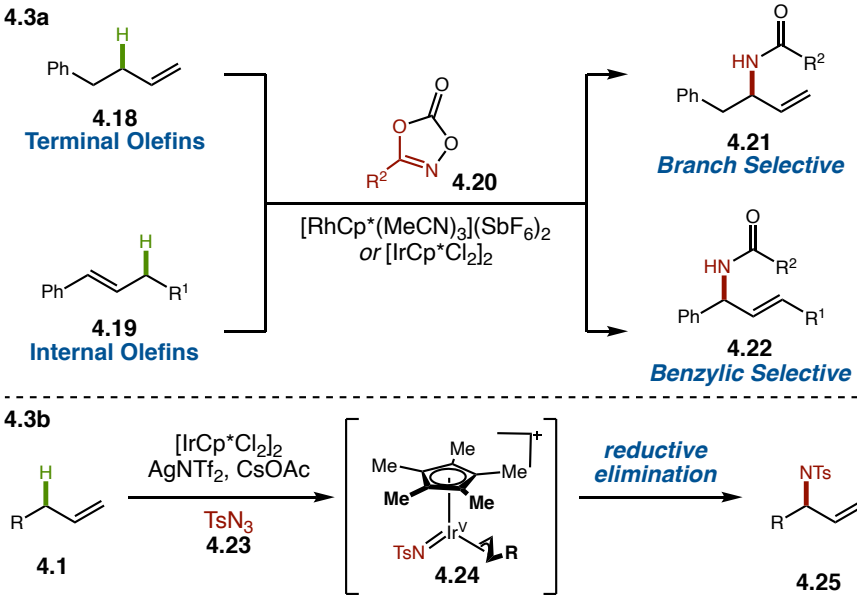

Figure 4.3: Allylic C–H amidation with dioxazolones and azides

Follow-up work from Kazerouni *et al.* expanded the scope of competent nitrenoid precursors in this transformation to azides (**4.23**, **Figure 4.3b**).[27] Under this "second generation" mechanistic paradigm, evidence has been growing to strongly suggest the Rh(III)-Rh(V) pathway that delivers key C–N bond formation *via* a reductive elimination pathway in the catalytic cycle

(**4.24** to **4.25**). This proposed pathway moves the key bond forming step the catalytic cycle, in contrast to the off-cycle S_N1-type bond formation like the "first generation" system. Now, the possibility for enantioinduction by switching from an achiral Cp* to a chiral Cp becomes a reality.

4.2 Design of a Planar Chiral Rhodium Indenyl Ligand Platform for Enantioselective C–H Functionalization

4.2.1 From Model System to Active Catalyst

As previously discussed in the first and second chapters of this dissertation, the scope of available chiral Cp platforms for use as enantioselective catalysis has been dominated by C_2-symmetric ligand platforms.[28] However, in the Blakey group, we sought to develop a new catalyst platform to induce enantioselectivity in our allylic amidation system. Outlined in Chapter 3 of this dissertation, work had already begun internally on a planar chiral indenyl platform. Specifically focused on indene ring slip delivering electronic asymmetry to a π-allyl intermediate, we wondered if this electronic control would be sufficient to provide enantioinduction in the allylic amidation reaction. The sulfoxide-tethered Baker-type catalyst scaffold **4.26** was proposed, but the presence of the sulfoxide tether occupied a coordination site on the rhodium center that would need to be available for dioxazolone coordination and nitrene formation (**Figure 4.4**).[29] Thus, working with Dr. Caitlin Farr and Dr. Amaan Kazerouni, we endeavored to explore if a simplified planar chiral indenyl catalyst without the sulfoxide tether (**4.27**) would act as a competent catalyst (See page 99 for contribution detail).

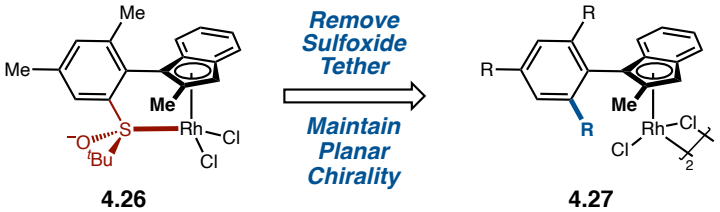

4.26 4.27

Figure 4.4: Planar chiral indenyl catalyst redesign

Through model studies examining the arylation stragety of indanone **4.28**, an intermediate in route to the Baker-type platform, we had accessed 2-methyl-3-phenylindene **4.29** (**Scheme 4.1a**).[30–32] We were able to complex this pre-ligand onto Rh(I) as a racemic mixture of two planar chiral enantiomers (***rac*-4.30**) prior to oxidation with iodine to the racemic Rh(III) diiodide dimer ***rac*-4.31** as the desired pre-catalyst for the system. Gratifyingly, the direct application of

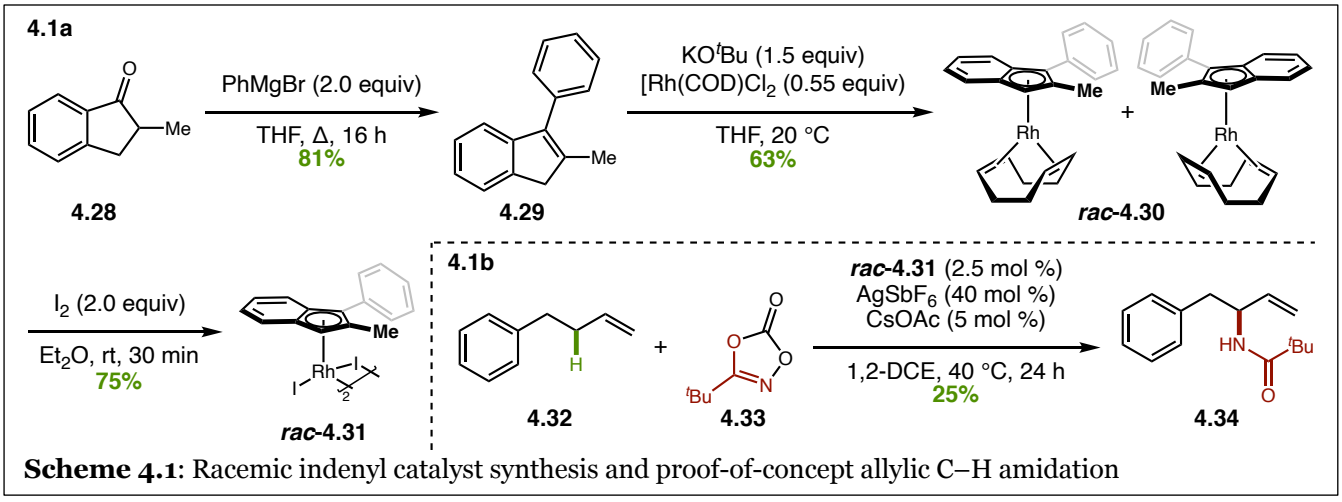

Scheme 4.1: Racemic indenyl catalyst synthesis and proof-of-concept allylic C–H amidation

racemic indenyl pre-catalyst **4.31** to the published allylic amidation conditions afforded the desired branched product **4.34** (**Scheme 4.1b**).[18] While the yield was modest, this result provided a proof-of-concept that asymmetrically substituted indenyl ligands would be effective catalysts in this system.

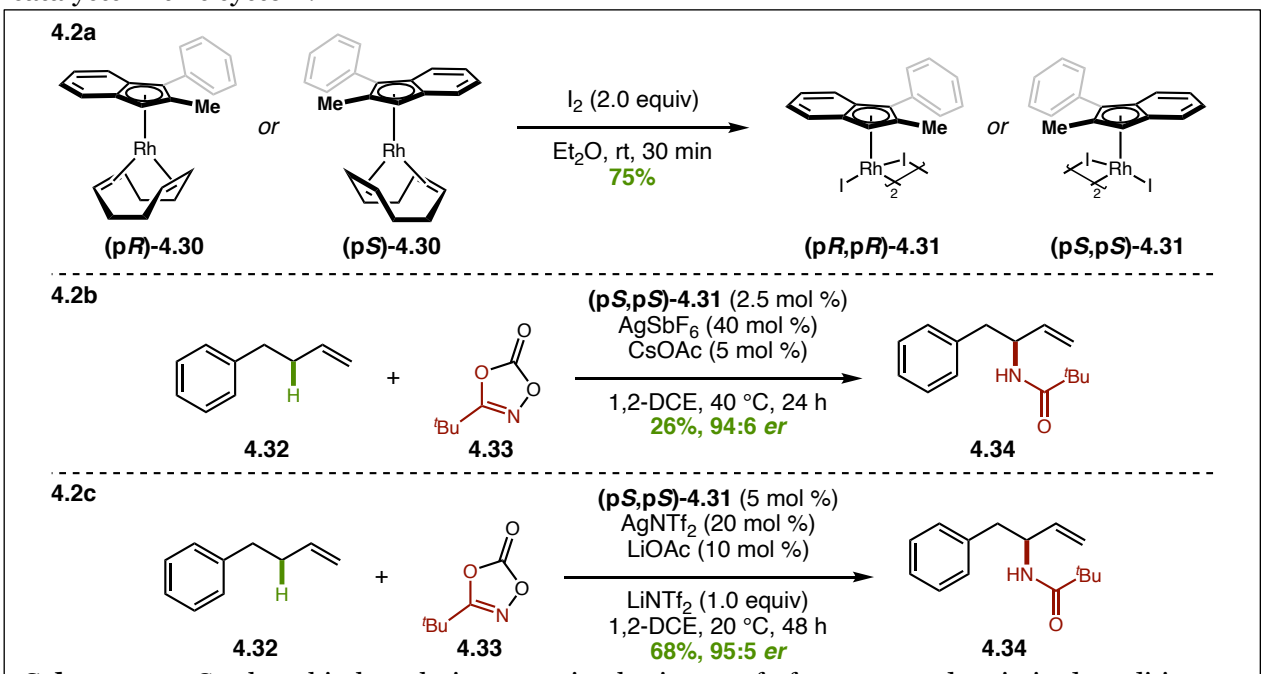

Scheme 4.2: Catalyst chiral resolution, enantioselective proof-of-concept, and optimized conditions

With this result in hand, Dr. Caitlin Farr took the lead on determining if the synthetic route was amenable to chiral resolution. In fact, the Rh(I) indene complex ***rac*-4.30** was surprisingly stable, avoiding air oxidation under ambient storage conditions, and the planar chiral enantiomers (**(p*R*)-4.30** and **(p*S*)-4.30**) were separable by chiral preparative HPLC (**Scheme**

4.2a). Upon chiral resolution, each enantiomer could be oxidized separately to the enantiopure Rh(III) dihalide pre-catalyst (**(p*R*,p*R*)-4.31** or **(p*S*,p*S*)-4.31**). Application of the enantioenriched Rh(III) indenyl pre-catalyst to the same allylic amidation test reaction successfully generated enantioenriched allylic amide **4.34** in a still modest 26% yield with an excellent 94:6 *er* (**Scheme 4.2b**). After a brief survey of catalyst and reaction conditions, Dr. Farr was able to increase the yield of this reaction to 68% while maintaining a high enantioselectivity with a 95:5 *er* (**Scheme 4.2c**).

4.2.2 Stereochemical Determination of the Catalyst and Allylic Amide Products

With a successful and highly enantioselective catalyst in hand, one of my primary roles on this project was to determine the stereochemistry of both the enantiopure 2-methyl-3-phenylindenyl catalyst and the allylic amide products being formed.

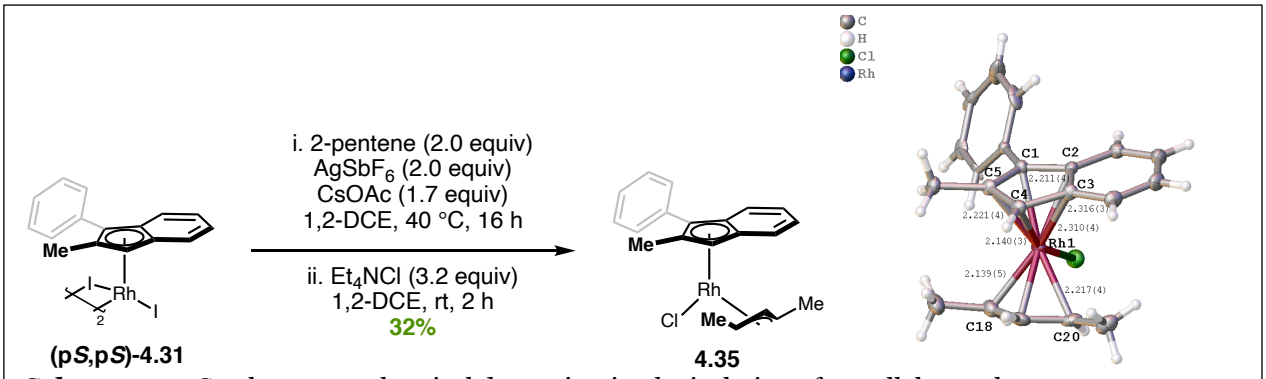

Scheme 4.3: Catalyst stereochemical determination by isolation of a π-allyl complex

The first goal was to determine the catalyst stereochemistry. In previous mechanistic studies conducted in our group, extensive work had been completed related to the synthesis of RhCp* π-allyl complexes.[14,18] Utilizing this work, and Baker's stoichiometric studies, as precedent we were able to synthesize a Rh(2-Me-3-Ph-Ind) π-allyl complex (**4.35**) and successfully isolate a single crystal sufficient for x-ray diffraction studies **Scheme 4.3**.[32] The crystallographic data confirmed that the $P2_1$ space group for this crystal was chiral, allowing us to confidently determine that the conformation observed was for a single enantiomer. Once complexed to rhodium, the indenyl ligand should not disassociate from the rhodium metal center. Thus, we extrapolated that the observed planar enantiomer **4.35** would be consistent between the isolated π-allyl complex and

the diiodide dimer pre-catalyst and determined this crystal structure as having come from the **(p*S*,p*S*)-4.31** enantiomer of pre-catalyst.

Interestingly, and analogous to observations from Baker,[29,32] this structure also provides crystallographic evidence for the indenyl ring slip and the *trans* effect on the π-allyl ligand. The Rh-C1, Rh-C5, and Rh-C4 bonds to the more localized allylic fragment of the indene are 2.211, 2.221, and 2.140 Å, respectively (**Scheme 4.3**). In contrast, the Rh-C2 and Rh-C3 bonds are a lengthened 2.316 and 2.310 Å as the benzene moiety begins to restore aromaticity and lift away from the metal center. Translating these observations to the π-allyl fragment, the Rh-C20 bond (trans to the more localized allylic fragment of the indene) is 2.217 Å while the Rh-C18 bond (trans to the benzene moiety that is lifting away from the metal center) is a shorter 2.139 Å. This data will become important during stoichiometric, mechanistic, and computational studies discussed in later sections.

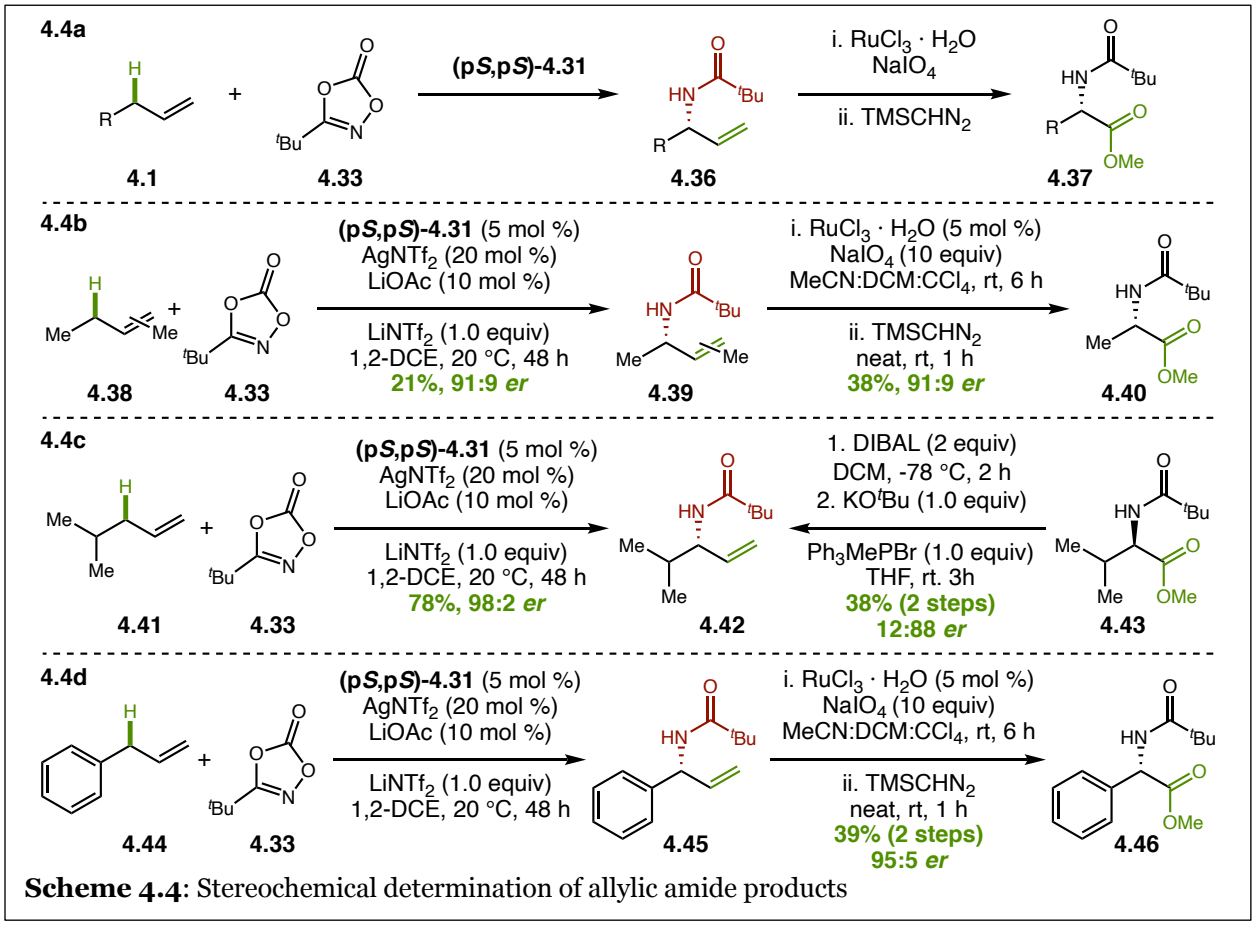

Scheme 4.4: Stereochemical determination of allylic amide products

For the stereochemical determination of the products, we envisioned a scheme to transform the amidated products **4.36** into amino acid derivatives **4.37** *via* oxidative cleavage of the resulting olefin to the carboxylic acid and capping this as the methyl ester (**Scheme 4.4a**). When we used *tert*-butyl dioxazolone (**4.33**), the amide fuctions like a pivaloyl protecting group. Through purchase of enantiopure of amino acid methyl ester precursors and subsequent pivaloyl protection of the nitrogen, enantiomerically pure standards for each substrate were obtained. With respect to the olefin substrates for these tests, we chose 2-pentene (**4.38**), 4-methylpentene (4.**41**), and allyl benzene (**4.44**). Careful attention was taken during the choice of these olefins as we sought to modulate the steric and electronic identity of the homoallylic position from small alkyl (**4.38**) to bulkier branched alkyl (**4.41**), and finally to an aromatic group (**4.44**). After allylic amidation with *tert*-butyl dioxazolone (**4.33**), oxidative cleavage of the olefin, and esterification, these olefins were transformed into pivaloyl protected alanine (**4.40**, **Scheme 4.4b**), valine (**4.43**, **Scheme 4.4c**), and phenylalanine (**4.46**, **Scheme 4.4d**), respectively. HPLC analysis confirmed that the same major stereocenter was formed in each case, showcasing that the same source of enantioinduction was in operation across a range of steric and electronic effects.

4.2.3 Reaction Scope

Having synthesized a highly enantioselective catalyst and determined the stereochemistry of both the catalyst and the products, we investigated the scope of this reaction. For examining the dioxazolone scope, we chose 4-methylpentene **4.41** as the olefin, having explored this substrate during stereochemical investigations. Sterically small methyl (**4.47**), bulky *tert*-butyl (**4.42**), and cyclic cyclohexyl (**4.48**) dioxazolones were well tolerated (**Figure 4.5a**). The presence of heteroatoms in the form of ether **4.49** and carbamate **4.50** experienced success with moderate yields but high selectivity. Aryl containing dioxazolones bearing benzyl and phenyl substituents afforded the amidated products **4.51** and **4.52** in lower yields (37%, and 13%, respectively) but still with high selectivities (99:1 *er*, and 99:1 *er*). The reduced yield of **4.52** with phenyl dioxazolone is consistent with previous racemic

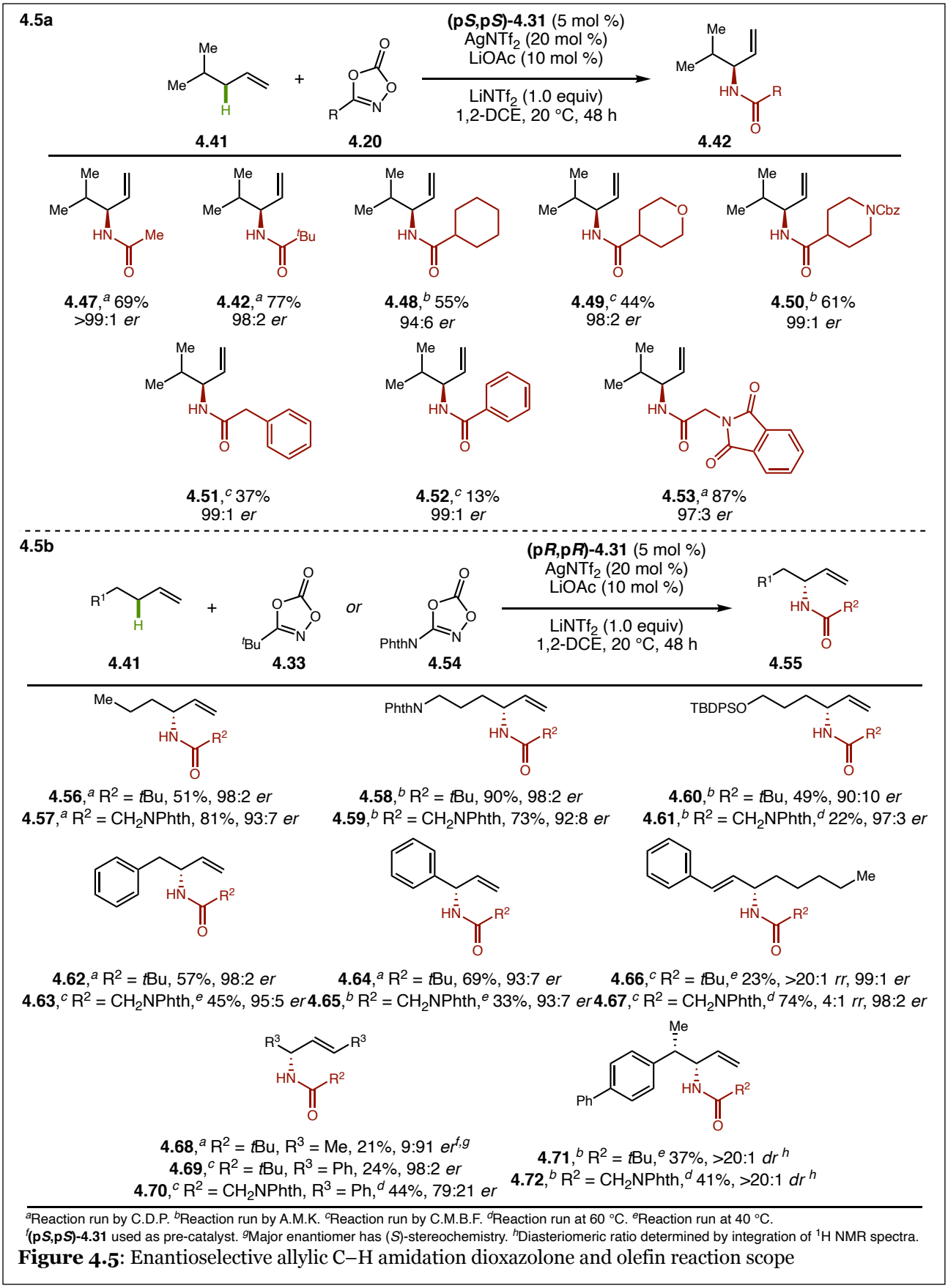

[a]Reaction run by C.D.P. [b]Reaction run by A.M.K. [c]Reaction run by C.M.B.F. [d]Reaction run at 60 °C. [e]Reaction run at 40 °C.
[f](pS,pS)-4.31 used as pre-catalyst. [g]Major enantiomer has (S)-stereochemistry. [h]Diasteriomeric ratio determined by integration of ^{1}H NMR spectra.

Figure 4.5: Enantioselective allylic C–H amidation dioxazolone and olefin reaction scope

reaction results and is believed to arise from the dioxazolone interacting with rhodium prior to π-allyl formation. Finally, a glycine-derived dioxazolone afforded allylic amide **4.53** with 87% yield and a 97:3 *er*, highlighting the capability of utilizing an amino-acid derived dioxazolone in this chemistry.

During investigation of the olefin scope, we began to discern subtle nuances in the balances of stereoelectronic effects in this reaction. As such, each olefin substrate was examined with both *tert*-butyl dioxazolone **4.33** and glycine-derived dioxazolone **4.54** (**Figure 4.5b**). Simple linear hexene (**4.56**-**4.57**) as well as similar straight chain terminal alkenes featuring carbamate (**4.58**-**4.59**) or silyl ether (**4.60**-**4.61**) functionality were functionalized with moderate to good yields and consistently with high selectivities. Aryl containing terminal olefins and were well tolerated for selectivity albeit with variable yields (**4.62**-**4.65**). This system was able to functionalize 1,2-dibstituted, internal olefins in low to moderate yield but, primarily, with good selectivity (**4.66**-**4.70**). Notably, the 2-pentene (**4.68**) and 1,3-diphenylpropene (**4.69**-**4.70**) substrates, which go through ostensible symmetrical π-allyl intermediates, were successful in the desymmetrization of the intermediate. Finally, the presence of a homoallylic stereocenter proceeded with excellent diasterioselectivity when reacted with the matched catalyst pair (**4.71**-**4.72**).

4.2.4 Mechanistic and Computational Studies

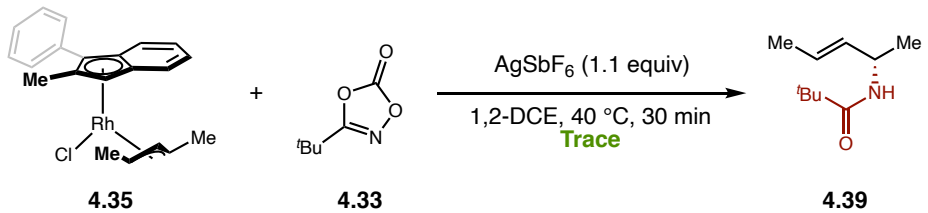

4.35 **4.33** **4.39**

Scheme 4.5: Stoichiometric amidation of π-allyl complex

In addition to isolation of the Rh(2-Me-3-Ph-Ind) π-allyl complex **4.35** for determination of stereochemistry, we also used this complex stoichiometrically to further probe the Rh(III)-Rh(V) mechanistic proposal. Reaction of complex **4.35** with *tert*-butyl dioxazolone **4.33** and a halide scavenger afforded trace amounts of the allylic amide **4.39** (**Scheme 4.5**).[1] Delivering the same enantiomer as the catalytic reaction, this result suggests that

reductive elimination from the nitrene intermediate would have occurred to the termini of the π-allyl that is respectively longer, *trans* to the localized allyl fragment of the indene.

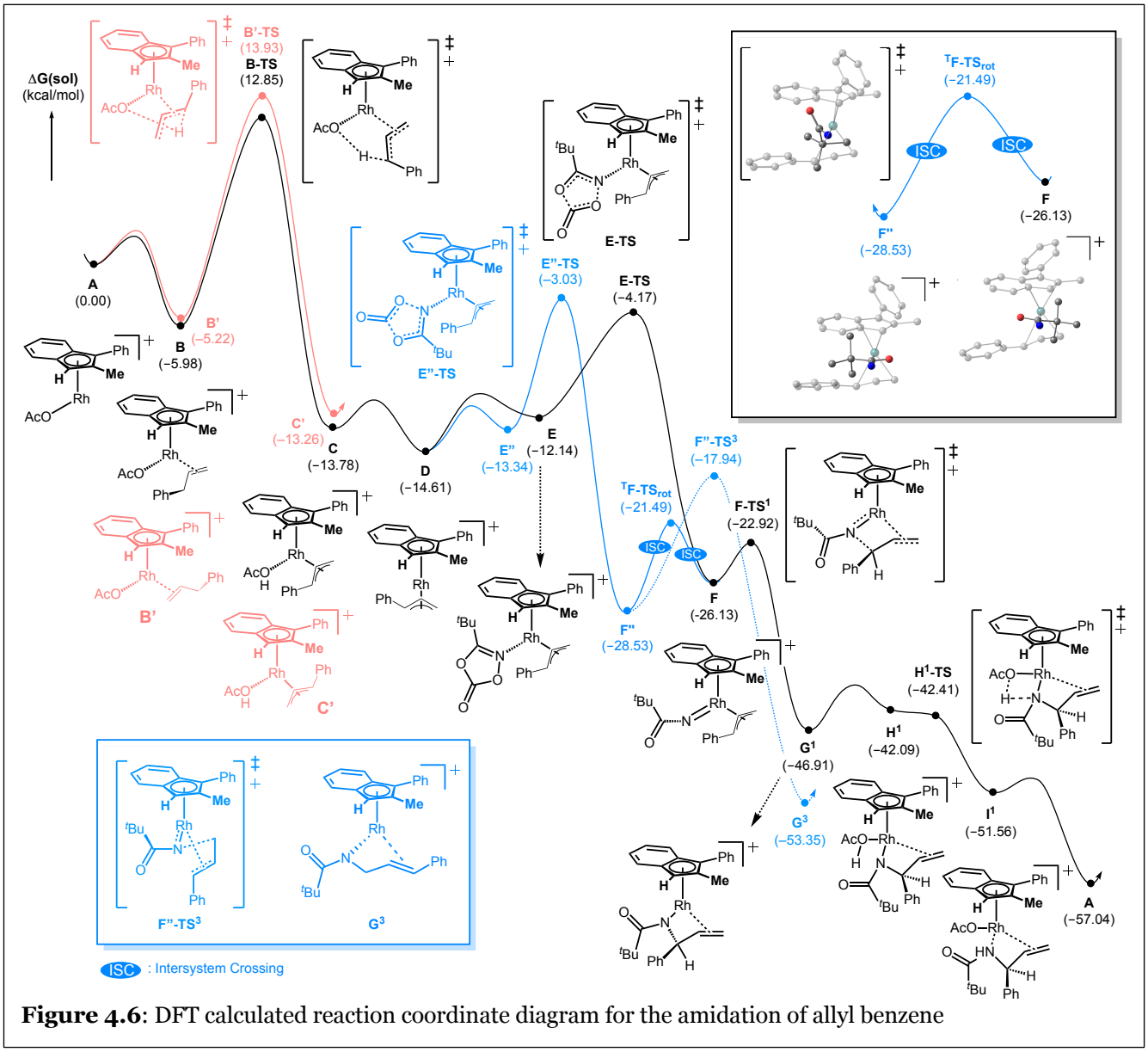

Figure 4.6: DFT calculated reaction coordinate diagram for the amidation of allyl benzene

To further uncover the source of regio- and enantioselectivity in this reaction, mechanistic studies were performed in collaboration with the Baik group at the Korea Advanced Institute of Science and Technology (KAIST). Density functional theory (DFT) calculations of key intermediates afforded the mechanistic pathway outlined in **Figure 4.6**.[1] First, olefin coordination to **A** affords **B** or **B'** before rate- and enantiodetermining C–H activation. Here, the energy difference between **B-TS** and **B'-TS** is largely controlled by steric differences between the

removed, planar benzene moiety of the indene and the proximity of the methyl substituent at the indene 2-position. After C–H activation (**C**), ligand exchange (**C** to **D** to **E**) allows the dioxazolone to coordinate providing **E** or **E”**. The orientation of the dioxazolone coordination effects the energy difference between **E-TS** and **E”-TS**, with the orientation of **F”** being slightly lower in energy than **F**. However, while reductive elimination to **G**[3] would afford a more thermodynamically stable linear product, electronic bias from the indene ring slip helps in directing reductive elimination to afford the branched product observed. Due in part to this bias, **F”** can enter a triplet energy state through ^{T}**F”-TS**$_{rot}$ to allow the dioxazolone to rotate to **F**. Guided by the indene ring slip, reductive elimination from **F** to the internal position of the π-allyl leads to **G**[1]. Finally, protodemetalation and release of the olefin product reforms complex **A**.

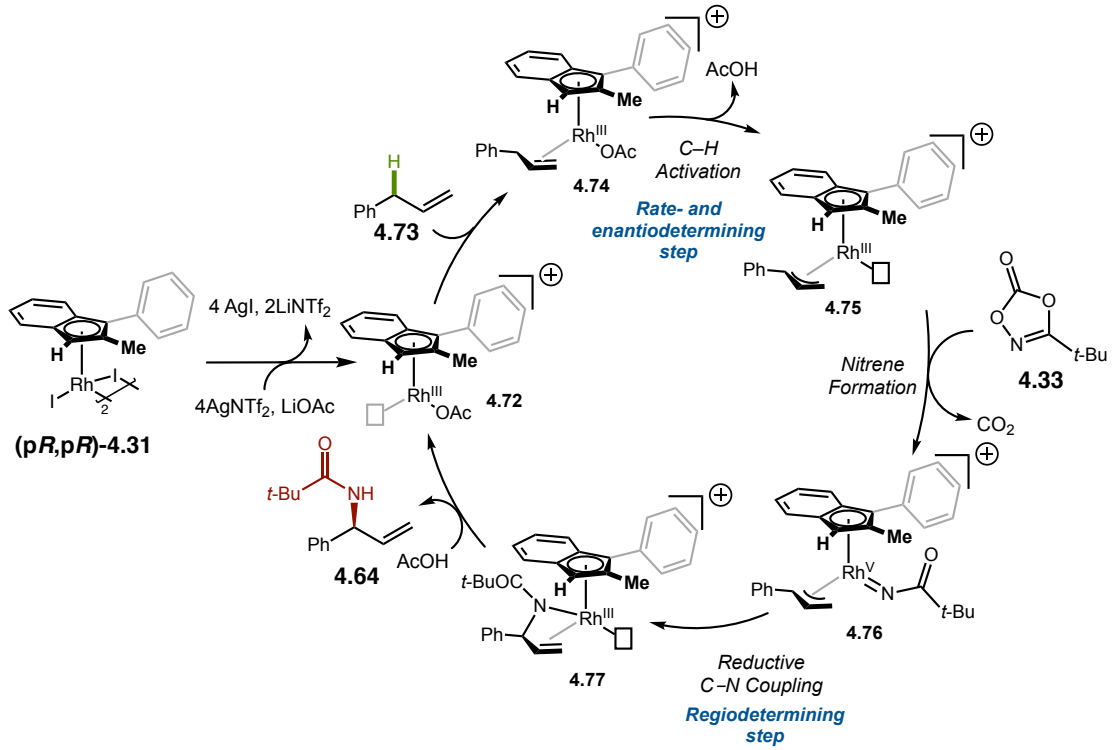

Figure 4.7: Proposed catalytic cycle for the allylic C–H amidation of allyl benzene with *tert*-butyl dioxazolone

The combination of observed reactivity trends, computational insight from the Baik group, and previous stoichiometric investigations allow for the proposal of the catalytic cycle in **Figure 4.7**.[1] Initially, the diiodide dimer pre-catalyst **(p*R*,p*R*)-4.31** is activated through halide abstraction and acetate coordination to enter the catalytic cycle as **4.72**. Olefin (**4.73**)

coordination provides **4.74** which can undergo rate- and enantiodetermining C–H activation, forming **4.75**. Coordination of dioxazolone **4.33**, CO_2 extrusion, and 2-electron oxidation of the metal center generates Rh(V) nitrenoid **4.76**. The high oxidation state of rhodium promotes facile regiodetermining reductive elimination to the lengthened termini of the π-allyl *syn* to the benzene moiety of the indene (**4.77**). Finally, protodemetallation and release of olefin **4.64** forms the product and allows the rhodium complex to reenter the catalytic cycle as **4.72**.

4.3 Conclusion

Through these studies we have disclosed the development of a simplified planar chiral rhodium indenyl complex capable of acting as an enantioselective catalyst for an allylic C–H amidation reaction. The simple ligand scaffold can be accessed in 2-steps allowing for rapid diversification of the scaffold. Crystallographic evidence supports the transmission of an electronic asymmetry guided by the ring slip of the indene. This electronic asymmetry plays a significant role in the regiodetermining step of the catalytic cycle, which can also act as the enantiodetermining step when desymmeterizing an otherwise symmetrical π-allyl intermediate. Since the publication of this work, several additional generations of the indenyl catalyst platform have been synthesized and used during enantioselective catalytic studies. Current work by Patrick Gross is aimed at demonstrating the enantioselective ability of this platform to act on reactions outside of allylic C–H functionalization chemistry.

4.4 References

(1) Farr, C. M. B.; Kazerouni, A. M.; Park, B.; Poff, C. D.; Won, J.; Sharp, K. R.; Baik, M. H.; Blakey, S. B. Designing a Planar Chiral Rhodium Indenyl Catalyst for Regio- And Enantioselective Allylic C-H Amidation. *J. Am. Chem. Soc.* **2020**, *142*, 13996–14004.

(2) Burman, J. S.; Blakey, S. B. Regioselective Intermolecular Allylic C–H Amination of Disubstituted Olefins via Rhodium/π-Allyl Intermediates. *Angew. Chem. Int. Ed.* **2017**, *56*, 13666–13669.

(3) Chen, M. S.; White, M. C. A Sulfoxide-Promoted, Catalytic Method for the Regioselective Synthesis of Allylic Acetates from Monosubstituted Olefins via C-H Oxidation. *J. Am. Chem. Soc.* **2004**, *126*, 1346–1347.

(4) Chen, M. S.; Prabagaran, N.; Labenz, N. A.; White, M. C. Serial Ligand Catalysis: A Highly Selective Allylic C-H Oxidation. *J. Am. Chem. Soc.* **2005**, *127*, 6970–6971.

(5) Fraunhoffer, K. J.; White, M. C. Syn-1,2-Amino Alcohols via Diastereoselective Allylic C-H Amination. *J. Am. Chem. Soc.* **2007**, *129*, 7274.

(6) Young, A. J.; White, M. C. Catalytic Intermolecular Allylic C-H Alkylation. *J. Am. Chem. Soc.* **2008**, *130*, 14090.

(7) Reed, S. A.; White, M. C. Catalytic Intermolecular Linear Allylic C-H Amination via Heterobimetallic Catalysis. *J. Am. Chem. Soc.* **2008**, *130*, 3316.

(8) Reed, S. A.; Mazzotti, A. R.; White, M. C. A Catalytic, Bronsted Base Strategy for Intermolecular Allylic C-H Amination. *J. Am. Chem. Soc.* **2009**, *131*, 11701–11706.

(9) Pattillo, C. C.; Strambeanu, J. I.; Calleja, P.; Vermeulen, N. A.; Mizuno, T.; White, M. C. Aerobic Linear Allylic C-H Amination: Overcoming Benzoquinone Inhibition. *J. Am. Chem. Soc.* **2016**, *138*, 1265–1272.

(10) Campbell, A. N.; White, P. B.; Guzei, I. A.; Stahl, S. S. Allylic C-H Acetoxylation with a 4,5-Diazafluorenone-Ligated Palladium Catalyst: A Ligand-Based Strategy To Achieve Aerobic Catalytic Turnover. *J. Am. Chem. Soc.* **2010**, *132*, 15116–15119.

(11) Cochet, T.; Bellosta, V.; Roche, D.; Ortholand, J.-Y.; Greiner, A.; Cossy, J. Rhodium(Iii)-Catalyzed Allylic C–H Bond Amination. Synthesis of Cyclic Amines from ω-Unsaturated N-Sulfonylamines. *Chem. Commun.* **2012**, *48*, 10745–10747.

(12) Shibata, Y.; Kudo, E.; Sugiyama, H.; Uekusa, H.; Tanaka, K. Facile Generation and Isolation of π-Allyl Complexes from Aliphatic Alkenes and an Electron-Deficient Rh(III) Complex: Key Intermediates of Allylic C–H Functionalization. *Organometallics* **2016**, *35*, 1547–1552.

(13) Nelson, T.; Blakey, S. B. Intermolecular Allylic C–H Etherification of Internal Olefins. *Angew. Chem. Int. Ed.* **2018**, *57*, 14911-14915.

(14) Harris, R. J.; Park, J.; Nelson, T. A. F.; Iqbal, N.; Salgueiro, D. C.; Bacsa, J.; Macbeth, C. E.; Baik, M. H.; Blakey, S. B. The Mechanism of Rhodium-Catalyzed Allylic C-H Amination. *J. Am. Chem. Soc.* **2020**, *142*, 5842–5851.

(15) Evans, P. A.; Nelson, J. D. Conservation of Absolute Configuration in the Acyclic Rhodium-Catalyzed Allylic Alkylation Reaction: Evidence for an Enyl (σ + π) Organorhodium Intermediate. *J. Am. Chem. Soc.* **1998**, *120*, 5581–5582.

(16) Satoh, T.; Miura, M. Oxidative Coupling of Aromatic Substrates with Alkynes and Alkenes under Rhodium Catalysis. *Chem. Eur. J.* **2010**, *16*, 11212–11222.

(17) Vásquez-Céspedes, S.; Wang, X.; Glorius, F. Plausible Rh(V) Intermediates in Catalytic C–H Activation Reactions. *ACS Catal.* **2017**, *8*, 242–257.

(18) Burman, J. S.; Harris, R. J.; Farr, C. M. B.; Bacsa, J.; Blakey, S. B. Rh(III) and Ir(III)Cp∗ Complexes Provide Complementary Regioselectivity Profiles in Intermolecular Allylic C-H Amidation Reactions. *ACS Catal.* **2019**, *9*, 5474–5479.

(19) Lei, H.; Rovis, T. Ir-Catalyzed Intermolecular Branch-Selective Allylic C–H Amidation of Unactivated Terminal Olefins Scheme 1. Catalytic Allylic C–H Amidation. *J. Am. Chem. Soc.* **2019**, *141*, 2268–2273.

(20) Knecht, T.; Mondal, S.; Ye, J. H.; Das, M.; Glorius, F. Intermolecular, Branch-Selective,

and Redox-Neutral Cp*IrIII-Catalyzed Allylic C–H Amidation. *Angew. Chem. Int. Ed.* **2019**, *58*, 7117–7121.

(21) Park, Y.; Jee, S.; Kim, J. G.; Chang, S. Study of Sustainability and Scalability in the Cp*Rh(III)-Catalyzed Direct C-H Amidation with 1,4,2-Dioxazol-5-Ones. *Org. Process Res. Dev.* **2015**, *19*, 1024–1029.

(22) Shin, K.; Park, S.-W.; Chang, S. Cp*Ir(III)-Catalyzed Mild and Broad C–H Arylation of Arenes and Alkenes with Aryldiazonium Salts Leading to the External Oxidant-Free Approach. *J. Am. Chem. Soc.* **2015**, *137*, 8584–8592.

(23) Park, Y.; Park, K. T.; Kim, J. G.; Chang, S. Mechanistic Studies on the Rh(III)-Mediated Amido Transfer Process Leading to Robust C-H Amination with a New Type of Amidating Reagent. *J. Am. Chem. Soc.* **2015**, *137*, 4534–4542.

(24) Park, Y.; Heo, J.; Baik, M. H.; Chang, S. Why Is the Ir(III)-Mediated Amido Transfer Much Faster Than the Rh(III)-Mediated Reaction? A Combined Experimental and Computational Study. *J. Am. Chem. Soc.* **2016**, *138*, 14020–14029.

(25) Park, J.; Lee, J.; Chang, S. Iterative C–H Functionalization Leading to Multiple Amidations of Anilides. *Angew. Chem. Int. Ed.* **2017**, *56*, 4256–4260.

(26) Hwang, Y.; Park, Y.; Chang, S. Mechanism-Driven Approach To Develop a Mild and Versatile C–H Amidation through IrIII Catalysis. *Chem. Eur. J.* **2017**, *23* 11147–11152.

(27) Kazerouni, A. M.; Nelson, T. A. F.; Chen, S. W.; Sharp, K. R.; Blakey, S. B. Regioselective Cp*Ir(III)-Catalyzed Allylic C-H Sulfamidation of Allylbenzene Derivatives. *J. Org. Chem.* **2019**, *84*, 13179–13185.

(28) Mas-Roselló, J.; Herraiz, A. G.; Audic, B.; Laverny, A.; Cramer, N. Chiral Cyclopentadienyl Ligands: Design, Syntheses, and Applications in Asymmetric Catalysis. *Ang. Chem. Int. Ed.* **2021**, *60*, 13198-13224.

(29) Baker, R. W. Asymmetric Induction via the Structural Indenyl Effect. *Organometallics* **2018**, *37*, 433-440.

(30) Biosca, M.; Salomó, E.; De La Cruz-Sánchez, P.; Riera, A.; Verdaguer, X.; Pàmies, O.; Diéguez, M. Extending the Substrate Scope in the Hydrogenation of Unfunctionalized Tetrasubstituted Olefins with Ir-P Stereogenic Aminophosphine-Oxazoline Catalysts. *Org. Lett.* **2019**, *21*, 807–811.

(31) Nalesnik, T. E.; Freudenberger, J. H.; Orchin, M. Hydrogenation Reactions with Hydridocobalt Tetracarbonyl. *J. Organomet. Chem.* **1981**, *221*, 193–197.

(32) Baker, R. W.; Radzey, H.; Lucas, N. T.; Turner, P. Stereospecific Syntheses and Structures of Planar Chiral Bidentate H5:KS-Indenyl-Sulfanyl and -Sulfinyl Complexes of Rhodium(III). *Organometallics* **2012**, *31*, 5622–5633.

Explanation of Contributions

The following describes the individual contributions of each of the co-first authors on the publication of enantioselective allylic amidation. Christopher David Poff completed the racemic catalyst synthesis, initial racemic reactivity test, stereochemical elucidation of the catalyst and products, and selected substrates within the dioxazolone and olefin scopes. Dr. Caitlin Farr completed the initial catalyst chiral resolution, initial enantioselective reactivity test, reaction optimization, and selected substrates within the dioxazolone and olefin scopes. Dr. Amaan Kazerouni completed selected substrates within the dioxazolone and olefin scopes as well as much of the racemic reactions to collect HPLC traces for full characterization. Bohyun Park was the primary graduate student from the Baik group working on the computationally generated reaction coordinate diagram.

4.5 Supplementary Information

4.5.1 General Information

All reactions were carried out under nitrogen atmosphere with anhydrous solvents in oven- or flame-dried glassware using standard Schlenk technique, unless otherwise stated. Anhydrous dichloromethane (DCM), diethyl ether (Et_2O), tetrahydrofuran (THF), and toluene were obtained by passage through activated alumina using a *Glass Contours* solvent purification system. 1,2-dichloroethane (DCE), 2,2,2-trifluoroethanol, 1,1,1,3,3,3-hexaflouroisopropanol (HFIP) were distilled over calcium hydride (CaH_2) and stored over activated molecular sieves. Solvents for workup, extraction, and column chromatography were used as received from commercial suppliers without further purification. 2-methyl-3-phenyl-1*H*-indene (2-Me-3-Ph-Ind), ((±)-[Rh(2-Me-3-Ph-Ind)(COD)]), (*S,S*)-[Rh(2-Me-3-Ph-Ind)I_2]$_2$, and (*R,R*)-[Rh(2-Me-3-Ph-Ind)I_2]$_2$ were stored and weighed in a nitrogen-filled glovebox. All other chemicals were purchased from Millipore Sigma, Strem Chemicals, Oakwood Chemicals, Alfa Aesar, or Combi-Blocks and used as received without further purification, unless otherwise stated.

^{1}H and ^{13}C nuclear magnetic resonance (NMR) spectra were recorded on a Varian Inova 600 spectrometer (600 MHz ^{1}H, 151 MHz ^{13}C), a Bruker 600 spectrometer (600 MHz ^{1}H, 151 MHz ^{13}C), a Varian Inova 500 spectrometer (500 MHz ^{1}H, 126 MHz ^{13}C), and a Varian Inova 400 spectrometer (400 MHz ^{1}H, 126 MHz ^{13}C) at room temperature in $CDCl_3$ (neutralized and dried over K_2CO_3 and activated molecular sieves) with internal $CHCl_3$ as the reference (7.26 ppm for ^{1}H, 77.16 ppm for ^{13}C), unless otherwise stated. Chemical shifts (δ values) were reported in parts per million (ppm) and coupling constants (*J* values) in Hz. Multiplicity was indicated using the following abbreviations: s = singlet, d = doublet, t = triplet, q = quartet, qn = quintet, m = multiplet, br = broad. High resolution mass spectra (HRMS) were obtained using a Thermo Electron Corporation Finigan LTQFTMS (at the Mass Spectrometry Facility, Emory University). High Pressure Liquid Chromatography (HPLC) was performed on an Agilent 1100 series HPLC utilizing CHIRALPAK AD-H, AS-H, OD-H and OJ-H 4.6 x 150 mm analytical columns and a 4.6

x 250 mm Whelk column by Regis Technologies. Analytical thin layer chromatography (TLC) was performed on precoated glass-backed Silicycle SiliaPure® 0.25 mm silica gel 60 plates and visualized with UV light, ethanolic *p*-anisaldehyde, ethanolic bromocresol green, or aqueous potassium permanganate ($KMnO_4$). Flash column chromatography was performed using Silicycle SiliaFlash® F60 silica gel (40-63 μm) on a Biotage Isolera One system. Preparatory TLC was performed on precoated glass-backed Silicycle SiliaPure® 1.0 mm silica gel 60 plates. We acknowledge the use of shared instrumentation provided by grants from the NIH and the NSF.

4.5.2 Experimental Section

4.5.2.1 General Procedures

General Procedure A (Optimization of Enantioselective Allylic C–H Amidation): In a nitrogen-filled glovebox, base, silver salt, additive, and $[Rh(2\text{-Me-}3\text{-Ph-Ind})I_2]_2$ (*(*p*R*,p*R)* or *(*p*S*,p*S*), as indicated) were added to an oven-dried 4-mL vial equipped with a magnetic stir-bar and a teflon-septum screw cap. The vial was capped and brought out of the glovebox. 4-phenylbutene (0.015 mL, 0.10 mmol, 1.0 equiv) was added as a stock solution in DCE (0.25 mL), followed by *t*-Bu dioxazolone (0.0286 g, 0.20 mmol, 2.0 equiv) as a stock solution in DCE (0.25 mL). The reaction was stirred at the indicated temperature under a balloon of nitrogen for the time indicated. A solution of 1,4-dinitrobenzene (0.25 equiv) in dichloromethane was added as an internal standard. The reaction was filtered through a pipette containing celite with EtOAc (8 mL) and the filtrate was concentrated under reduced pressure. Product yield was determined by integration against 1,4-dinitrobenzene in the crude ^{1}H NMR spectra. Crude purification by preparatory thin layer chromatography on silica gel provided product for analysis by chiral normal phase HPLC on OD-H column in 5% isopropanol in hexanes.

General Procedure B (Enantioselective Allylic C–H Amidation of Unactivated Olefins): In a nitrogen-filled glovebox, LiOAc (0.0006 g, 0.010 mmol, 0.10 equiv), $AgNTf_2$

(0.0078 g, 0.020 mmol, 0.20 equiv), $LiNTf_2$ (0.0290 g, 0.10 mmol, 1.0 equiv), and [Rh(2-Me-3-Ph-Ind)I_2]$_2$ (0.0056 g, 0.05 mmol, 0.005 equiv, (*(p**R,R**)* or *(p**S,S**)*, as indicated) were added to an oven-dried 4-mL vial equipped with a magnetic stir-bar and a teflon- septum screw cap. The vial was capped and brought out of the glovebox. The olefin (0.10 mmol, 1.0 equiv) was added as a stock solution in DCE (0.25 mL), followed by the dioxazolone (0.20 mmol, 2 equiv) as a stock solution in DCE (0.25 mL). The reaction was stirred at room temperature (unless otherwise indicated) under a balloon of nitrogen for 48 hours. The reaction was filtered through a pipette containing celite with EtOAc (10 mL) and the filtrate was concentrated under reduced pressure. Purification by flash chromatography on silica gel provided the amide products.

4.5.2.3 Catalyst Preparation

Synthesis and Resolution of [Rh(2-Me-3-Ph-Ind)I_2]$_2$ (4.31)

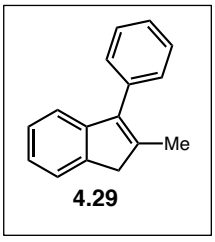

4.29

A 250 mL flame dried 3-neck round bottom flask equipped with a stir bar and reflux condenser under nitrogen was placed into a 0 °C ice/water bath. 2-methylindan-1-one[1] (1.32 g, 9.01 mmol, 1.0 equiv) was dissolved in anhydrous THF (40.0 mL) and added to the round bottom flask. After 5 minutes, phenylmagnesium bromide (3.27 g, 18.0 mmol, 2.0 equiv) was added. The ice bath was removed and the reaction allowed to warm to room temperature. The reaction was heated to reflux and allowed to stir while refluxing for 16 hours. The reaction was cooled to room temperature and quenched with DI water (20 mL). Concentrated HCl (20 mL) and Et_2O (20 mL) were added and the reaction was allowed to stir open to air for 16 hours. The layers were separated, and the aqueous layer extracted 3x with Et_2O (20 mL). The organic layers were combined and washed with $NaHCO_3$ (3x 50 mL), DI water (1x 50 mL) and brine (1x 50 mL). The organic extract was dried over $MgSO_4$, filtered, and the filtrate was concentrated under reduced pressure. Purification by flash chromatography (100% hexanes) afforded 2-methyl-3-phenyl-1*H*-indene **(4.28)** (1.50 g,

81% yield) as a white solid. **^{1}H NMR** ($CDCl_3$, 500 MHz) δ 7.51 – 7.41 (m, 4H), 7.40 – 7.35 (m, 1H), 7.26 – 7.24 (m, 1H), 7.16 – 7.20 (m, 1H), 3.48 (s, 1H), 2.17 (s, 2H) ppm.

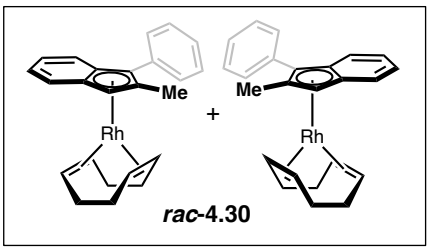

***rac*-4.30**

In a nitrogen-filled glovebox, 2-methyl-3-phenyl-1*H*-indene (0.0580 g, 0.281 mmol, 1.1 equiv), [Rh(COD)Cl_2] (0.0756 g, 0.153 mmol, 0.6 equiv), and potassium *tert*-butoxide (0.0430 g, 0.383 mmol, 1.5 equiv) were added to an oven-dried 4 mL vial equipped with a magnetic stir bar. A Teflon-septum screw cap was added and the vial was brought out of the glovebox. THF (2.0 mL) was added to the vial and the reaction stirred at room temperature under a balloon of nitrogen for 16 hours. The reaction was filtered through a pipette containing celite with hexanes (6 mL) and the filtrate was concentrated under reduced pressure. Purification by flash chromatography on silica gel with hexanes provided (±)-1,5-cyclooctadiene(η^5-2-methyl-3-phenylinden-1*H*-yl)rhodium(I) ((±)-[Rh(2-Me-3-Ph-Ind)(COD)]) **[*rac*-4.30]** (0.0960 g, 90% yield) as a yellow oil. **^{1}H NMR** ($CDCl_3$, 600 MHz) δ 7.46 – 7.39 (m, 4H), 7.29 (tt, J = 6.0, 2.8 Hz, 1H), 7.27 – 7.24 (m, 2H), 7.07 – 7.01 (m, 2H), 5.01 (s, 1H), 3.86 (td, J = f7.4, 3.4 Hz, 2H), 3.62 (tt, J = 7.3, 3.0 Hz, 2H), 2.50 (d, J = 1.5 Hz, 3H), 1.97 – 1.83 (m, 4H), 1.79 – 1.67 (m, 4H) ppm. **^{13}C NMR** ($CDCl_3$, 151 MHz) δ 135.12, 129.28, 128.38, 126.15, 122.50, 121.80, 119.21, 117.32, 112.32 (d, $J_{C–Rh}$ = 2.2 Hz), 111.60 (d, $J_{C–Rh}$ = 2.7 Hz), 107.79 (d, $J_{C–Rh}$ = 5.0 Hz), 95.47 (d, $J_{C–Rh}$ = 3.6 Hz), 76.55 (d, $J_{C–Rh}$ = 4.7 Hz), 71.98, 71.89, 69.11, 69.02, 31.43, 31.33, 14.80 ppm. **HRMS** (+APCI) calculated for $C_{24}H_{25}Rh[M]^+$ 416.10058, found 416.10045.

Chiral Resolution – Semi-prep HPLC (Chiralcel OD-H column, 0% 2-propanol in hexanes, 20 mL/min) **(p*S*)-4.30** t = 16.2 min. **(p*R*)-4.30** t = 26.9 min. Utilizing a 10 x 250 mm column with stacked injections of variable sizez (10 mg/mL concentration) we have been able to resolve up to 307 mg of racemic monomer in a 12 hour period.

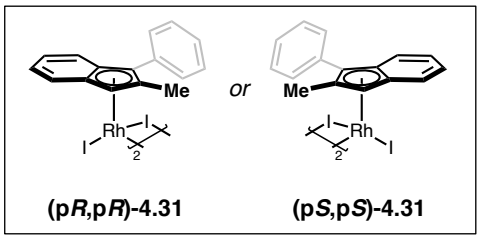

(p*R*,p*R*)-4.31 **(p*S*,p*S*)-4.31**

To a 20 mL scintillation vial containing *(S)*-[Rh(2-Me-3-Ph-Ind)(COD)] [**(p*S*)-4.30**] (0.0515 g, 0.124 mmol, 2.0 equiv) and a stir bar, iodine (0.0785 g, 0.309 mmol, 5.0 equiv) was added and the vial was sealed with a rubber septum. Anhydrous Et_2O (5.0 mL) was added and the reaction stirred for 24 hours under a balloon of nitrogen. The reaction was filtered through a Büchner funnel and washed with Et_2O (50 mL, or until the filtrate is clear). Collected and dried the filtered material to afford (*S,S*)-(2-methyl-3-phenylinden-1*H*-yl)rhodium(III) diiodide dimer ((*S,S*)-[Rh(2-Me-3-Ph-Ind)I_2]$_2$) **[(p*S*,p*S*)-4.31]** as a black solid (0.0593 g, 85% yield). **^{1}H NMR** (DMSO-d_6, 600 MHz) δ 7.87 – 7.84 (m, 4H), 7.69 (dt, J = 8.5, 1.1 Hz, 2H), 7.63 – 7.56 (m, 2H), 7.51 – 7.48 (m, 6H), 7.44 – 7.41 (m, 2H), 6.46 (s, 2H), 2.25 (s, 6H) ppm**. ^{13}C NMR** (DMSO-d_6, 151 MHz) δ 133.55, 132.42, 130.89, 129.20, 128.86, 128.41, 127.72, 125.49, 111.39 (d, $J_{C–Rh}$ = 5.5 Hz), 107.32 (d, $J_{C–Rh}$ = 3.6 Hz), 103.61 (d, $J_{C–Rh}$ = 4.7 Hz), 94.84 (d, $J_{C–Rh}$ = 6.0 Hz), 77.87 (d, $J_{C–Rh}$ = 7.1 Hz), 13.61 ppm. **HRMS** (+APCI) calculated for $C_{32}H_{26}I_3Rh_2$ $[M - I]^+$ 996.72731, found 996.7258.

(*R,R*)-[Rh(2-M3-3-Ph-Ind)I_2]$_2$ [**(p*R*,p*R*)-4.31**] was prepared using the above procedure starting from **(p*R*)-4.30**.

4.5.2.4 Determination of Stereochemistry

Catalyst Stereochemistry

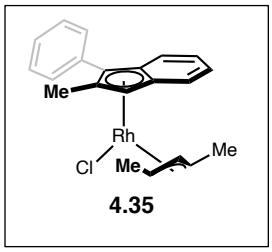

4.35

In a nitrogen filled glove box, *(S,S)*-[Rh(2-Me-3-Ph-Ind)I_2]$_2$ (0.0121 g, 0.0108 mmol. 0.5 equiv), silver hexafluoroantimonate (0.0148 g, 0.0431 mmol, 2.0 equiv), and cesium acetate (0.007 mg, 0.0360 mmol, 1.7 equiv) were added to a 7 mL vial equipped with a stir bar. The vial was sealed with a teflon cap and removed from the box. To the reaction vial was added 1,2-dichloroethane (2.0 mL) and 2-pentene (0.066 mL, 0.0413 mmol, 2.0 equiv). The vial was placed into a 40 °C heating

block and allowed to stir under a balloon of nitrogen for 16 hours. A solution of tetraethylammonium chloride (0.0114 g, 0.0688 mmol, 3.2 equiv)) in 1,2-dichloroethane (3.0 mL) was prepared and sonicated for 30 minutes. The reaction vial was cooled to room temperature and the solution of tetraethylammonium chloride in 1,2-dichloroethane was added. The reaction continued to stir at room temperature for 2 hours. The reaction was filtered through celite eluting with excess dichloromethane and the filtrate concentrated in vacuo. The crude material was purified on silica (25:75 EtOAc/hexanes) to provide (*E*)-(η^5-*S*-2-methyl-3-phenylinden-1*H*-yl)(η^3-pent-3-enyl)rhodium(III) chloride **(4.35)** (0.0028 g, 32 % yield) as a red solid. Single crystals suitable for X-Ray were obtained by vapor diffusion of pentane into chloroform. **^{1}H NMR** ($CDCl_3$, 600 MHz) δ 7.78 – 7.74 (m, 2H), 7.52 – 7.47 (m, 2H), 7.45 – 7.37 (m, 4H), 7.14 – 7.11 (m, 2H), 5.08 (s, 1H), 4.68 (td, *J* = 10.2, 1.9 Hz, 1H), 3.46 – 3.39 (m, 1H), 3.38 – 3.32 (m, 1H), 2.04 (d, *J* = 1.5 Hz, 3H), 1.52 (d, *J* = 6.9 Hz, 3H), 1.29 (d, *J* = 6.4 Hz, 3H) ppm. **^{13}C NMR** ($CDCl_3$, 151 MHz) δ 131.78, 130.57, 128.76, 128.35, 128.10, 127.57, 122.66, 121.06, 111.59, 111.14 (d, $J_{C–Rh}$ = 3.6 Hz), 108.45 (d, $J_{C–Rh}$ = 7.0), 90.53 (d, $J_{C–Rh}$ = 6.2 Hz), 79.27 (d, $J_{C–Rh}$ = 9.0 Hz), 74.99 (d, $J_{C–Rh}$ = 11.6 Hz), 32.08, 22.85, 19.71, 19.46, 14.27, 12.12 ppm. **HRMS** (+APCI) calculated for $C_{21}H_{22}Rh$ [M – Cl]$^+$ 377.07711, found 377.07680.

Stereochemical assignment of the indene ring in the π-allyl complex was used to assume stereochemistry of the $[Rh(2\text{-Me-3-Ph-Ind})I_2]_2$ starting material.

Product Stereochemistry

Stereochemistry of *N-(4-methylpent-1-en-3-yl)pivalamide* was assigned by converting methyl pivaloyl-*D*-valinate[2] to the corresponding olefin product by reduction to the aldehyde and subsequent Wittig reaction. HPLC data was then compared to the reaction HPLC data for the same substrate, shown below. All substrates with alkyl substituents at the homoallylic position were assigned by analogy.

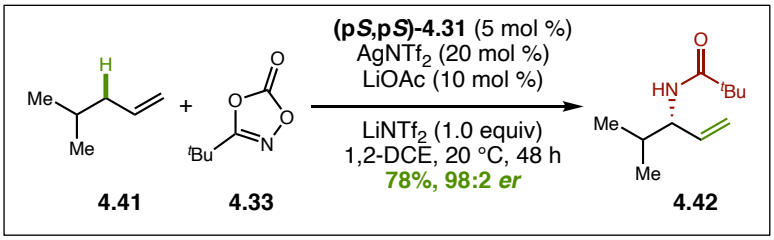

(S)-N-(4-methylpent-1-en-3-yl)acetamide* (4.42):** See ***Dioxazolone Scope for full experimental. **HPLC** (OJ-H column, 10% 2-propanol in Hexanes, 1 mL/min) t_M = 5.6 min, t_m = 5.0 min, 98:2 e.r.

***(±)-N-(4-methylpent-1-en-3-yl)acetamide* ((±)-4.42):**

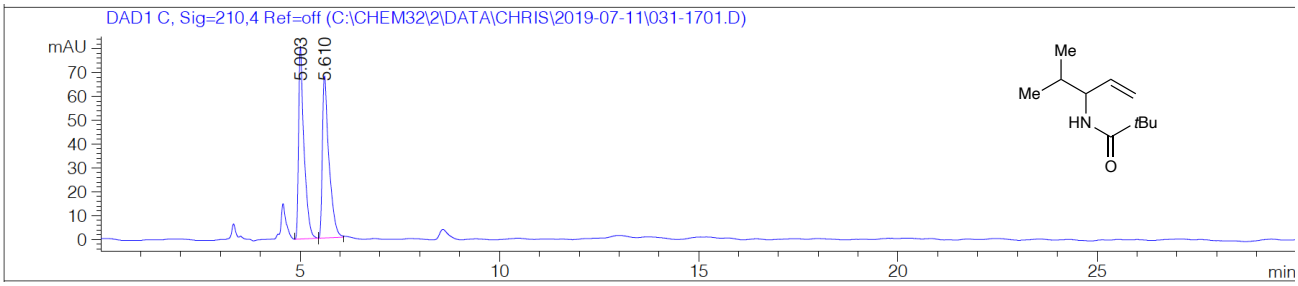


```
Signal 1: DAD1 C, Sig=210,4 Ref=off

Peak RetTime Type  Width     Area      Height     Area
  #   [min]        [min]   [mAU*s]     [mAU]       %
----|-------|----|-------|----------|----------|--------|
   1   5.003 VV    0.1348  767.14093   80.80962  50.2210
   2   5.610 VB    0.1585  760.38782   67.99258  49.7790

Totals :                  1527.52875  148.80220
```

(S)-N-(4-methylpent-1-en-3-yl)acetamide (4.42):

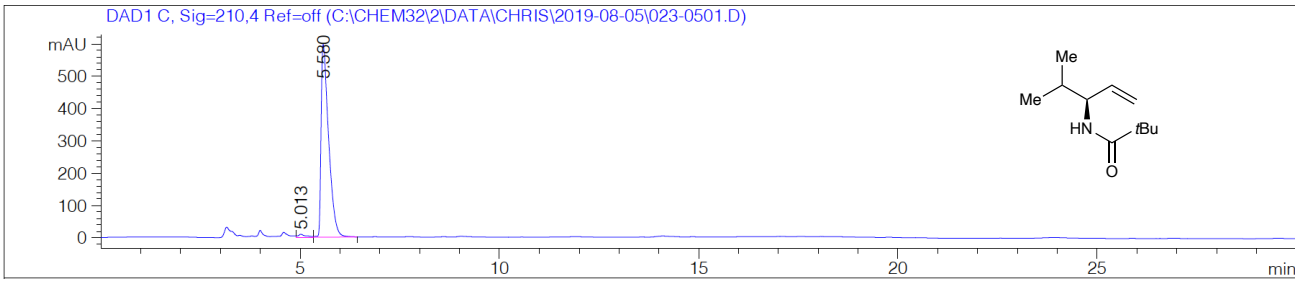

Signal 2: DAD1 C, Sig=210,4 Ref=off

Peak #	RetTime [min]	Type	Width [min]	Area [mAU*s]	Height [mAU]	Area %
1	5.013	VV	0.1808	126.23240	9.27309	1.6162
2	5.580	VB	0.1861	7684.32129	597.17950	98.3838
Totals :				7810.55369	606.45259	

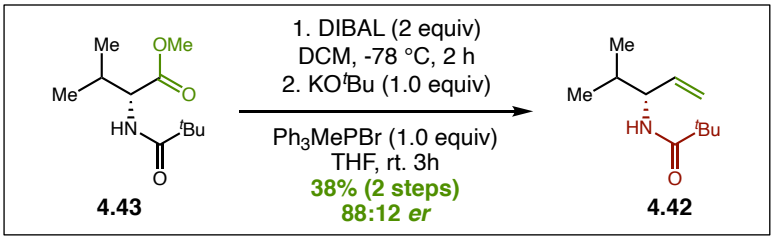

***(R)-N-(4-methylpent-1-en-3-yl)pivalamide* (4.S1):** To an oven-dried 7 mL vial equipped with a stir bar was added methyl pivaloyl-*D*-valinate[2] (0.0741 g, 0.344 mmol, 1.0 equiv) and the atmosphere was exchanged with N_2. The solid was dissolved in DCM (2.0 mL) and cooled to -78 °C in an acetone/dry ice bath. DIBAL-H (0.720 mL, 0.723 mmol, 2.1 equiv) was added to the reaction vial over 20 minutes via syringe pump and the reaction allowed to stir at -78 °C for 2 hours. The reaction was quenched with DI H_2O (4 mL) and allowed to come to room temperature. A white solid was filtered away by passing the reaction through a cotton plug before the layers were separated and the organic layer was washed with brine (4 mL), dried over $MgSO_4$, filtered, and concentrated *in vacuo*. The Wittig reagent was prepared by adding methyltriphenylphosphonium bromide (0.123 g, 0.344 mmol, 1.0 equiv) and potassium *tert*-butoxide (0.0386 g, 0.344 mmol, 1.0 equiv) to a flame dried 7 mL vial equipped with a stir bar. The vial was sealed, and the atmosphere exchanged with N_2 before the addition of anhydrous THF (2.0 mL). The vial was stirred at room temperature for 5 minutes. The crude aldehyde was dissolved in anhydrous THF (2.0 mL) and added dropwise to the vial containing the yellow Wittig reagent. The reaction stirred at room temperature until the yellow color had changed to white (3 hours). The reaction was concentrated *in vacuo* and purified on silica gel (10-50% EtOAc in hexanes) to afford **(4.S1)** (0.0239 g, 38% yield, 2 steps) as a white solid. **^{1}H NMR** ($CDCl_3$, 400 MHz) δ 5.76 (ddd, J = 17.0, 10.6, 5.5 Hz, 1H), 5.54 (s, 1H), 5.15 – 5.05 (m, 2H), 4.35 (dtt, J = 8.9, 5.5, 1.6 Hz, 1H), 1.81 (qnd, J = 6.9, 5.6 Hz, 1H), 1.22 (s, 9H), 0.90 (d, J = 6.9 Hz, 3H), 0.88 (d, J = 7.0 Hz, 3H) ppm. **HPLC** (OJ-H column, 10% 2-propanol in Hexanes, 1 mL/min) t_M = 5.0 min, t_m = 5.9 min, 88:11 e.r.

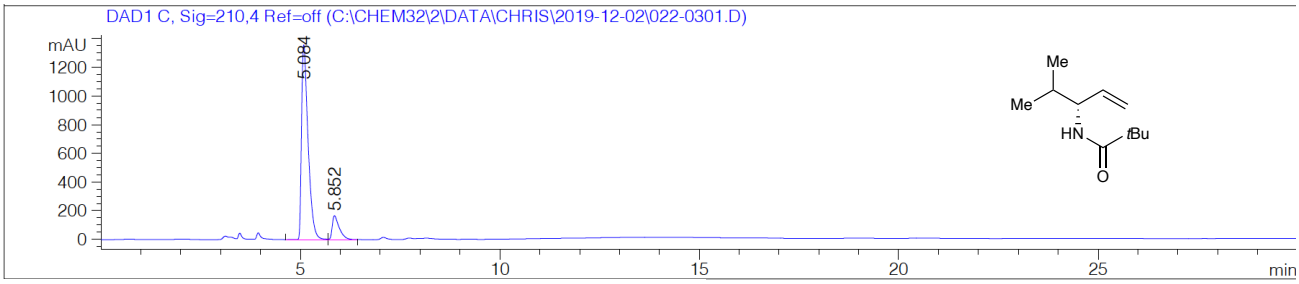

Signal 1: DAD1 C, Sig=210,4 Ref=off

Peak #	RetTime [min]	Type	Width [min]	Area [mAU*s]	Height [mAU]	Area %
1	5.084	VV	0.1704	1.56517e4	1359.12085	88.3109
2	5.852	VB	0.1806	2071.69434	167.13620	11.6891
Totals :				1.77234e4	1526.25705	

Stereochemistry of *N-(1-phenylallyl)pivalamide* assigned by converting the amidated product of the reaction between allyl benzene and *tert*-butyl dioxazolone to its *N*-pivaloyl phenylglycine methyl ester derivative by oxidative cleavage of the olefin and methyl protection of the resulting carboxylic acid. Comparison to the HPLC traces of *N*-pivaloyl-*D*-phenylglycine methyl ester and *N*-pivaloyl-*L*-phenylglycine methyl ester, formed from their enantiopure amino acid precursors, allowed for final stereochemical assignment. All substrates with aryl substituents at the homoallylic position are assigned by analogy.

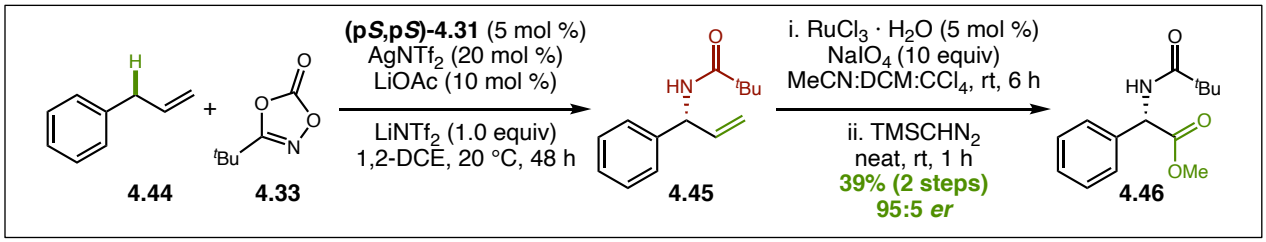

***N-pivaloyl-L-phenylglycine methyl ester* (4.46)**: **(4.45)** was prepared using the same procedure as **(4.64)** utilizing the *(S,S)*-[Rh(2-Me-3-Ph-Ind)I_2]$_2$ catalyst in place of the *(R,R)*-[Rh(2-Me-3-Ph-Ind)I_2]$_2$ catalyst. To a 7 mL oven dried vial equipped with stir bar was added sodium periodate (0.1310 g, 1.15 mmol, 10.0 equiv) and ruthenium(III) chloride hydrate (0.2460 mg, 0.00575 mmol, 5 mol %), the vial was sealed, and atmosphere exchanged with N_2. **(4.45)**

(0.0360 mg, 0.166 mmol) was dissolved in CCl_4 (1.44 mL) and 1.0 mL of the **4.45** solution (0.0250 mg, 0.115 mmol, 1.0 equiv), MeCN (1.0 mL), and DCM (1.0 mL) were added to the reaction vial and the reaction stirred at room temperature for 4 hours. The reaction was poured into a 1:1 DCM:DI H_2O mixture (10 mL). The organic layer was separated, and the aqueous layer extracted 3x with DCM (5 mL). The combined organic layers were dried over $MgSO_4$, filtered, and concentrated *in vacuo*. To the crude carboxylic acid was added (diazomethyl)trimethylsilane (0.1310 g, 1.15 mmol, 10.0 equiv) and the reaction stirred at room temperature for 1 hour. The reaction was concentrated *in vacuo* and then purified on silica gel (10-50% EtOAc in Hexanes) to afford **(4.46)** (0.0112 g, 39% yield) as a white solid. **^{1}H NMR** ($CDCl_3$, 500 MHz) δ 7.40 – 7.27 (m, 5H), 6.61 (d, J = 6.7 Hz, 1H), 5.53 (d, J = 6.8 Hz, 1H), 3.73 (s, 3H), 1.22 (s, 9H) ppm. **HPLC** (AS-H column, 5% 2-propanol in Hexanes, 1 mL/min) t_M = 7.0 min, t_m = 10.0 min, 94:6 e.r.

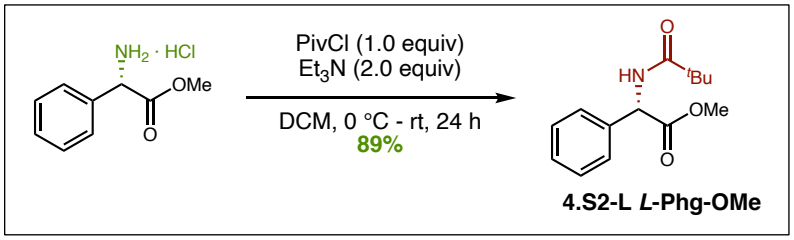

***N-pivaloyl-L-phenylglycine methyl ester* (4.S2-L *L*-Phg-OMe)** (HPLC Standards): To a 20 mL flame dried round bottom flask equipped with a stir bar, added methyl-(*S*)-2-amino-2-phenylacetate hydrochloride (0.5041 g, 2.50 mmol, 1.0 equiv) sealed with a rubber septum exchanged the atmosphere with N_2. Added DCM (8.0 mL) and placed into a 0 °C ice/water bath for 30 minutes before the addition of Et_3N (0.0073 L, 5.00 mmol, 2.0 equiv) and pivaloyl chloride (0.000308 L, 2.50 mmol, 1.0 equiv). The reaction was allowed to stir for 24 hours and warmed to room temperature. The reaction was poured into a separatory funnel containing EtOAc (40 mL) and DI H_2O (40 mL). The organic layer was separated, and the aqueous layer extracted with EtOAc (3x15 mL). The combined organic layers were dried over $MgSO_4$, filtered, and concentrated *in vacuo*. Purification on silica gel (10-50% EtOAc in hexanes) afforded **(4.S2-L *L*-Phg-OMe)** (0.5532 g, 89% yield, single enantiomer) as a white solid. **^{1}H NMR** ($CDCl_3$, 500 MHz) δ 7.41 –

7.29 (m, 5H), 6.61 (d, *J* = 6.7 Hz, 1H), 5.53 (d, *J* = 6.8 Hz, 1H), 3.73 (s, 3H), 1.22 (s, 9H) ppm. **HPLC** (AS-H column, 5% 2-propanol in Hexanes, 1 mL/min) *t* = 7.0 min.

***N-pivaloyl-D-phenylglycine methyl ester* (4.SD *D*-Phg-OMe)** HPLC standard prepared according to the same procedure utilizing methyl-(*R*)-2-amino-2-phenylacetate hydrochloride as the starting material. **^{1}H NMR** ($CDCl_3$, 500 MHz) δ 7.41 – 7.29 (m, 5H), 6.61 (d, *J* = 6.7 Hz, 1H), 5.53 (d, *J* = 6.8 Hz, 1H), 3.73 (s, 3H), 1.22 (s, 9H) ppm. **HPLC** (AS-H column, 5% 2-propanol in Hexanes, 1 mL/min) *t* = 9.6 min.

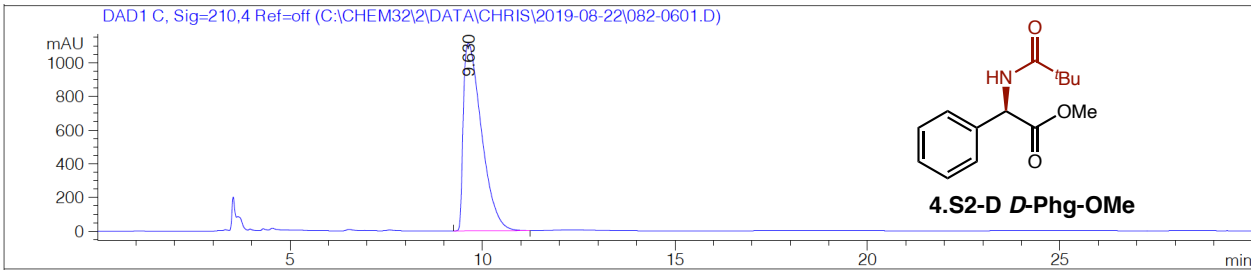

Signal 1: DAD1 C, Sig=210,4 Ref=off

Peak #	RetTime [min]	Type	Width [min]	Area [mAU*s]	Height [mAU]	Area %
1	9.630	BB	0.5104	3.66984e4	1113.71863	100.0000
Totals :				3.66984e4	1113.71863	

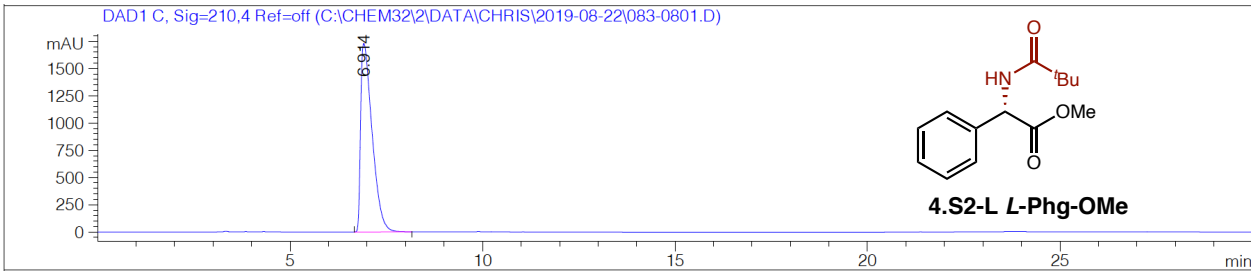

Signal 1: DAD1 C, Sig=210,4 Ref=off

Peak #	RetTime [min]	Type	Width [min]	Area [mAU*s]	Height [mAU]	Area %
1	6.914	BB	0.3150	3.60334e4	1730.04883	100.0000
Totals :				3.60334e4	1730.04883	

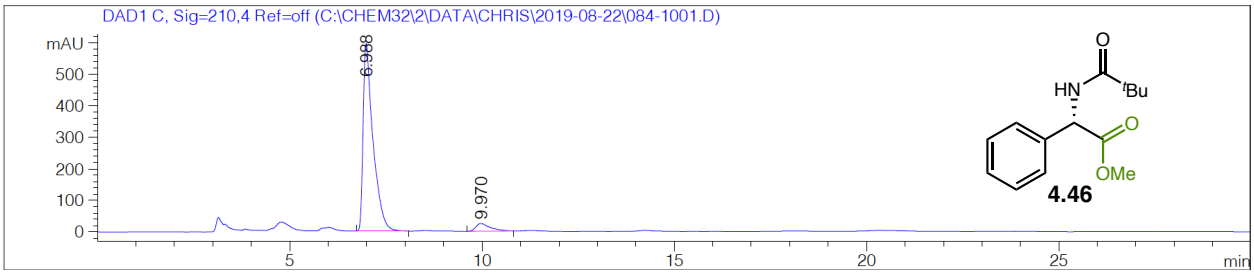

Signal 1: DAD1 C, Sig=210,4 Ref=off

Peak #	RetTime [min]	Type	Width [min]	Area [mAU*s]	Height [mAU]	Area %
1	6.988	BB	0.2569	1.06587e4	595.19495	94.4866
2	9.970	BB	0.3668	621.94397	24.28669	5.5134
Totals :				1.12806e4	619.48164	

Enantiomeric ratio of *(S,E)-N-(pent-3-en-2-yl)pivalamide* (**4.39**) assigned by converting the amidated product of the reaction between 2-pentene and tert-butyl dioxazolone to its N-pivaloyl alanine methyl ester derivative by oxidative cleavage of the olefin and methyl protection of the resulting carboxylic acid. Comparison to the HPLC traces of N-pivaloyl-D-alanine methyl ester and N-pivaloyl-L-alanine methyl ester, formed from their enantiopure amino acid precursors, allowed for final assignment of stereochemistry.

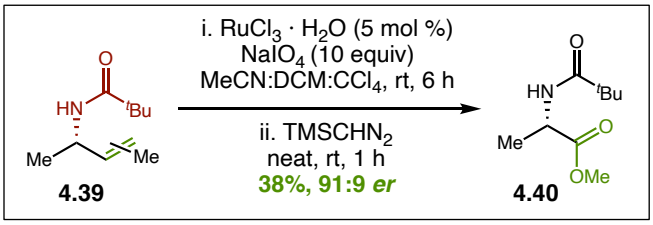

N-pivaloyl-L-alanine methyl ester (**4.40**): To a 4 mL oven dried vial equipped with stir bar was added sodium periodate (0.2540 g, 1.19 mmol, 10.0 equiv), ruthenium(III) chloride hydrate (0.0013 g, 0.00594 mmol, 5 mol %), and (**4.39**) (0.0201 g, 0.119 mmol), the vial was sealed, and atmosphere exchanged with N2. To the reaction vial was added CCl4 (0.60 mL), MeCN (0.6 mL), and DI H2O (0.9 mL) were added to the reaction vial and the reaction stirred at room temperature for 3 hours. The reaction was poured into a 1:1 DCM:DI H2O mixture (10 mL). The organic layer was separated, and the aqueous layer extracted 3x with DCM (5 mL). The combined organic layers were dried over MgSO4, filtered, and concentrated in vacuo. To the crude carboxylic acid was

added (diazomethyl)trimethylsilane (0.1360 g, 1.19 mmol, 10.0 equiv) and the reaction stirred at room temperature for 1 hour. The reaction was concentrated in vacuo and then purified on silica gel (10-50% EtOAc in Hexanes) to afford (**4.40**) (0.0084 g, 38% yield). **^{1}H NMR** ($CDCl_3$, 500 MHz) δ 6.18 (s, 1H), 4.57 (qn, J = 7.2 Hz, 1H), 3.75 (s, 3H), 1.40 (d, J = 7.2 Hz, 3H), 1.21 (s, 9H).) ppm. **HPLC** (OJ-H column, 1% 2-propanol in Hexanes, 1 mL/min) t_M = 9.7 min, t_m = 11.0 min, 91:9 e.r.

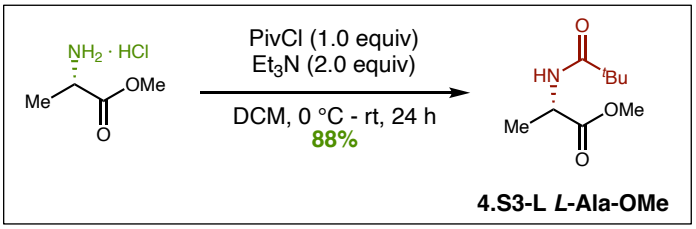

N-pivaloyl-L-phenylglycine methyl ester **(4.S3-L *L*-Ala-OMe)** (HPLC Standards): To a 20 mL flame dried round bottom flask equipped with a stir bar, added methyl-L-alaninate hydrochloride (0.2000 g, 1.43 mmol, 1.0 equiv) sealed with a rubber septum exchanged the atmosphere with N2. Added DCM (8.0 mL) and placed into a 0 °C ice/water bath for 30 minutes before the addition of Et3N (0.0004 L, 2.87 mmol, 2.0 equiv) and pivaloyl chloride (0.000176 L, 1.43 mmol, 1.0 equiv). The reaction was allowed to stir for 24 hours and warmed to room temperature. The reaction was poured into a separatory funnel containing EtOAc (40 mL) and DI H2O (40 mL). The organic layer was separated, and the aqueous layer extracted with EtOAc (3x15 mL). The combined organic layers were dried over MgSO4, filtered, and concentrated in vacuo. Aqueous wash afforded (**4.S3-L *L*-Ala-OMe**) (0.2363 g, 88% yield, single enantiomer) as a white solid. **^{1}H NMR** ($CDCl_3$, 500 MHz) δ 6.18 (s, 1H), 4.57 (qn, J = 7.2 Hz, 1H), 3.75 (s, 3H), 1.40 (d, J = 7.2 Hz, 3H), 1.21 (s, 8H) ppm. HPLC (OJ-H column, 1% 2-propanol in Hexanes, 1 mL/min) *t* = 10.8 min.

N-pivaloyl-D-alanine methyl ester **(4.S3-D *D*-Ala-OMe)** HPLC standard prepared according to the same procedure utilizing methyl-D-alaninatehydrochloride as the starting material provided (**4.S3-D *D*-Ala-OMe**) (0.2420 g, 90% yield, single enantiomer). **^{1}H NMR**

(CDCl3, 500 MHz) δ 6.18 (s, 1H), 4.57 (qn, J = 7.2 Hz, 1H), 3.75 (s, 3H), 1.40 (d, J = 7.2 Hz, 3H), 1.21 (s, 8H) ppm. **HPLC** (OJ-H column, 1% 2-propanol in Hexanes, 1 mL/min) *t* = 9.4 min.

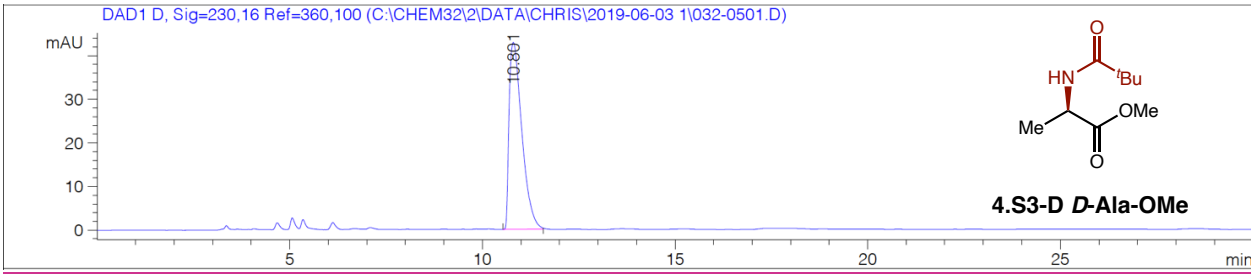

Signal 1: DAD1 D, Sig=230,16 Ref=360,100

Peak #	RetTime [min]	Type	Width [min]	Area [mAU*s]	Height [mAU]	Area %
1	10.801	BB	0.3567	985.87683	42.81202	100.0000
Totals :				985.87683	42.81202	

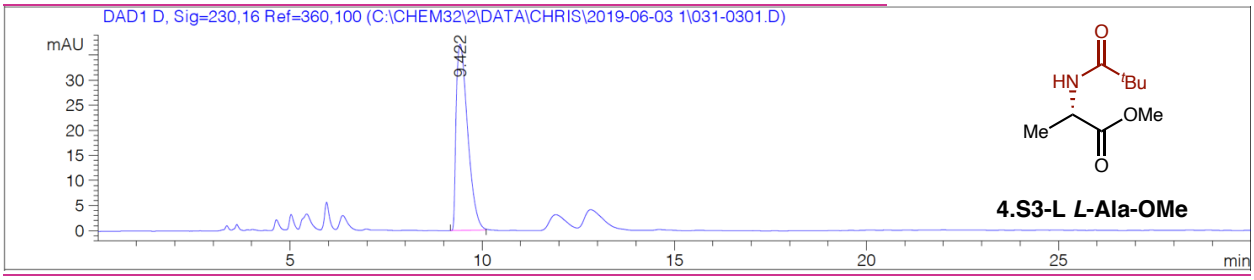

Signal 1: DAD1 D, Sig=230,16 Ref=360,100

Peak #	RetTime [min]	Type	Width [min]	Area [mAU*s]	Height [mAU]	Area %
1	9.422	BB	0.3203	764.51672	37.11811	100.0000
Totals :				764.51672	37.11811	

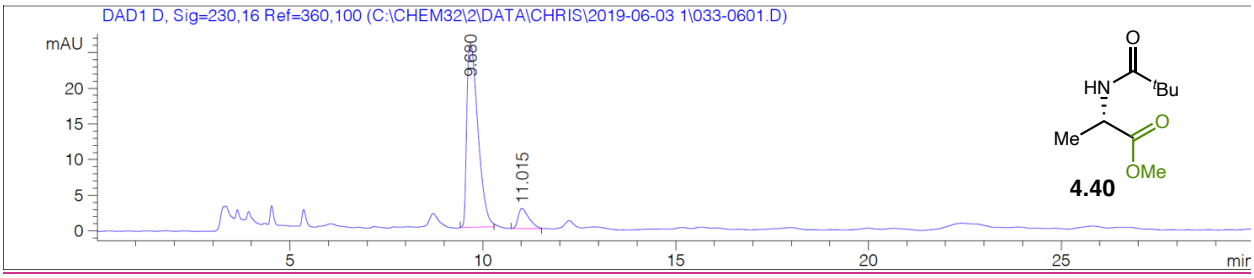

Signal 1: DAD1 D, Sig=230,16 Ref=360,100

Peak #	RetTime [min]	Type	Width [min]	Area [mAU*s]	Height [mAU]	Area %
1	9.680	BB	0.3139	522.02844	25.81386	90.6337
2	11.015	BB	0.2908	53.94768	2.79983	9.3663
Totals :				575.97612	28.61368	

4.5.2.5 Characterization of Enantioselective Allylic C–H Amidation Products

All racemic runs were carried out with the designated alkene and dioxazolone, utilizing $[IrCp^*Cl_2]_2$ as the catalyst under previously reported conditions.[3]

Dioxazolone Scope – Selected reactions completed by C.D.P.

-For the remaining substrates, see supplementary reference 8.

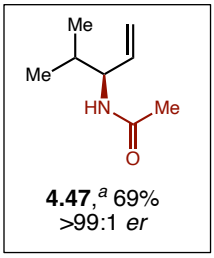

(S)-N-(4-methylpent-1-en-3-yl)acetamide (**4.47**): Prepared according to **General Procedure B** using 4-methylpentene (0.0127 mL, 0.10 mmol, 1.0 equiv), 3-methyl-1,4,2-dioxazol-5-one (0.0202 g, 0.20 mmol, 2.0 equiv), LiOAc (0.0006 g, 0.010 mmol, 0.10 equiv), AgNTf2 (0.0078 g, 0.020 mmol, 0.20 equiv), LiNTf2 (0.0290 g, 0.10 mmol, 1.0 equiv), and (S,S)-[Rh(2-Me-3-Ph-Ind)I2]2 (0.0056 g, 0.005 mmol, 0.05 equiv) in DCE (0.5 mL) at room temperature for 48 hours. Purified by flash chromatography on silica gel (90-100% EtOAc in Hexanes) to provide **4.47** (0.0098 g, 69% yield, >99:1 e.r.) as a yellow oil. **^{1}H NMR** ($CDCl_3$, 600 MHz) δ 5.74 (ddd, J = 17.5, 10.2, 5.9 Hz, 1H), 5.41 (s, 1H), 5.17 – 5.11 (m, 2H), 4.34 (dtt, J = 9.1, 5.9, 1.6 Hz, 1H), 2.02 (s, 3H), 1.80 (qnd, J = 6.9, 5.7 Hz, 1H), 0.91 (d, J = 4.8 Hz, 3H), 0.90 (d, J = 4.9 Hz, 3H) ppm. **^{13}C NMR** ($CDCl_3$, 151 MHz) δ 169.43, 136.67, 115.62, 56.58, 32.01, 23.52, 18.64, 18.19 ppm. **HRMS** (+APCI) calculated for

C8H16NO $[M+H]^+$ 142.12264, found 142.12267. **HPLC** (AD-H column, 1% 2-propanol in Hexanes, 1 mL/min) t_M = 19.1 min, t_m = 22.8 min, >99:1 e.r.

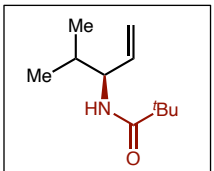

4.42,[a] 77%
98:2 *er*

(S)-N-(4-methylpent-1-en-3-yl)pivalamide (**4.42**): Prepared according to **General Procedure B** using 4- methylpentene (0.0253 mL, 0.20 mmol, 1.0 equiv), 3-(tert-butyl)-1,4,2-dioxazol-5-one (0.0573 g, 0.40 mmol, 2.0 equiv), LiOAc (0.0012 g, 0.020 mmol, 0.10 equiv), AgNTf2 (0.0155 g, 0.040 mmol, 0.20 equiv), LiNTf2 (0.0574 g, 0.20 mmol, 1.0 equiv), and (S,S)-[Rh(2-Me-3-Ph-Ind)I2]2 (0.0112 g, 0.01 mmol, 0.05 equiv) in DCE (0.5 mL) at room temperature for 48 hours. Purified by flash chromatography on silica gel (10-50% EtOAc in Hexanes) to provide **4.42** (0.0285 g, 78% yield, 98:2 e.r.) as a white solid. **^{1}H NMR** ($CDCl_3$, 600 MHz) δ 5.77 (ddd, J = 17.1, 10.6, 5.6 Hz, 1H), 5.54 (s, 1H), 5.13 – 5.07 (m, 2H), 4.38 – 4.32 (m, 1H), 1.82 (qnd, J = 6.9, 5.6 Hz, 1H), 1.22 (s, 9H), 0.90 (d, J = 6.8 Hz, 3H), 0.89 (d, J = 6.8 Hz, 3H) ppm. **^{13}C NMR** ($CDCl_3$, 151 MHz) δ 177.66, 137.13, 115.15, 55.86, 38.92, 32.10, 27.71, 18.80, 17.98 ppm. **HRMS** (+APCI) calculated for C11H22NO $[M+H]^+$ 184.16926, found 184.16959. **HPLC** (OJ-H column, 10% 2- propanol in Hexanes, 1 mL/min) t_M = 5.6 min, t_m = 5.0 min, 98:2 e.r.

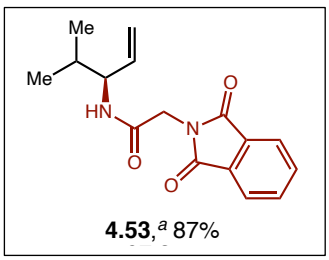

4.53,[a] 87%

(S)-2-(1,3-dioxoisoindolin-2-yl)-N-(4-methylpent-1-en-3-yl)acetamide (**4.53**): Prepared according to **General Procedure B** using 4-methylpentene (0.0127 mL, 0.10 mmol, 1.0 equiv), 2-((5-oxo-1,4,2- dioxazol-3-yl)methyl)isoindoline-1,3-dione (0.0492 g, 0.20 mmol, 2.0 equiv), LiOAc (0.0006 g, 0.010 mmol, 0.10 equiv), AgNTf2 (0.0078 g, 0.020 mmol, 0.20 equiv), LiNTf2 (0.0290 g, 0.10 mmol, 1.0 equiv), and (S,S)-[Rh(2-Me-3-Ph-Ind)I2]2 (0.0056 g, 0.005 mmol, 0.05 equiv) in DCE (0.5 mL) at room temperature for 48 hours. Purified by flash chromatography on silica gel (20-50% EtOAc in Hexanes) to provide **4.53** (0.0250 g, 87% yield, 97:3 e.r.) as a white solid**. ^{1}H NMR** ($CDCl_3$, 600 MHz) δ 7.89 (dd, J = 5.4, 3.1 Hz, 2H),

7.75 (dd, J = 5.5, 3.0 Hz, 2H), 5.74 (ddd, J = 17.2, 10.5, 5.9 Hz, 1H), 5.66 (d, J = 9.1 Hz, 1H), 5.20 – 5.13 (m, 2H), 4.37 (s, 2H), 4.35 (ddt, J = 9.0, 5.8, 1.6 Hz, 1H), 1.88 – 1.78 (m, 1H), 0.91 (d, J = 6.8 Hz, 3H), 0.90 (d, J = 6.9 Hz, 3H) ppm. **^{13}C NMR** ($CDCl_3$, 151 MHz, $CDCl_3$) δ 167.79, 165.45, 136.07, 134.28, 132.01, 123.68, 116.17, 57.04, 41.18, 32.03, 18.68, 18.08 ppm. **HRMS** (+APCI) calculated for $C_{16}H_{19}NO_3$ $[M+H]^+$ 287.13902, found 287.13889. **HPLC** (OJ-H column, 10% 2-propanol in Hexanes, 1 mL/min) t_M = 20.2 min, t_m = 17.9 min, 97:3 e.r.

Olefin Scope – Selected reactions completed by C.D.P.

-For the remaining substrates, see supplementary reference 8.

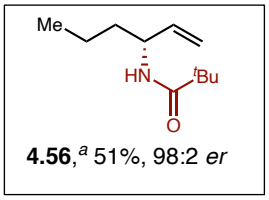

4.56,[a] 51%, 98:2 *er*

(R)-N-(hex-1-en-3-yl)pivalamide (**4.56**): Prepared according to **General Procedure B** using hex-1-ene (0.0084 g, 0.10 mmol, 1.0 equiv), 3-(tert-butyl)-1,4,2-dioxazol-5-one (0.0286 g, 0.20 mmol, 2.0 equiv), (R,R)- [Rh(2-Me-3-Ph-Ind)I2]2 (0.0056 g, 0.005 mmol, 0.05 equiv), LiOAc (0.0006 g, 0.010 mmol, 0.10 equiv), AgNTf2 (0.0078 g, 0.020 mmol, 0.20 equiv), and LiNTf2 (0.0290 g, 0.10 mmol, 1.0 equiv) in DCE (0.5 mL) at room temperature for 48 hours. Purified by flash chromatography on silica gel (10-30% EtOAc in Hexanes) to provide **4.56** (0.0297 g, 90% yield, 98:2 e.r.) as a white solid. **^{1}H NMR** ($CDCl_3$, 500 MHz) δ 5.82 – 5.73 (m, 1H), 5.45 (s, 1H), 5.15 – 5.05 (m, 2H), 4.50 – 4.42 (m, 1H), 1.58 – 1.50 (m, 1H), 1.50 – 1.40 (m, 1H), 1.40 – 1.30 (m, 2H), 1.22 (s, 9H), 0.95 – 0.91 (m, 3H) ppm. **^{13}C NMR** ($CDCl_3$, 126 MHz) δ 177.77, 139.00, 114.43, 50.78, 38.89, 37.24, 27.81, 19.14, 14.04 ppm. **HRMS** (+APCI) calculated for $C_{11}H_{22}NO$ $[M+H]^+$ 184.16959, found 184.16954. **HPLC** (WHELK column, 1% 2-propanol in Hexanes, 1 mL/min) t_M = 18.4 min, t_m = 16.1 min, 98:2 e.r.

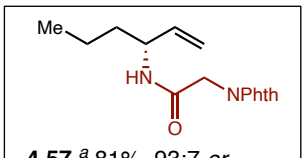

4.57,[a] 81%, 93:7 *er*

(R)-2-(1,3-dioxoisoindolin-2-yl)-N-(hex-1-en-3-yl)acetamide (**4.57**): Prepared according to **General Procedure B** using hex-1-ene (0.0084 g, 0.10 mmol, 1.0 equiv), 2-((5-oxo-1,4,2-dioxazol-3-

yl)methyl)isoindoline-1,3- dione (0.0492 g, 0.20 mmol, 2.0 equiv), (R,R)-[Rh(2-Me-3-Ph-Ind)I2]2 (0.0056 g, 0.005 mmol, 0.05 equiv), LiOAc (0.0006 g, 0.010 mmol, 0.10 equiv), AgNTf2 (0.0078 g, 0.020 mmol, 0.20 equiv), and LiNTf2 (0.0290 g, 0.10 mmol, 1.0 equiv) in DCE (0.5 mL) at room temperature for 48 hours. Purified by flash chromatography on silica gel (10-30% EtOAc in Hexanes) to provide **4.57** (0.0297 g, 90% yield, 93:7 e.r.) as a white solid. **^{1}H NMR** (CDCl3, 600 MHz) δ 7.92 – 7.85 (m, 2H), 7.78 – 7.71 (m, 2H), 5.75 (ddd, J = 17.2, 10.4, 5.7 Hz, 1H), 5.59 (d, J = 8.3 Hz, 1H), 5.21 – 5.07 (m, 2H), 4.47 (dqd, J = 7.3, 5.9, 1.6 Hz, 1H), 4.35 (s, 2H), 1.56 – 1.45 (m, 2H), 1.40 – 1.30 (m, 2H), 0.92 (t, J = 7.3 Hz, 3H) ppm. **^{13}C NMR** (CDCl3, 151 MHz) δ 167.93, 165.44, 137.96, 134.40, 134.34, 132.21, 132.18, 123.81, 115.43, 51.78, 41.18, 41.12, 37.03, 19.06, 13.95 ppm. **HRMS** (+APCI) calculated for C16H19N2O3 $[M+H]^+$ 287.13902, found 287.13888. **HPLC** (AD-H column, 5% 2-propanol in Hexanes, 1 mL/min) t_M = 29.1 min, t_m = 31.6 min, 93:7 e.r

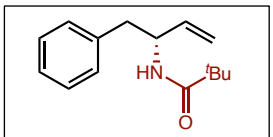

4.62,[a] 57%, 98:2 *er*

(R)-N-(1-phenylbut-3-en-2-yl)pivalamide (**4.62**): Prepared according to **General Procedure B** using 4- phenylbutene (0.0127 mL, 0.10 mmol, 1.0 equiv), 3-(tert-butyl)-1,4,2-dioxazol-5-one (0.0338 g, 0.20 mmol, 2.0 equiv), (R,R)-[Rh(2-Me-3-Ph-Ind)I2]2 (0.0056 g, 0.005 mmol, 0.05 equiv), LiOAc (0.0006 g, 0.010 mmol, 0.10 equiv), AgNTf2 (0.0078 g, 0.020 mmol, 0.20 equiv), and LiNTf2 (0.0290 g, 0.10 mmol, 1.0 equiv) in DCE (0.5 mL) at room temperature for 48 hours. Purified by flash chromatography on silica gel (10-25% EtOAc in Hexanes) to provide **4.62** (0.0132 g, 57% yield, 98:2 e.r.) as a white solid. **^{1}H NMR** (CDCl3, 600 MHz) δ 7.30 – 7.27 (m, 2H), 7.24 – 7.20 (m, 1H), 7.19 – 7.15 (m, 2H), 5.85 (ddd, J = 17.2, 10.5, 5.2 Hz, 1H), 5.46 (d, J = 8.2 Hz, 1H), 5.12 – 5.05 (m, 2H), 4.78 (dtdt, J = 8.4, 6.8, 5.2, 1.7 Hz, 1H), 2.92 (dd, J = 13.7, 6.6 Hz, 1H), 2.83 (dd, J = 13.7, 6.8 Hz, 1H), 1.12 (s, 9H) ppm. **^{13}C NMR** (CDCl3, 151 MHz) δ 177.71, 138.05, 137.35, 129.65, 128.50, 126.77, 114.91, 51.55, 41.03, 38.86, 27.65 ppm. **HRMS** (+APCI) calculated for C15H22NO

$[M+H]^+$ 232.16959, found 232.16947. **HPLC** (OD-H column, 5% 2-propanol in Hexanes, 1 mL/min) t_M = 8.4 min, t_m = 7.6 min, 98:2 e.r.

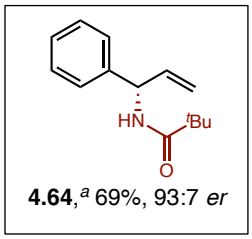

4.64,[a] 69%, 93:7 *er*

(S)-N-(1-phenylallyl)pivalamide (**4.64**): Prepared according to **General Procedure B** using allyl benzene (0.0132 mL, 0.10 mmol, 1.0 equiv), 3-(tert-butyl)-1,4,2-dioxazol-5-one (0.0286 g, 0.20 mmol, 2.0 equiv), LiOAc (0.0006 g, 0.010 mmol, 0.10 equiv), AgNTf2 (0.0078 g, 0.020 mmol, 0.20 equiv), LiNTf2 (0.0290 g, 0.10 mmol, 1.0 equiv), and (R,R)-[Rh(2-Me-3-Ph-Ind)I2]2 (0.0056 g, 0.200 mmol, 0.005 equiv) in DCE (0.5 mL) at room temperature for 48 hours. Purified by flash chromatography on silica gel (10-30% EtOAc in Hexanes) to provide **4.64** (0.0150 g, 69% yield, 93:7 e.r.) as a colorless solid. **^{1}H NMR** ($CDCl_3$, 600 MHz) δ 7.37 – 7.33 (m, 2H), 7.30 – 7.27 (m, 3H), 6.02 (ddd, J = 17.1, 10.4, 5.3 Hz, 1H), 5.85 (s, 1H), 5.62 (dd, J = 7.9, 5.5 Hz, 1H), 5.29 – 5.13 (m, 2H), 1.23 (s, 9H) ppm. **^{13}C NMR** ($CDCl_3$, 151 MHz) δ 173.37, 140.84, 137.50, 128.78, 127.61, 127.11, 115.68, 54.78, 38.79, 27.61 ppm. **HRMS** (+APCI) calculated for $C_{14}H_{20}NO$ $[M+H]^+$ 218.15339, found 218.15394. **HPLC** (OJ-H column, 10% 2-propanol in Hexanes, 1 mL/min)) t_M = 9.1 min, t_m = 8.1 min, 93:7 e.r.

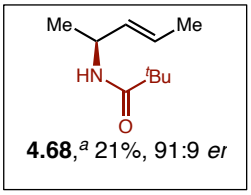

4.68,[a] 21%, 91:9 *er*

(S,E)-N-(1,3-diphenylallyl)pivalamide (**4.68**): Prepared according to General Procedure B using (E)-prop-1- ene-1,3-diyldibenzene (0.0194 g, 0.10 mmol, 1.0 equiv), 3-(tert-butyl)-1,4,2-dioxazol-5-one (0.0286 g, 0.20 mmol, 2.0 equiv), (S,S)-[Rh(2-Me-3-Ph-Ind)I2]2 (0.0056 g, 0.005 mmol, 0.05 equiv), LiOAc (0.0006 g, 0.010 mmol, 0.10 equiv), AgNTf2 (0.0078 g, 0.020 mmol, 0.20 equiv), and LiNTf2 (0.0290 g, 0.10 mmol, 1.0 equiv) in DCE (0.5 mL) at 40 °C for 48 hours. Purified by flash chromatography on silica gel (5- 30% EtOAc in Hexanes) to provide **4.68** (0.0065 g, 21% yield, 91:9 e.r.) as a white solid. **^{1}H NMR** ($CDCl_3$, 600 MHz) δ 7.37 (t, J = 7.2 Hz, 4H), 7.34 – 7.28 (m, 5H), 7.26 – 7.22 (m, 1H), 6.51 (dd, J = 16.0, 1.5 Hz, 1H), 6.35 (dd, J = 15.9, 6.1 Hz, 1H), 5.98 (d, J = 8.0 Hz, 1H), 5.80

(ddd, J = 8.0, 6.2, 1.3 Hz, 1H), 1.25 (s, 9H) ppm. **^{13}C NMR** ($CDCl_3$, 151 MHz) δ 177.49, 141.27, 136.62, 131.62, 129.23, 128.96, 128.71, 127.94, 127.75, 127.15, 126.69, 54.63, 38.98, 27.78 ppm. **HRMS** (+APCI) calculated for $C_{20}H_{24}NO$ $[M+H]^+$ 294.18524, found 294.185123. **HPLC** (AD-H column, 5% 2-propanol in Hexanes, 1 mL/min) t_M = 16.2 min, t_m = 13.8 min, 98:2 e.r.

4.5.2.6 X-Ray Crystallographic Data – Collected by Dr. John Bacsa

Experimental. Single orange plate-shaped crystals of CCDC 196624 (CDPoff-0035-0071) (4.35) were recrystallised from a mixture of pentane and $CHCl_3$ by vapor diffusion. A suitable crystal 0.50×0.14×0.09 mm^3 was selected and mounted on a loop with paratone oil on an XtaLAB Synergy-S diffractometer. The crystal was kept at T = 100.0(2) K during data collection. The structure was solved with the **ShelXT** (Sheldrick, 2015) structure solution program using the Intrinsic Phasing solution method and by using **Olex$_2$** (Dolomanov et al., 2009) as the graphical interface. The model was refined with version 2018/3 of **ShelXL** (Sheldrick, 2015) us20rthogonalizuares minimisation.

Crystal Data. $C_{21}H_{22}ClRh$, M_r = 412.74, monoclinic, $P2_1$ (No. 4), a = 6.9777(6) Å, b = 17.2222(15) Å, c = 7.2610(10) Å, β = 98.216(10)°, $\alpha = \gamma$ = 90°, V = 863.60(16) $Å^3$, T = 10.0(2) K, Z = 2, Z' = 1, $\mu(MoK_\alpha)$ = 1.140 mm^{-1}, 15658 reflections measured, 5214 unique (R_{int} = 0.0562) which were used in all calculations. The final wR_2 was 0.0946 (all data) and R_1 was 0.0422 (I > 2σ(I)).

Compound	**CCDC 1966524 (CDPoff-0035-0071)**
Formula	$C_{21}H_{22}ClRh$
$D_{calc.}$/ g cm^{-3}	1.587
μ/mm^{-1}	1.140
Formula Weight	412.74
Colour	orange
Shape	plate
Size/mm^3	0.50×0.14×0.09
T/K	100.0(2)
Crystal System	monoclinic
Flack Parameter	-0.02(3)
Hooft Parameter	-0.01(2)
Space Group	$P2_1$
a/Å	6.9777(6)
b/Å	17.2222(15)
c/Å	7.2610(10)
α/°	90
β/°	98.216(10)
γ/°	90
V/Å^3	863.60(16)
Z	2
Z'	1
Wavelength/Å	0.71073
Radiation type	MoK□
Θ_{min}/°	2.365
Θ_{max}/°	30.506
Measured Refl.	15658
Independent Refl.	5214
Reflections with I > 2σ(I)	4605
R_{int}	0.0562
Parameters	260
Restraints	168
Largest Peak	1.105
Deepest Hole	-1.289
GooF	1.019
wR_2 (all data)	0.0946
wR_2	0.0920
R_1 (all data)	0.0500
R_1	0.0422

Structure Quality Indicators

Reflections:	d min (Mo)	0.70	I/σ	15.7	Rint	5.62%	complete 100% (IUCr)	100%
Refinement:	Shift	-0.009	Max Peak	1.1	Min Peak	-1.3	GooF	1.019	Flack	-.02(3)

An orange plate-shaped crystal with dimensions 0.50×0.14×0.09 mm^3 was mounted on a loop with paratone oil. Data were collected using an XtaLAB Synergy, Dualflex, HyPix diffractometer equipped with an Oxford Cryosystems low-temperature device operating at T = 100.0(2) K.

Data were measured using ω scans using MoK_α radiation. The total number of runs and images was based on the strategy calculation from the program **CrysAlisPro** (Rigaku, V1.171.40.53, 2019). The maximum resolution that was achieved was Θ = 30.506° (0.70 Å).

The diffraction pattern was indexed and the unit cell was refined using **CrysAlisPro** (Rigaku, V1.171.40.53, 2019) on 7723 reflections, 49% of the observed reflections.

Data reduction, scaling and absorption corrections were performed using **CrysAlisPro** (Rigaku, V1.171.40.53, 2019). The final completeness is 100.00 % out to 30.506° in Θ. A numerical absorption correction based on Gaussian integration over a multifaceted crystal model was performed using **CrysAlisPro** (Rigaku, V1.171.40.53, 2019). An empirical absorption correction using spherical harmonics as implemented in SCALE3 ABSPACK was also applied. The absorption coefficient μ of this material is 1.140 mm^{-1} at this wavelength (λ = 0.711Å) and the minimum and maximum transmissions are 0.441 and 1.000.

The structure was solved and the space group $P2_1$ (# 4) determined by the **ShelXT** (Sheldrick, 2015) structure solution program using Intrinsic Phasing and refined by Least Squares using version 2018/3 of **ShelXL** (Sheldrick, 2015). All non-hydrogen atoms were refined

anisotropically. Most Hydrogen atom positions were calculated geometrically and refined using the riding model. Hydrogen atom positions for the allyl group were located and refined freely.

There is a single molecule in the asymmetric unit, which is represented by the reported sum formula. In other words: Z is 2 and Z' is 1.

The Flack parameter was refined to -0.02(3). Determination of absolute structure using Bayesian statistics on Bijvoet differences using the Olex2 results in -0.01(2). Note: The Flack parameter is used to determine chirality of the crystal studied, the value should be near 0, a value of 1 means that the stereochemistry is wrong, and the model should be inverted. A value of 0.5 means that the crystal consists of a racemic mixture of the two enantiomers.

Images of the Crystal on the Diffractometer

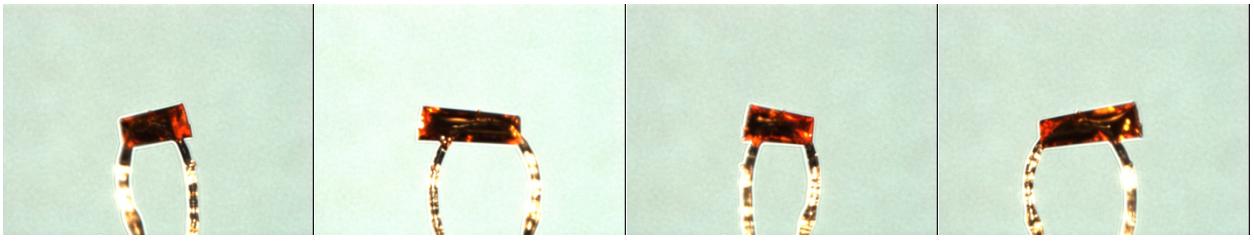

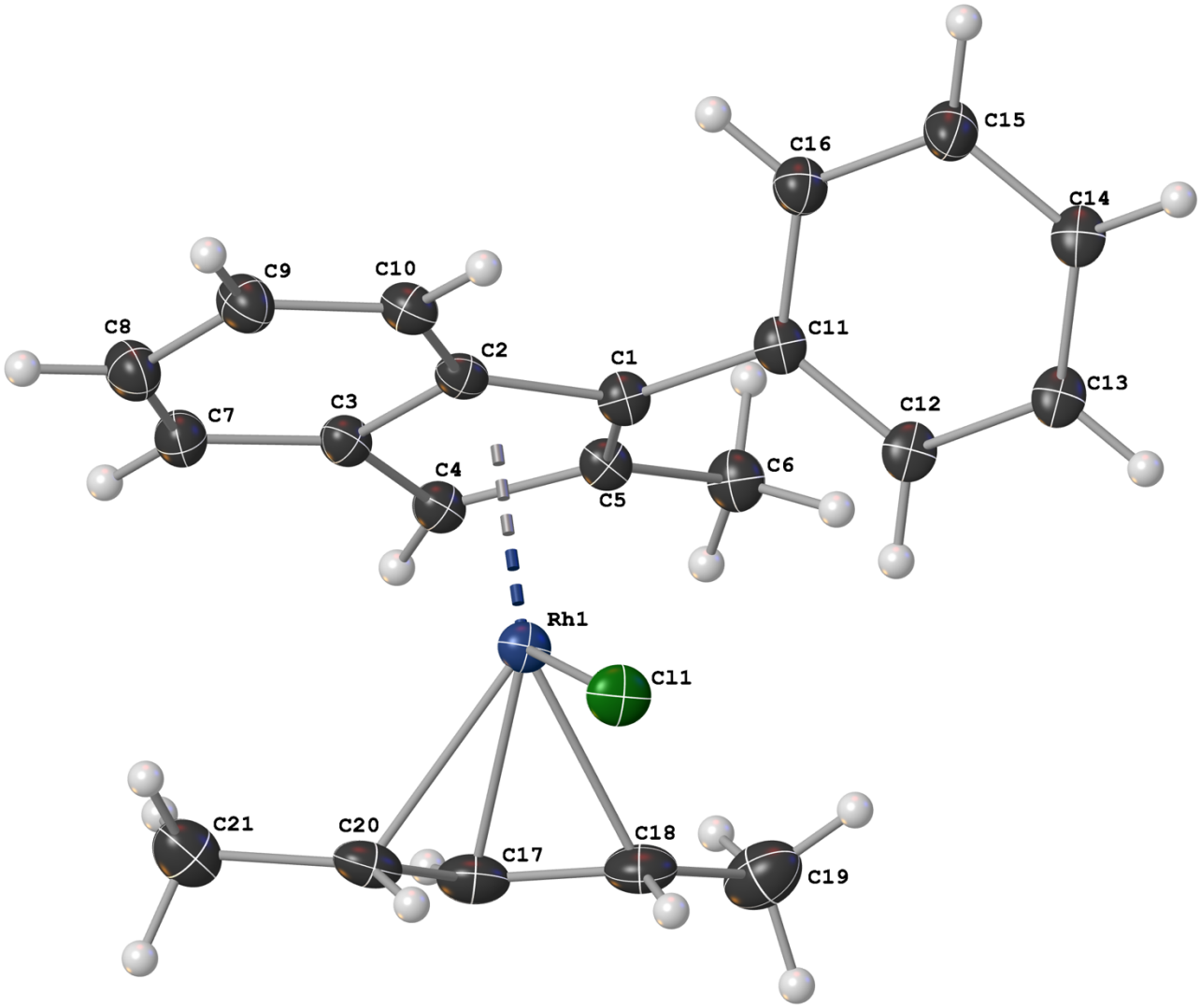

Figure S1: Crystal Structure for **CCDC 1966524** (CDPoff-0035-0071)

Data Plots: Diffraction Data

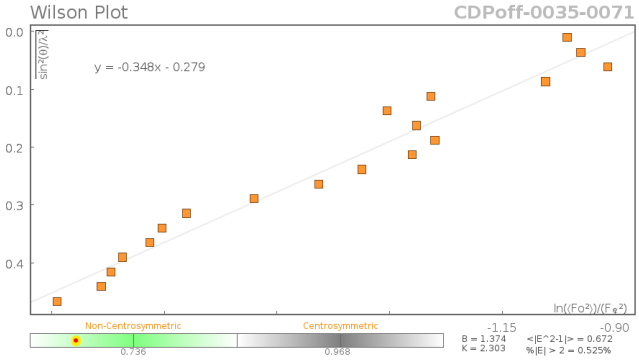

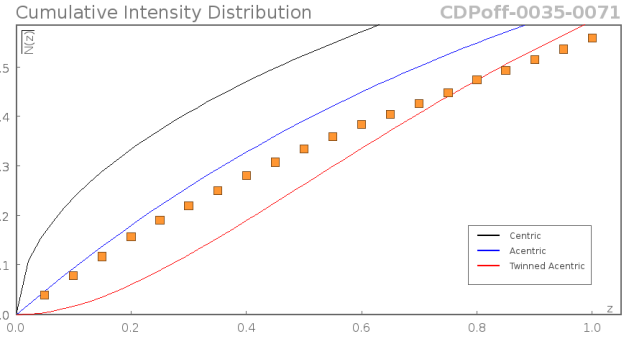

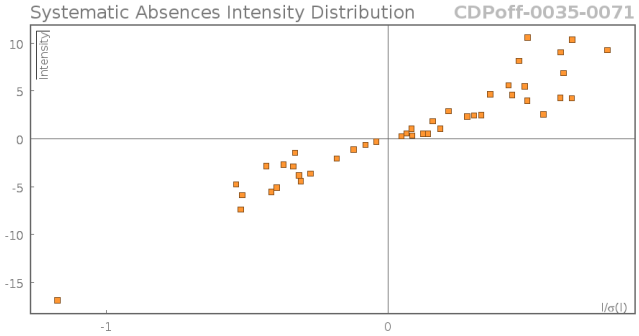

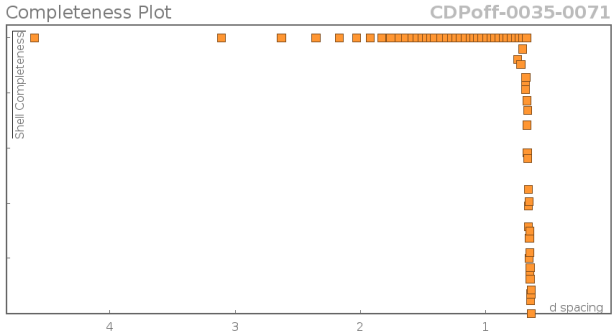

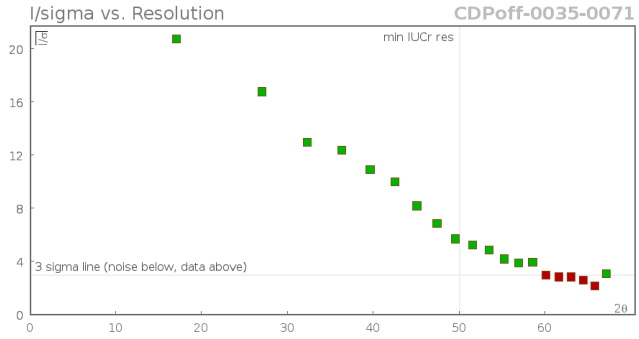

Data Plots: Refinement and Data

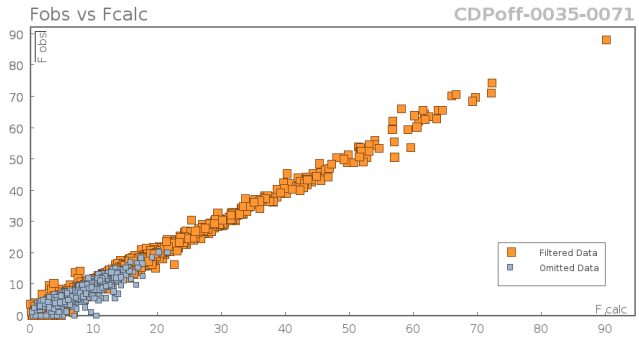

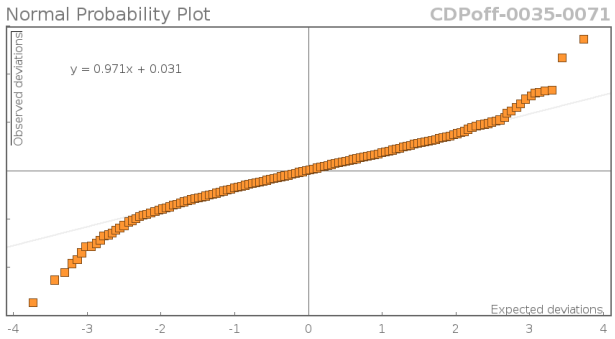

Reflection Statistics

Total reflections (after filtering)	15701	Unique reflections	5214
Completeness	0.99	Mean I/σ	14.41
hkl_{max} collected	(9, 26, 10)	hkl_{min} collected	(-10, -26, -11)
hkl_{max} used	(9, 24, 10)	hkl_{min} used	(-9, -24, 0)
Lim d_{max} collected	20.0	Lim d_{min} collected	0.7
d_{max} used	8.61	d_{min} used	0.7
Friedel pairs	3382	Friedel pairs merged	0
Inconsistent equivalents	20	R_{int}	0.0562
R_{sigma}	0.0636	Intensity transformed	0
Omitted reflections	0	Omitted by user (OMIT hkl)	0
Multiplicity	(4540, 2898, 1239, 393, 127, 48, 26, 9, 1)	Maximum multiplicity	11
Removed systematic absences	43	Filtered off (Shel/OMIT)	1110

Table 4.S1: Fractional Atomic Coordinates ($\times 10^4$) and Equivalent Isotropic Displacement Parameters ($Å^2 \times 10^3$) for **CCDC 1966524** (CDPoff-0035-0071). U_{eq} is defined as 1/3 of the trace of the orthogonalised U_{ij}.

Atom	x	y	z	U_{eq}
C1	3493(8)	5176(3)	3938(8)	18.0(9)
C2	2884(6)	4397(4)	3332(6)	17.2(7)
C3	4493(8)	3885(3)	3711(8)	18.9(9)
C4	6097(7)	4355(3)	4600(7)	18.9(8)
C5	5524(7)	5149(3)	4539(8)	17.3(9)
C6	6840(8)	5831(4)	4967(8)	22.9(11)
C7	4270(8)	3097(4)	3305(8)	22.7(10)
C8	2507(9)	2831(4)	2510(9)	25.8(10)
C9	912(8)	3332(4)	2097(9)	25.3(10)
C10	1064(8)	4107(4)	2532(8)	20.7(9)
C17	5855(9)	4075(4)	8896(10)	27.5(11)
C18	5284(7)	4837(4)	9205(9)	26.7(12)
C19	6649(10)	5496(5)	9495(10)	36.2(14)
C20	4433(7)	3502(4)	8549(8)	24.4(10)
C21	4828(9)	2691(4)	7975(10)	31.1(12)
Cl1	891.8(17)	4641.3(17)	7406.5(19)	23.3(3)
Rh1	4021.2(4)	4459.1(16)	6485.9(5)	16.8(1)
C11_1	2319(12)	5894(3)	3763(8)	18.4(8)
C12_1	2231(13)	6376(3)	5274(8)	18(2)
C13_1	1235(13)	7075(3)	5056(8)	20(2)
C14_1	300(12)	7288(3)	3335(9)	19(2)
C15_1	337(13)	6810(3)	1840(8)	25(3)
C16_1	1345(14)	6105(3)	2058(8)	22(3)
C11_2	2314(11)	5885(3)	3502(8)	18.4(8)

Atom	x	y	z	U_{eq}
C12_2	2018(12)	6415(3)	4867(8)	23(2)
C13_2	987(12)	7093(3)	4406(8)	21.9(19)
C14_2	230(11)	7239(3)	2587(8)	23(2)
C15_2	442(12)	6706(3)	1237(8)	24(2)
C16_2	1503(12)	6026(3)	1697(8)	20(2)

Table 4.S2: Anisotropic Displacement Parameters (×10⁴) **CCDC 19665245** (CDPoff-0035-0071). The anisotropic displacement factor exponent takes the form: $-2\pi^2[h^2a^{*2} \times U_{11} + \ldots + 2hka^* \times b^* \times U_{12}]$

Atom	U_{11}	U_{22}	U_{33}	U_{23}	U_{13}	U_{12}
C1	12.5(13)	20.3(13)	22(2)	0.1(13)	3.6(13)	-0.3(10)
C2	15.9(12)	20.0(13)	16.1(17)	2.8(15)	4.1(11)	0.5(10)
C3	17.5(12)	19.8(12)	20(2)	1.4(12)	3.8(12)	1.7(10)
C4	16.3(14)	20.6(14)	20.1(19)	1.5(13)	4.1(13)	1.7(10)
C5	12.2(13)	20.0(15)	20(2)	1.1(13)	4.3(13)	0.0(9)
C6	18(2)	23.0(16)	28(3)	-0.2(18)	4(2)	-3.9(15)
C7	24.1(14)	19.9(12)	24(2)	0.0(13)	3.2(14)	1.2(10)
C8	26.6(15)	21.1(13)	29(3)	1.5(15)	0.2(14)	-1.2(10)
C9	24.9(14)	22.5(14)	27(3)	1.9(14)	-0.8(15)	-2.1(11)
C10	17.9(12)	22.1(13)	22(2)	3.6(14)	1.6(13)	-1.6(11)
C17	26(2)	37.5(15)	19(3)	6.0(16)	3(2)	-0.4(13)
C18	23(2)	37.5(15)	19(3)	2.8(17)	-2(2)	-1.7(14)
C19	33(3)	44.7(19)	31(3)	-6(2)	6(3)	-10(2)
C20	21.2(19)	32.6(15)	19(3)	8.7(16)	2.9(18)	4.0(13)
C21	26(3)	33.2(16)	35(3)	6.4(18)	10(2)	4.0(16)
Cl1	12.4(5)	31.4(8)	27.2(6)	0.9(5)	7.0(4)	2.3(4)
Rh1	10.87(16)	20.79(16)	19.05(17)	0.9(2)	3.20(11)	0.81(19)
C11_1	11.5(15)	19.6(12)	24.5(16)	0.1(11)	3.5(12)	-1.3(11)
C12_1	6(5)	23(2)	26.0(19)	-2.3(17)	2(2)	-1(3)
C13_1	8(4)	23(2)	27(3)	-4(2)	-1(3)	0(3)
C14_1	7(4)	22(3)	28(3)	-3(2)	-1(3)	-2(3)
C15_1	24(5)	23(3)	27(3)	-2.7(18)	-3(3)	4(3)
C16_1	19(6)	22(3)	25.4(18)	-0.6(16)	1(2)	2(3)
C11_2	11.5(15)	19.6(12)	24.5(16)	0.1(11)	3.5(12)	-1.3(11)
C12_2	18(5)	24(2)	25.6(19)	-2.1(15)	0.8(19)	5(3)
C13_2	15(4)	23(2)	27(2)	-2.6(19)	0(2)	3(2)
C14_2	19(4)	23(3)	27(3)	-2.8(19)	-1(3)	4(3)
C15_2	23(4)	22(3)	27(2)	-1.8(16)	-1(2)	4(3)
C16_2	16(4)	20(3)	24.8(17)	-0.3(14)	2.3(16)	0(3)

Table 4.S3: Bond Lengths in Å for **CCDC 1966524** (CDPoff-0035-0071).

Atom	Atom	Length/Å
C1	C2	1.455(8)
C1	C5	1.423(7)
C1	Rh1	2.210(5)
C1	C11_1	1.479(7)
C1	C11_2	1.481(7)
C2	C3	1.423(7)
C2	C10	1.410(7)
C2	Rh1	2.316(4)
C3	C4	1.455(8)
C3	C7	1.394(7)
C3	Rh1	2.310(6)
C4	C5	1.425(7)
C4	Rh1	2.138(5)
C5	C6	1.495(7)
C5	Rh1	2.222(5)
C7	C8	1.361(8)
C8	C9	1.407(8)
C9	C10	1.372(8)
C17	C18	1.399(8)
C17	C20	1.397(9)
C17	Rh1	2.120(7)
C18	C19	1.477(9)
C18	Rh1	2.145(7)
C20	C21	1.493(8)
C20	Rh1	2.219(6)
Cl1	Rh1	2.3938(12)
C11_1	C12_1	1.384(6)
C11_1	C16_1	1.373(6)
C12_1	C13_1	1.388(6)
C13_1	C14_1	1.374(7)
C14_1	C15_1	1.366(7)
C15_1	C16_1	1.401(7)
C11_2	C12_2	1.384(6)
C11_2	C16_2	1.373(6)
C12_2	C13_2	1.388(6)
C13_2	C14_2	1.374(7)
C14_2	C15_2	1.366(7)
C15_2	C16_2	1.401(7)

Table 4.S4: Bond Angles in ° for **CCDC 1966524** (CDPoff-0035-0071).

Atom	Atom	Atom	Angle/°
C2	C1	Rh1	75.3(3)
C2	C1	C11_1	127.6(5)

Atom	Atom	Atom	Angle/°
C2	C1	C11_2	124.5(5)
C5	C1	C2	107.4(4)
C5	C1	Rh1	71.7(3)
C5	C1	C11_1	124.6(5)
C5	C1	C11_2	126.1(5)
C11_1	C1	Rh1	124.3(4)
C11_2	C1	Rh1	131.3(4)
C1	C2	Rh1	67.3(3)
C3	C2	C1	108.9(4)
C3	C2	Rh1	71.8(3)
C10	C2	C1	131.1(5)
C10	C2	C3	119.9(6)
C10	C2	Rh1	125.8(3)
C2	C3	C4	106.1(5)
C2	C3	Rh1	72.3(3)
C4	C3	Rh1	64.6(3)
C7	C3	C2	120.1(5)
C7	C3	C4	133.7(5)
C7	C3	Rh1	125.1(4)
C3	C4	Rh1	77.4(3)
C5	C4	C3	109.0(4)
C5	C4	Rh1	74.1(3)
C1	C5	C4	107.6(4)
C1	C5	C6	126.5(5)
C1	C5	Rh1	70.8(3)
C4	C5	C6	125.9(5)
C4	C5	Rh1	67.8(3)
C6	C5	Rh1	128.3(4)
C8	C7	C3	119.0(5)
C7	C8	C9	121.6(5)
C10	C9	C8	121.0(5)
C9	C10	C2	118.4(5)
C18	C17	Rh1	71.8(4)
C20	C17	C18	118.8(6)
C20	C17	Rh1	75.1(4)
C17	C18	C19	123.4(5)
C17	C18	Rh1	69.9(4)
C19	C18	Rh1	122.4(4)
C17	C20	C21	123.8(5)
C17	C20	Rh1	67.4(4)
C21	C20	Rh1	121.2(4)
C1	Rh1	C2	37.4(2)
C1	Rh1	C3	62.4(2)
C1	Rh1	C5	37.46(18)
C1	Rh1	C20	165.9(2)
C1	Rh1	Cl1	96.36(14)
C2	Rh1	Cl1	94.87(11)
C3	Rh1	C2	35.84(19)
C3	Rh1	Cl1	123.31(15)
C4	Rh1	C1	63.78(19)

Atom	Atom	Atom	Angle/°
C4	Rh1	C2	62.01(16)
C4	Rh1	C3	37.9(2)
C4	Rh1	C5	38.09(19)
C4	Rh1	C18	112.85(18)
C4	Rh1	C20	109.62(18)
C4	Rh1	Cl1	156.67(14)
C5	Rh1	C2	61.43(19)
C5	Rh1	C3	62.3(2)
C5	Rh1	Cl1	129.79(14)
C17	Rh1	C1	150.9(2)
C17	Rh1	C2	151.9(2)
C17	Rh1	C3	116.2(2)
C17	Rh1	C4	96.8(2)
C17	Rh1	C5	114.1(2)
C17	Rh1	C18	38.3(2)
C17	Rh1	C20	37.5(2)
C17	Rh1	Cl1	106.10(18)
C18	Rh1	C1	126.7(2)
C18	Rh1	C2	164.0(2)
C18	Rh1	C3	147.3(2)
C18	Rh1	C5	104.7(2)
C18	Rh1	C20	66.9(2)
C18	Rh1	Cl1	88.52(13)
C20	Rh1	C2	128.8(2)
C20	Rh1	C3	104.5(2)
C20	Rh1	C5	143.13(18)
C20	Rh1	Cl1	86.79(12)
C12_1	C11_1	C1	121.3(5)
C16_1	C11_1	C1	119.7(5)
C16_1	C11_1	C12_1	118.9(4)
C11_1	C12_1	C13_1	120.5(4)
C14_1	C13_1	C12_1	120.0(4)
C15_1	C14_1	C13_1	120.1(4)
C14_1	C15_1	C16_1	119.9(4)
C11_1	C16_1	C15_1	120.5(5)
C12_2	C11_2	C1	121.7(5)
C16_2	C11_2	C1	119.4(5)
C16_2	C11_2	C12_2	118.9(4)
C11_2	C12_2	C13_2	120.5(4)
C14_2	C13_2	C12_2	120.0(4)
C15_2	C14_2	C13_2	120.1(4)
C14_2	C15_2	C16_2	119.9(4)
C11_2	C16_2	C15_2	120.5(5)

Table 4.S5: Torsion Angles in ° for **CCDC 1966524** (CDPoff-0035-0071).

Atom	Atom	Atom	Atom	Angle/°
C1	C2	C3	C4	1.3(6)
C1	C2	C3	C7	178.2(5)
C1	C2	C3	Rh1	57.2(3)
C1	C2	C10	C9	-179.8(5)
C1	C11_1	C12_1	C13_1	175.4(8)
C1	C11_1	C16_1	C15_1	-175.5(8)
C1	C11_2	C12_2	C13_2	176.9(8)
C1	C11_2	C16_2	C15_2	-177.7(7)
C2	C1	C5	C4	-9.4(6)
C2	C1	C5	C6	168.6(5)
C2	C1	C5	Rh1	-67.4(3)
C2	C1	C11_1	C12_1	129.5(7)
C2	C1	C11_1	C16_1	-52.7(10)
C2	C1	C11_2	C12_2	130.9(7)
C2	C1	C11_2	C16_2	-49.6(9)
C2	C3	C4	C5	-7.2(6)
C2	C3	C4	Rh1	60.9(4)
C2	C3	C7	C8	1.3(8)
C3	C2	C10	C9	-1.5(8)
C3	C4	C5	C1	10.4(6)
C3	C4	C5	C6	-167.6(5)
C3	C4	C5	Rh1	70.3(4)
C3	C7	C8	C9	-0.2(9)
C4	C3	C7	C8	177.2(6)
C5	C1	C2	C3	5.0(6)
C5	C1	C2	C10	-176.6(5)
C5	C1	C2	Rh1	65.0(4)
C5	C1	C11_1	C12_1	-58.8(10)
C5	C1	C11_1	C16_1	119.0(8)
C5	C1	C11_2	C12_2	-67.3(9)
C5	C1	C11_2	C16_2	112.2(8)
C7	C3	C4	C5	176.6(6)
C7	C3	C4	Rh1	-115.3(7)
C7	C8	C9	C10	-1.9(10)
C8	C9	C10	C2	2.7(9)
C10	C2	C3	C4	-177.3(5)
C10	C2	C3	C7	-0.5(8)
C10	C2	C3	Rh1	-121.4(4)
C18	C17	C20	C21	172.4(6)
C18	C17	C20	Rh1	59.0(6)
C20	C17	C18	C19	-177.0(5)
C20	C17	C18	Rh1	-60.7(6)
Rh1	C1	C2	C3	-60.0(4)
Rh1	C1	C2	C10	118.4(5)
Rh1	C1	C5	C4	58.0(4)
Rh1	C1	C5	C6	-124.0(6)
Rh1	C1	C11_1	C12_1	31.7(10)
Rh1	C1	C11_1	C16_1	-150.6(6)

Atom	Atom	Atom	Atom	Angle/°
Rh1	C1	C11_2	C12_2	29.8(10)
Rh1	C1	C11_2	C16_2	-150.7(6)
Rh1	C2	C3	C4	-56.0(4)
Rh1	C2	C3	C7	120.9(5)
Rh1	C2	C10	C9	-89.9(6)
Rh1	C3	C4	C5	-68.1(3)
Rh1	C3	C7	C8	90.1(7)
Rh1	C4	C5	C1	-59.9(4)
Rh1	C4	C5	C6	122.1(5)
Rh1	C17	C18	C19	-116.3(7)
Rh1	C17	C20	C21	113.3(6)
C11_1	C1	C2	C3	177.9(6)
C11_1	C1	C2	C10	-3.7(9)
C11_1	C1	C2	Rh1	-122.2(6)
C11_1	C1	C5	C4	177.5(5)
C11_1	C1	C5	C6	-4.5(9)
C11_1	C1	C5	Rh1	119.5(6)
C11_1	C12_1	C13_1	C14_1	1.0(13)
C12_1	C11_1	C16_1	C15_1	2.3(12)
C12_1	C13_1	C14_1	C15_1	0.5(13)
C13_1	C14_1	C15_1	C16_1	-0.6(13)
C14_1	C15_1	C16_1	C11_1	-0.8(14)
C16_1	C11_1	C12_1	C13_1	-2.4(12)
C11_2	C1	C2	C3	169.7(5)
C11_2	C1	C2	C10	-11.9(9)
C11_2	C1	C2	Rh1	-130.4(6)
C11_2	C1	C5	C4	-173.7(5)
C11_2	C1	C5	C6	4.3(9)
C11_2	C1	C5	Rh1	128.3(6)
C11_2	C12_2	C13_2	C14_2	0.8(12)
C12_2	C11_2	C16_2	C15_2	1.9(11)
C12_2	C13_2	C14_2	C15_2	1.9(11)
C13_2	C14_2	C15_2	C16_2	-2.7(11)
C14_2	C15_2	C16_2	C11_2	0.8(12)
C16_2	C11_2	C12_2	C13_2	-2.7(11)

Table 4.S6: Hydrogen Fractional Atomic Coordinates (×10⁴) and Equivalent Isotropic Displacement Parameters (Å²×10³) for **CCDC 1966524** (CDPoff-0035-0071). U_{eq} is defined as 1/3 of the trace of the orthogonalised U_{ij}.

Atom	x	y	z	U_{eq}
H4	7301.38	4166.4	5124.06	23
H6A	7206.57	6029.73	3832.16	34
H6B	7977.85	5671.48	5782.33	34
H6C	6181.61	6227.96	5559.57	34
H7	5309.38	2757.25	3572.67	27
H8	2353.21	2305.13	2234.06	31
H9	-263.88	3135.31	1520.03	30

Atom	x	y	z	U_{eq}
H10	-6.02	4433.04	2304.95	25
H19A	7083.85	5558.47	10801.51	54
H19B	6011.12	5961.71	9009.31	54
H19C	7741.24	5395.23	8861.87	54
H21B	5995.35	2683.09	7417.63	47
H21A	3766.47	2510.81	7091.58	47
H21C	4977.53	2359.26	9048.27	47
H18	4038	4851.69	9811.7	0
H20	3208.21	3582.51	9167.8	0
H17	7178.5	3963.4	8586.61	0
H12_1	2844.57	6229.65	6445.2	22
H13_1	1200.76	7399.11	6074.56	24
H14_1	-359.06	7758.05	3188.93	23
H15_1	-305.4	6952.55	677.7	30
H16_1	1354.92	5777.68	1041.27	27
H12_2	2514.39	6315.13	6102.78	27
H13_2	808.19	7449.28	5329.5	26
H14_2	-428.07	7700.49	2273.85	28
H15_2	-117.47	6795.08	13.89	29
H16_2	1660.22	5667.35	772.97	24

Table 4.S7: Atomic Occupancies for all atoms that are not fully occupied in **CCDC 1966524** (CDPoff-0035-0071).

Atom	Occupancy
C11_1	0.444(11)
C12_1	0.444(11)
H12_1	0.444(11)
C13_1	0.444(11)
H13_1	0.444(11)
C14_1	0.444(11)
H14_1	0.444(11)
C15_1	0.444(11)
H15_1	0.444(11)
C16_1	0.444(11)
H16_1	0.444(11)
C11_2	0.556(11)
C12_2	0.556(11)
H12_2	0.556(11)
C13_2	0.556(11)
H13_2	0.556(11)
C14_2	0.556(11)
H14_2	0.556(11)
C15_2	0.556(11)
H15_2	0.556(11)
C16_2	0.556(11)
H16_2	0.556(11)

checkCIF/PLATON report

Structure factors have been supplied for datablock(s) cdpoff-0035-0071

THIS REPORT IS FOR GUIDANCE ONLY. IF USED AS PART OF A REVIEW PROCEDURE FOR PUBLICATION, IT SHOULD NOT REPLACE THE EXPERTISE OF AN EXPERIENCED CRYSTALLOGRAPHIC REFEREE.

No syntax errors found. CIF dictionary Interpreting this report

CCDC 1966524

Datablock: cdpoff-0035-0071

Bond precision: C-C = 0.0086 A		Wavelength=0.71073	
Cell:	a=6.9777(6)	b=17.2222(15)	c=7.261(1)
	alpha=90	beta=98.216(10)	gamma=90
Temperature:	100 K		
	Calculated	Reported	
Volume	863.61(16)	863.60(16)	
Space group	P 21	P 1 21 1	
Hall group	P 2yb	P 2yb	
Moiety formula	C21 H22 Cl Rh	C21 H22 Cl Rh	
Sum formula	C21 H22 Cl Rh	C21 H22 Cl Rh	
Mr	412.75	412.74	
Dx,g cm-3	1.587	1.587	
Z	2	2	
Mu (mm-1)	1.140	1.140	

F000	420.0	420.0
F000'	418.17	
h,k,lmax	9,24,10	9,24,10
Nref	5266[2713]	5214
Tmin,Tmax	0.828,0.906	0.441,1.000
Tmin'	0.568	

Correction method= # Reported T Limits: Tmin=0.441 Tmax=1.000

AbsCorr = GAUSSIAN

Data completeness= 1.92/0.99 Theta(max)= 30.506

R(reflections)= 0.0422(4605) wR2(reflections)= 0.0946(5214)

S = 1.019 Npar= 260

The following ALERTS were generated. Each ALERT has the format **test-name_ALERT_alert-type_alert-level**.

Click on the hyperlinks for more details of the test.

Alert level C

PLAT342_ALERT_3_C Low Bond Precision on C-C Bonds ..... 0.0086 Ang.

Alert level G

PLAT002_ALERT_2_G Number of Distance or Angle Restraints on AtSite 17 Note

PLAT003_ALERT_2_G Number of Uiso or Uij Restrained non-H Atoms ... 27 Report

PLAT171_ALERT_4_G The CIF-Embedded .res File Contains EADP Records 2 Report

PLAT175_ALERT_4_G The CIF-Embedded .res File Contains SAME Records 1 Report

PLAT176_ALERT_4_G The CIF-Embedded .res File Contains SADI Records 2 Report

PLAT186_ALERT_4_G The CIF-Embedded .res File Contains ISOR Records 1 Report

PLAT187_ALERT_4_G The CIF-Embedded .res File Contains RIGU Records 9 Report

PLAT301_ALERT_3_G Main Residue Disorder .....(Resd 1) 26% Note

PLAT380_ALERT_4_G Incorrectly? Oriented X(sp2)-Methyl Moiety ..... C21 Check

PLAT720_ALERT_4_G Number of Unusual/Non-Standard Labels ..... 22 Note

PLAT811_ALERT_5_G No ADDSYM Analysis: Too Many Excluded Atoms .... ! Info

PLAT860_ALERT_3_G Number of Least-Squares Restraints ..... 168 Note

PLAT912_ALERT_4_G Missing # of FCF Reflections Above STh/L= 0.600 5 Note

PLAT978_ALERT_2_G Number C-C Bonds with Positive Residual Density. 4 Info

---

0 **ALERT level A** = Most likely a serious problem - resolve or explain

0 **ALERT level B** = A potentially serious problem, consider carefully

1 **ALERT level C** = Check. Ensure it is not caused by an omission or oversight

14 **ALERT level G** = General information/check it is not something unexpected

0 ALERT type 1 CIF construction/syntax error, inconsistent or missing data

3 ALERT type 2 Indicator that the structure model may be wrong or deficient

3 ALERT type 3 Indicator that the structure quality may be low

8 ALERT type 4 Improvement, methodology, query or suggestion

1 ALERT type 5 Informative message, check

It is advisable to attempt to resolve as many as possible of the alerts in all categories. Often the minor alerts point to easily fixed oversights, errors and omissions in your CIF or refinement strategy, so attention to these fine details can be worthwhile. In order to resolve some of the more serious problems it may be necessary to carry out additional measurements or structure

refinements. However, the purpose of your study may justify the reported deviations and the more serious of these should normally be commented upon in the discussion or experimental section of a paper or in the "special_details" fields of the CIF. checkCIF was carefully designed to identify outliers and unusual parameters, but every test has its limitations and alerts that are not important in a particular case may appear. Conversely, the absence of alerts does not guarantee there are no aspects of the results needing attention. It is up to the individual to critically assess their own results and, if necessary, seek expert advice.

Publication of your CIF in IUCr journals

A basic structural check has been run on your CIF. These basic checks will be run on all CIFs submitted for publication in IUCr journals (*Acta Crystallographica*, *Journal of Applied Crystallography*, *Journal of Synchrotron Radiation*); however, if you intend to submit to *Acta Crystallographica Section C* or *E* or *IUCrData*, you should make sure that full publication checks are run on the final version of your CIF prior to submission.

Publication of your CIF in other journals

Please refer to the *Notes for Authors* of the relevant journal for any special instructions relating to CIF submission.

PLATON version of 07/08/2019; check.def file version of 30/07/2019

Datablock cdpoff-0035-0071 - ellipsoid plot

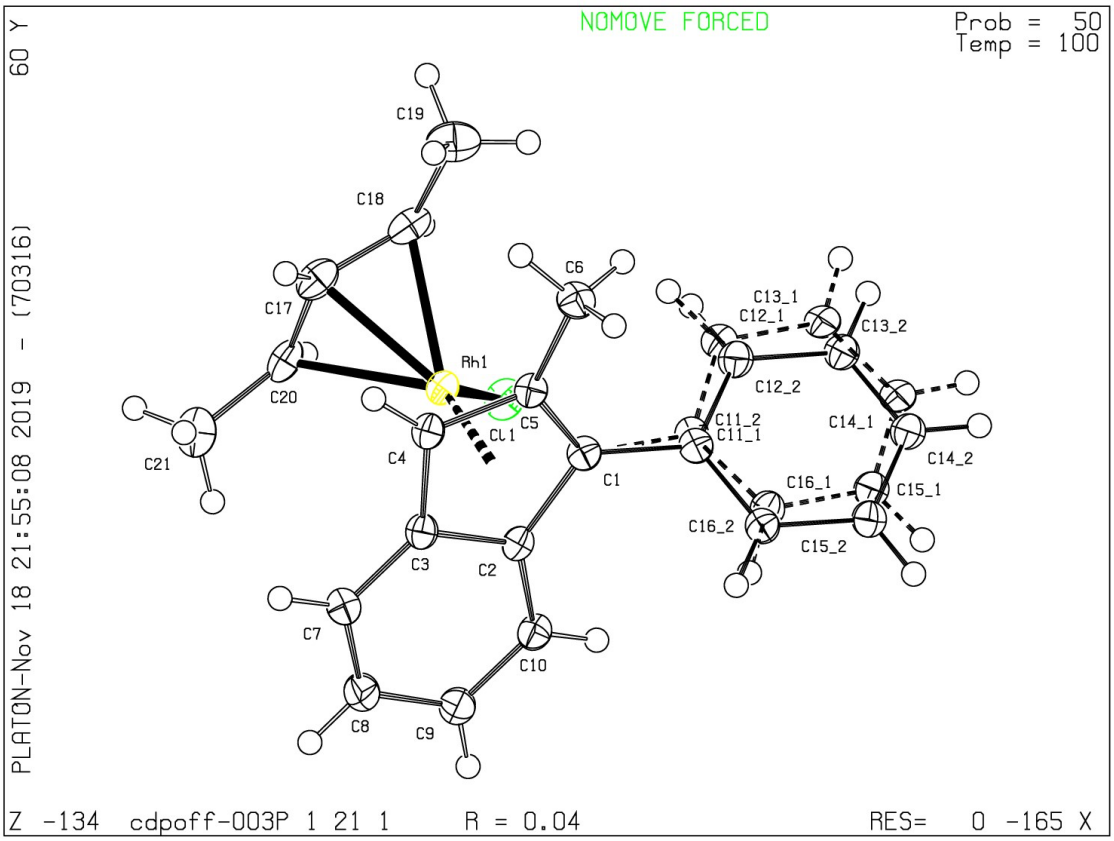

4.5.3 Supplementary References

(1) Yan, Z.; Chong S.; Lin, H.; Yang, Q.; Wang, X.; Zhang, W.; Zhang, X.; Zeng, Z.; Su X. Design, synthesis and biological evaluation of tetrazole-containing RXRα ligands as anticancer agents. *Eur. J. Med. Chem.* **2019**, *164*, 562-575.

(2) Abe, I.; Nakao, Y.; Nakahara, T. *N*-Pivaloyl Methyl Esters as Novel Derivatives of Amino Acid Enantiomers for Chiral-Phase Capillary Gas Chromatography. *Chem. Lett.* **1997**, 629-630.

(3) Burman, J. S.; Harris, R. J.; Farr, C. M. B.; Bacsa, J.; Blakey, S. B. Rh(III) and Ir(III)Cp* Complexes Provide Complimentary Regioselectivity Profiles in Allylic C–H Amidation Reactions. *ACS Catal.* **2019**, *9*, 5474-5479.

(4) CrysAlisPro Software System, Rigaku Oxford Diffraction, (2019).

(5) O.V. Dolomanov and L.J. Bourhis and R.J. Gildea and J.A.K. Howard and H. Puschmann, Olex2: A complete structure solution, refinement and analysis program, *J. Appl. Cryst.*, (2009), **42**, 339-341.

(6) Sheldrick, G.M., Crystal structure refinement with ShelXL, *Acta Cryst.*, (2015), **C27**, 3-8.

(7) Sheldrick, G.M., ShelXT-Integrated space-group and crystal-structure determination, *Acta Cryst.*, (2015), **A71**, 3-8.

(8) Farr, C. M. B.; Kazerouni, A. M.; Park, B.; Poff, C. D.; Won, J.; Sharp, K. R.; Baik, M.-H.; Blakey, S. B. Designing a Planar Chiral Rhodium Indenyl Catalyst for Regio- and Enantioselective Allylic C–H Amidation. *J. Am. Chem. Soc.* **2020**, *142*, 13996-14004.

4.5.4 Spectra and HPLC Data

***2-Methyl-3-phenyl-1H-indene* (4.29)**

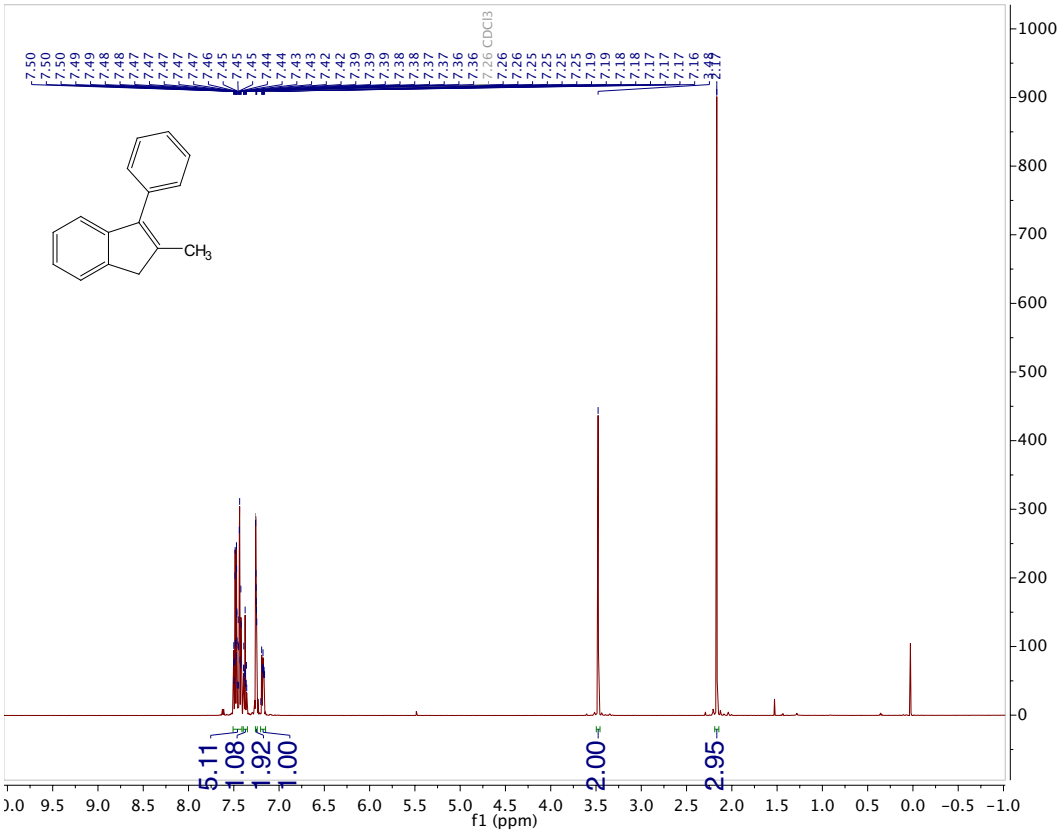

(±)-1,5-cyclooctadiene(η⁵-2-methyl-3-phenylinden-1H-yl)rhodium(I) (rac-4.30)

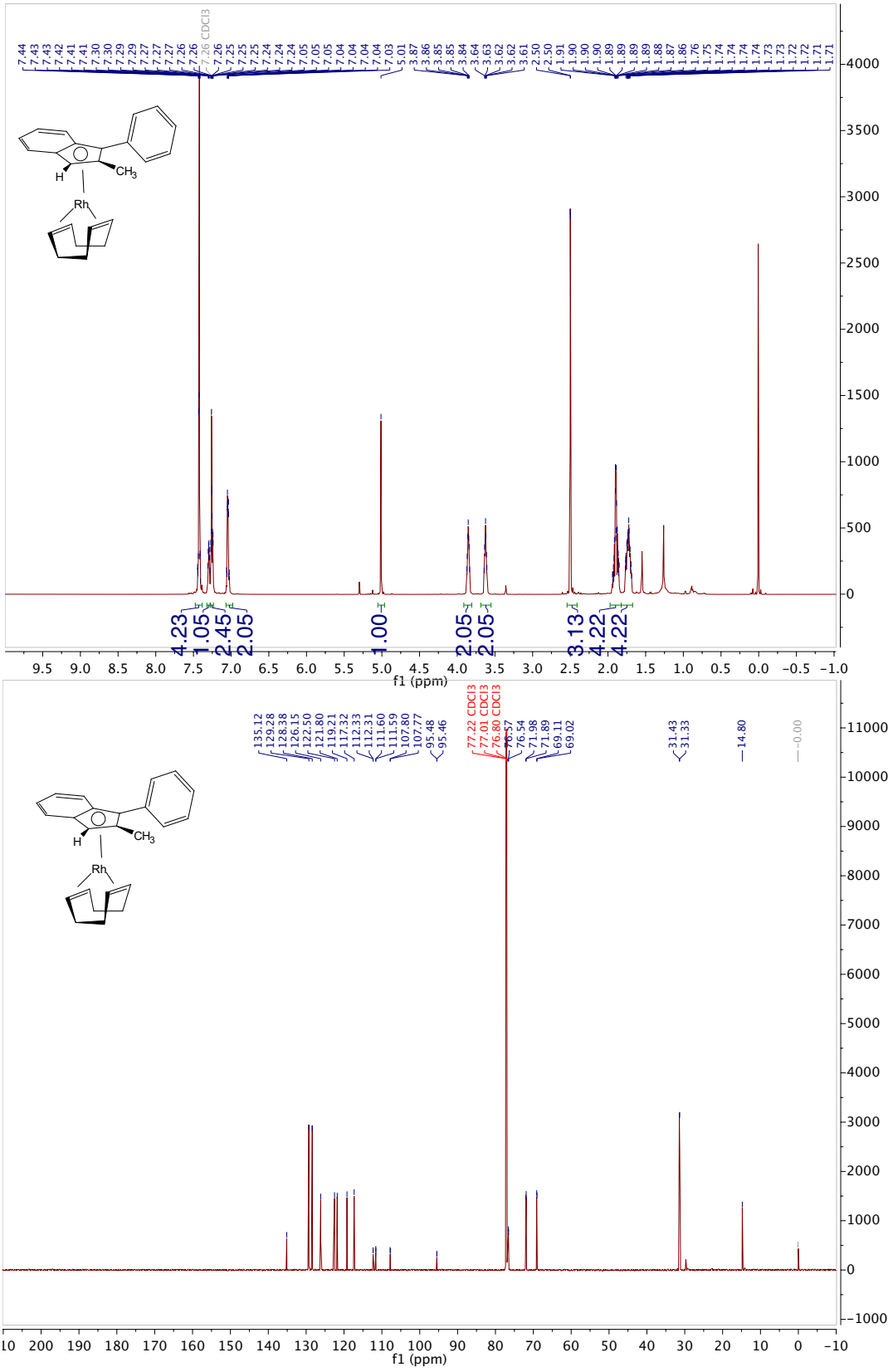

***(±)-1,5-cyclooctadiene(η^5-2-methyl-3-phenylinden-1H-yl)rhodium(I)* (rac-4.30)**

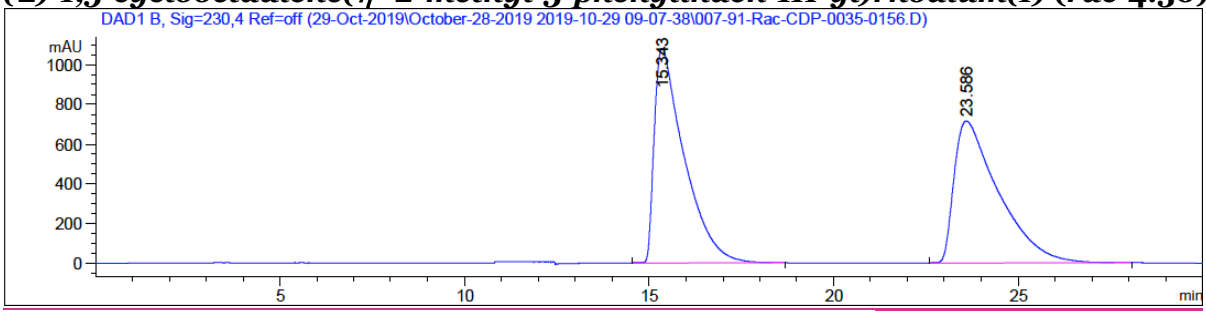

Signal 2: DAD1 B, Sig=230,4 Ref=off

Peak #	RetTime [min]	Type	Width [min]	Area [mAU*s]	Height [mAU]	Area %
1	15.343	BB	0.6713	6.09575e4	1081.97058	50.4581
2	23.586	BB	0.9789	5.98507e4	715.51105	49.5419
Totals :				1.20808e5	1797.48163	

***(pS)-1,5-cyclooctadiene(η^5-2-methyl-3-phenylinden-1H-yl)rhodium(I)* (p*S*-4.30)**

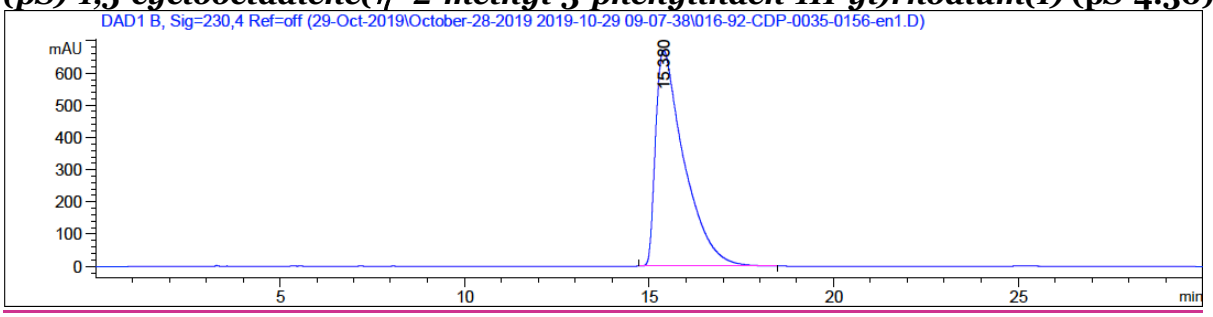

Signal 2: DAD1 B, Sig=230,4 Ref=off

Peak #	RetTime [min]	Type	Width [min]	Area [mAU*s]	Height [mAU]	Area %
1	15.380	BB	0.6345	3.57966e4	669.86053	100.0000
Totals :				3.57966e4	669.86053	

***(pR)-1,5-cyclooctadiene(η^5-2-methyl-3-phenylinden-1H-yl)rhodium(I)* (p*R*-4.30)**

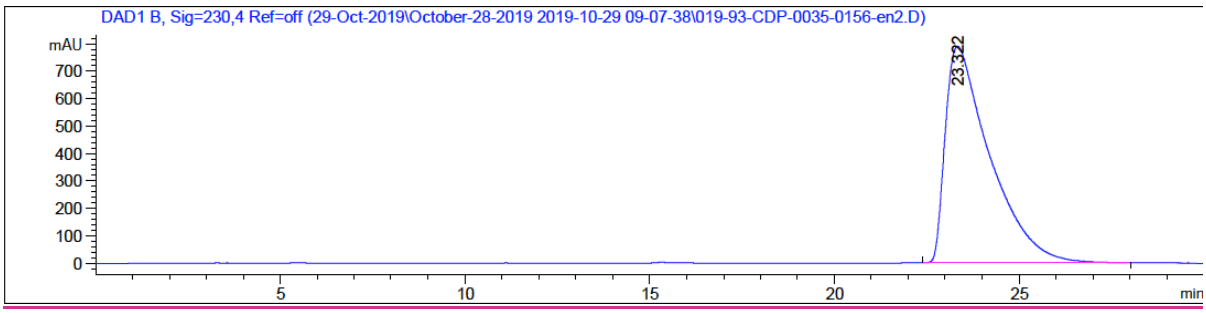

Signal 2: DAD1 B, Sig=230,4 Ref=off

Peak #	RetTime [min]	Type	Width [min]	Area [mAU*s]	Height [mAU]	Area %
1	23.322	BB	0.9844	6.60966e4	789.35767	100.0000
Totals :				6.60966e4	789.35767	

(S,S)-[Rh(2-Me-3-Ph-Ind)I$_2$]$_2$ [(p*S*,p*S*)-4.31]

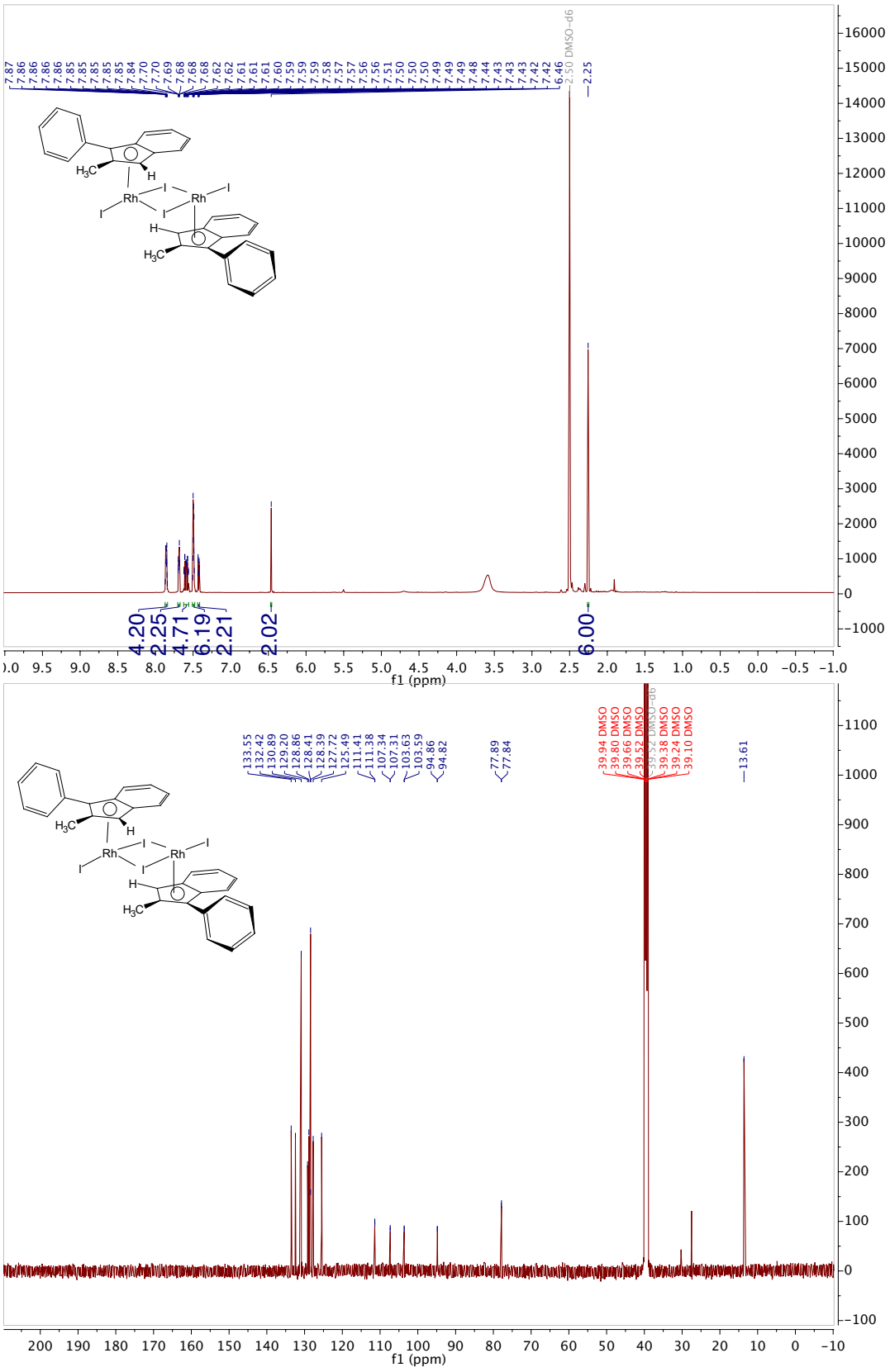

***(E)-(η⁵-S-2-methyl-3-phenylinden-1H-yl)(η³-pent-3-enyl)rhodium(III) chloride* (4.35)**

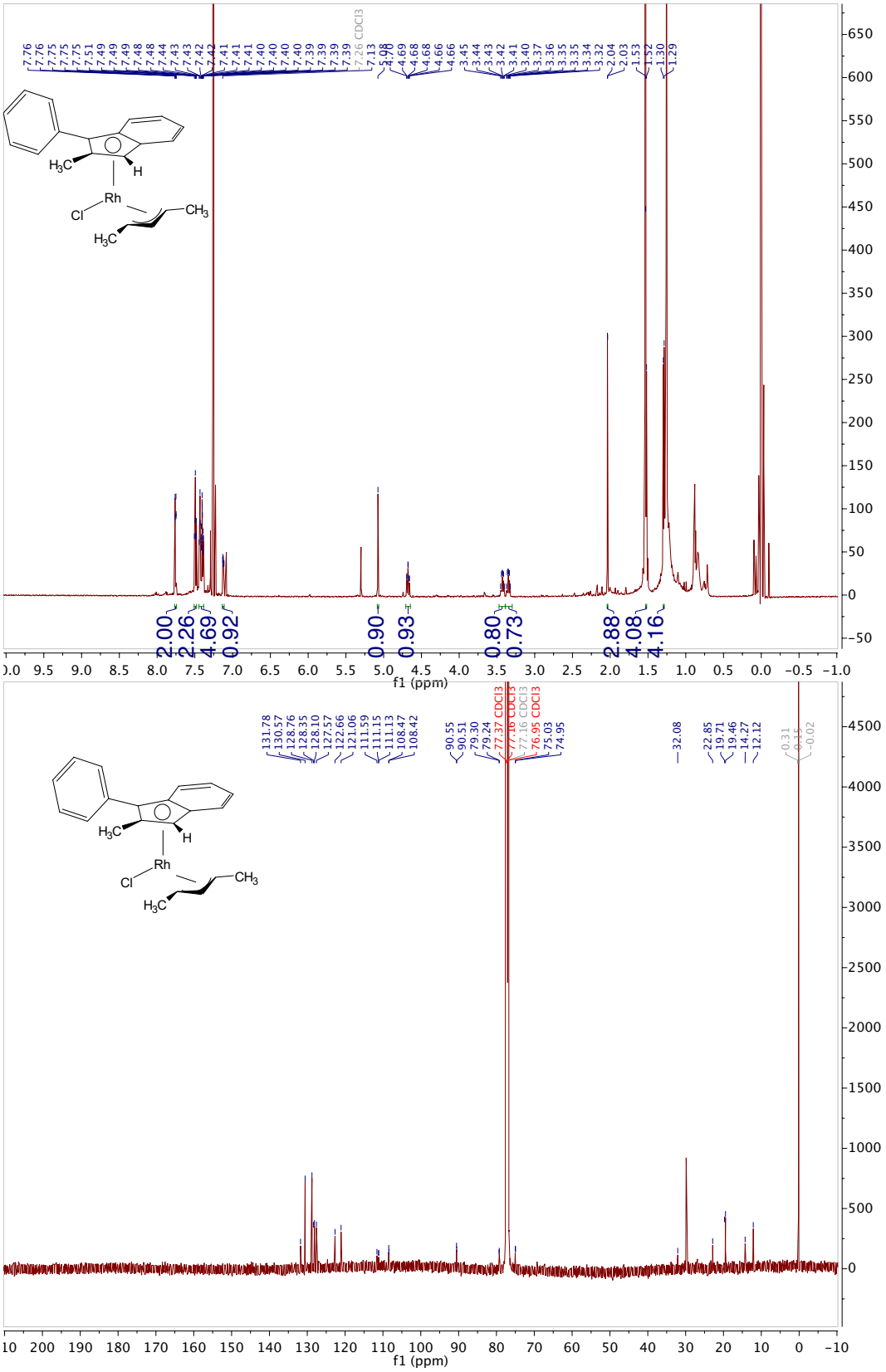

***(R)-N-(4-methylpent-1-en-3-yl)pivalamide* (4.S1)**

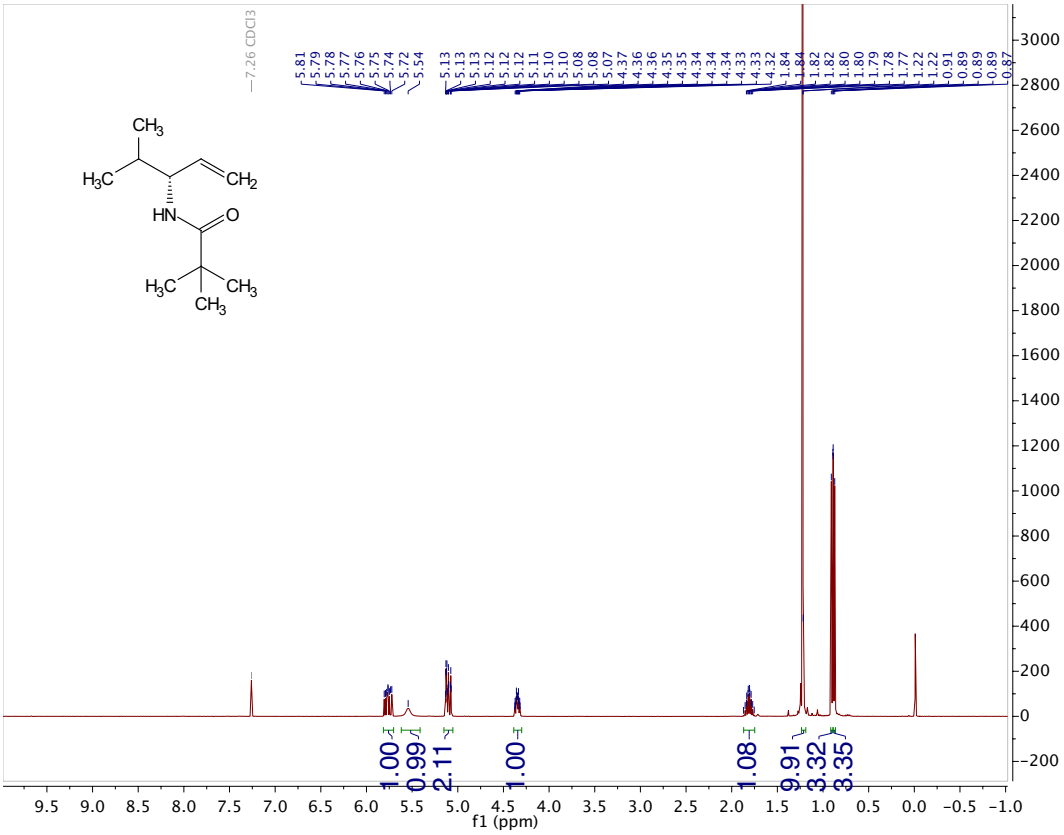

***N-pivaloyl-D-phenylglycine methyl ester* (4.S2-D *D*-Phg-OMe)**

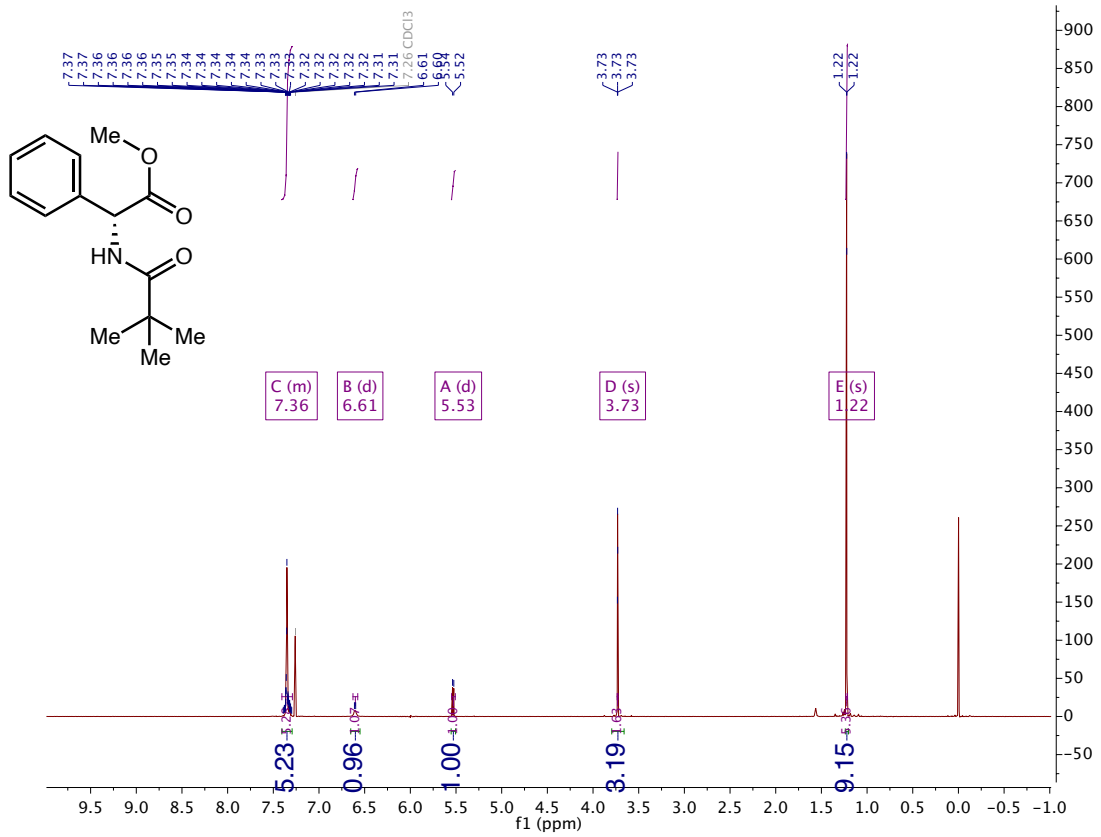

***N-pivaloyl-L-phenylglycine methyl ester* (4.S2-L *L*-Phg-OMe)**

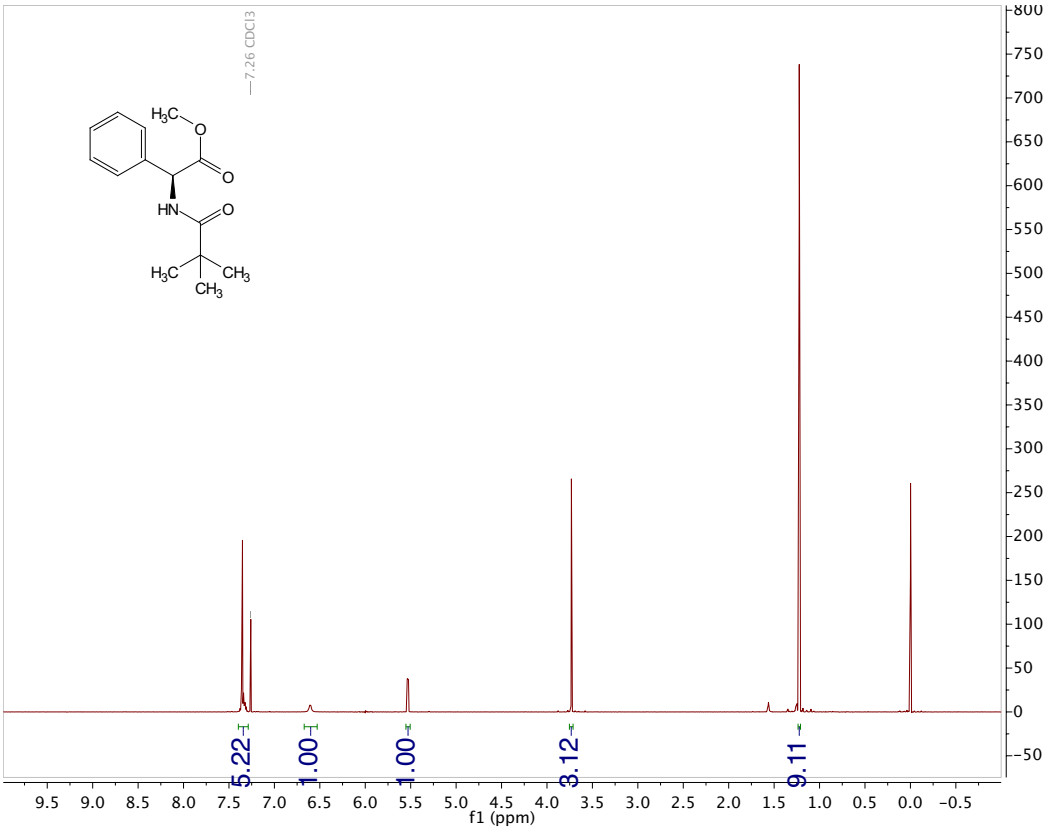

***Methyl pivaloyl-L-alaninate* (4.S3-L *L*-Ala-OMe)**

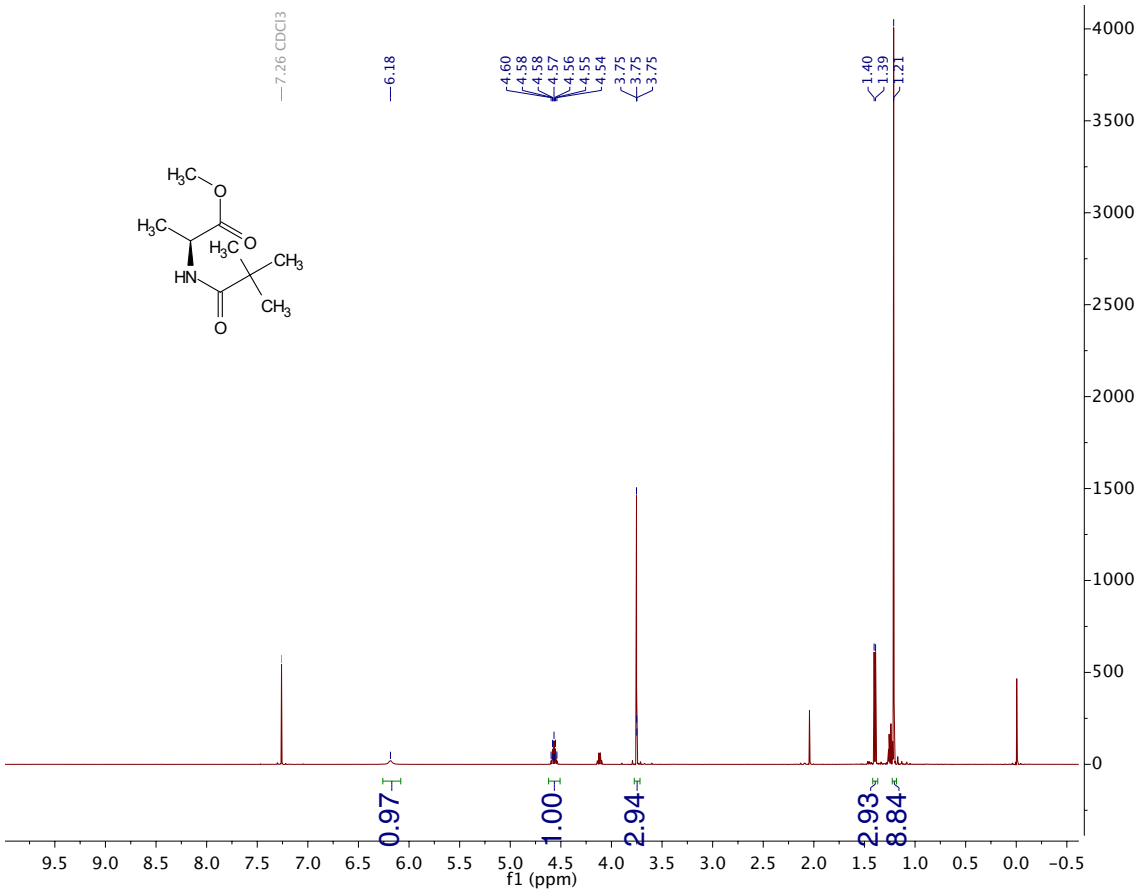

***Methyl pivaloyl-D-alaninate* (4.S3-D *D*-Ala-OMe)**

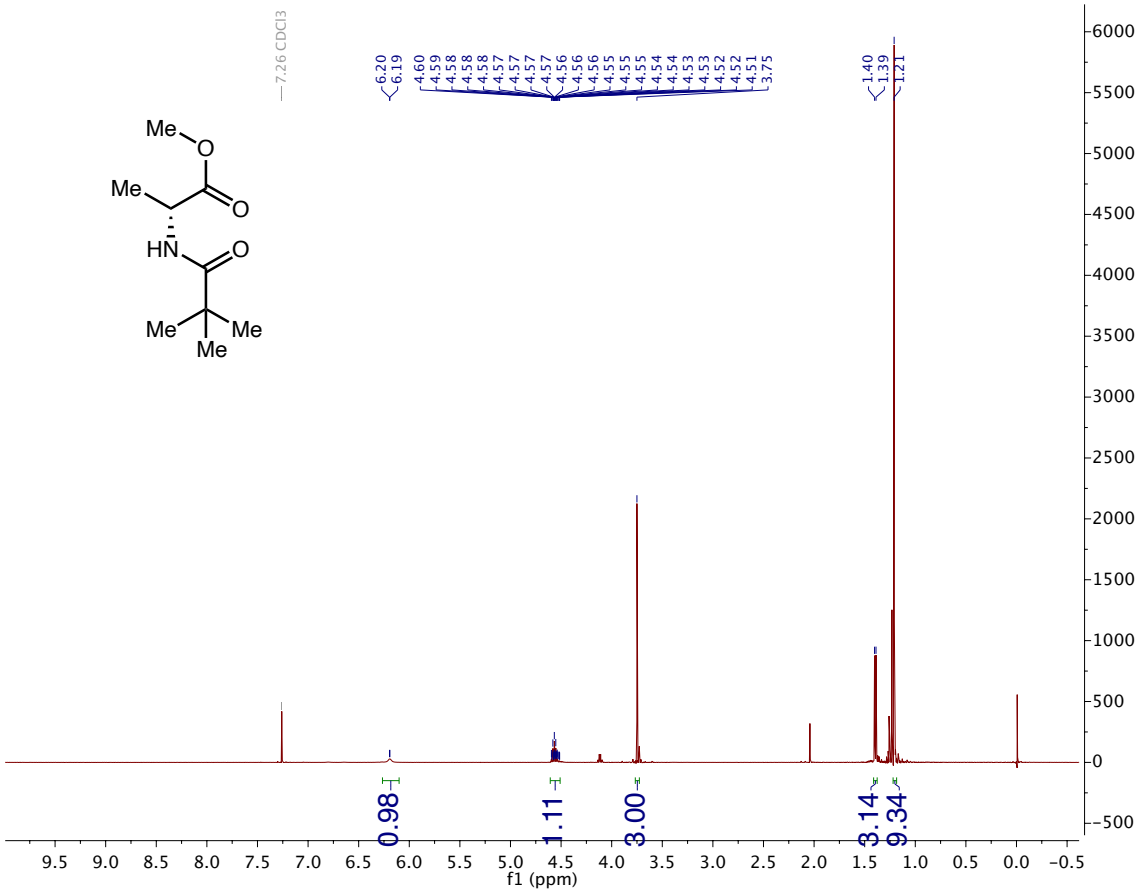

***(S)-N-(4-methylpent-1-en-3-yl)acetamide* (4.47)**

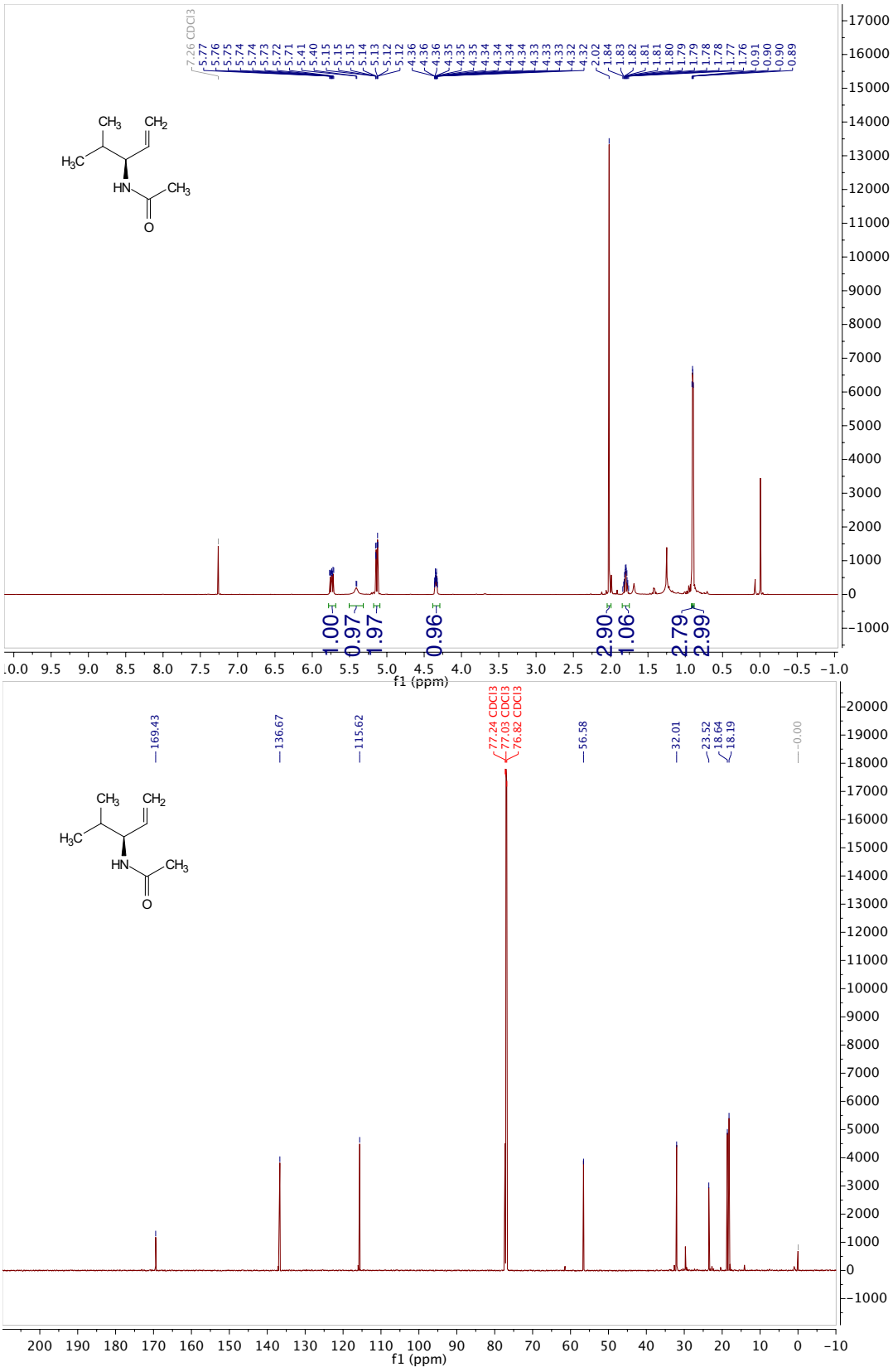

(±)-N-(4-methylpent-1-en-3-yl)acetamide (±-4.47)

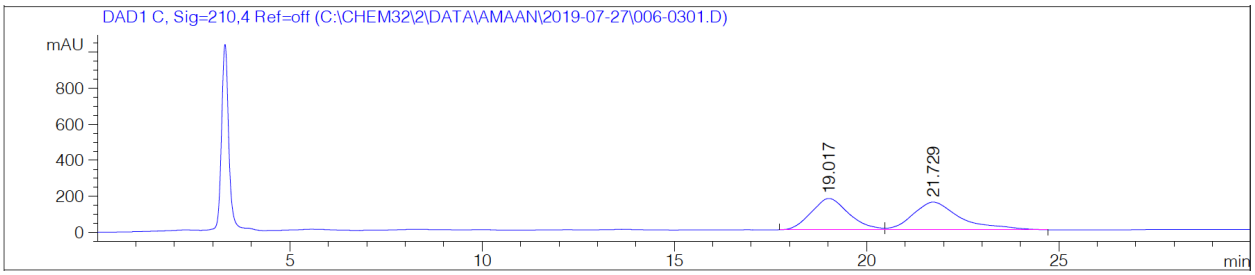

Signal 1: DAD1 C, Sig=210,4 Ref=off

Peak #	RetTime [min]	Type	Width [min]	Area [mAU*s]	Height [mAU]	Area %
1	19.017	BV	0.9845	1.18197e4	174.45068	47.1135
2	21.729	VB	1.1997	1.32681e4	154.53239	52.8865
Totals :				2.50878e4	328.98308	

(S)-N-(4-methylpent-1-en-3-yl)acetamide (4.47)

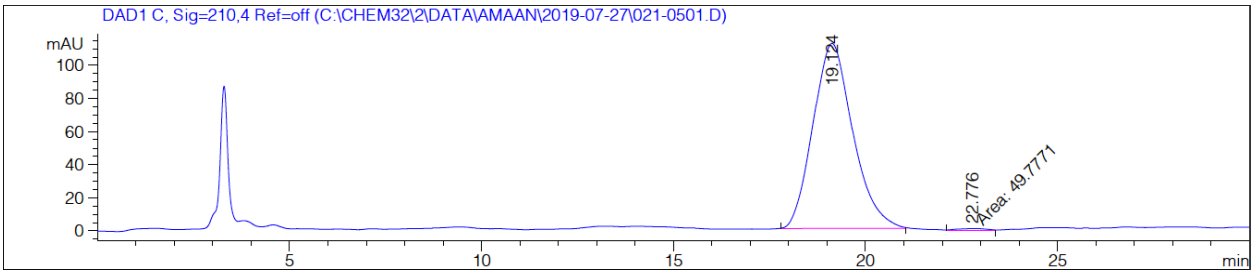

Signal 1: DAD1 C, Sig=210,4 Ref=off

Peak #	RetTime [min]	Type	Width [min]	Area [mAU*s]	Height [mAU]	Area %
1	19.124	BB	1.0659	8066.80420	111.78791	99.3867
2	22.776	MM	0.8456	49.77714	9.81139e-1	0.6133
Totals :				8116.58134	112.76905	

(S)-N-(4-methylpent-1-en-3-yl)pivalamide (4.42)

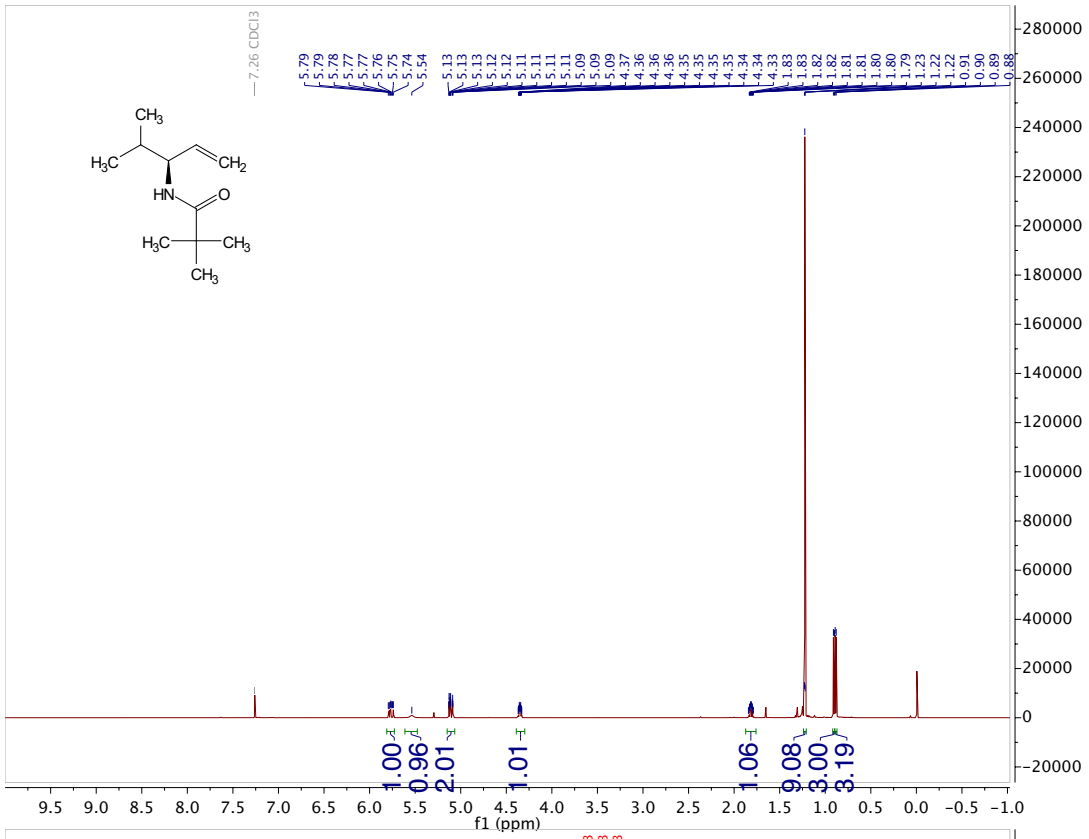

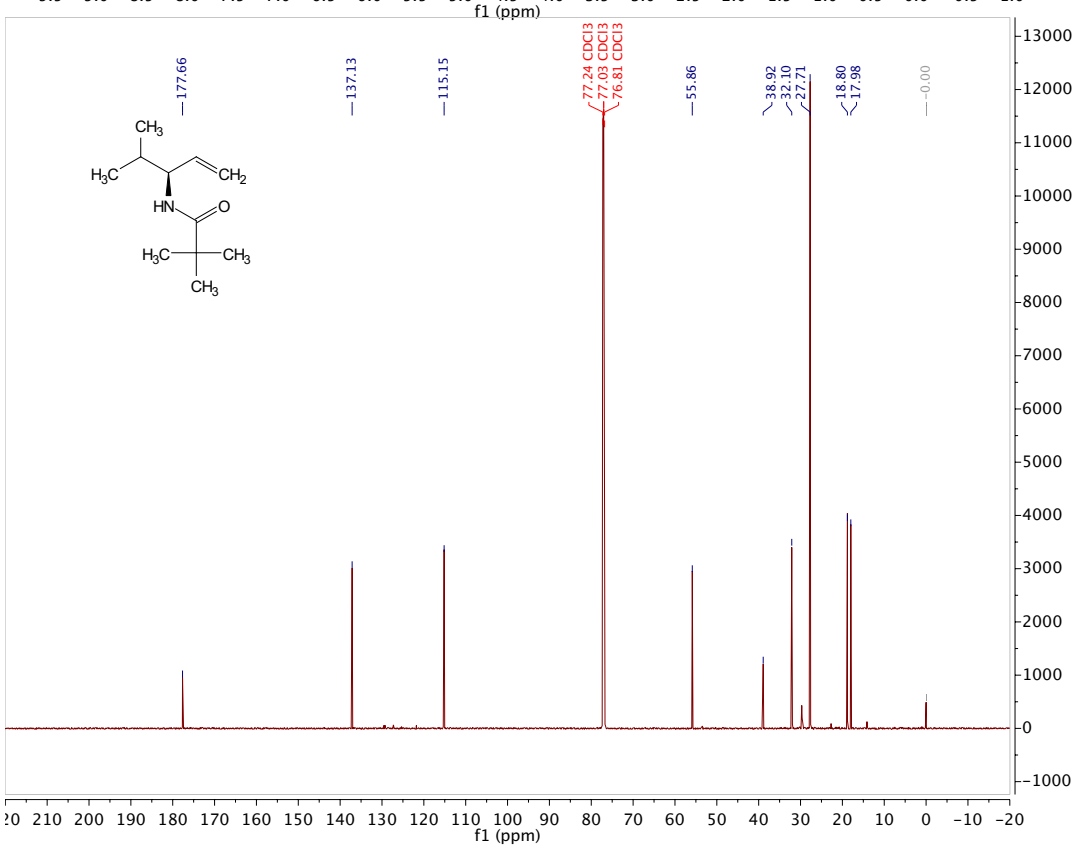

(±)-N-(4-methylpent-1-en-3-yl)pivalamide (±-4.42)

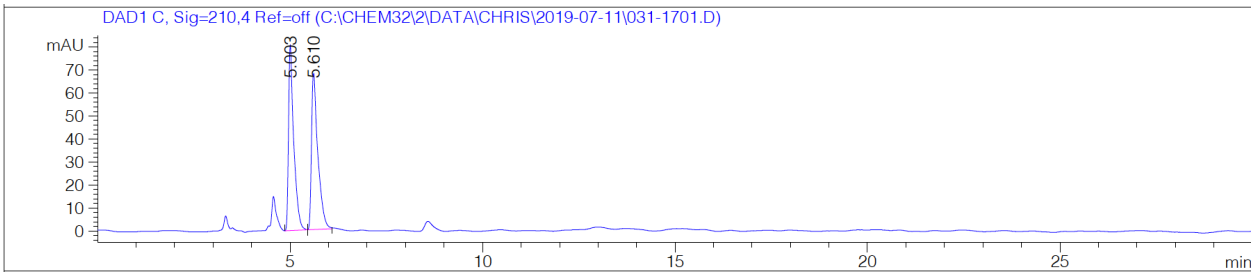

Signal 1: DAD1 C, Sig=210,4 Ref=off

Peak #	RetTime [min]	Type	Width [min]	Area [mAU*s]	Height [mAU]	Area %
1	5.003	VV	0.1348	767.14093	80.80962	50.2210
2	5.610	VB	0.1585	760.38782	67.99258	49.7790
Totals :				1527.52875	148.80220	

(S)-N-(4-methylpent-1-en-3-yl)pivalamide (4.42)

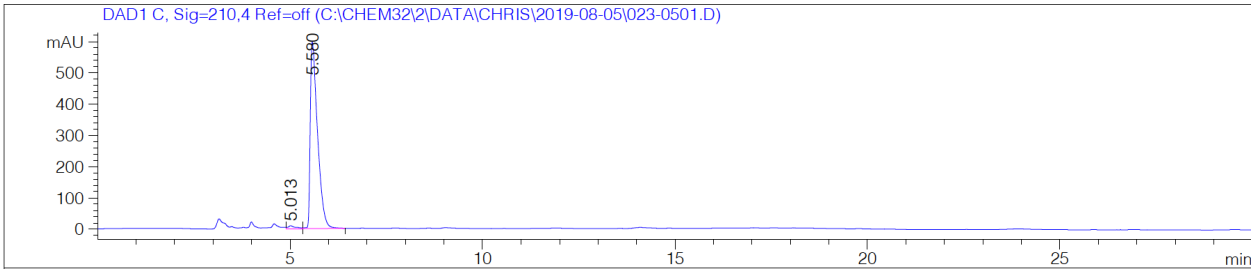

Signal 2: DAD1 C, Sig=210,4 Ref=off

Peak #	RetTime [min]	Type	Width [min]	Area [mAU*s]	Height [mAU]	Area %
1	5.013	VV	0.1808	126.23240	9.27309	1.6162
2	5.580	VB	0.1861	7684.32129	597.17950	98.3838
Totals :				7810.55369	606.45259	

***(S)-2-(1,3-dioxoisoindolin-2-yl)-N-(4-methylpent-1-en-3-yl)acetamide* (4.53)**

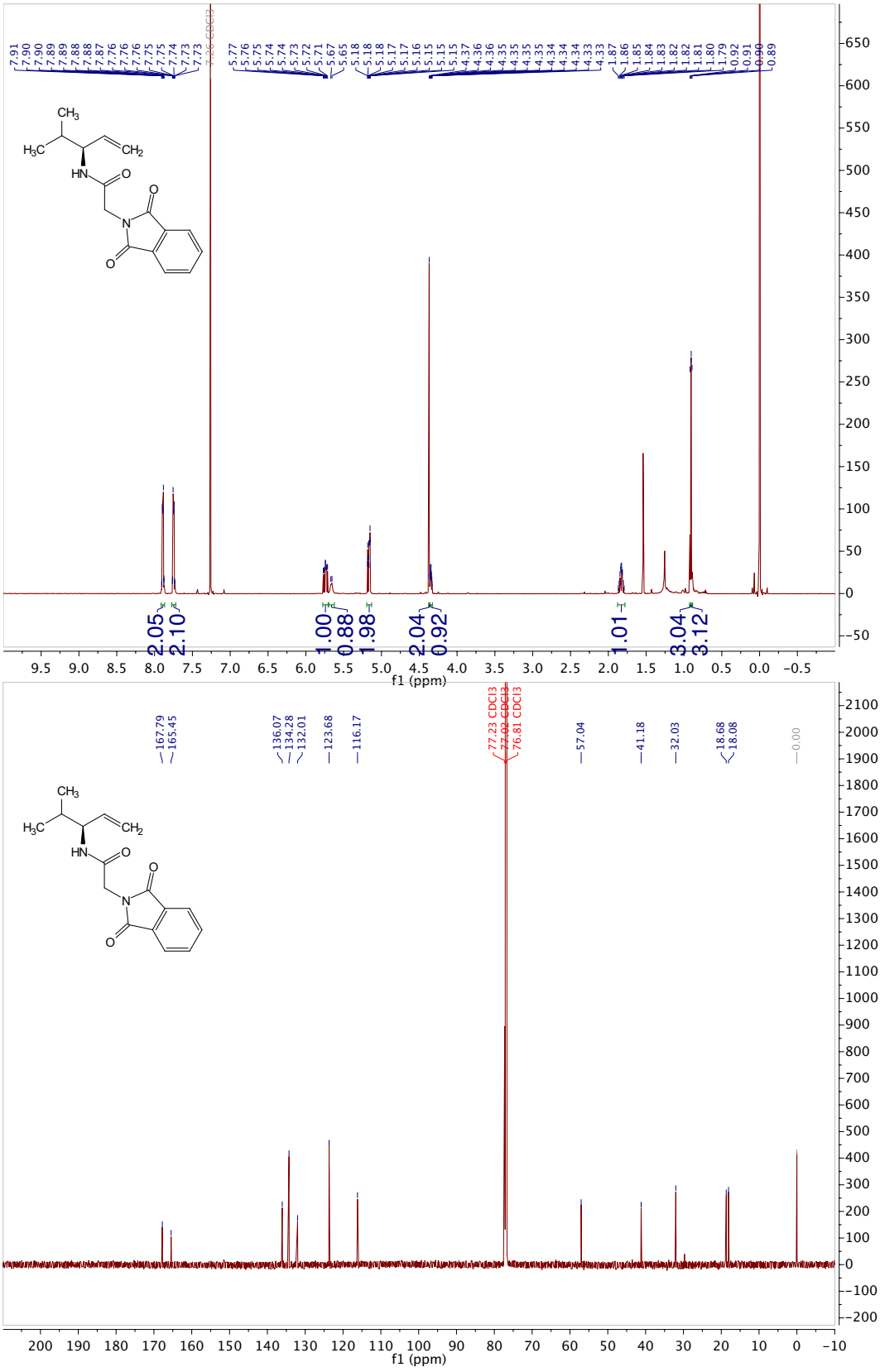

(±)-2-(1,3-dioxoisoindolin-2-yl)-N-(4-methylpent-1-en-3-yl)acetamide (±-4.53)

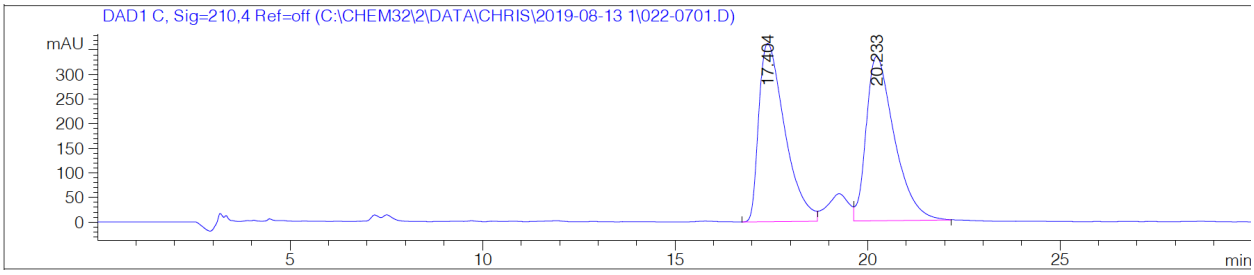

Signal 1: DAD1 C, Sig=210,4 Ref=off

Peak #	RetTime [min]	Type	Width [min]	Area [mAU*s]	Height [mAU]	Area %
1	17.404	BV	0.7204	1.70021e4	362.99741	49.9559
2	20.233	VB	0.7666	1.70322e4	334.19327	50.0441
Totals :				3.40343e4	697.19067	

(S)-2-(1,3-dioxoisoindolin-2-yl)-N-(4-methylpent-1-en-3-yl)acetamide (4.53)

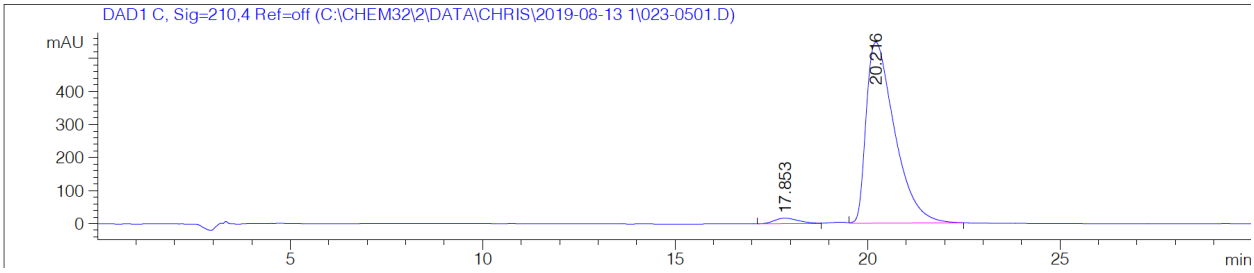

Signal 1: DAD1 C, Sig=210,4 Ref=off

Peak #	RetTime [min]	Type	Width [min]	Area [mAU*s]	Height [mAU]	Area %
1	17.853	BV	0.6325	740.67694	16.66547	2.5624
2	20.216	VB	0.7857	2.81644e4	547.89539	97.4376
Totals :				2.89050e4	564.56085	

(R)-N-(hex-1-en-3-yl)pivalamide (4.56)

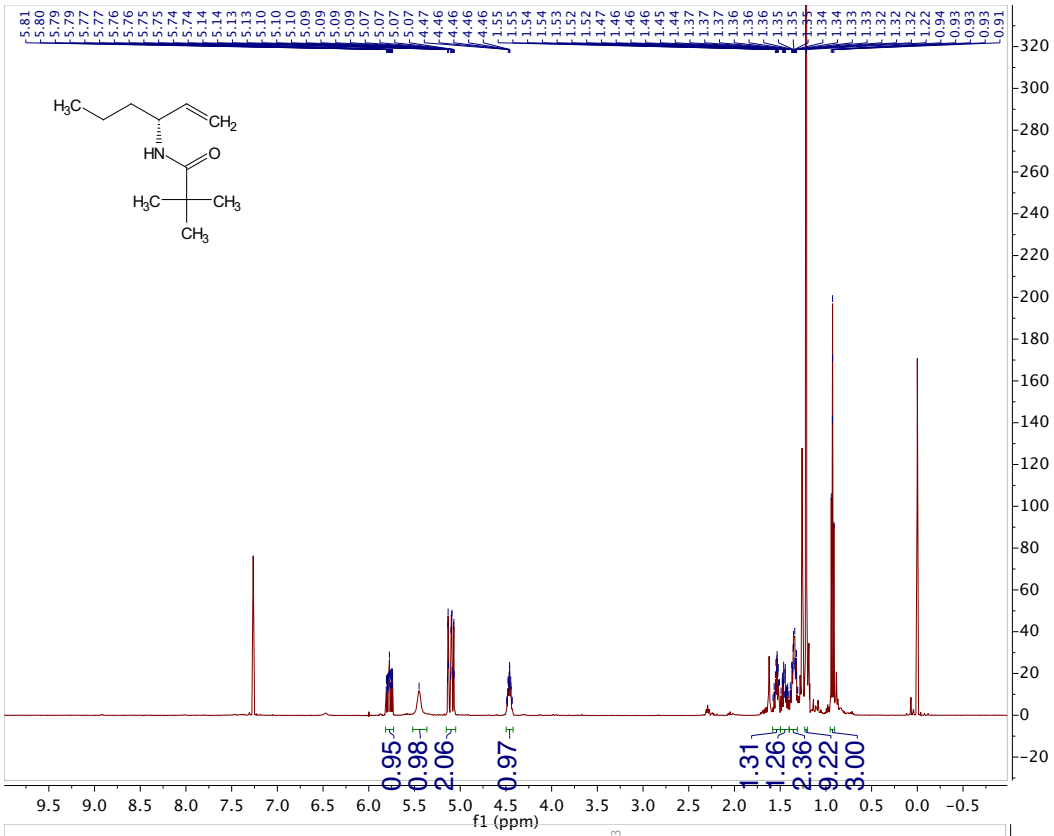

(±)-N-(hex-1-en-3-yl)pivalamide (±-4.56)

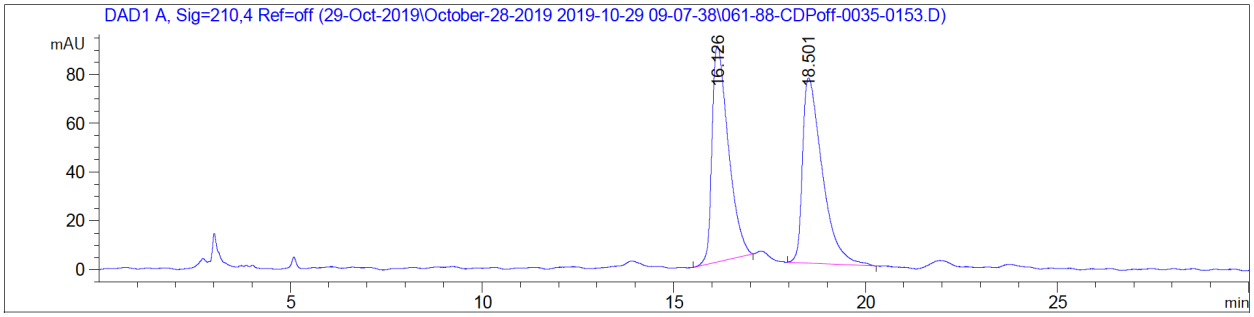

Signal 1: DAD1 A, Sig=210,4 Ref=off

Peak #	RetTime [min]	Type	Width [min]	Area [mAU*s]	Height [mAU]	Area %
1	16.126	BB	0.3726	2631.26929	88.56808	49.1456
2	18.501	BB	0.4307	2722.75781	75.95327	50.8544
Totals :				5354.02710	164.52135	

(R)-N-(hex-1-en-3-yl)pivalamide (4.56)

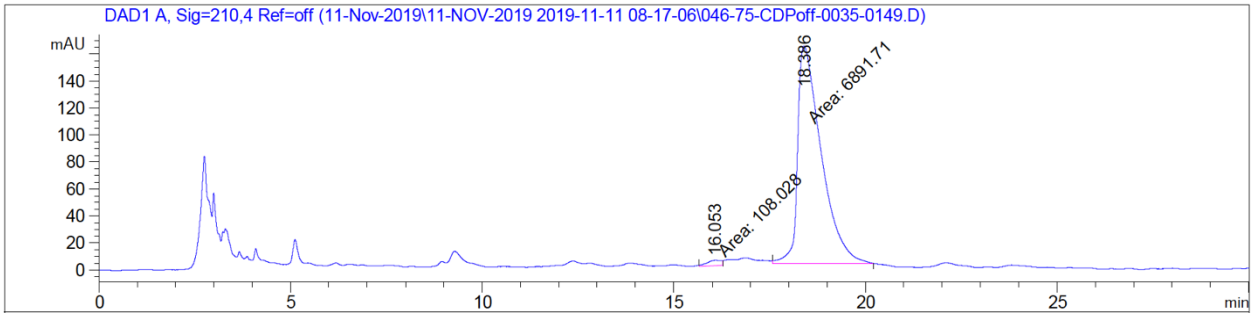

Signal 1: DAD1 A, Sig=210,4 Ref=off

Peak #	RetTime [min]	Type	Width [min]	Area [mAU*s]	Height [mAU]	Area %
1	16.053	MM	0.4373	108.02784	4.11707	1.5433
2	18.386	MM	0.7130	6891.71094	161.10773	98.4567
Totals :				6999.73878	165.22480	

***(R)-2-(1,3-dioxoisoindolin-2-yl)-N-(hex-1-en-3-yl)acetamide* (4.57)**

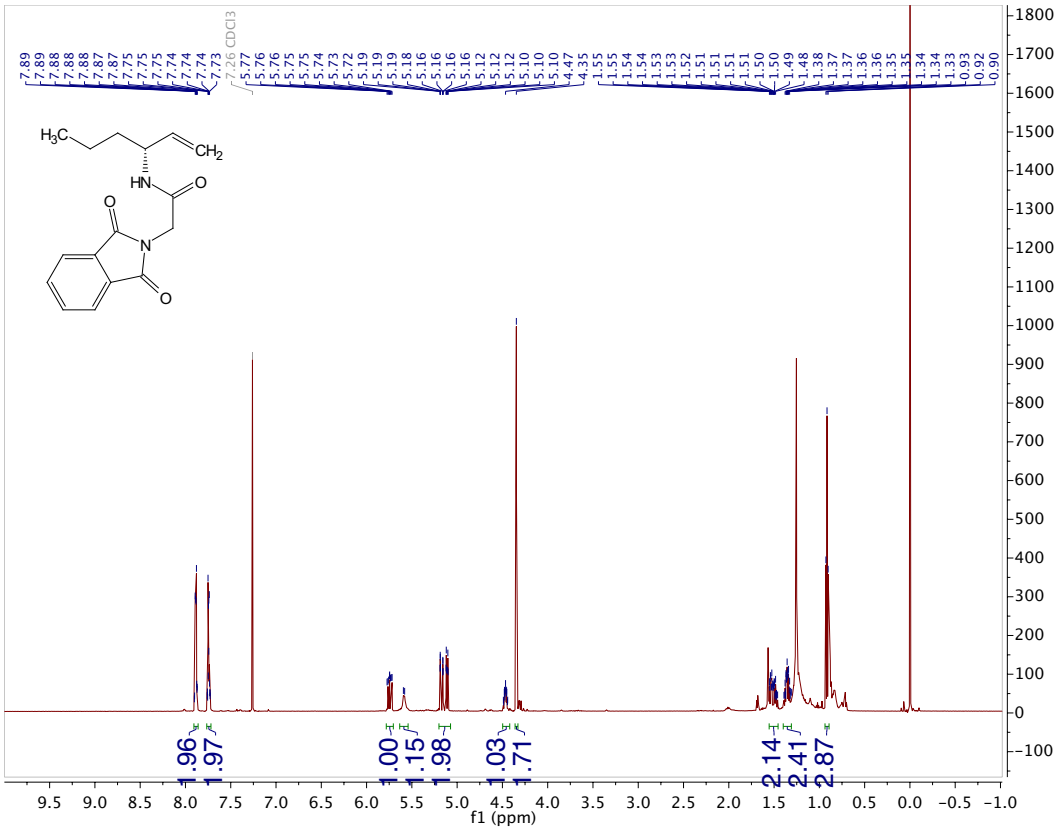

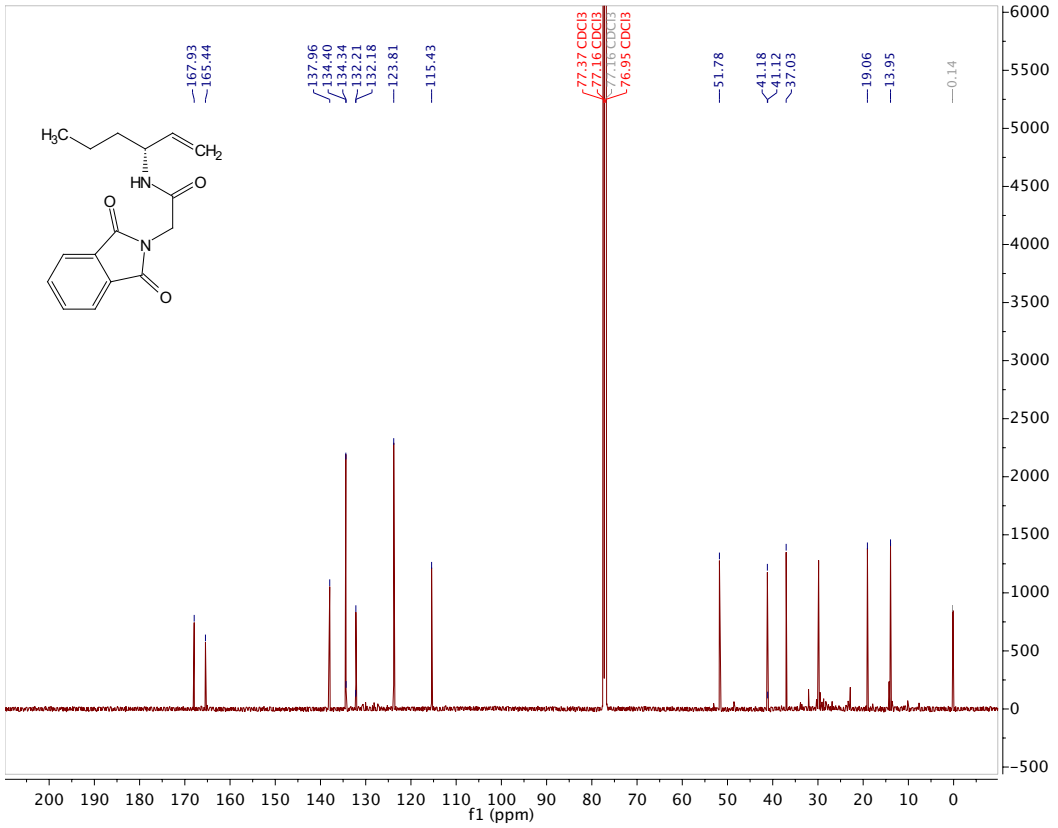

(±)-2-(1,3-dioxoisoindolin-2-yl)-N-(hex-1-en-3-yl)acetamide (±-4.57)

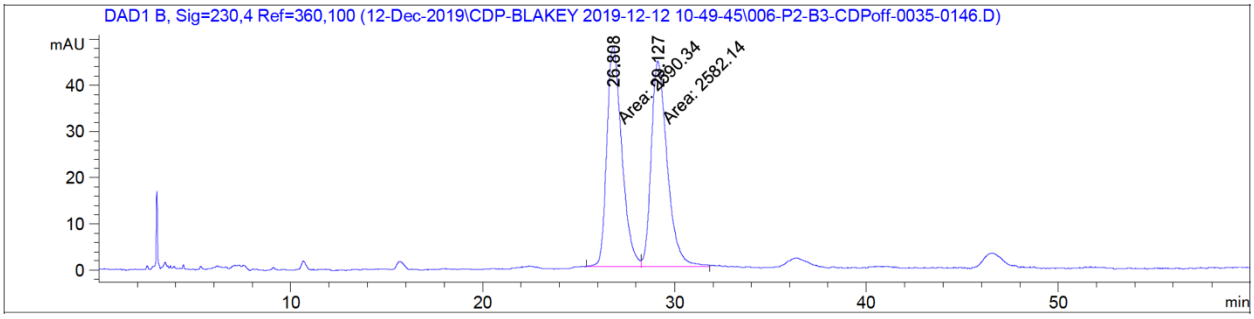

Signal 2: DAD1 B, Sig=230,4 Ref=360,100

Peak #	RetTime [min]	Type	Width [min]	Area [mAU*s]	Height [mAU]	Area %
1	26.808	MF	0.9051	2590.33911	47.69818	50.0793
2	29.127	FM	0.9676	2582.13672	44.47890	49.9207
Totals :				5172.47583	92.17709	

(R)-2-(1,3-dioxoisoindolin-2-yl)-N-(hex-1-en-3-yl)acetamide (4.57)

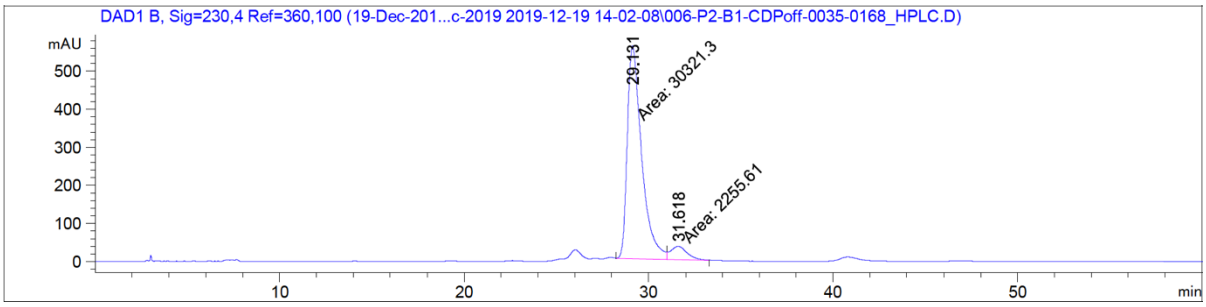

Signal 2: DAD1 B, Sig=230,4 Ref=360,100

Peak #	RetTime [min]	Type	Width [min]	Area [mAU*s]	Height [mAU]	Area %
1	29.131	MF	0.9020	3.03213e4	560.25873	93.0761
2	31.618	FM	1.0542	2255.60840	35.66072	6.9239
Totals :				3.25769e4	595.91945	

***(R)-N-(1-phenylbut-3-en-2-yl)pivalamide* (4.62)**

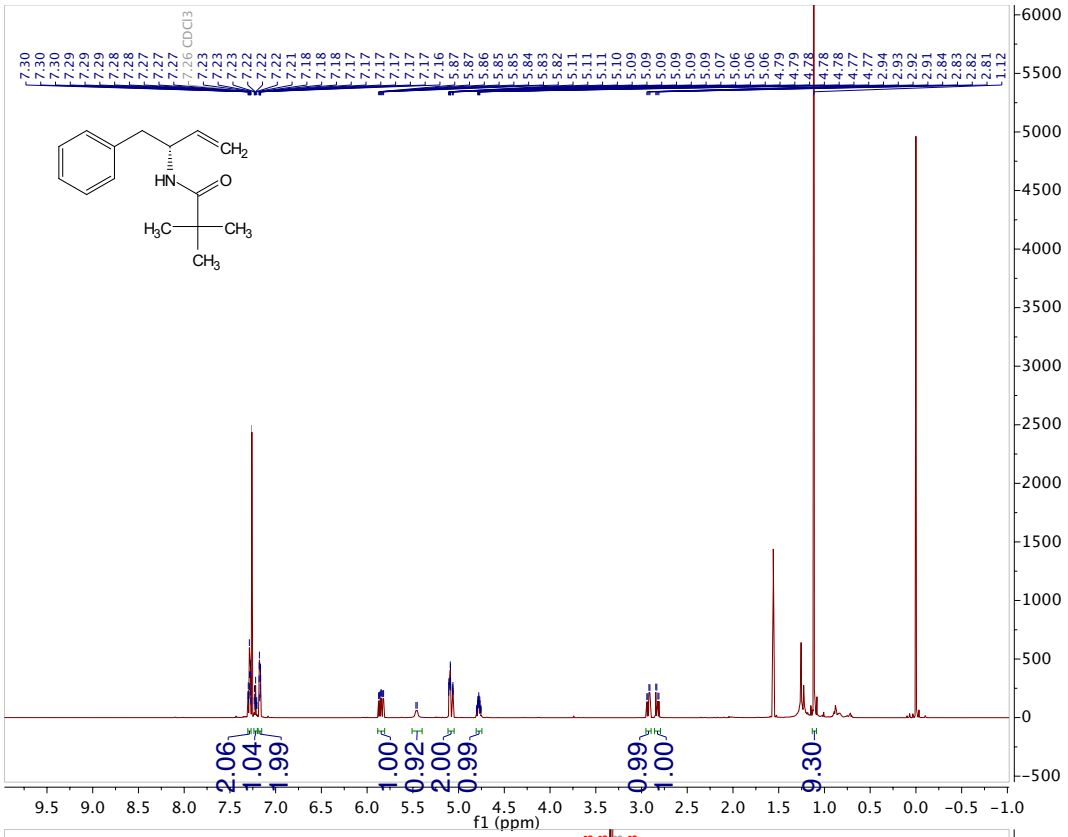

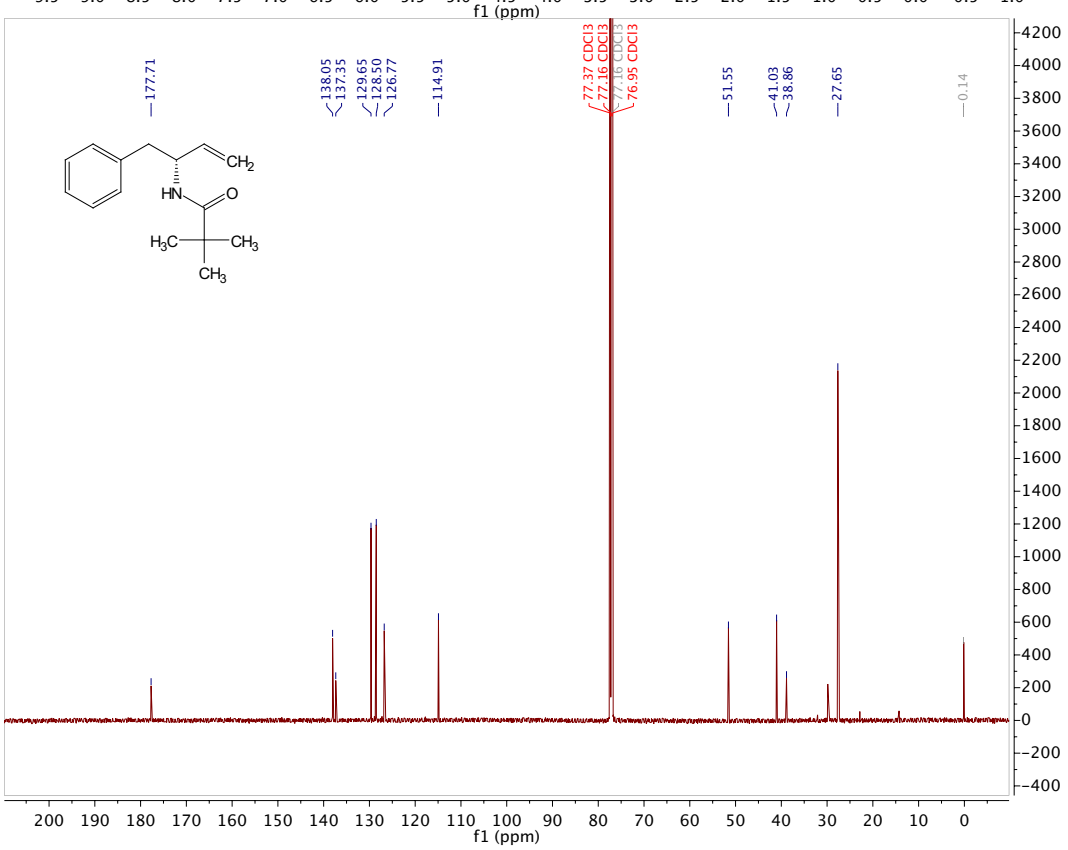

(±)-N-(1-phenylbut-3-en-2-yl)pivalamide (±-4.62)

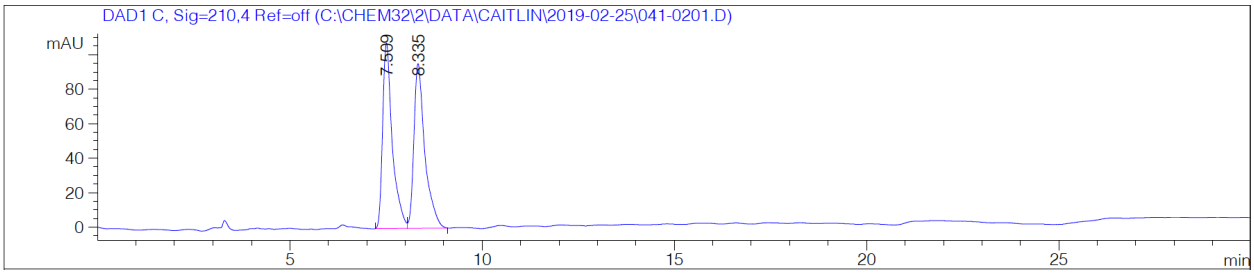

Signal 1: DAD1 C, Sig=210,4 Ref=off

Peak #	RetTime [min]	Type	Width [min]	Area [mAU*s]	Height [mAU]	Area %
1	7.509	BV	0.2528	1852.07629	107.60557	49.7381
2	8.335	VB	0.2887	1871.58264	95.46971	50.2619
Totals :				3723.65894	203.07528	

(R)-N-(1-phenylbut-3-en-2-yl)pivalamide (4.62)

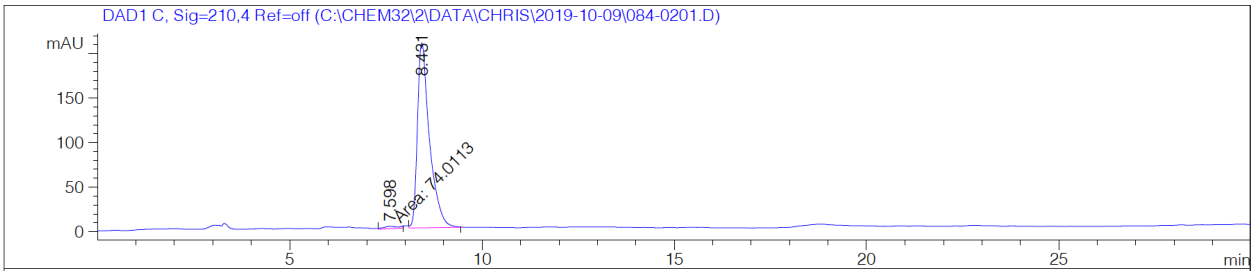

Signal 2: DAD1 C, Sig=210,4 Ref=off

Peak #	RetTime [min]	Type	Width [min]	Area [mAU*s]	Height [mAU]	Area %
1	7.598	MM	0.4611	74.01132	2.67536	1.6245
2	8.431	VB	0.3117	4481.90283	207.74052	98.3755
Totals :				4555.91415	210.41588	

(S)-N-(1-phenylallyl)pivalamide (4.64)

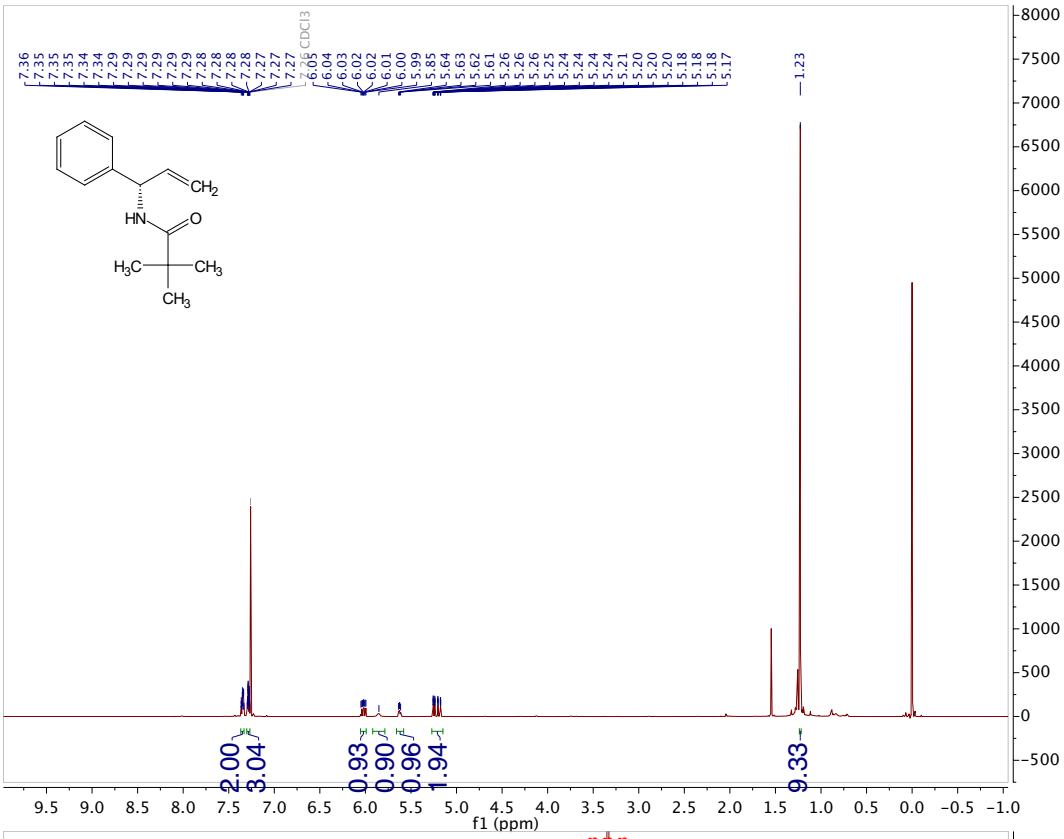

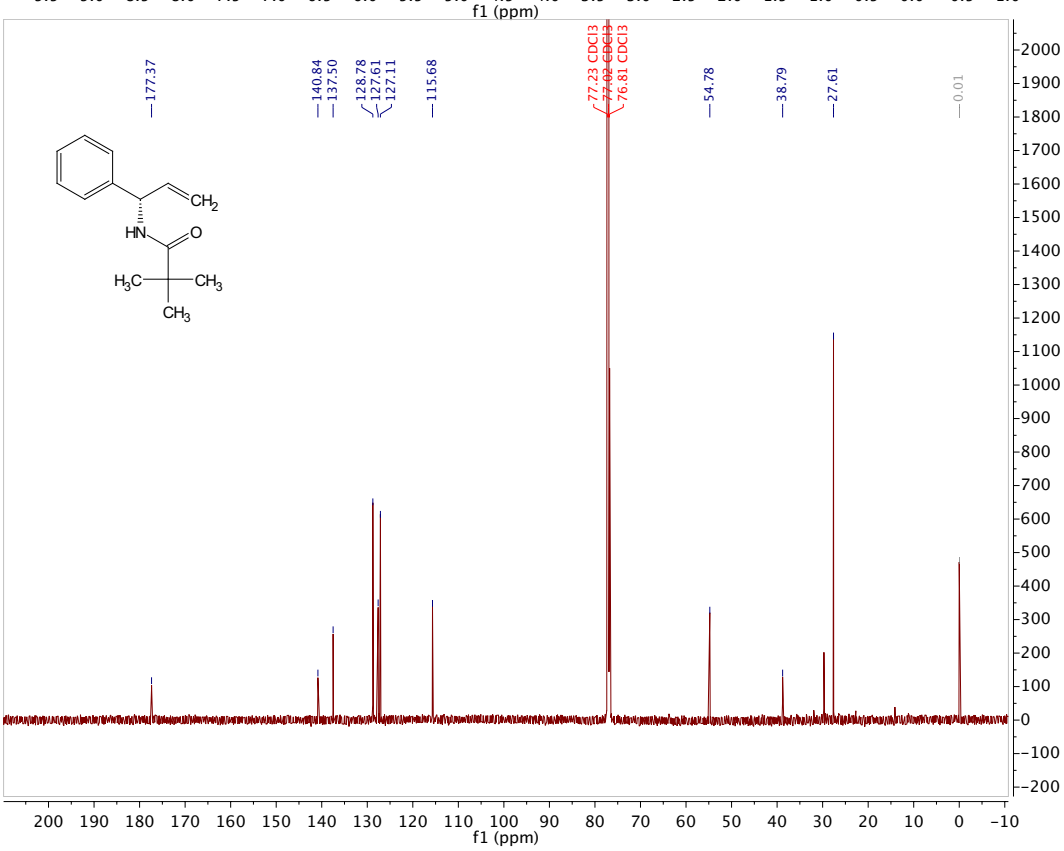

(±)-N-(1-phenylallyl)pivalamide (±-4.64)

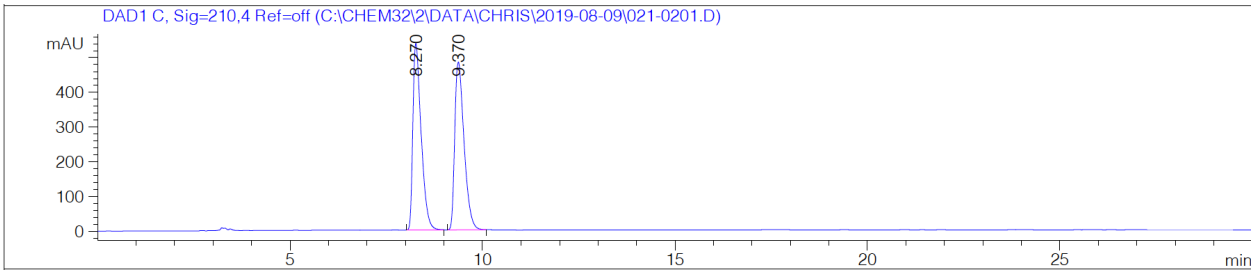

Signal 1: DAD1 C, Sig=210,4 Ref=off

Peak #	RetTime [min]	Type	Width [min]	Area [mAU*s]	Height [mAU]	Area %
1	8.270	BB	0.2251	7979.37158	537.64404	49.9904
2	9.370	BB	0.2526	7982.44971	483.54959	50.0096
Totals :				1.59618e4	1021.19363	

(S)-N-(1-phenylallyl)pivalamide (4.64)

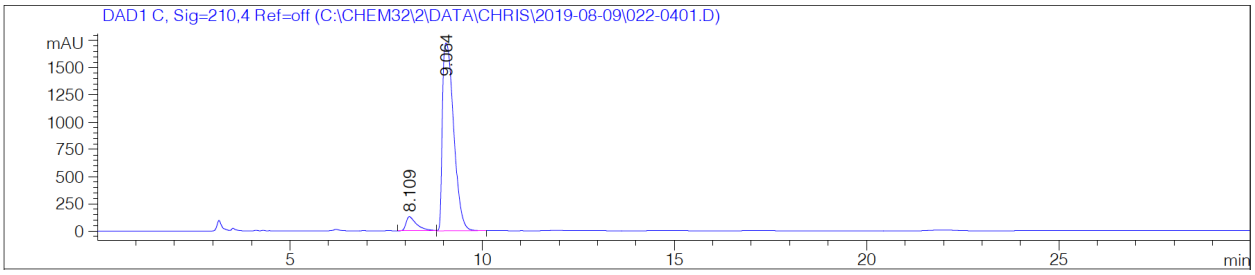

Signal 2: DAD1 C, Sig=210,4 Ref=off

Peak #	RetTime [min]	Type	Width [min]	Area [mAU*s]	Height [mAU]	Area %
1	8.109	VV	0.2769	2515.46436	130.49010	6.6902
2	9.064	VB	0.3233	3.50839e4	1725.01147	93.3098
Totals :				3.75993e4	1855.50157	

***(S,E)-N-(pent-3-en-2-yl)pivalamide* (4.68)**

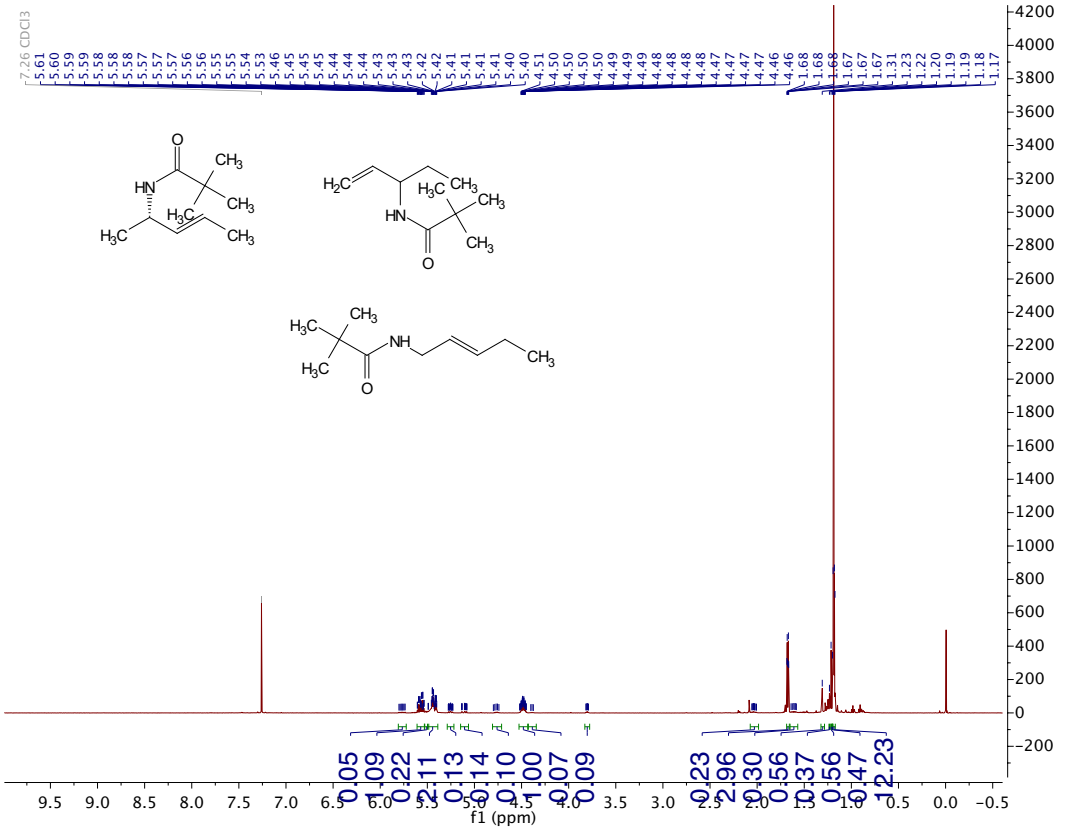

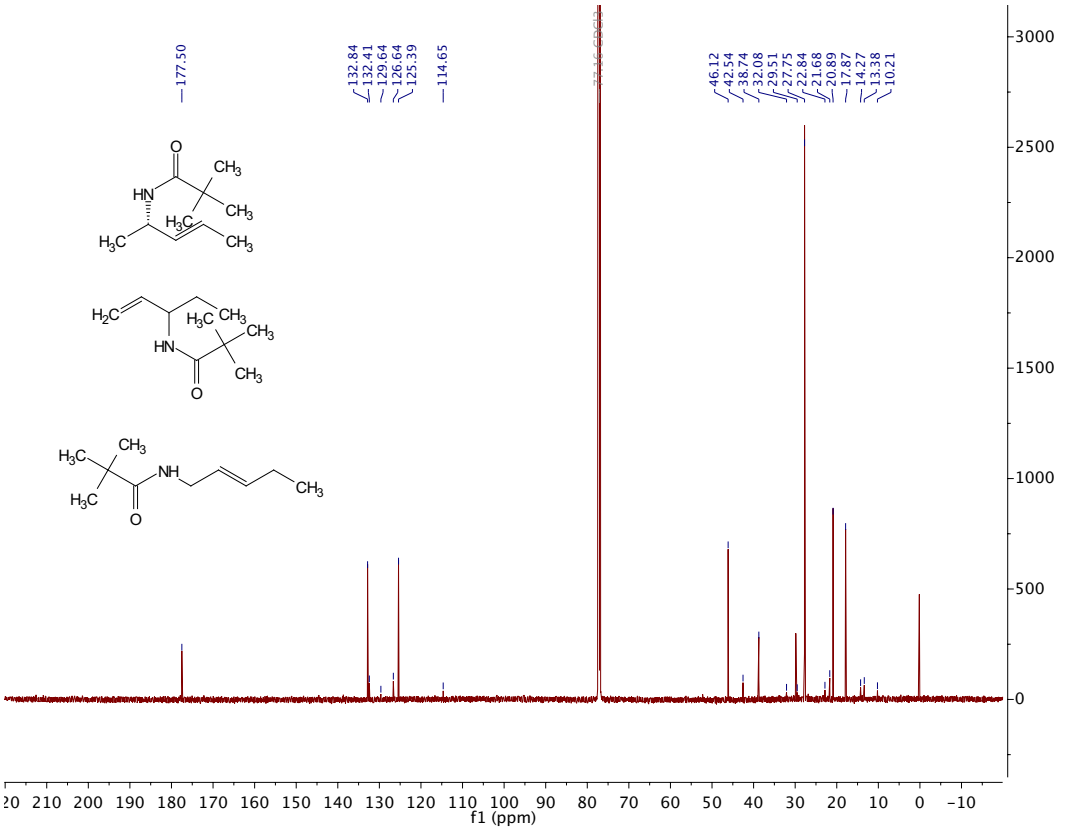

Chapter 5. Towards a Peptide Macrocyclization Strategy *via* the Cobalt-Catalyzed 1,2-Carboamidation of Acrylamides

In this chapter, we will discuss the progress towards a peptide macrocyclization strategy *via* the cobalt-catalyzed 1,2-carboamidation of acrylamides. We are continuing to use group IX transition metal catalysis; however, we are endeavoring to push new boundaries in base metal catalysis for the development of greener processes. This work has been conducted in collaboration with Sophia Xu, a current undergraduate in the Blakey lab, under my mentorship.

5.1 Introduction to Ribosomally-Synthesized and Post-Translationally Modified Peptides

5.1.1 Overview of Several Key Peptides Under Investigation by the Blakey Group

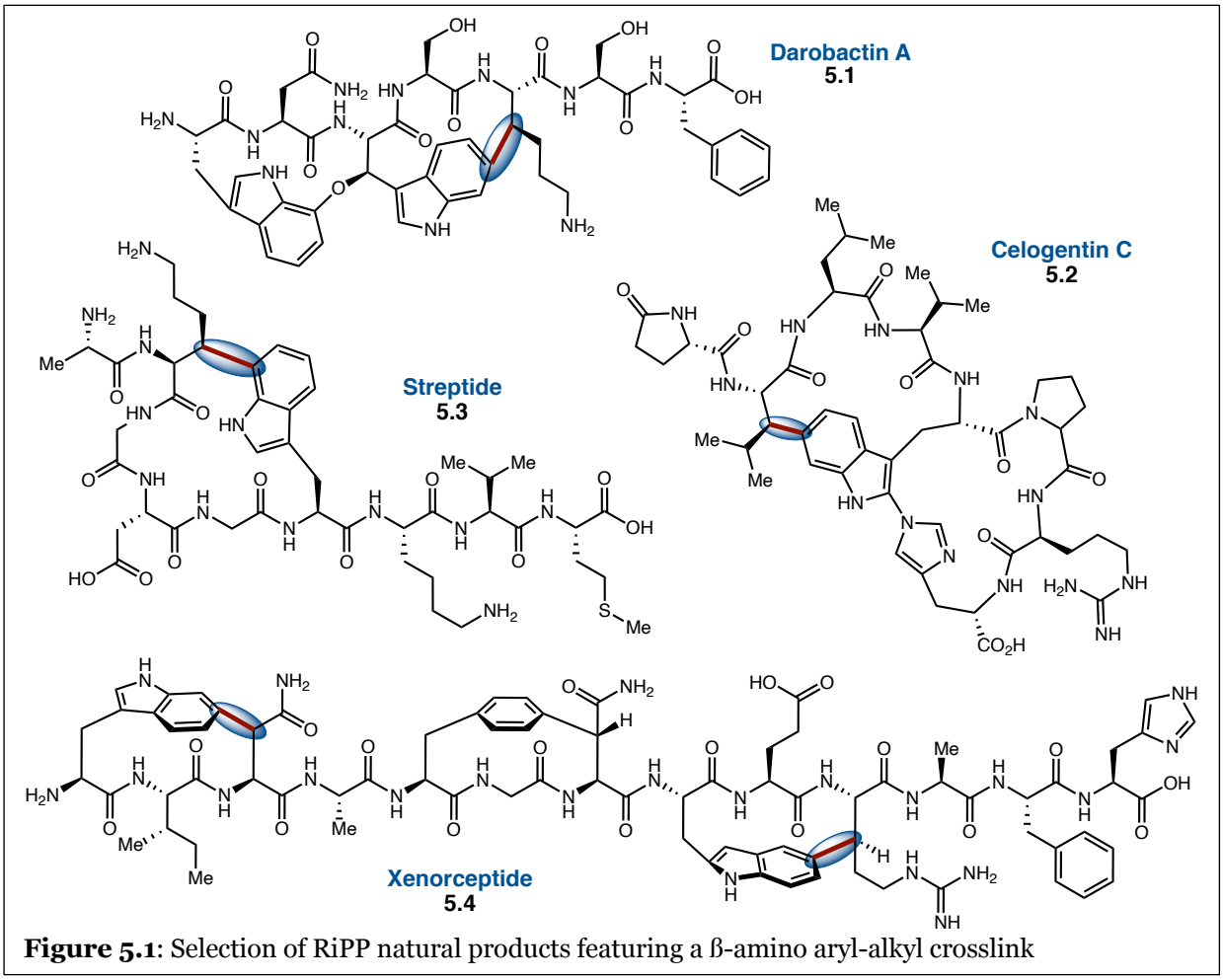

Figure 5.1: Selection of RiPP natural products featuring a ß-amino aryl-alkyl crosslink

Recently, the Blakey lab has begun work towards the development of new synthetic strategies to access ribosomally-synthesized and post-translationally modified peptides (RiPPs, **Figure 5.1**).[1,2] This class of natural products features a wide variety of molecules with diverse bioactivities. From a biosynthetic perspective, many of these natural products are synthesized in a linear fashion and then undergo post-translational modifications including cyclization to deliver the final compound.[1] These cyclization points also represent some of the key synthetic challenges when attempting to carry out a total synthesis of molecules within this class. Specifically, we have had an increased focus on a ß-amino aryl-alkyl crosslink highlighted in the molecules darobactin A (**5.1**), celogentin C (**5.2**), streptide (**5.3**), and xenorceptide (**5.4**).

5.1.2 Key Synthetic Strategies to Access RiPPs

While a full review manuscript on RiPPs featuring C-C crosslinks is in preparation by David Laws III and Eleda Plouch, two current graduate students in the Blakey group, this section will narrowly focus on emerging strategies to access the ß-amino aryl-alkyl crosslink of several key RiPPs (**Figure 5.1**).[3] As mentioned in the previous section, this disconnection represents the primary challenge that arises during the synthesis of compounds featuring this moiety. From a synthetic perspective, total or partial synthetic routes have been disclosed for celogentin C (**5.2**),[4–8] streptide (**5.3**),[9] and xenorceptide (**5.4**).[10] Darobactin A (**5.1**) has, thus far, only been obtained through isolation of the natural product, and a published total synthesis has yet to be disclosed.

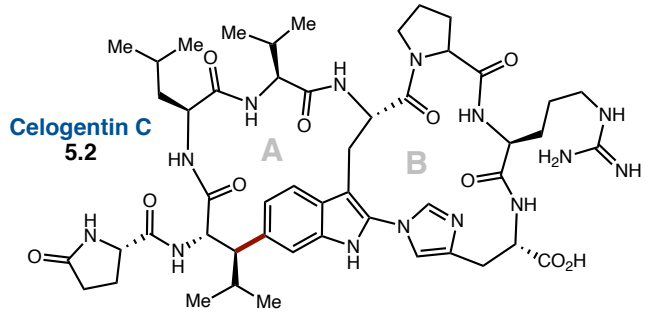

Figure 5.2: Structural analysis of Celogentin C

The RiPP that has been the explored most extensively is celogentin C (**5.2**), having three total syntheses along with several strategies to access the aryl-alkyl crosslink specifically.[4–8] While the biosynthetic route to celogentin C forms the linear pepetide first and then cyclizes, the total syntheses and partial syntheses have focused

on forming the western (A) ring initially and then building out the eastern (B) ring (**Figure 5.2**). We will focus on the synthesis of the western ring as this is where the key crosslink resides.

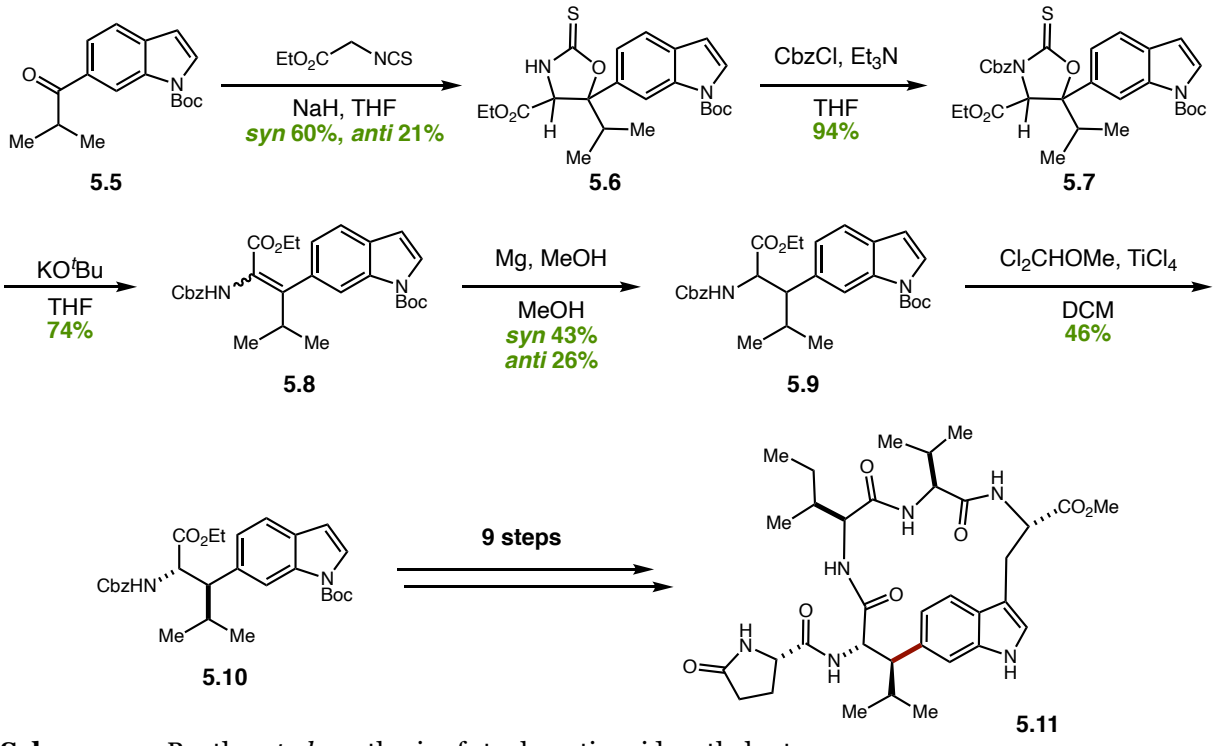

Scheme 5.1: Bentley *et al.* synthesis of stephanotic acid methyl ester

The first strategy towards the synthesis of the western macrocycle comes from Bentley *et al.* in their synthesis of the related stephanotic acid methyl ester (**5.11**, **Scheme 5.1**).[4] Stephanotic acid is a single residue change away from the celogentin family. This route begins with the aryl-alkyl bond installed in the form of ketone **5.5**. Ketone **5.5** is elaborated to thioxo-oxazolidinone **5.6** as a mixture of diastereomers. Nitrogen protection (**5.7**) and elimination afford olefin **5.8** which can be then be reduced to amino acid ester **5.9**, at which point the *syn*- and *anti*-enantiomeric pairs could be separated. The *anti*-enantiomers were then formylated at the 3-position of the indole to provide their desired indole core **5.10**. After nine additional steps, and purification by preparative HPLC, the desired stephanotic acid was complete. While this route effectively delivered the crosslink, lack of stereocontrol limits its overall utility. Additionally, this route lacks ease of diversification as the identity of the crosslinked alkyl group must be present in the starting material from the beginning of the synthesis.

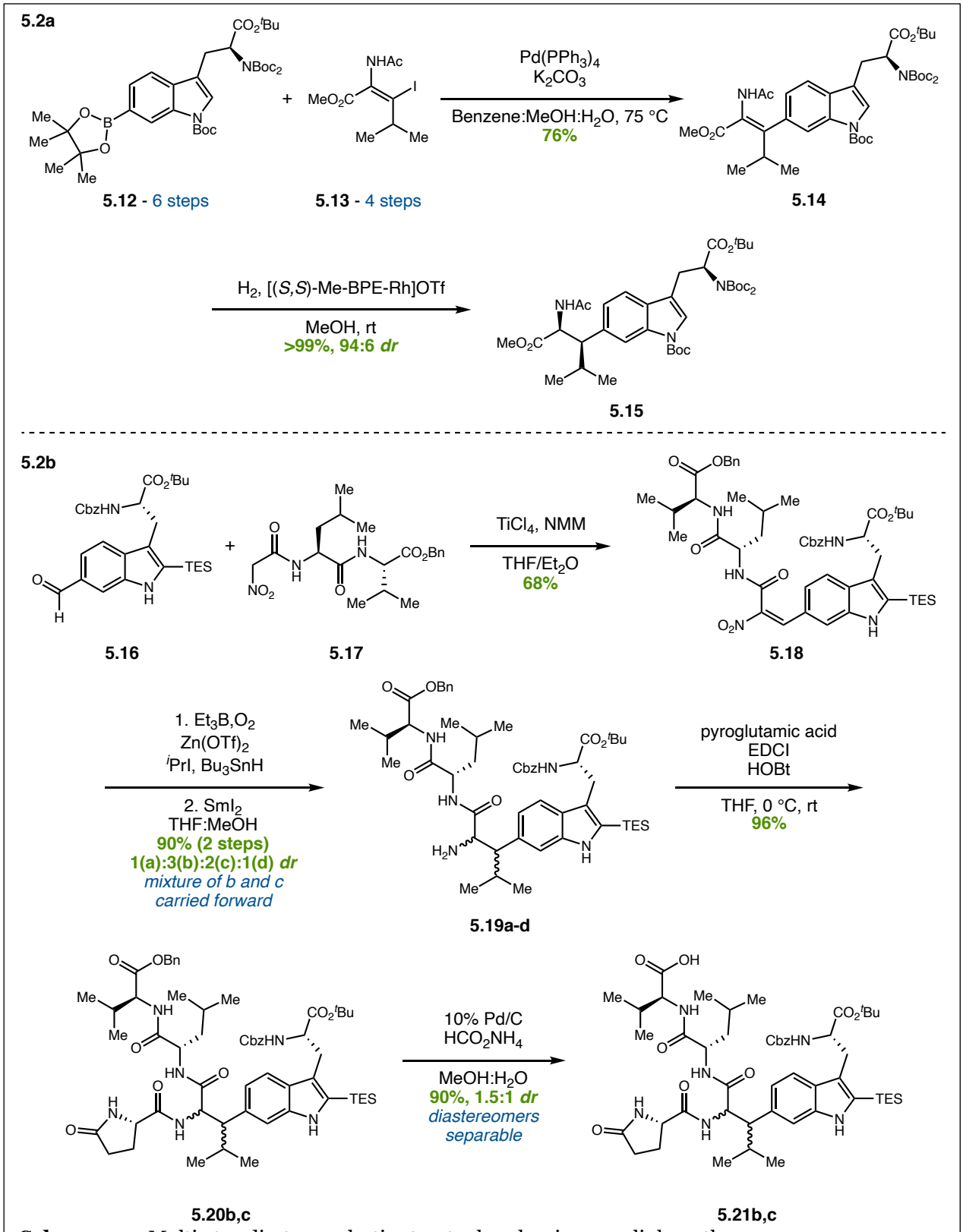

Scheme 5.2: Multi-step diastereoselective tryptophan-leucine crosslink syntheses

The next effort comes from Michaux *et al.* who, again, disclosed a partial synthesis aimed at

this disconnection specifically.[5] This report targeted the stereospecific synthesis of **5.14** with the goal of carrying out a rhodium catalyzed asymmetric hydrogenation to afford the product with the desired stereochemistry (**Scheme 5.2a**). Olefin **5.14** could be accessed in 76% yield through the Suzuki cross coupling of tryptophan boronic ester **5.12** and vinyl iodide **5.13**. Optimization of the hydrogenation provided excellent yield and stereocontrol, however, multi-step synthesis of the Suzuki coupling partners limits the overall usefulness to this system specifically.

Two total synthetic efforts have been disclosed from Castle and coworkers utilizing an identical scheme that involved Knoevenagel condensation, radical conjugate addition to a Michael acceptor, and nitro reduction to access the aryl-alkyl crosslinked product (**Scheme 5.2b**).[6,7] The Knoevenagel condensation occurred between aldehyde **5.16** and amino acid derived nitro compound **5.17** to afford Michael acceptor **5.18**. Radical conjugate addition of an *iso*-propyl group to the Michael acceptor and reduction of the nitro group provided the primary amine provides **5.19a-d**. While this route successfully afforded access to the crosslinked products, stereochemistry of the Michael addition and reduction was severely limited. Fortunately for their syntheses, the major diastereomer formed (**5.19b**) had the same stereochemistry as the natural product. However, this outcome was entirely determined by the native selectivity of the transformation and further manipulations of the molecule were required to allow for separation of the diastereomers (**5.21b-c**).

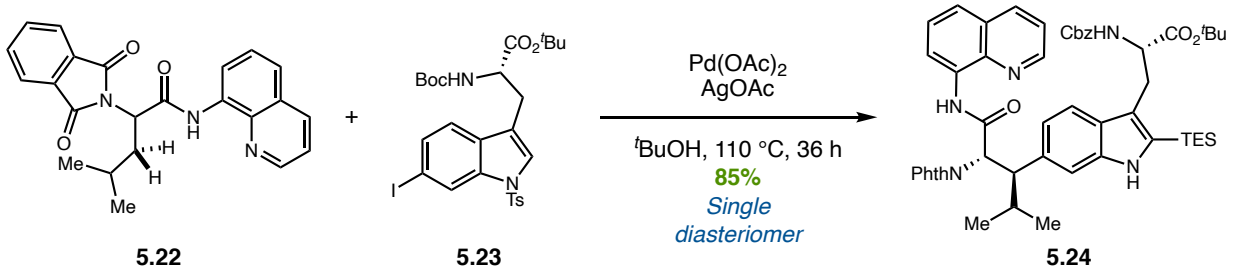

Scheme 5.3: Directed asymmetric C–H arylation to access the tryptophan-leucine crosslink

The final total synthesis of celogentin C from Feng *et al.* introduces the most used strategy to access this type of ß-amino aryl-alkyl crosslink, a palladium catalyzed, 8-aminoquinoline directed asymmetric C(sp^3)–H arylation reaction (**Scheme 5.3**).[8,11] In the context of celogentin C (**5.2**),

reaction of phthalimide **5.22** with indole iodide **523** provided crosslinked **5.24** in high yield and in a single diastereomer.[8] Examination of the expected palladacycle intermediate **5.25** (**Figure 5.3**), and studies with mono-protected amines, showed that the presence of the phthalimide conveniently doubly protected the nitrogen and provided significant steric bulk to guide the diastereoselectivity of the transformation.

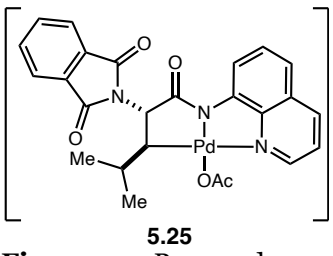

5.25

Figure 5.3: Proposed catalytic intermediate in the 8-aminoquinoline directed ß-C–H arylation

This palladium catalyzed directed asymmetric C–H arylation strategy was generalized by Chen and coworkers in 2018 for the synthesis of this kind of crosslink.[11] Further, this strategy has been applied to the total syntheses of streptide (**5.3**) and partial synthesis of xenorceptide (**5.4**), the only other RiPPs featuring this specific disconnection that have been explored.[9,10]

5.2 Blakey Group Strategy to Access the Key ß-Amino Aryl-Alkyl Disconnection

5.2.1 Application of Previous Methodology and New Synthetic Plan

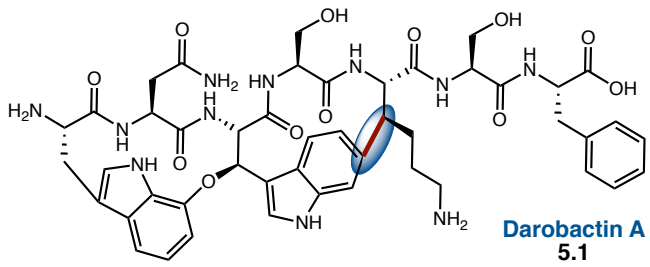

Figure 5.4: RiPP natural product targeted by the Blakey group for total synthesis

As mentioned in the previous section, the palladium catalyzed, 8-aminoquinoline directed asymmetric C–H arylation reaction has attracted the most attention in the published routes to access key ß-amino aryl-alkyl crosslinks in RiPP natural products.[8–11] However, we in the Blakey group wanted to develop a new and generalizable strategy to access molecules of this natural product class that didn't require the installation and removal of a directing group. We specifically sought to develop a method that would utilize our rhodium indenyl catalyst platform, discussed extensively in Chapter 4, for an asymmetric C–H functionalization strategy.[12] To develop this strategy, we have begun targeting darobactin A (**5.1**), the final RiPP natural product containing the key ß-amino aryl-alkyl crosslink that has not been accessed synthetically (**Figure 5.4**).

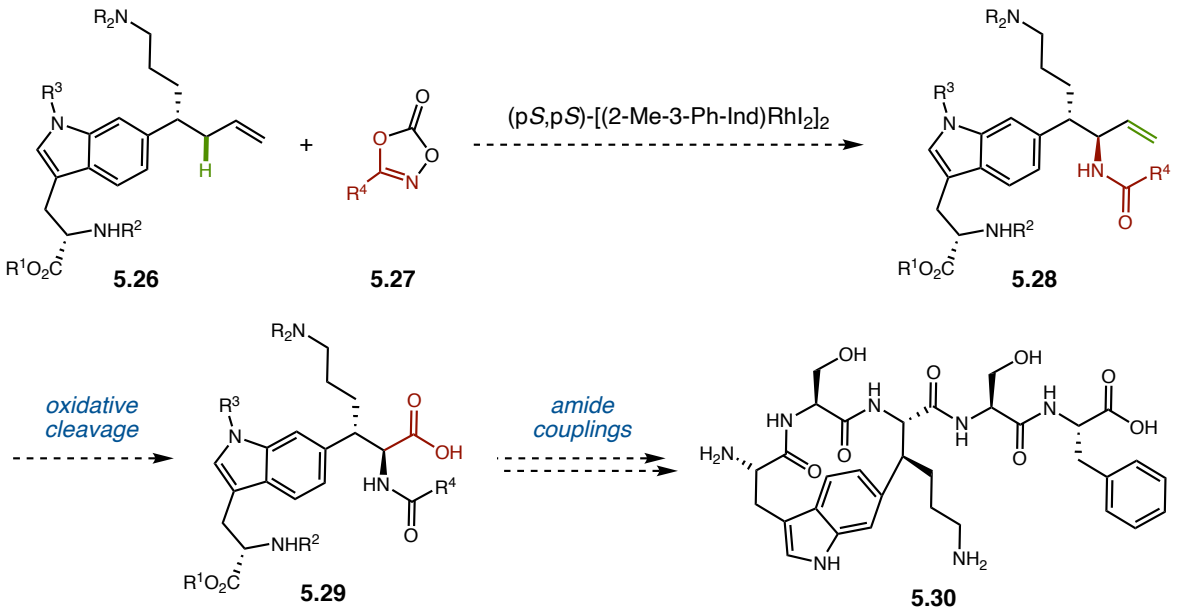

Scheme 5.4: Proposed route to the eastern ring of darobactin A utilizing the Blakey group's enantioselective allylic C–H amidation reaction for key bond disconnections

A general scheme was developed where we could begin with tryptophan derived **5.26** (**Scheme 5.4**). With the homo-allylic stereocenter already installed, enantioselective allylic amidation would provide protected amide **5.28**.[12] Oxidative cleavage of the olefin to carboxylic acid **5.29** would allow for the installation of additional residues to this terminus of the compound, and conventional amide couplings would be utilized to afford macrocycle **5.30**.[13,14] Unfortunately, several key challenges arose in this potential method. First, while enantioselective allylic amidation of **5.26** could, in theory, afford the desired stereochemical outcome of the ß-amino aryl-alkyl crosslink, the olefin product delivered (**5.28**) would require further oxidative manipulations for continuation in the synthesis. Additionally, the presence of a homoallylic stereocenter was shown to elicit a match/mismatched scenario with the catalyst.[12] The desired stereochemical outcome for darobactin A could require the use of a mismatched catalyst substrate pair, effectively eliminating this strategy.

While investigating alternative strategies, we discovered a report from the Glorius group for the 1,2-carboamination of electron-deficient acrylates **5.32** for the synthesis of unnatural amino acids **5.33** (**Scheme 5.5a**).[15] Subsequent work from the Liu group in the same year disclosed the

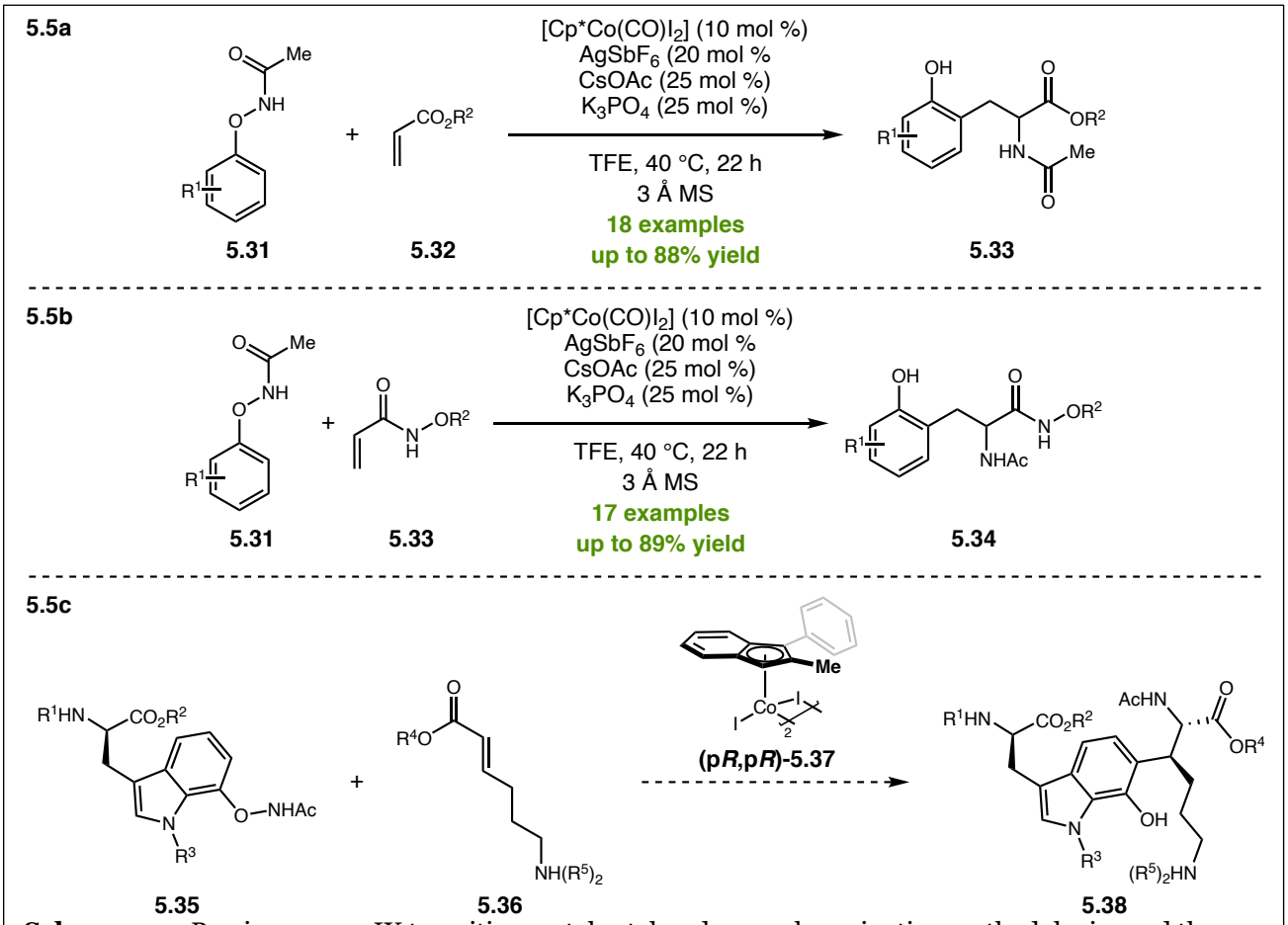

Scheme 5.5: Previous group IX transition metal catalyzed 1,2-carboamination methodologies and the strategic plan for application to the total synthesis of RiPPs including darobactin A

rhodium catalyzed 1,2-carboamination of acrylamides **5.33** (**Scheme 5.5b**).[16] From these reports we proposed a new synthetic strategy to access the desired ß-amino aryl-alkyl crosslink. Outlining this strategy in the context of darobactin A (**Scheme 5.5c**), we envisioned a strategy where we could carry out the enantioselective 1,2-carboamination of olefin **5.36** with tryptophan derived **5.35**. This strategy would set both stereocenters concurrently, and *syn* carboamination of a *trans* olefin precursor would afford the desired stereochemistry (**5.38**).

5.2.2 Development and Optimization of the Cobalt-Catalyzed 1,2-Carboamidation of Acrylamides

For this synthetic plan to work, several advances had to be made on the published 1,2-carboamination chemistry.[15,16] First, 1,2-disubstituted olefins (**5.36**) have yet to successfully be functionalized in any of the previous methodologies. Next, an enantioselective version of this

reaction had yet to be disclosed. Finally, to make this a generalizable way to access different RiPP natural products, we wondered if this could be used as a late stage macrocyclization platform to better mimic the biosynthetic machinery.

We initially focused on the use of our chiral rhodium indenyl platform to develop an enantioselective version of the 1,2-carboamidation platform,[12] however, a report detailing this transformation was published by the Cramer group during our initial foray into this reaction.[17] Therefore, we turned our attention to the more-ambitious use of 1,2-carboamidation as a late stage macrocyclization strategy.

Efforts at developing a cobalt centered chiral indenyl catalyst (**5.37**, **Scheme 5.5c**) were unsuccessful, so we first focused on developing the racemic platform, with the goal of later applying a chiral cobalt catalyst to the reaction. In the Glorius' groups initial work, 1,2-carboamidation had been successful on the acrylate platform but had not been tested on acrylamides.[15] While acrylamides had been successful in the rhodium catalyzed reaction, these acrylamides used required specific electronic tuning to prevent early ß-hydride elimination in the reaction, and so the rhodium catalysis would not be useful for the desired reactivity.[16]

We began by conducting an initial proof-of-concept reaction of the 1,2-carboamidation on a model system of phenoxyacetamide **5.39** and acrylamide **5.40** under conditions identical to the acrylate report.[15] To our pleasure, the reaction successfully provided **5.41**, albeit with low conversion. From this initial result, we began an optimization study to improve the yield of this reaction.

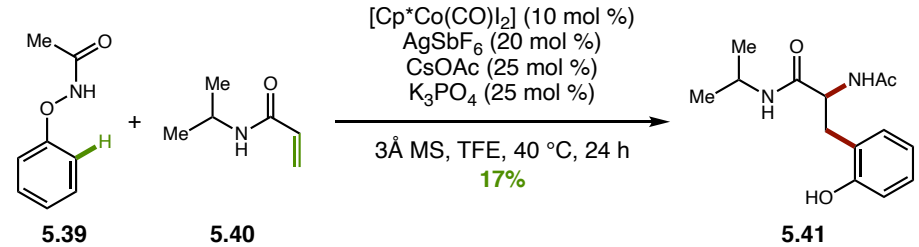

Scheme 5.6: Proof-of-concept 1,2-carboamidation of acrylamides

Early work on the reaction demonstrated that amino acid derived hydroxamates behaved differently than simple phenoxyacetamide **5.39**. With peptide macrocyclization in mind, reaction

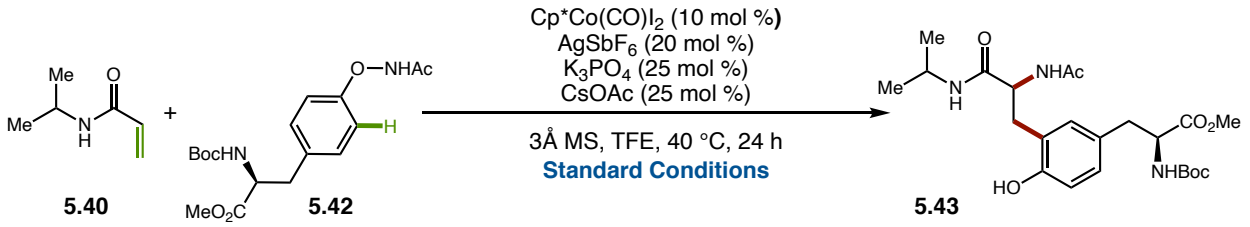

Entry	Deviation from std. cond.	Assay Yield* (Isolated)
1	None	25 (20)
2	AgOAc, No $AgSbF_6$	41
3	AgOAc	20
4	No Co	n.r.
5	No K_3PO_4	11
6	No CsOAc	36[a]
7	No $AgSbF_6$	54
8	No $AgSbF_6$, 60 °C	81
9	No $AgSbF_6$, 80 °C	71

*Assay yield determined by ^{1}H NMR integration against methyl 3,5-dinitrobenzoate. [a]Yield represents an average of two results.

Table 5.1: Optimization of 1,2-carboamidation of acrylamides with amino acid derived hydroxamates

optimization was shifted to the use of amino acid derived hydroxamate **5.42** (**Table 5.1**).[17] First, we applied standard reaction conditions to the tyrosine hydroxamate **5.42** and validated the internal standard (**Entry 1**). To simplify reaction conditions, we first explored to see if we could combine the silver source and acetate source into a single component and saw an increase in yield (**Entry 2**). We confirmed that it was not just the change from cesium acetate to silver acetate (**Entry 3**) and then began control experiments to identify which components of the reaction mixture were necessary as our results suggested that not every component was required for reactivity. Removal of the cobalt catalyst, as expected, shut down the reaction entirely (**Entry 4**). During the Glorius group's initial optimization, they noted that potassium phosphate tribasic was not necessary but served to increase the yield, which also proved to be true in our reaction (**Entry 5**).[15] Removal of the acetate source afforded a slight increase in yield compared to standard conditions (**Entry 6**), though there is still sufficient base present from the potassium phosphate tribasic. Interestingly, removal of silver from the reaction afforded the highest reproducible yield observed (**Entry 7**). Several recent studies of rhodium and iridium catalyzed reactions proceeding through nitrenoid intermediates, including undisclosed preliminary data from our group, suggest the importance of the identity of the halide and the role it may play in reactive intermediates.[18–20]

A similar effect may be at play in this reaction since the removal of silver afforded such a large improvement in the yield. Increasing the temperature from 40 °C to 60 °C improved the yield from 54% to 81% (**Entry 8**). However, there was a limit to this relative increase as the reaction at 80 °C, above the solvent boiling point, did not perform as well (**Entry 9**).

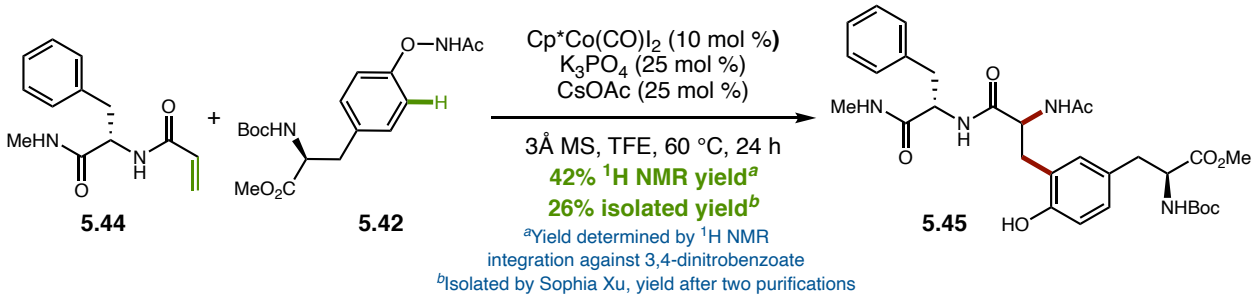

Scheme 5.7: Intermolecular model system for dipeptide formation *via* 1,2-carboamidation

With optimized reaction conditions in hand, we wanted to expand this simple model system to a more complex peptide-based model prior to examining a macrocyclization (**Scheme 5.7**). To this end, we designed phenylalanine diamide **5.44**, which we could access from commercially available phenylalanine (see **5.5 Supporting Information** for details). Application of this designer diamide to the same conditions afforded **5.45** as a ~1:1 mixture of diastereomers. While the intermolecular 1,2-carboamidation with this final model system does not provide any diastereoselectivity, we predict there is a potential for inherent selectivity in a full peptide platform due to secondary structures providing a bias for folding in a specific conformation.[21]

5.2.3 Tyrosine Hydroxamate Studies and Linear Peptide Design/Synthesis

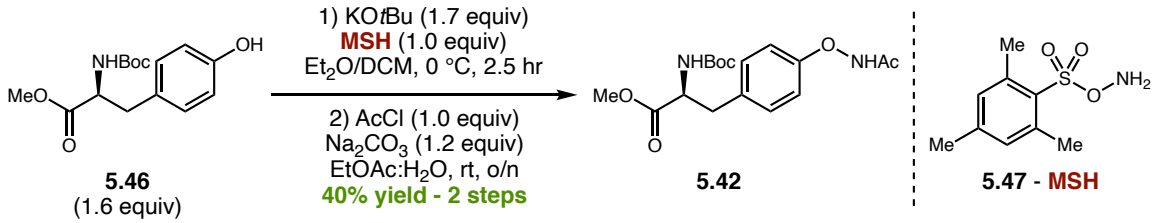

Scheme 5.8: Published route to access phenol-derived hydroxamate functionality

During the completion of the reaction development and initial model studies, we had been utilizing previously disclosed methods to access the necessary pre-functionalized tyrosine substrate **5.42** (**Scheme 5.8**).[22,23] This starting material synthesis involved the amination of Boc-Tyr-OMe (**5.46**) with MSH (**5.47**) followed by acetylation. However, **5.47** is a known explosion

hazard, even when specific safe handling precautions are taken.[24] After a near-miss incident involving a multi-gram quantity of **5.47** violently decomposing in our chemical fridge, we decided it would be prudent for the future of this project to design a safer route to access tyrosine **5.42**.

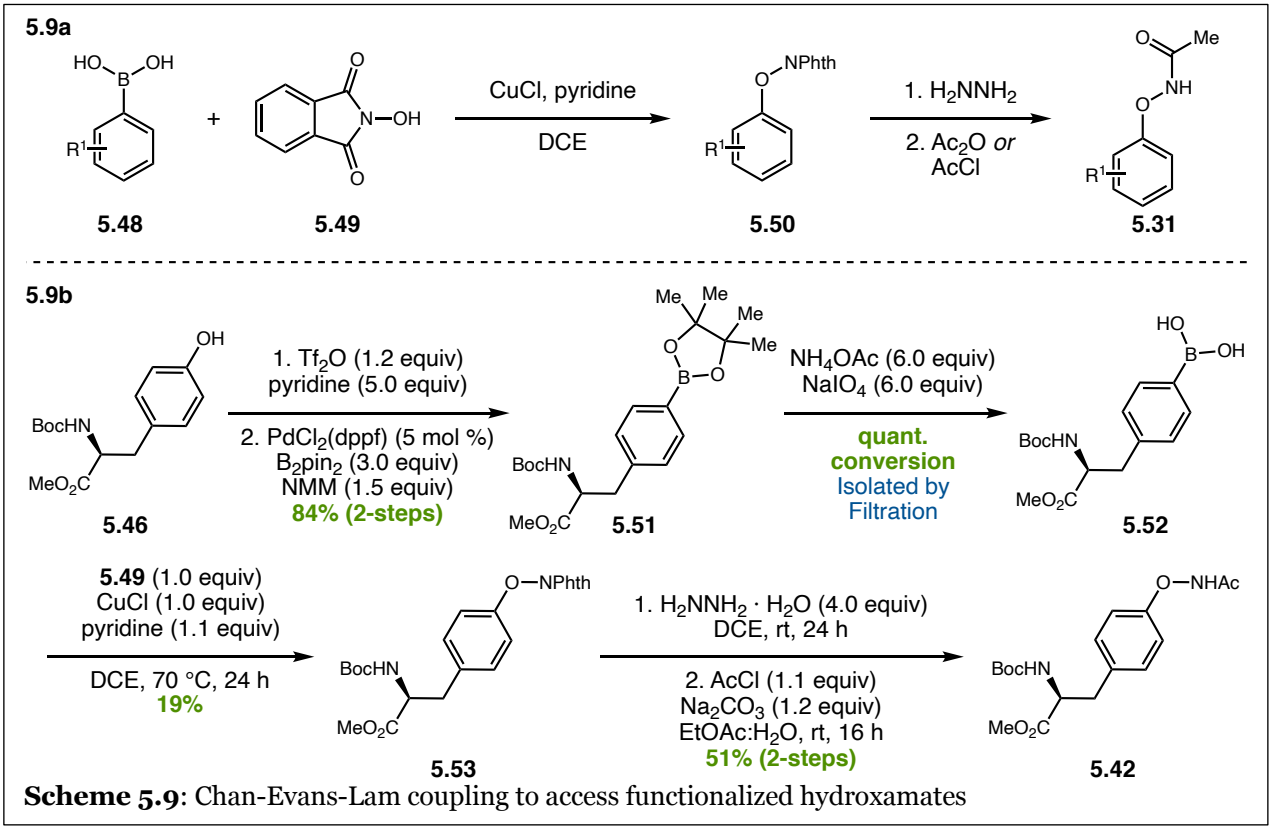

Scheme 5.9: Chan-Evans-Lam coupling to access functionalized hydroxamates

For this, we turned to the synthesis of phenoxyacetamide **5.31** for inspiration (**Scheme 5.9a**).[25] When the boronic acid of the desired aryl functionality (**5.48**) is commercially available, the route to access phenoxyacetamides proceeds *via* the Chan-Evans-Lam coupling with *N*-hydroxyphthalimide **5.49** to install the N–O bond (**5.50**).[26] Deprotection of the phthalimide with hydrazine and acylation affords **5.31**.[25,26] Therefore, we decided to design a route to access tyrosine boronic acid **5.52** and use the Chan-Evans-Lam coupling to install the N-O bond here as well (**Scheme 5.9b**). Starting from readily available tyrosine **5.46**, triflation of the phenol followed by installation of a pinacol boronic ester provides Boc-Tyr(Bpin)-OMe (**5.51**) in 84% yield with a single purification.[27] Conversion of boronic ester **5.51** to acid **5.52** affords the coupling partner for the Chan-Evans-Lam reaction with *N*-hydroxyphthalimide **5.49**.[26,27] Finally, hydrazine deprotection of phthalimide **5.53** and acetylation provide tyrosine **5.42**.[25,26] This route,

while longer, provides safe and scalable access to tyrosine **5.42** without the use of large quantities of unstable **5.47** (**Scheme 5.8**). Currently, Michael Hollerbach and Sophia Xu are working towards improving or modifying several synthetic steps to achieve the greatest utility of this route.

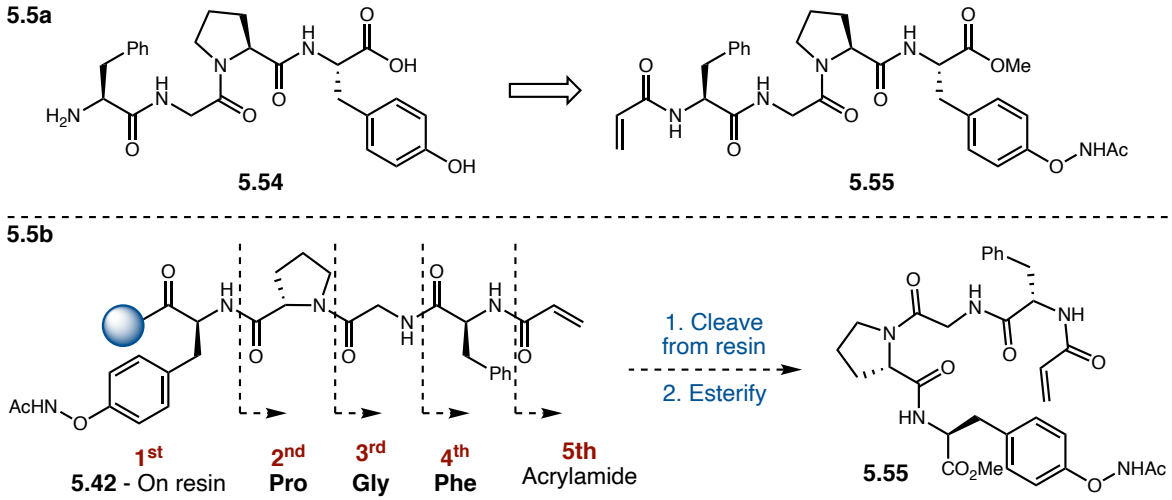

Figure 5.5: Synthetic design and plan of the linear peptide sequence for cyclization *via* 1,2-carboamidation

During the reaction discovery and optimization, Sophia Xu was working towards the synthesis of the linear peptide for cyclization. The functionalized linear sequence **5.55** chosen for initial study was derived from phenylalanine-glycine-proline-tyrosine **5.54** (**Figure 5.5a**). This sequence would provide a favorable 18-membered ring size for the resulting macrocycle and included a proline-glycine pair to encourage angle compression of the linear peptide backbone and improve the likelihood of productive reactivity.[21] For the synthesis of the linear peptide, our original plan was to load pre-functionalized tyrosine **5.42** onto a solid phase peptide synthesizer (SPPS), build the linear sequence, cap the *N*-terminus as an acrylamide, cleave the peptide from the resin, and protect the resultant carboxylic acid for cyclization. However, when Sophia conducted preliminary studies with functionalized tyrosine **5.56** to examine its ability to tolerate SPPS coupling conditions, she recovered tyrosine **5.57**, the result of N–O bond cleavage in the starting material in addition to Fmoc deprotection (**Figure 5.6a**). Through a deep dive into the literature, Sophia discovered that the functionalized tyrosine **5.58** was likely undergoing a Lossen-type rearrangement to cleave the N–O bond (**Figure 5.6b**).[28]

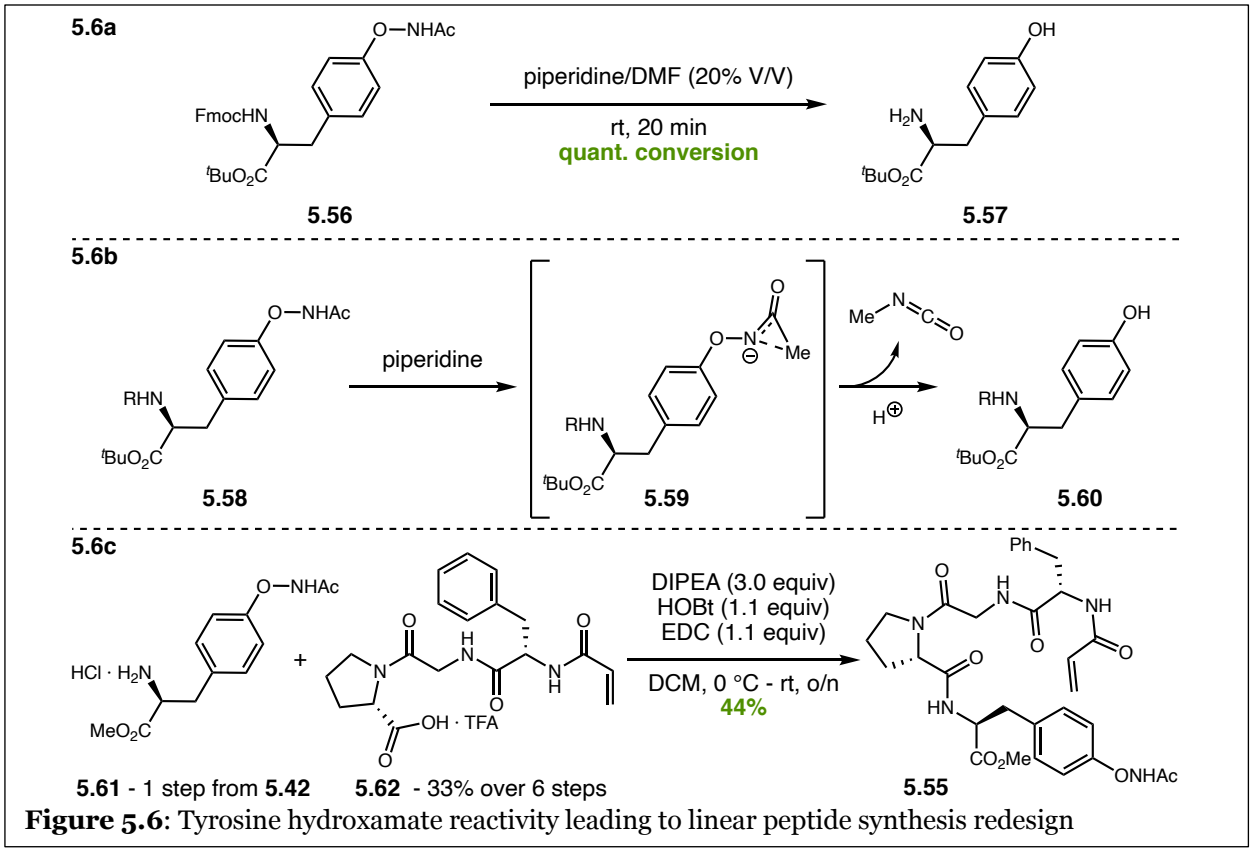

Figure 5.6: Tyrosine hydroxamate reactivity leading to linear peptide synthesis redesign

After further investigation, Sophia discovered that functionalized tyrosine **5.58** would undergo this rearrangement and N–O bond cleavage under most SPPS conditions available for continued amide coupling after installation of the tyrosine. Therefore, she redesigned the route to access the linear peptide sequence. The revised method begins with solution phase synthesis of a peptide trimer and *N*-terminus installation of the acrylamide (**5.62**, **Figure 5.6c**).[29–31] Then the functionalized tyrosine **5.61** can be installed as the last step in the sequence before cyclization.[30,31] Through this modified order of residue installation, she has been able to access the complete linear peptide **5.55** and is working to investigate the proof-of-concept peptide macrocyclization.

5.3 Conclusion

During these studies, we have made significant progress towards a peptide macrocyclization strategy through the cobalt-catalyzed 1,2-carboamidation of acrylamides. The development of this methodology involved the optimization of previous acrylate literature to the desired acrylamide system. Successful intermolecular model studies have detailed the ability of the optimized conditions to form dipeptide functionality. If successful, macrocyclization following linear peptide synthesis will allow for access to the targeted ß-amino aryl-alkyl crosslink in a manner that more closely mimics the biosynthetic pathway. Additionally, we have developed a safe and scalable alternative route to access phenol-derived phenoxyacetamide functionality that avoids the use of inherently explosive reagents. Currently, work is being continued by Sophia Xu to investigate the proof-of-concept intramolecular macrocyclization and, further, to investigate a range of linear peptide sequences capable of utilizing this methodology.

5.4 References

(1) Arnison, P. G.; Bibb, M. J.; Bierbaum, G.; Bowers, A. A.; Bugni, T. S.; Bulaj, G.; Camarero, J. A.; Campopiano, D. J.; Challis, G. L.; Clardy, J.; et al. Ribosomally Synthesized and Post-Translationally Modified Peptide Natural Products: Overview and Recommendations for a Universal Nomenclature. *Nat. Prod. Rep.* **2012**, *30*, 108–160.

(2) Montalbán-López, M.; Scott, T. A.; Ramesh, S.; Rahman, I. R.; Van Heel, A. J.; Viel, J. H.; Bandarian, V.; Dittmann, E.; Genilloud, O.; Goto, Y.; et al. New Developments in RiPP Discovery, Enzymology and Engineering. *Nat. Prod. Rep.* **2021**, *38*, 130–239.

(3) Swain, J. A.; Walker, S. R.; Calvert, M. B.; Brimble, M. A. The Tryptophan Connection: Cyclic Peptide Natural Products Linked via the Tryptophan Side Chain. *Nat. Prod. Rep.* **2022**. Advance Article. https://doi.org/10.1039/d1np00043h.

(4) Bentley, D. J.; Slawin, A. M. Z.; Moody, C. J. Total Synthesis of Stephanotic Acid Methyl Ester. *Org. Lett.* **2006**, *8*, 1975–1978.

(5) Michaux, J.; Retailleau, P.; Campagne, J.-M. Synthesis of the Central Tryptophan-Leucine Residue of Celogentin C. *Synlett* **2008**, *10*, 1532-1536.

(6) Ma, B.; Litvinov, D. N.; He, L.; Banerjee, B.; Castle, S. L. Total Synthesis of Celogentin C. *Angew. Chem. Int. Ed.* **2009**, *48*, 6104–6107.

(7) Ma, B.; Banerjee, B.; Litvinov, D. N.; He, L.; Castle, S. L. Total Synthesis of the Antimitotic Bicyclic Peptide Celogentin C. *J. Am. Chem. Soc.* **2010**, *132*, 1159-1171.

(8) Feng, Y.; Chen, G. Total Synthesis of Celogentin C by Stereoselective C-H Activation. *Angew. Chem. Int. Ed.* **2010**, *49*, 958–961.

(9) Isley, N. A.; Endo, Y.; Wu, Z.-C.; Covington, B. C.; Bushin, L. B.; Seyedsayamdost, M. R.; Boger, D. L. Total Synthesis and Stereochemical Assignment of Streptide. *J. Am. Chem. Soc.* **2019**, *141*, 17361-17369.

(10) Quynh Ngoc Nguyen, T.; Wei Tooh, Y.; Sugiyama, R.; Phuong Diep Nguyen, T.; Purushothaman, M.; Chuan Leow, L.; Hanif, K.; How Sheng Yong, R.; Agatha, I.;

Winnerdy, F. R.; et al. Post-Translational Formation of Strained Cyclophanes in Bacteria. *Nat. Chem.* **2020**, *12*, 1042-1053.

(11) Zhang, X.; Lu, G.; Sun, M.; Mahankali, M.; Ma, Y.; Zhang, M.; Hua, W.; Hu, Y.; Wang, Q.; Chen, J.; et al. A General Strategy for Synthesis of Cyclophane-Braced Peptide Macrocycles via Palladium-Catalysed Intramolecular Sp 3 C–H Arylation. *Nat. Chem.* **2018**, *10*, 540-548.

(12) Farr, C. M. B.; Kazerouni, A. M.; Park, B.; Poff, C. D.; Won, J.; Sharp, K. R.; Baik, M. H.; Blakey, S. B. Designing a Planar Chiral Rhodium Indenyl Catalyst for Regio- And Enantioselective Allylic C-H Amidation. *J. Am. Chem. Soc.* **2020**, *142*, 13996–14004.

(13) White, C. J.; Yudin, A. K. Contemporary Strategies for Peptide Macrocyclization. *Nat. Chem.* **2011**, *3*, 509-524.

(14) Bechtler, C.; Lamers, C. Macrocyclization Strategies for Cyclic Peptides and Peptidomimetics. *RSC Med. Chem* **2021**, *12*, 1351.

(15) Lerchen, A.; Knecht, T.; Daniliuc, C. G.; Glorius, F. Unnatural Amino Acid Synthesis Enabled by the Regioselective Cobalt(III)-Catalyzed Intermolecular Carboamination of Alkenes. *Angew. Chem. Int. Ed.* **2016**, *55*, 15166–15170.

(16) Hu, Z.; Tong, X.; Liu, G. Rhodium(III) Catalyzed Carboamination of Alkenes Triggered by C–H Activation of N-Phenoxyacetamides under Redox-Neutral Conditions. *Org. Lett.* **2016**, *18*, 1702–1705.

(17) Ozols, K.; Onodera, S.; Woźniak, Ł.; Cramer, N. Cobalt(III)-Catalyzed Enantioselective Intermolecular Carboamination by C–H Functionalization. *Angew. Chem. Int. Ed.* **2021**, *60*, 655–659.

(18) Wang, H.; Jung, H.; Song, F.; Zhu, S.; Bai, Z.; Chen, D.; He, G.; Chang, S.; Chen, G. Nitrene-Mediated Intermolecular N–N Coupling for Efficient Synthesis of Hydrazides. *Nat. Chem.* **2021**, *13*, 378-385.

(19) Lee, S.; Rovis, T. Rh(III)-Catalyzed Three-Component Syn-Carboamination of Alkenes

Using Arylboronic Acids and Dioxazolones. *ACS Catal.* **2021**, *11*, 8585–8590.

(20) Lee, S.; Semakul, N.; Rovis, T. Direct Regio- and Diastereoselective Synthesis of δ -Lactams from Acrylamides and Unactivated Alkenes Initiated by Rh III -Catalyzed C–H Activation . *Angew. Chem. Int. Ed.* **2020**, *59*, 4965-4969.

(21) Blankenstein, J.; Zhu, J. Conformation-Directed Macrocyclization Reactions. *Eur. J. Org. Chem.* **2005**, *10*, 1949–1964.

(22) Li, B.; Lan, J.; Wu, D.; You, J. Rhodium(III)-Catalyzed Ortho -Heteroarylation of Phenols through Internal Oxidative C–H Activation: Rapid Screening of Single-Molecular White-Light-Emitting Materials . *Angew. Chem. Int. Ed.* **2015**, *54*, 14008–14012.

(23) Yan, D.; Wang, G.; Xiong, F.; Sun, W. Y.; Shi, Z.; Lu, Y.; Li, S.; Zhao, J. A Selenium-Catalysed Para-Amination of Phenols. *Nat. Commun.* **2018**, *9*, 1–9.

(24) Bernardes, G. J. L.; Chalker, J. M.; Errey, J. C.; Davis, B. G. Facile Conversion of Cysteine and Alkyl Cysteines to Dehydroalanine on Protein Surfaces: Versatile and Switchable Access to Functionalized Proteins. *J. Am. Chem. Soc.* **2008**, *130*, 5052–5053.

(25) Liu, G.; Shen, Y.; Zhou, Z.; Lu, X. Rhodium(III)-Catalyzed Redox-Neutral Coupling of N-Phenoxyacetamides and Alkynes with Tunable Selectivity. *Angew. Chem. Int. Ed.* **2013**, *52*, 6033–6037.

(26) Petrassi, H. M.; Sharpless, K. B.; Kelly, J. W. The Copper-Mediated Cross-Coupling of Phenylboronic Acids and N-Hydroxyphthalimide at Room Temperature: Synthesis of Aryloxyamines. *Org. Lett.* **2001**, *3*, 139–141.

(27) Feng, Z.; Min, Q. Q.; Xiao, Y. L.; Zhang, B.; Zhang, X. Palladium-Catalyzed Difluoroalkylation of Aryl Boronic Acids: A New Method for the Synthesis of Aryldifluoromethylated Phosphonates and Carboxylic Acid Derivatives. *Angew. Chem. Int. Ed.* **2014**, *53*, 1669–1673.

(28) Jašíková, L.; Hanikýřová, E.; Škríba, A.; Jašík, J.; Roithová, J. Metal-Assisted Lossen Rearrangement. *J. Org. Chem.* **2012**, *77*, 2829–2836.

(29) Marafon, G.; Crisma, M.; Moretto, A. Intrinsically Photoswitchable α/β Peptides toward Two-State Foldamers. *Angew. Chem. Int. Ed.* **2018**, *57*, 10217–10220.

(30) Ghosh, K. C.; Duttagupta, I.; Bose, C.; Banerjee, P.; Gayen, A. K.; Sinha, S. Synthesis and Anticancer Activities of Proline-Containing Cyclic Peptides and Their Linear Analogs and Congeners. *Synth. Commun.* **2019**, *49*, 221–236.

(31) Suzuki, Y.; Takagi, N.; Sano, T.; Chimuro, T. Design and Synthesis of a Novel Fluorescent Protein Probe for Easy and Rapid Electrophoretic Gel Staining by Using a Commonly Available UV-Based Fluorescent Imaging System. *Electrophoresis* **2013**, *34*, 2464–2472.

5.5 Supporting Information

5.5.1 General Information

All reactions were carried out under nitrogen atmosphere with anhydrous solvents in oven- or flame-dried glassware using standard Schlenk technique, unless otherwise stated. Anhydrous dichloromethane (DCM), diethyl ether (Et2O), tetrahydrofuran (THF), and toluene were obtained by passage through activated alumina using a Glass Contours solvent purification system. 2,2,2-trifluoroethanol was distilled over calcium hydride (CaH_2) and stored over activated molecular sieves. Solvents for workup, extraction, and column chromatography were used as received from commercial suppliers without further purification. Unless otherwise reported, compounds L-Phe-NHMe,[1] **5.39**,[2] **5.42**,[3] and $[Cp^*Co(CO)I_2]$[4] were synthesized according to previously reported procedures. All other chemicals were purchased from Millipore Sigma, Strem Chemicals, Oakwood Chemicals, Alfa Aesar, or Combi-Blocks and used as received without further purification, unless otherwise stated.

^{1}H and 13C nuclear magnetic resonance (NMR) spectra were recorded on a Varian Inova 600 spectrometer (600 MHz 1 H, 151 MHz 13C), a Bruker 600 spectrometer (600 MHz 1 H, 151 MHz 13C), a Varian Inova 500 spectrometer (500 MHz 1 H, 126 MHz 13C), and a Bruker 400 spectrometer (400 MHz 1 H, 126 MHz 13C) at room temperature in CDCl3 (dried over activated molecular sieves) with internal CHCl3 as the reference (7.26 ppm for 1 H, 77.16 ppm for 13C), unless otherwise stated. Chemical shifts (δ values) were reported in parts per million (ppm) and coupling constants (J values) in Hz. Multiplicity was indicated using the following abbreviations: s = singlet, d = doublet, t = triplet, q = quartet, qn = quintet, m = multiplet, br = broad. High resolution mass spectra (HRMS) were obtained using a Thermo Electron Corporation Finigan LTQFTMS (at the Mass Spectrometry Facility, Emory University). High Pressure Liquid Chromatography (HPLC) was performed on an Agilent 1100 series HPLC utilizing CHIRALPAK AD-H, AS-H, OD-H and OJ-H 4.6 x 150 mm analytical columns. Analytical thin layer chromatography (TLC) was performed on precoated glass-backed Silicycle SiliaPure® 0.25 mm

silica gel 60 plates and visualized with UV light, ethanolic p-anisaldehyde, ethanolic bromocresol green, or aqueous potassium permanganate (KMnO4). Flash column chromatography was performed using Silicycle SiliaFlash® F60 silica gel (40- 63 μm) on a Biotage Isolera One system. Preparatory TLC was performed on precoated glass-backed Silicycle SiliaPure® 1.0 mm silica gel 60 plates. We acknowledge the use of shared instrumentation provided by grants from the NIH and the NSF.

5.5.2 Experimental Section

5.5.2.1 General Procedures

General Procedure 1 (1,2-carboamidation of acrylamide, based off of acrylate procedure): To an oven-dried 4 mL vial equipped with a stir bar and 3 Å MS in a nitrogen-filled glove box, added phenoxyacetamide (1.0 equiv), K_3PO_4 (25 mol %), $AgSbF_6$ (20 mol %), CsOAc (25 mol %), and [Cp*Co(CO)I_2] (10 mol %), sealed with a teflon-cap and removed from the glove box. A stock solution of *N*-isopropylacrylamide **5.40** in TFE was prepared by dissolving **5.40** (0.0127 mg) in TFE (1.6 mL) and 1.0 mL (1.0 equiv, 0.07 M total concentration) was added to the reaction vial. The vial was placed into a pre-heated 40 °C heating block under a balloon of nitrogen and allowed to stir for 24 hours before being removed and cooled to room temp. After cooling, the reaction was filtered through a plug of silica and concentrated *in vacuo* before analysis by ^{1}H NMR. Purification on silica affords title compound.

General Procedure 2 (1,2-carboamidation optimization procedure): To an oven-dried 4 mL vial equipped with a stir bar and 3 Å MS in a nitrogen-filled glove box, added **5.42** (1.0 equiv, 0.0284 mmol), K_3PO_4 (25 mol %, 0.0071 mmol), $AgSbF_6$ (20 mol %, 0.0056 mmol), CsOAc (25 mol %, 0.0071 mmol), and [Cp*Co(CO)I_2] (10 mol %, 0.0028 mmol) as necessary, sealed with a teflon-cap and removed from the glove box. A stock solution of *N*-isopropylacrylamide **5.40** in DCM was prepared by dissolving **5.40** (1.0 equiv, 0.0284 mmol) in TFE and 0.3 mL (0.1 M total

concentration) was added to the reaction vial. The vial was placed into a pre-heated heating block at the stated temperature under a balloon of nitrogen and allowed to stir for 24 hours before being removed and cooled to room temp. After cooling, a stock solution of methyl 3,5-dinitrobenzoate (0.0284 mmol) in DCM was added and the reaction was filtered through a plug of silica and concentrated *in vacuo* before analysis by ^{1}H NMR. Purification on silica affords title compound.

5.5.2.2 Experimental Procedures for Compounds Synthesized by C.D.P.

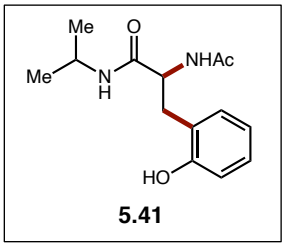

5.41

***2-acetamido-3-(2-hydroxyphenyl)-N-isopropylpropanamide* (5.41)** – Synthesized according to **General Procedure 1** from phenoxyacetamide **5.39** (0.0010 g, 0.0662 mmol), *N*-isopropylacrylamide **5.40** (0.0075 g, 0.0662 mmol), K_3PO_4 (0.0035 g, 0.0165 mmol), [Cp*Co(CO)I_2] (0.0032 g, 0.00662 mmol), $AgSbF_6$ (0.0046 g, 0.0132 mmol), and CsOAc (0.0032 g, 0.0165 mmol). Purification by flash chromatography on silica (75% EtOAc in hexanes) afforded **5.41** (3.0 mg, 17% yield) as a white solid. **^{1}H NMR** ($CDCl_3$, 600 MHz) δ 9.05 (s, 1H), 7.22 – 7.15 (m, 1H), 6.99 (ddd, *J* = 9.4, 7.8, 1.5 Hz, 2H), 6.82 (td, *J* = 7.4, 1.3 Hz, 1H), 6.76 (s, 1H), 5.42 (s, 1H), 4.27 (ddd, *J* = 10.0, 6.1, 2.0 Hz, 1H), 4.06 – 3.98 (m, 1H), 3.27 (dd, *J* = 14.4, 2.0 Hz, 1H), 2.74 (dd, *J* = 14.4, 9.9 Hz, 1H), 2.09 (s, 3H), 1.10 (d, *J* = 6.6 Hz, 3H), 1.04 (d, *J* = 6.6 Hz, 3H). **HRMS** (+APCI) calculated for $C_{14}H_{21}N_2O_3$ $[M+H]^+$ 264.1474, found 265.1547.

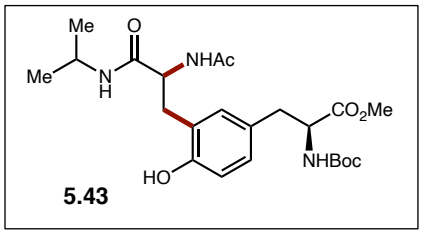

5.43

***Methyl (2S)-3-(3-(2-acetamido-3-(isopropylamino)-3-oxopropyl)-4-hydroxyphenyl)-2-((tert-butoxycarbonyl)amino)propanoate* (5.43)** – Synthesized according to **General Procedure 2** from Boc-Tyr(NHAc)-OMe **5.42** (0.0150 g, 0.0426 mmol), *N*-isopropylacrylamide **5.40** (0.0048 g, 0.0426 mmol), K_3PO_4 (0.0023 g, 0.0106 mmol), [Cp*Co(CO)I_2] (0.0020 g, 0.00426 mmol), $AgSbF_6$ (0.0030 g, 0.00851 mmol), and CsOAc (0.0020 g, 0.0106 mmol). Purification by preparative TLC

(100% EtOAc) afforded **5.43** (0.0040 g, 20% yield, ~1:1 mixture of diastereomers) as a white solid. **^{1}H NMR** ($CDCl_3$, 600 MHz) δ 9.16 (d, *J* = 109.2 Hz, 1H), 7.08 – 6.72 (m, 4H), 6.60 (s, 1H), 6.29 (d, *J* = 6.5 Hz, 1H), 5.73 (s, 1H), 4.96 (d, *J* = 9.5 Hz, 1H), 4.61 – 4.45 (m, 2H), 4.37 (s, 1H), 4.03 (dq, *J* = 13.1, 6.7 Hz, 1H), 3.74 (d, *J* = 48.1 Hz, 3H), 3.40 – 3.11 (m, 1H), 2.97 (d, *J* = 6.1 Hz, 1H), 2.77 – 2.58 (m, 1H), 2.11 (d, *J* = 6.4 Hz, 3H), 1.23 (s, 9H), 1.18 – 1.03 (m, 6H). **HRMS** (+APCI) calculated for $C_{23}H_{35}N_3NaO_7$ $[M+Na]^+$ 488.2373, found 488.2355.

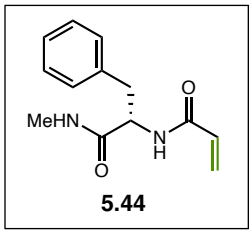

5.44

***(S)-N-(1-(methylamino)-1-oxo-3-phenylpropan-2-yl)acrylamide* (5.44)** – To a flame-dried 100 mL RBF equipped with a stir bar was added *L*-Phe-NHMe (1.2641 g, 7.09 mmol, 1.0 equiv) before sealing with a rubber septum and exchanging the atmosphere with N_2. The reaction was dissolved in DCM (25.0 mL, 0.3 M) and placed into a 0 °C ice/water bath. After cooling for 5 minutes, Et_3N (1.5788 g, 15.6 mmol, 2.2 equiv) was added and the reaction stirred for an additional 10 minutes at 0 °C. Acryloyl chloride (0.7703 g, 8.51 mmol, 1.2 equiv) was added and the reaction allowed to stir under a balloon of nitrogen and warm to room temperature. After 16 hours, celite was added and the reaction was concentrated *in vacuo*. Purification on silica (100% EtOAc) afforded **5.44** (0.9212 g, 56% yield) as a white solid. **^{1}H NMR** (400 MHz, $CDCl_3$) δ 7.33 – 7.28 (m, 2H), 7.25 – 7.20 (m, 3H), 6.39 (d, *J* = 7.8 Hz, 1H), 6.28 (dd, *J* = 17.0, 1.4 Hz, 1H), 6.10 (dd, *J* = 17.0, 10.3 Hz, 1H), 5.70 (s, 1H), 5.67 (dd, *J* = 10.2, 1.4 Hz, 1H), 4.65 (td, *J* = 8.1, 6.0 Hz, 1H), 3.16 (dd, *J* = 13.6, 6.0 Hz, 1H), 3.03 (dd, *J* = 13.6, 8.3 Hz, 1H), 2.70 (d, *J* = 4.9 Hz, 3H). **^{13}C NMR** ($CDCl_3$, 101 MHz) δ 171.16, 165.21, 136.67, 130.30, 129.24, 128.72, 127.30, 127.08, 54.83, 38.61, 26.20. **HRMS** (+APCI) calculated for $C_{13}H_{17}O_2N_2$ $[M+H]^+$ 233.1285, found 233.1279.

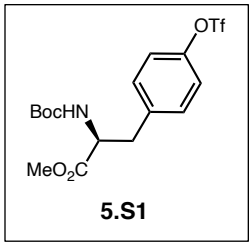

5.S1

***Methyl (S)-2-((tert-butoxycarbonyl)amino)-3-(4-(((trifluoromethyl)sulfonyl)oxy)phenyl)proponate* (5.S1)** – To a flame-dried 100 mL RBF equipped with a stir bar was added Boc-Tyr-OMe (2.0050 g, 6.79 mmol, 1.0 equiv) before sealing with a rubber septum and exchanging the atmosphere with nitrogen. The Boc-Tyr-OMe was dissolved in DCM (20.0 mL, 0.35 M total concentration) and pyridine (2.86 g, 33.94 mmol, 5.0 equiv) was added before the reaction was cooled to 0 °C in a ice/water bath. Tf_2O (2.2984 g, 8.15 mmol, 1.2 equiv) was added to the reaction flask and allowed to stir at 0 °C under a balloon of nitrogen. After 1 hour, the reaction was diluted with DCM (50.0 mL) and washed with DI H_2O (50.0 mL), 1N NaOH (50.0 mL), saturated Cu_2SO_4 (3 x 50.0 mL), and brine (50.0 mL). The organic layer was dried over Na_2SO_4, filtered to remove the drying agent, and concentrated *in vacuo* to afford **5.S1** (2.8250 g, 97% yield) as a clear oil. **^{1}H NMR** (500 MHz, $CDCl_3$) δ 7.25 – 7.16 (m, 4H), 5.02 (d, *J* = 8.2 Hz, 1H), 4.60 (q, *J* = 6.8 Hz, 1H), 3.71 (s, 3H), 3.17 (dd, *J* = 13.9, 5.8 Hz, 1H), 3.04 (dd, *J* = 13.9, 6.6 Hz, 1H), 1.41 (s, 9H).[5]

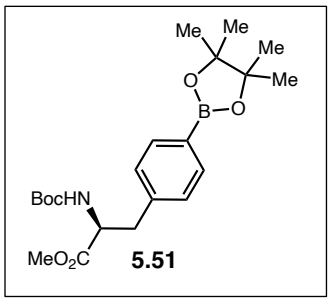

5.51

***Methyl (S)-2-((tert-butoxycarbonyl)amino)-3-(4-(4,4,5,5-tetramethyl-1,3,2-dioxaborolan-2-yl)phenyl)propanoate* (5.51)** – To a 250 mL RBF equipped with a stir bar was added **5.S1** (5.0440 g, 11.80 mmol, 1.0 equiv) and $PdCl_2$(dppf) (0.4384 g, 0.590 mmol, 5 mol %) before sealing with a rubber septum and exchanging the atmosphere with nitrogen. The solids were then dissolved in 1,4-dioxane (30.0 mL, 0.4 M total concentration), and *N*-methylmorpholine (1.7906 g, 11.70 mmol, 1.5 equiv) and pinacol borane (4.5312 g, 35.41 mmol, 3.0 equiv) were added. The reaction was placed into a pre-heated 70 °C heating block and allowed to stir under a balloon of nitrogen. After 16 hours, the reaction was cooled to room temperature, filtered over a pad of celite, celite added and concentrated *in vacuo*. Purifiication on silica (10% EtOAc in hexanes) afforded **5.51** (4.0586 g, 84% yield) as a pale-

yellow oil. **^{1}H NMR** (500 MHz, $CDCl_3$) δ 7.73 (d, *J* = 7.9 Hz, 2H), 7.12 (d, *J* = 7.6 Hz, 2H), 4.94 (d, *J* = 8.5 Hz, 1H), 4.58 (d, *J* = 7.3 Hz, 1H), 3.70 (s, 3H), 3.10 (qd, *J* = 13.8, 5.9 Hz, 2H), 1.42 (s, 9H), 1.34 (s, 12H).[5]

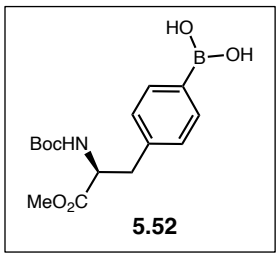

5.52

***(S)-(4-(2-((tert-butoxycarbonyl)amino)-3-methoxy-3-oxopropyl)phenyl)boronic acid* (5.52)** – To a 250 mL flame-dried RBF equipped with a stir bar was added NH_4OAc (3.994 g, 51.81 mmol, 6.0 equiv) and $NaIO_4$ (11.08 g, 51.81 mmol, 6.0 equiv) before sealing with a rubber septum and exchanging the atmosphere with nitrogen. **5.51** (3.500 g, 8.64 mmol. 1.0 equiv) was dissolved in acetone (9 mL) and added to the reaction flask followed by additional acetone (50.0 mL) and DI H_2O (30.0 mL). The reaction stirred at room temperature under a balloon of nitrogen for 48 hours before being diluted with Et_2O (100.0 mL) and filtered through a pad of celite. The solvent was removed *in vacuo* to afford **5.52** (2.79 g, >99% yield) as a white solid. **^{1}H NMR** (500 MHz, $CDCl_3$) δ 7.99 (d, *J* = 7.3 Hz, 2H), 7.18 (t, *J* = 7.9 Hz, 2H), 5.01 (d, *J* = 8.3 Hz, 1H), 4.69 – 4.54 (m, 2H), 3.72 (s, 3H), 3.29 – 2.90 (m, 2H), 1.42 (s, 9H).[5]

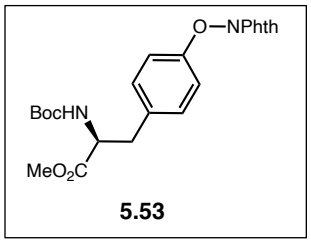

5.53

***Methyl (S)-2-((tert-butoxycarbonyl)amino)-3-(4-((1,3-dioxoisointolin-2-yl)oxy)phenyl)propanoate* (5.53)** – To a flame-dried 100 mL RBF equipped with a stir bar, added **5.52** (1.0065 g, 3.095 mmol, 1.0 equiv), activated 4Å molecular sieves (751 mg, 250 mg/mmol), *N*-hydroxyphthalimide (0.5048 g, 3.095 mmol, 1.0 equiv), and CuCl (0.3434 g, 3.095 mmol, 1.0 equiv). The mixture was dissolved in 1,2-DCE (20.0 mL) and pyridine (0.269 g, 3.404 mmol, 1.1 equiv). The reaction was heated to 70 °C and allowed to stir open to air. After 24 hours, the reaction was cooled to room temperature and celite was added. The mixture was concentrated *in vacuo* and purified by flash chromatography on silica (30% EtOAc in hexanes) to afford **5.53** (0.2644 g, 19% yield) as an off-white foam. **^{1}H NMR** (600 MHz, $CDCl_3$) δ 7.91 (dd, *J* = 5.4, 3.1

Hz, 2H), 7.83 – 7.78 (m, 2H), 7.15 – 7.07 (m, 4H), 4.95 (d, *J* = 8.3 Hz, 1H), 4.55 (q, *J* = 6.6 Hz, 1H), 3.70 (s, 3H), 3.09 (dd, *J* = 14.0, 5.8 Hz, 1H), 3.02 (dd, *J* = 14.0, 6.1 Hz, 1H), 1.41 (s, 9H). **^{13}C NMR** (151 MHz, $CDCl_3$) δ 172.27, 163.06, 158.15, 155.19, 135.05, 132.60, 130.74, 128.93, 124.13, 114.87, 80.17, 54.47, 52.42, 37.59, 28.42. **HRMS** (-APCI) calculated for $C_{23}H_{23}O_7N_2$ $[M-H]^-$ 439.1511, found 439.1514.

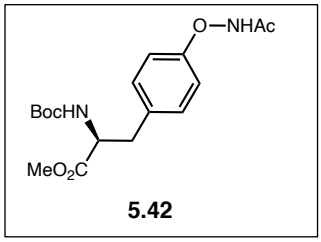

5.42

***Methyl (S)-3-(4-(acetamidooxy)phenyl)-2-((tert-butoxycarbonyl)amino)propanoate* (5.42)** – To a 25 mL flame-dried RBF equipped with a stir bar under a nitrogen atmosphere was added a solution of **5.53** (0.1925 g, 0.437 mmol, 1.0 equiv) in DCM (4.5 mL, 0.1 M). Hydrazine hydrate (0.0875 g, 1.75 mmol, 4.0 equiv) was added and the reaction stirred at room temperature under a balloon of nitrogen. After 24 hours, $MgSO_4$ (2 scoops) was added and the reaction continued to stir at room temperature. The reaction was filtered and the solid washed with DCM (10.0 mL) and EtOAc (10.0 mL) before solvent removal *in vacuo*. To a 10 mL flame-dried RBF equipped with a stir bar, added Na_2CO_3 (0.0562 g, 0.531 mmol, 1.2 equiv) before sealing and exchanging the atmosphere with nitrogen. The crude material from the first step was dissolved in EtOAc (1.3 mL) and the solution added to the reaction vial followed by DI H_2O (0.7 mL). Acetyl chloride (0.0374 g, 0.479 mmol, 1.1 equiv) was added and the reaction allowed to stir at room temperature under a balloon of nitrogen. After 16 hours, the reaction was quenched with saturated $NaHCO_3$ (2.5 mL). The aqueous layer was extracted with EtOAc (3 x 10 mL) and the combined organic layers dried over $MgSO_4$, filtered, and concentrated *in vauo*. Purification by flash chromatography on silica afforded **5.42** (0.0694 g, 51% yield) as a white solid. **^{1}H NMR** (400 MHz, $CDCl_3$) δ 7.20 – 6.91 (m, 4H), 4.96 (s, 1H), 4.54 (d, *J* = 7.4 Hz, 1H), 3.71 (s, 3H), 3.06 – 2.97 (m, 2H), 2.08 (s, 3H), 1.41 (s, 9H).[3]

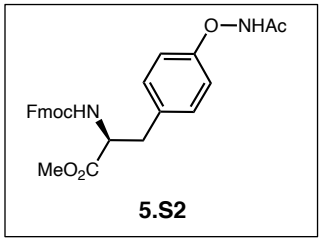

5.S2

***Methyl (S)-2-((((9H-fluoren-9-yl)methoxy)carbonyl)amino)-3-(4-acetamidooxy)phenyl)propanoate* (5.S2)** – To an oven-dried 15 mL reaction vial equipped with a stir bar, added KO^{t}Bu (0.6811 g, 6.07 mmol, 2.2 equiv) and Fmoc-Tyr-OMe (2.3034 g, 5.18 mmol, 1.0 equiv). The vial was sealed with a Teflon-cap, the atmosphere exchanged with nitrogen, and the solids dissolved in MeOH (7.0 mL). After 1.5 hours, the solvent was removed *in vacuo* and the crude residue dissolved in DCM (3.0 mL). Freshly prepared MSH (1.1878 g, 5.18 mmol, 1.0 equiv)[6] was dissolved in DCM (4.0 mL) and the MSH solution added slowly to the reaction vial. After 4 hours, the solvent was removed *in vacuo* and the vial sealed with a Teflon-cap and the atmosphere exchanged with nitrogen. The crude residue was dissolved in Et_2O (10.0 mL) and Ac_2O (1.1266 g, 11.04 mmol, 2.0 equiv) was added dropwise. The reaction stirred overnight at room temperature under a balloon of nitrogen. After 16 hours, the solvent was removed *in vacuo* and the crude material purified by flash chromatography on silica (25% EtOAc in hexanes) to afford **5.S2** (0.6300 g, 24% yield) as an off-white solid. **^{1}H NMR** (400 MHz, $CDCl_3$) δ 7.77 (d, *J* = 7.5 Hz, 2H), 7.61 – 7.56 (m, 2H), 7.41 (tt, *J* = 7.5, 1.0 Hz, 2H), 7.32 (tt, *J* = 7.4, 1.3 Hz, 2H), 7.10 (d, *J* = 8.4 Hz, 2H), 7.02 (d, *J* = 8.5 Hz, 2H), 5.29 (d, *J* = 8.2 Hz, 1H), 4.67 (dt, *J* = 8.3, 5.9 Hz, 1H), 4.46 (dd, *J* = 10.6, 7.2 Hz, 1H), 4.37 (dd, *J* = 10.6, 6.9 Hz, 1H), 4.22 (t, *J* = 7.0 Hz, 1H), 3.73 (s, 3H), 3.67 (dd, *J* = 7.0, 1.7 Hz, 1H), 3.21 – 3.01 (m, 2H), 2.30 (s, 3H). **^{13}C NMR** (101 MHz, $CDCl_3$) δ 171.89, 169.56, 155.67, 149.89, 143.93, 143.81, 141.43, 133.43, 130.56, 130.42, 127.85, 127.19, 125.23, 125.16, 121.82, 120.12, 120.10, 115.63, 67.06, 54.83, 52.56, 47.26, 37.68, 21.29. **HRMS** (+APCI) calculated for $C_{27}H_{27}N_2O_6$ $[M+H]^+$ 475.2088, found 475.2090.

5.5.2.3 Selected Experimental Data for Reactions Conducted by Sophia Xu

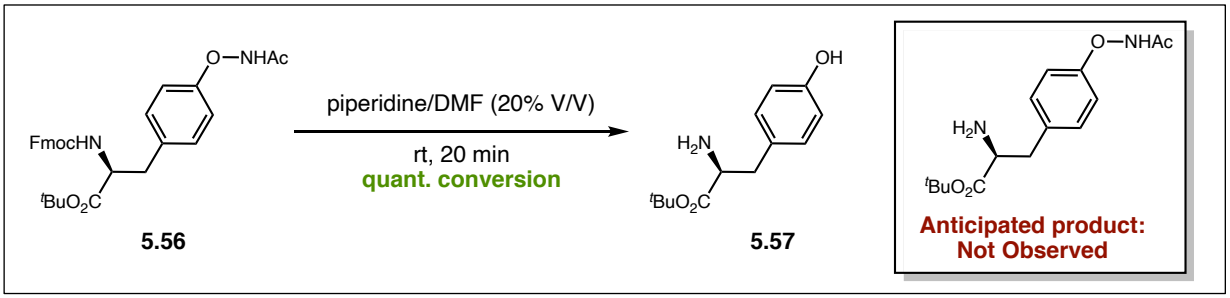

***L-Tyr-O^{t}Bu* (5.57)** – To a 4 mL oven-dried reaction vial, added Fmoc-Tyr(NHAc)-O^{t}Bu (0.0125 g, 0.0250 mmol, 1.0 equiv) and a stir bar. The atmosphere was exchanged with N_2 before the addition of DMF (0.8 mL) and piperidine (0.2 mL). The reaction was stirred at room temperature for 20 minutes. Solvent was removed *in vacuo*. Crude NMR data is consistent **5.57**,[7] and comparison to the starting material shows distinct shifts in the *para*-substituted aryl peaks after N–O bond cleaveage, loss of the amide methyl peak, and a change in the Fmoc peaks suggesting presence of the elimination side product of Fmoc deprotection.[8] **5.56 ^{1}H NMR** (400 MHz, $CDCl_3$) δ 7.77 (d, *J* = 7.5 Hz, 2H), 7.58 (dt, *J* = 7.5, 1.0 Hz, 2H), 7.44 – 7.37 (m, 2H), 7.35 – 7.28 (m, 2H), 7.16 (d, *J* = 8.2 Hz, 2H), 7.01 (d, *J* = 8.5 Hz, 2H), 5.30 (d, *J* = 8.0 Hz, 1H), 4.53 (q, *J* = 6.3 Hz, 1H), 4.44 (dd, *J* = 10.6, 7.2 Hz, 1H), 4.35 (dd, *J* = 10.6, 7.0 Hz, 1H), 4.22 (t, *J* = 7.1 Hz, 1H), 3.15 – 2.98 (m, 2H), 2.29 (s, 3H), 1.41 (s, 9H). **5.57 ^{1}H NMR** (400 MHz, $CDCl_3$) δ 7.00 (d, *J* = 8.4 Hz, 2H), 6.73 (d, *J* = 8.5 Hz, 2H), 3.59 (dd, *J* = 7.9, 5.2 Hz, 1H), 2.97 (dd, *J* = 14.4, 5.8 Hz, 1H), 2.75 (dd, *J* = 13.8, 8.0 Hz, 1H), 1.41 (s, 9H).

The following reaction was conducted as a model study to examine the tolerance of functionalized **5.42** to solution phase cross-coupling conditions and is provided herein solely for further, deconvoluted evidence that the N–O bond is preserved under these reaction conditions.

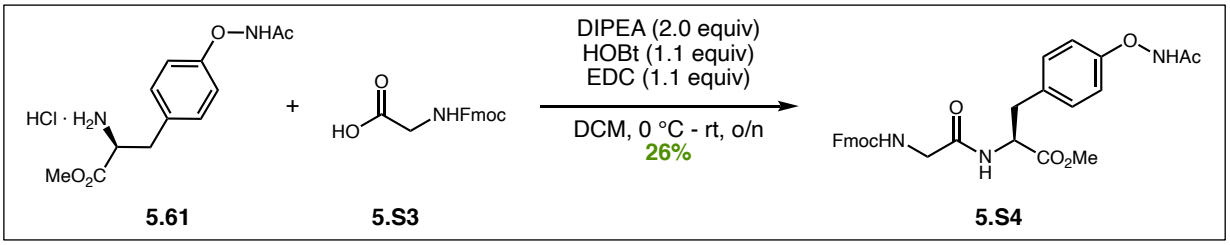

***Methyl (S)-2-(2-((((9H-fluoren-9-yl)methoxy)carbonyl)amino)acetamido)-3-(4-(acetamidooxy)phenyl)propanoate* (5.S4)** – **5.42** (0.1830 g, 0.520 mmol, 1.0 equiv) was dissolved in DCM (5.2 mL) in a 2-neck flame dried RBF. The atmosphere was exchanged with N_2 and the reaction cooled to 0 °C in an ice/water bath before the addition of HCl (5.2 mL, 4.0 M in dioxane). The reaction was allowed to warm to room temperature overnight. After 16 hours, the solvent was evaporated to afford **5.61** which was used without further purification. The flask containing crude **5.61** (0.520 mmol, 1.0 equiv) was placed under nitrogen before the addition of DCM (5.2 mL), and Hunig's base (0.18 mL, 1.04 mmol, 2.0 equiv). The solution was cooled to 0 °C in an ice/water bath. Under a positive pressure of nitrogen, Fmoc-Gly-OH **5.S3** (0.1576 g, 0.520 mmol, 1.0 equiv) and HOBt (0.0797 g, 0.0590 mmol, 1.1 equiv) were added and the reaction allowed to stir under N_2. After 15 minutes, EDC (0.1131 g, 0.0590 mmol 1.1 equiv) was added to the suspension and the reaction allowed to stir overnight under N_2 and warm to room temperature. After 16 hours, the solvent was removed under reduced pressure and the crude residue taken up in EtOAc (15 mL) and transferred to a separatory funnel. The organic layer was washed with cold 0.1 N HCl (3 x 15 mL) and $NaHCO_3$ (3 x 15 mL), dried over Na_2SO_4, the drying agent filtered, celite added, and the solvent removed *in vacuo*. Purification by flash chromatography on silica (0-100% EtOAc in hexanes) afforded **5.S4** (0.0562 g, 26%). **^{1}H NMR** (600 MHz, DMSO-d_6) δ 11.62 (s, 1H), 8.29 (d, J = 7.8 Hz, 1H), 7.89 (d, J = 7.6 Hz, 2H), 7.71 (d, J = 7.5 Hz, 2H), 7.50 (t, J = 6.2 Hz, 1H), 7.43 – 7.38 (m, 2H), 7.36 – 7.30 (m, 2H), 7.13 (d, J = 8.2 Hz, 2H), 6.89 (d, J = 8.2 Hz, 2H), 4.44 (td, J = 8.1, 5.7 Hz, 1H), 4.27 (d, J = 7.8 Hz, 2H), 4.22 (t, J

= 7.1 Hz, 1H), 3.65 (dd, *J* = 16.9, 6.3 Hz, 1H), 3.60 (s, 3H), 3.58 – 3.50 (m, 1H), 2.96 (dd, *J* = 13.8, 5.7 Hz, 1H), 2.87 (dd, *J* = 13.8, 8.6 Hz, 1H), 1.88 (s, 3H). **HRMS** (+APCI) calculated for $C_{29}H_{29}N_3O_7Na$ $[M+Na]^+$ 554.1903, found 554.1909.

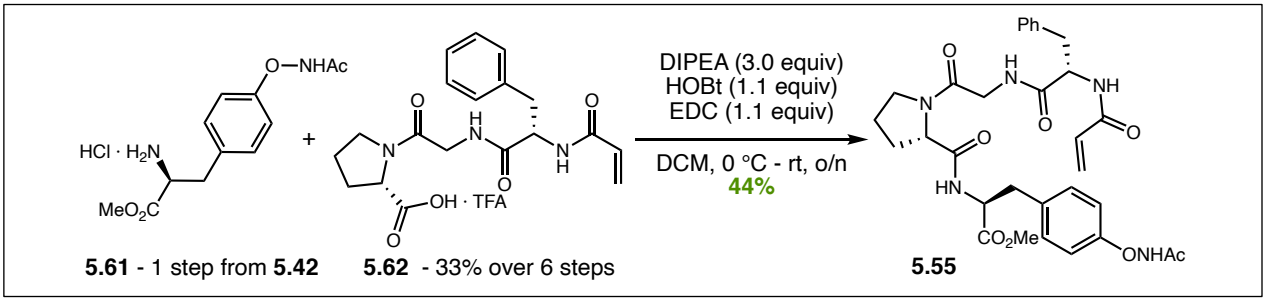

***Methyl (S)-3-(4-(acetamidooxy)phenyl)-2-((S)-1-(acryloyl-L-phenylalanylglycyl)pyrrolidine-2-carboxamido)propanoate* (5.55)** – **5.42** (0.2361 g, 0.670 mmol, 1.0 equiv) was dissolved in DCM (6.7 mL) in a 2-neck flame dried RBF. The atmosphere was exchanged with N_2 and the reaction cooled to 0 °C in an ice/water bath before the addition of HCl (6.7 mL, 4.0 M in dioxane). The reaction was allowed to warm to room temperature overnight. After 16 hours, the solvent was evaporated to afford **5.61** which was used without further purification. The flask containing crude **5.61** (0.670 mmol, 1.0 equiv) was placed under nitrogen before the addition of DCM (6.7 mL), and Hunig's base (0.45 mL, 2.01 mmol, 3.0 equiv). The solution was cooled to 0 °C in an ice/water bath. Under a positive pressure of nitrogen, **5.62** (0.2987 g, 0.670 mmol, 1.0 equiv) and HOBt (0.1014 g, 0.737 mmol, 1.1 equiv) were added and the reaction allowed to stir under N_2. After 15 minutes, EDC (0.1413 g, 0.737 mmol 1.1 equiv) was added to the suspension and the reaction allowed to stir overnight under N_2 and warm to room temperature. After 16 hours, the solution was washed with citric acid (10% v/v, 50 mL) and $NaHCO_3$ (50 mL), dried over Na_2SO_4, the drying agent filtered, and the solvent removed *in vacuo*. Purification by preparative HPLC afforded **5.55** (0.1784 g, 44%). Tentative assignment is supported by the following data. **^{1}H NMR** (400 MHz, DMSO-d_6) δ 11.63 (s, 1H), 8.58 – 8.07 (m, 3H), 7.31 – 7.19 (m, 4H), 7.16 (tdd, *J* = 7.9, 5.1, 2.1 Hz, 3H), 7.00 – 6.79 (m, 2H), 6.25 (ddd, *J* = 17.1, 10.2, 1.7 Hz, 1H), 5.99 (dd, *J* = 17.1, 2.2 Hz, 1H), 5.53 (dd, *J* = 10.2, 2.1 Hz, 1H), 4.10 – 3.74

(m, 2H), 3.58 (d, *J* = 14.0 Hz, 3H), 3.49 – 3.19 (m, 2H), 3.15 – 2.85 (m, 3H), 2.85 – 2.65 (m, 1H), 2.22 – 1.91 (m, 2H), 1.88 (s, 2H), 1.83 – 1.51 (m, 3H). **HPLC** (+APCI) $C_{31}H_{38}N_5O_8$ $[M+H]^+$ 608.2715, found 608.2719.

5.5.3 Supplementary References

(1) Nacsa, E. D.; MacMillan, D. W. C. Spin-Center Shift-Enabled Direct Enantioselective α-Benzylation of Aldehydes with Alcohols. *J. Am. Chem. Soc.* **2018**, *149*, 3322-3330.

(2) Liu, G.; Shen, Y.; Zhou, Z; Lu, X. Rhodium(III)-Catalyzed Redox-Neutral Coupling of N-Phenoxyacetamides and Alkynes with Tunable Selectivity. *Angew. Chem. Int. Ed.* **2013**, *52*, 6033-6037.

(3) a) Li, B.; Lan, J.; Wu, D.; You, J. Rhodium(III)-Catalyzed ortho- Heteroarylation of Phenols through Internal Oxidative C–H Activation: Rapid Screening of Single-Molecular White-Light-Emitting Materials. *Angew. Chem. Int. Ed.* **2015**, *54*, 14008-14012. b) Yan, D.; Want, G.; Xiong, F.; Sun, W. Y.; Shi, Z.; Lu, Y.; Li, S.; Zhao, J. A Selenium-Catalysed Para-Amination of Phenols. *Nat. Commun.* **2018**, *9*, 1-9.

(4) Sun, B.; Yoshino, T.; Matsunaga, S.; Kanai, M. A Cp*CoI_2-dimer as a precursor for cationic Co(III)-catalysis: Application to C–H phosphoramidation of indoles. *Chem. Commun.* **2015**, *51*, 4659-4661.

(5) Feng, Z.; Min, Q,-Q.; Xiao, Y.-L.; Zhang, B.; Zhang, X. Pallatium-Catalyzed Difluoroalkylaiton of Aryl Boronic Acids: A New Method for the Synthesis of Aryldifluoromethylated Phosphonates and Carboxylic Acid Derivatives. *Angew. Chem. Int. Ed.* **2014**, *53*, 1669-1673.

(6) Bernardes, G. J. L.; Chalker, J. M.; Errey, J. C.; Davis, B. G. Facile Conversion of Cysteine and Alkyl Cysteines to Dehydroalanine on Protein Surfaces: Versatile and Switchable Access to Functionalized Proteins. *J. Am. Chem. Soc.* **2008**, *130*, 5052-5053.

(7) Ooi, T.; Kameda, M.; Maruoka, K. Design of *N*-Spiro C_2-Symmetric Chiral Quaternary Ammonium Bromides as Novel Chiral Phase-Transfer Catalysts: Synthesis and Application to Practical Asymmetric Synthesis of α-Amino Acids. *J. Am. Chem. Soc.* **2003**, *125*, 5139-5151.

(8) Cho, B. P. A Novel and Practical Synthesis of Polycyclic Fluoranthrenes. *Tetrahedron Lett*. **1995**, *36*, 2403-2406.

5.5.4 Spectra

2-acetamido-3-(2-hydroxyphenyl)-N-isopropylpropanamide **(5.41)**

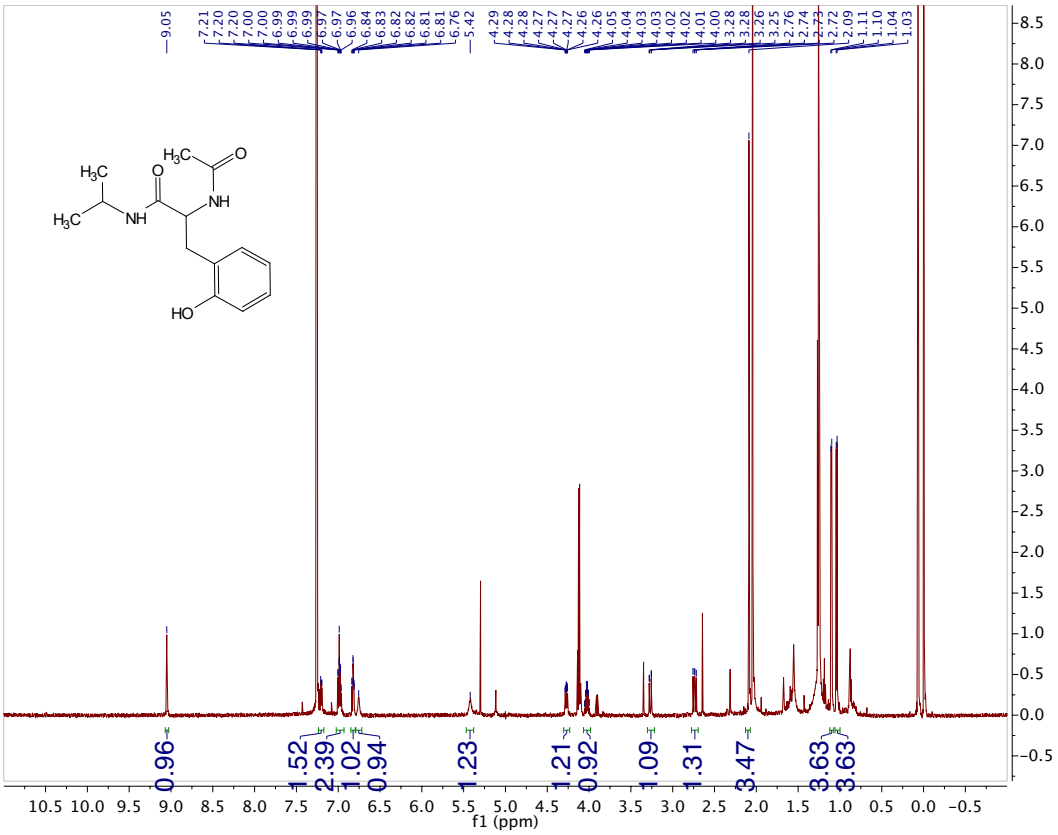

Methyl (2S)-3-(3-(2-acetamido-3-(isopropylamino)-3-oxopropyl)-4-hydroxyphenyl)-2-((tert-butoxycarbonyl)amino)propanoate **(5.43)**

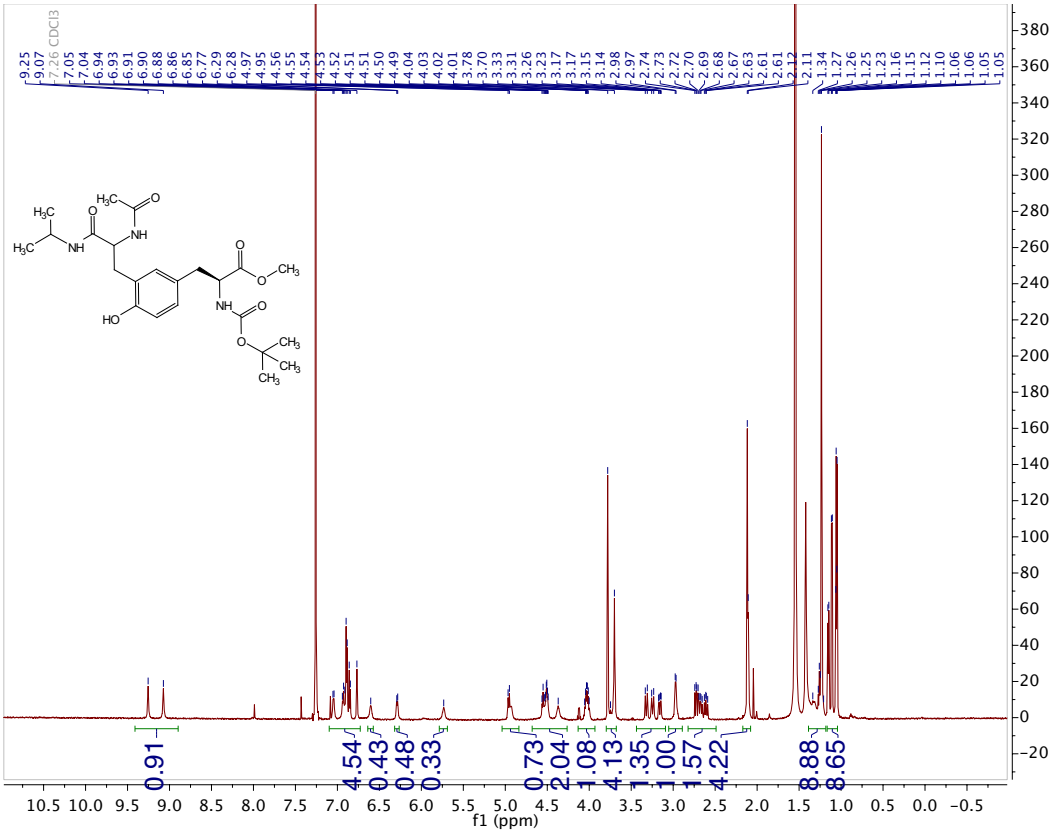

(S)-N-(1-(methylamino)-1-oxo-3-phenylpropan-2-yl)acrylamide **(5.44)**

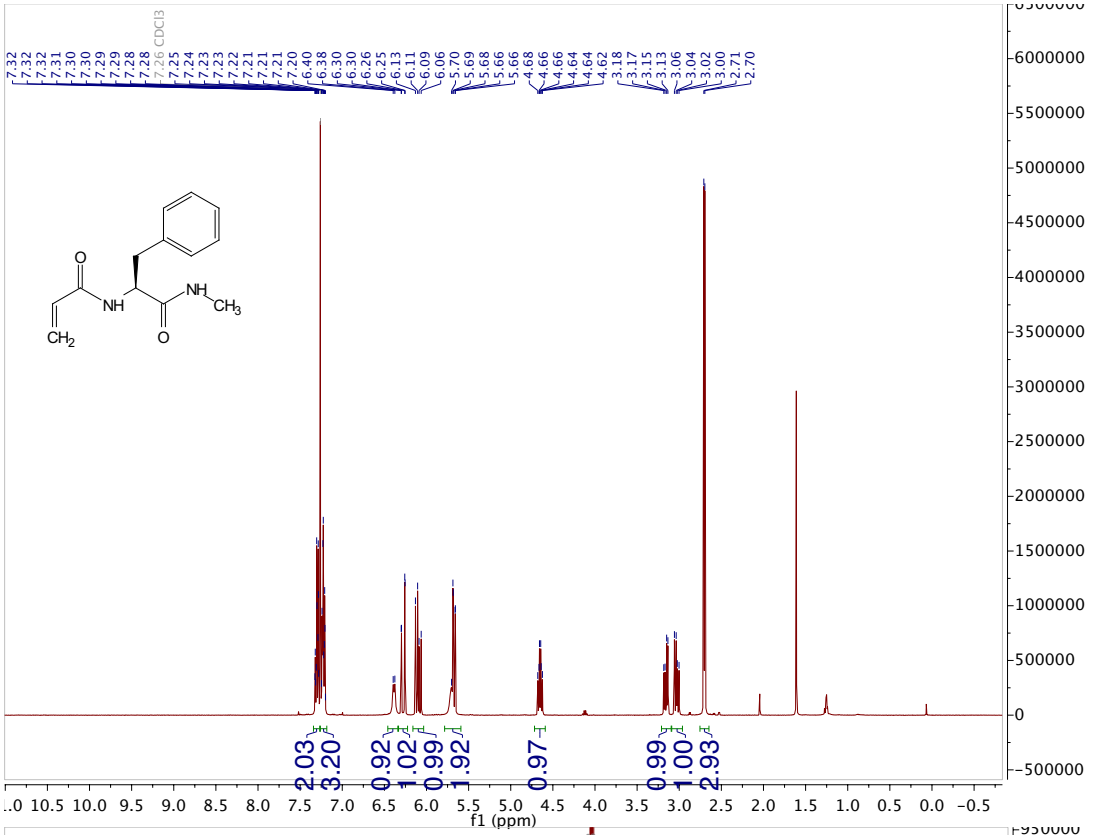

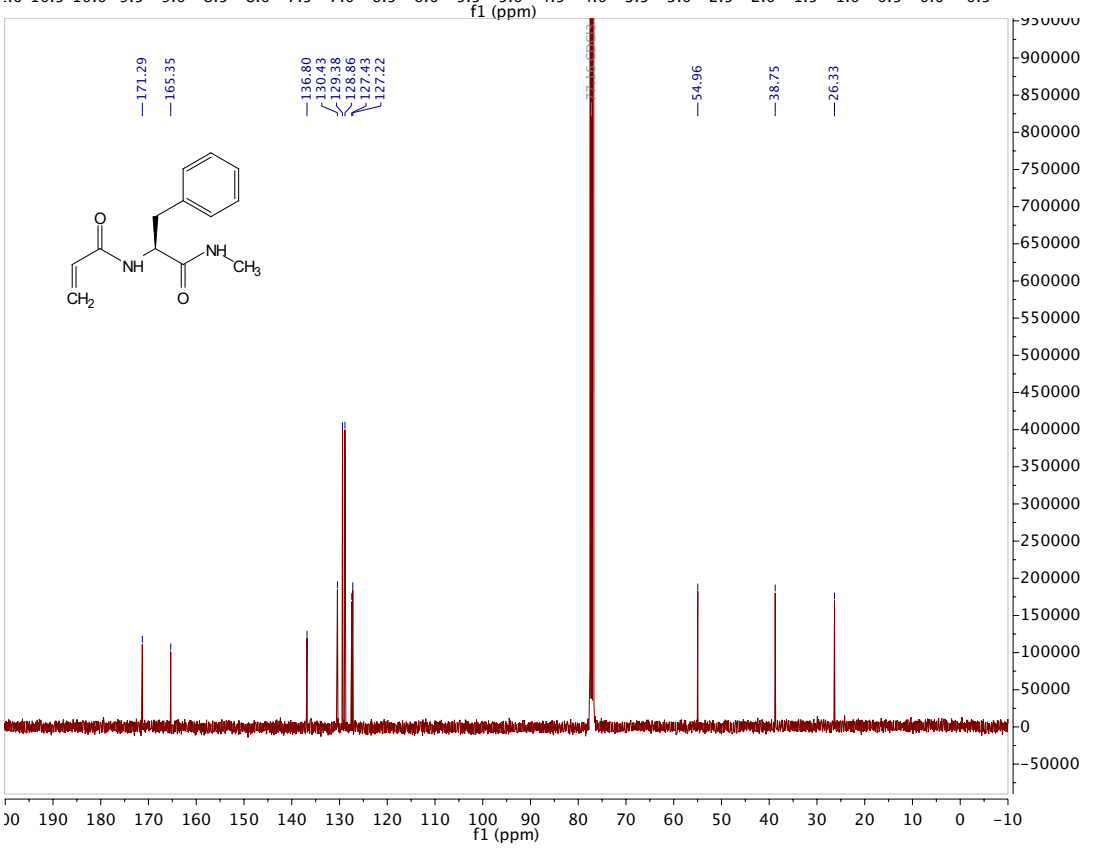

Methyl (S)-2-((tert-butoxycarbonyl)amino)-3-(4-(((trifluoromethyl)sulfonyl)oxy)phenyl)proponate **(5.S1)**

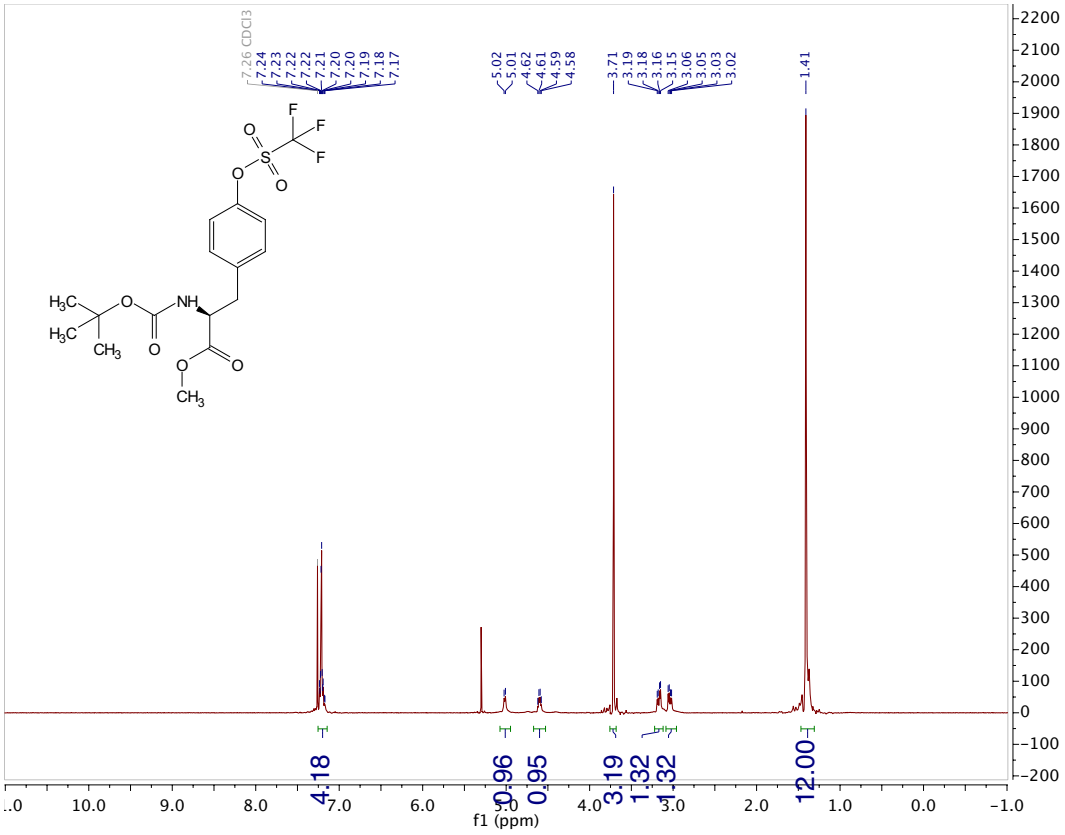

Methyl (S)-2-((tert-butoxycarbonyl)amino)-3-(4-(4,4,5,5-tetramethyl-1,3,2-dioxaborolan-2-yl)phenyl)propanoate **(5.51)**

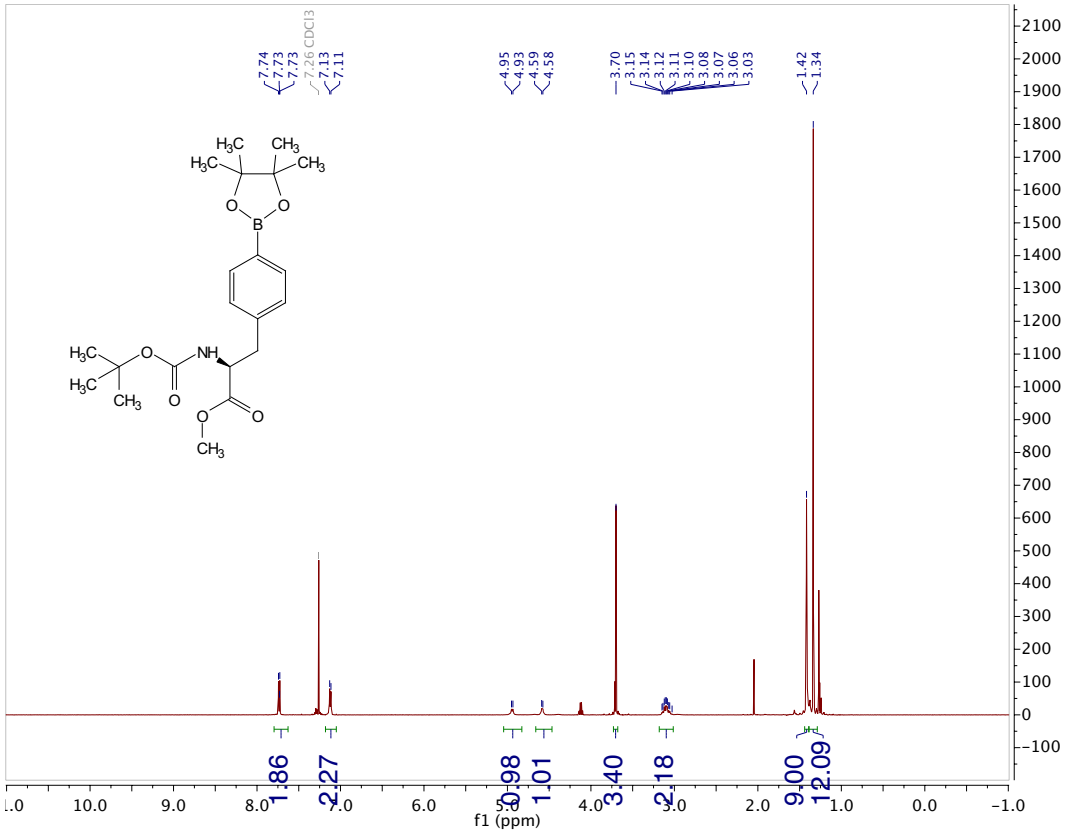

(S)-(4-(2-((tert-butoxycarbonyl)amino)-3-methoxy-3-oxopropyl)phenyl)boronic acid **(5.52)**

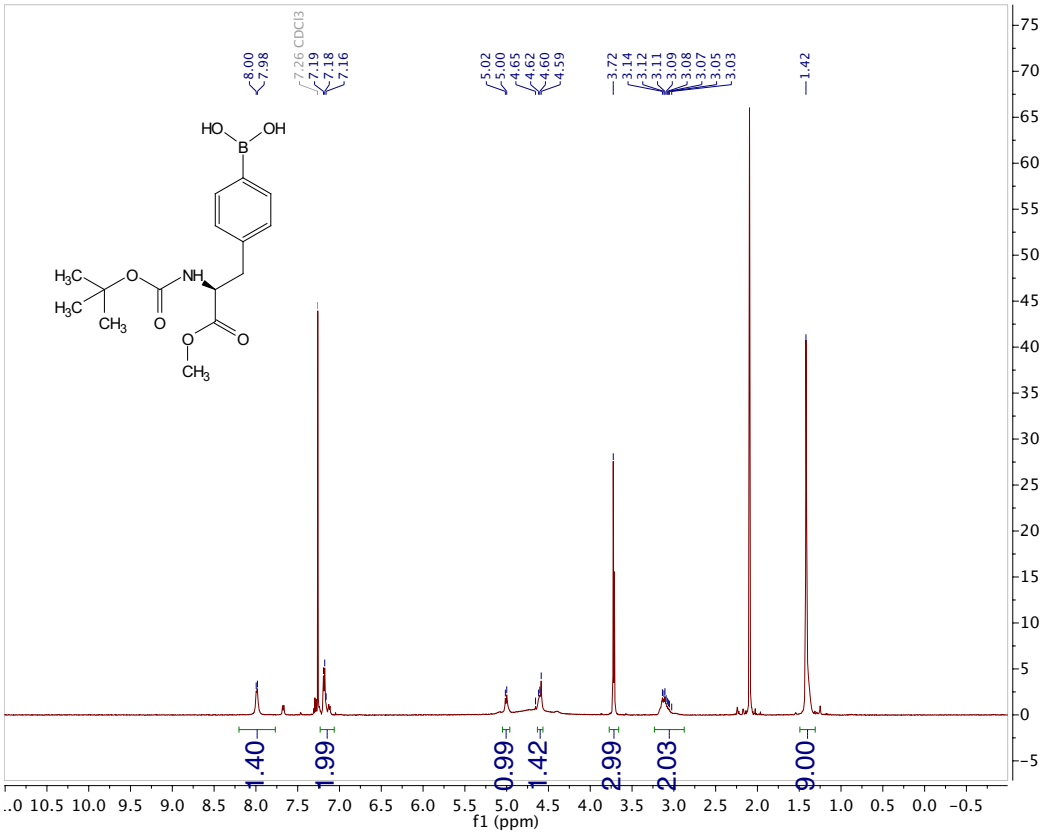

Methyl (S)-2-((tert-butoxycarbonyl)amino)-3-(4-((1,3-dioxoisointolin-2-yl)oxy)phenyl)propanoate **(5.53)**

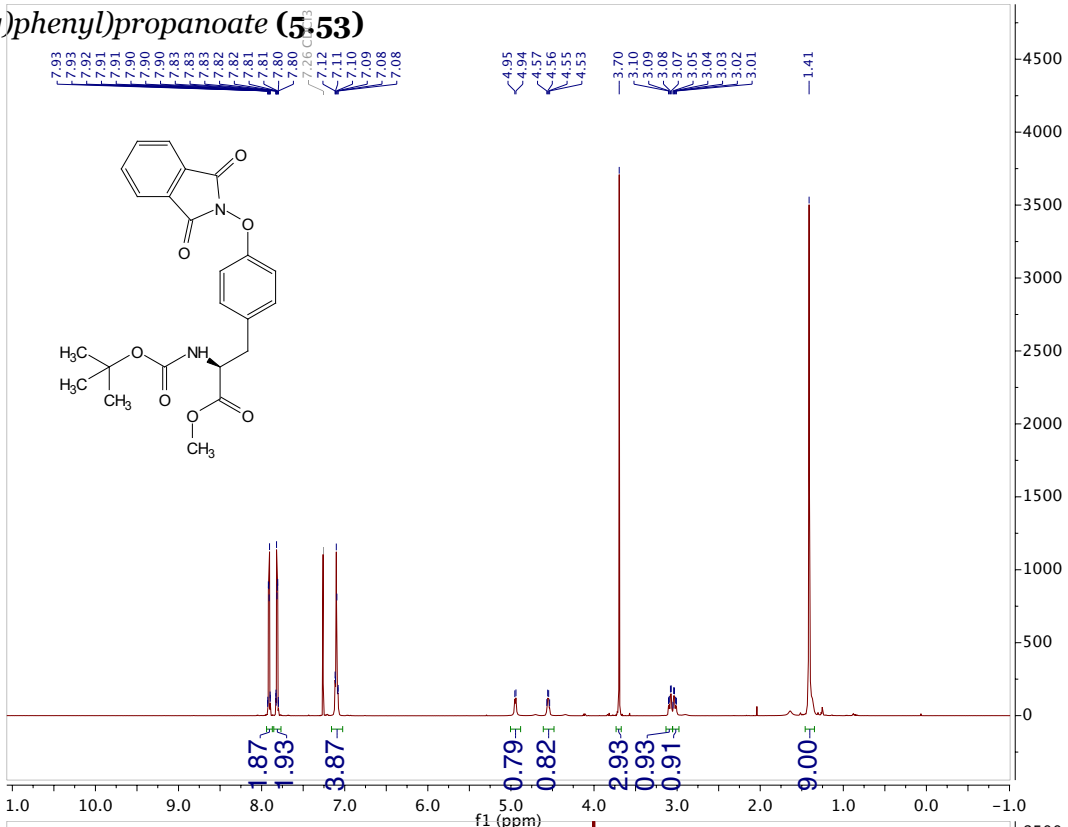

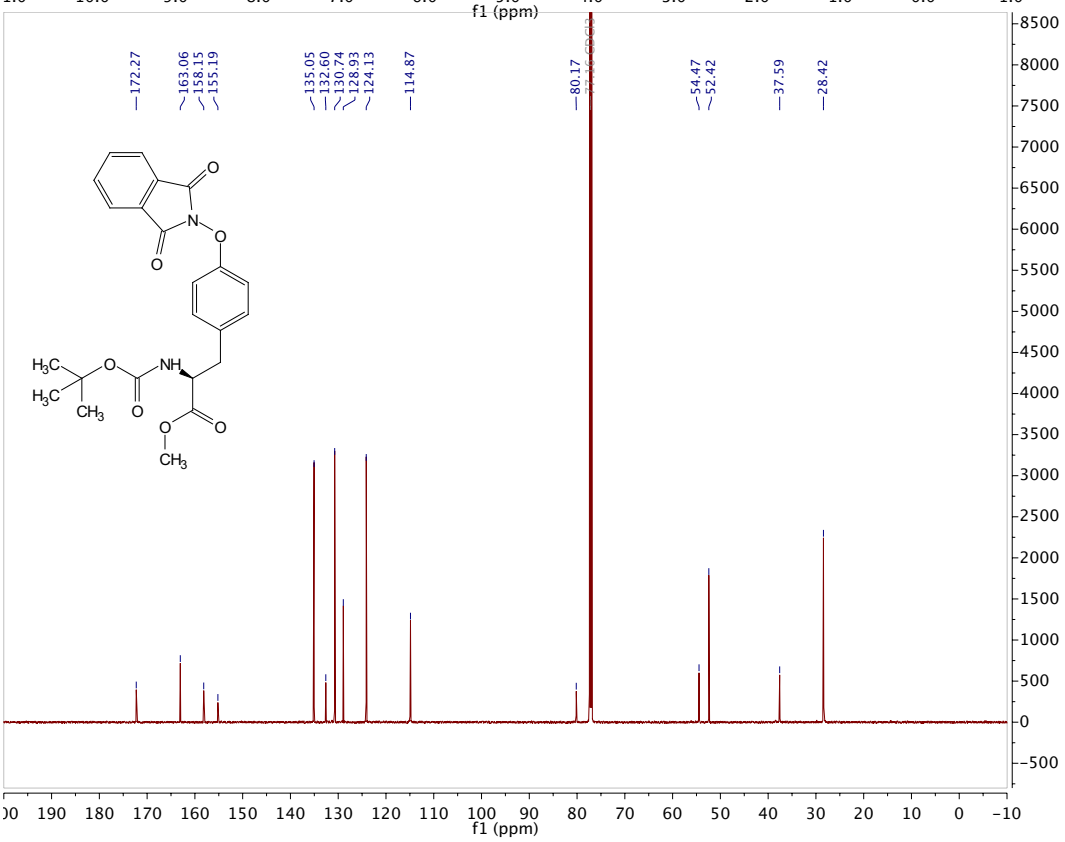

Methyl (S)-2-((((9H-fluoren-9-yl)methoxy)carbonyl)amino)-3-(4-acetamidooxy)phenyl)propanoate **(5.S2)**

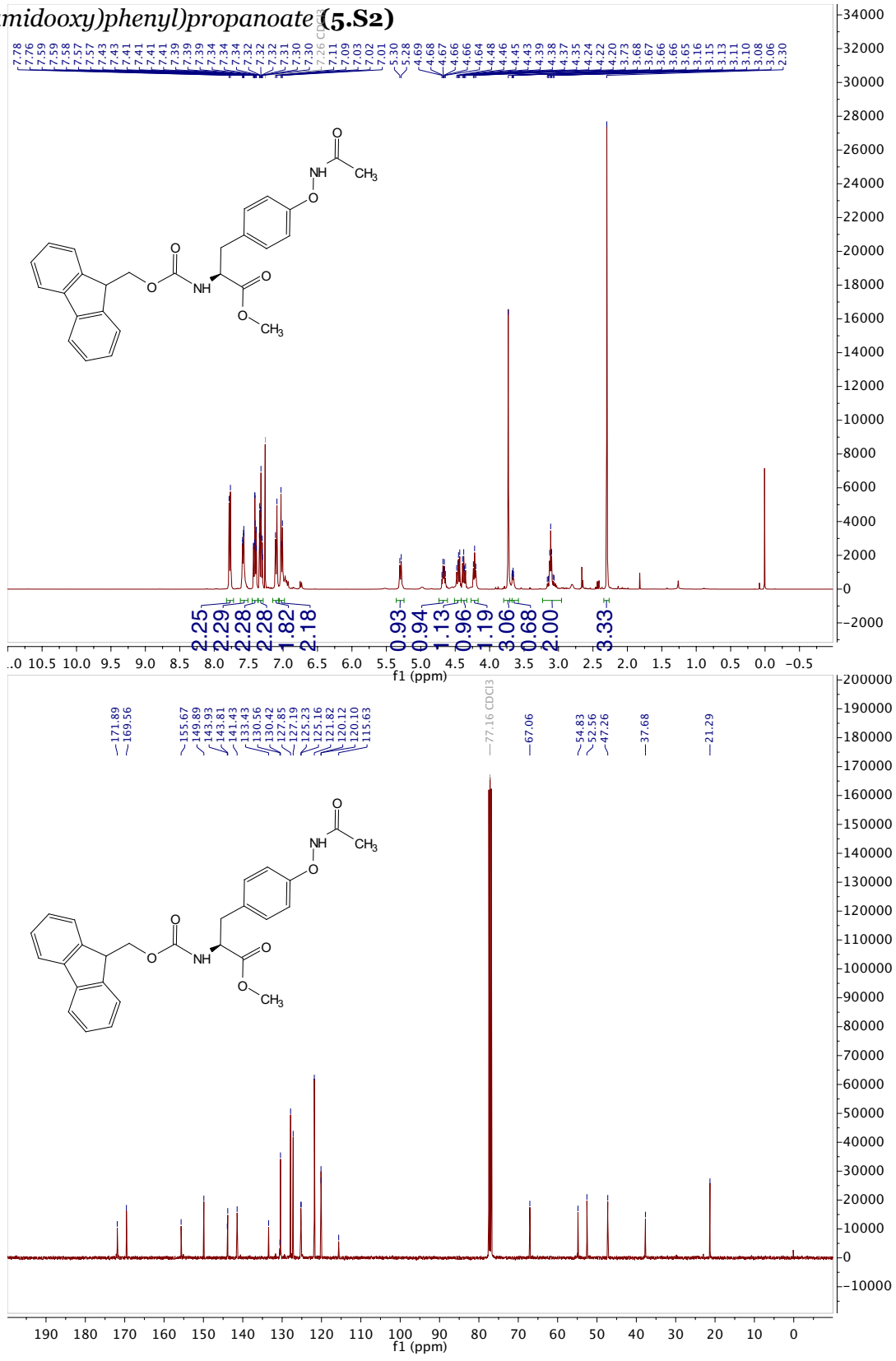

L-Tyr-O^{t}Bu **(5.57)** – Crude NMR and Starting Material (**5.56**) *Key changes in blue square box*

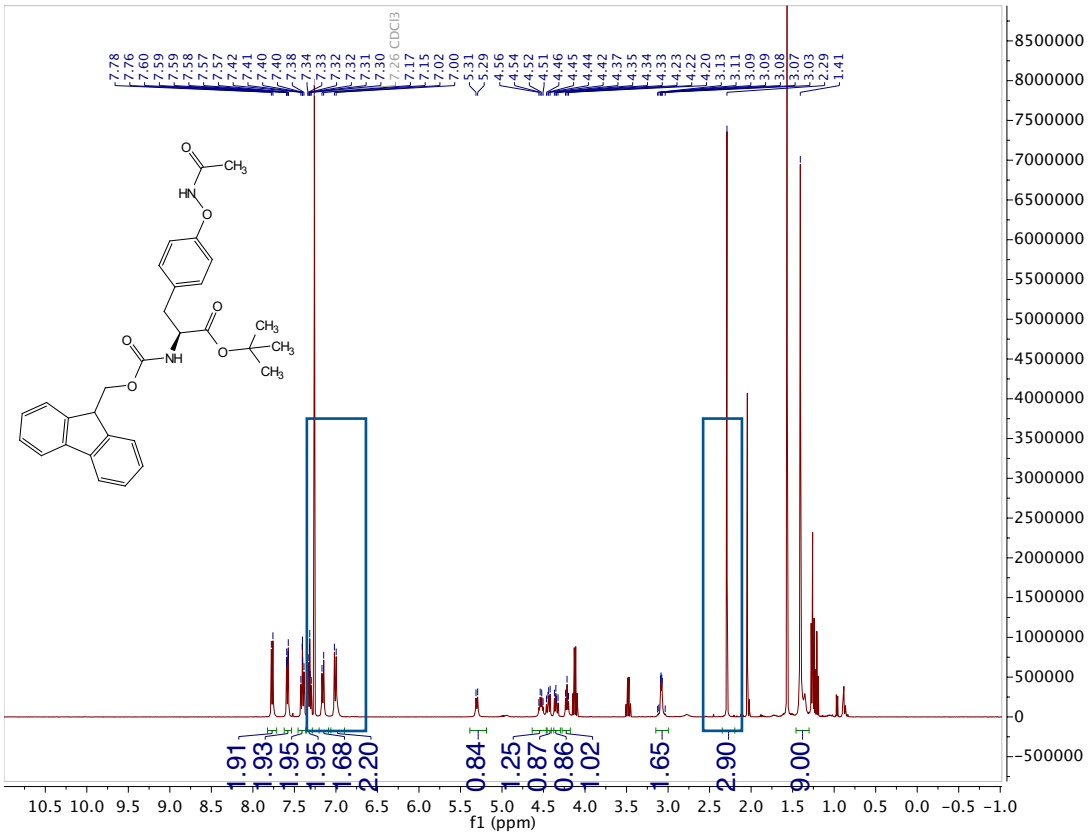

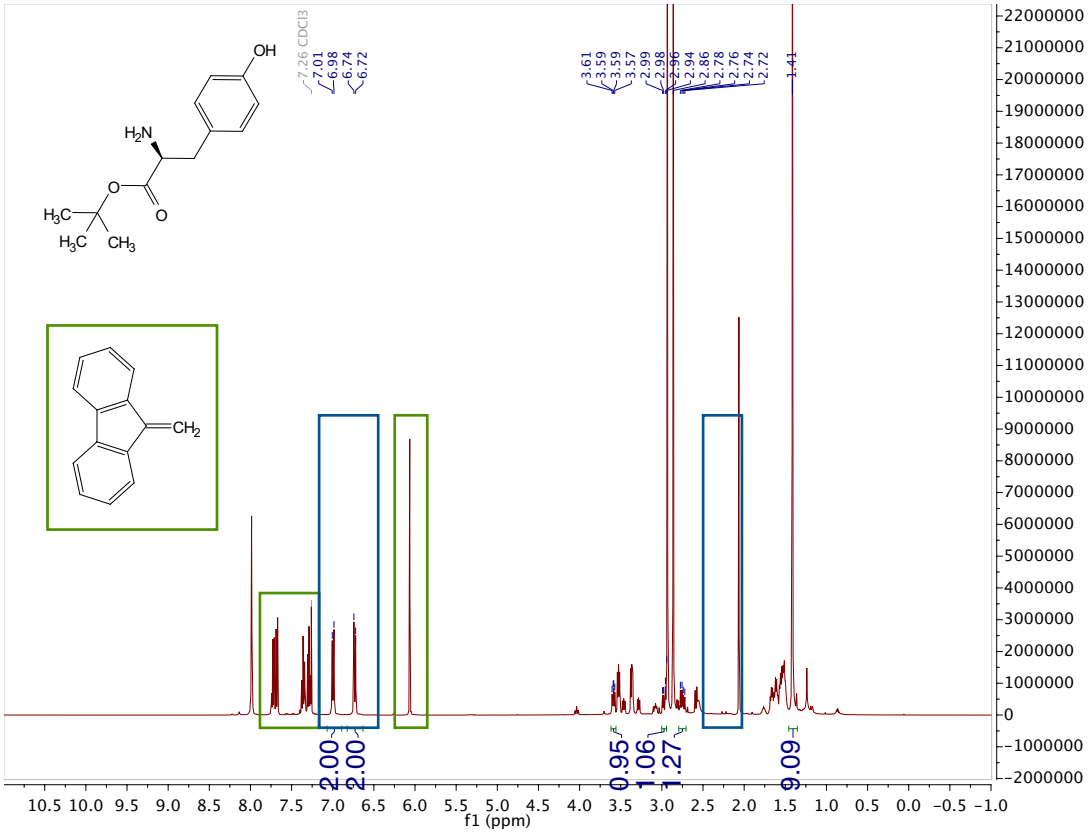

Methyl (S)-2-(2-((((9H-fluoren-9-yl)methoxy)carbonyl)amino)acetamido)-3-(4-(acetamidooxy)phenyl)propanoate **(5.S4)**

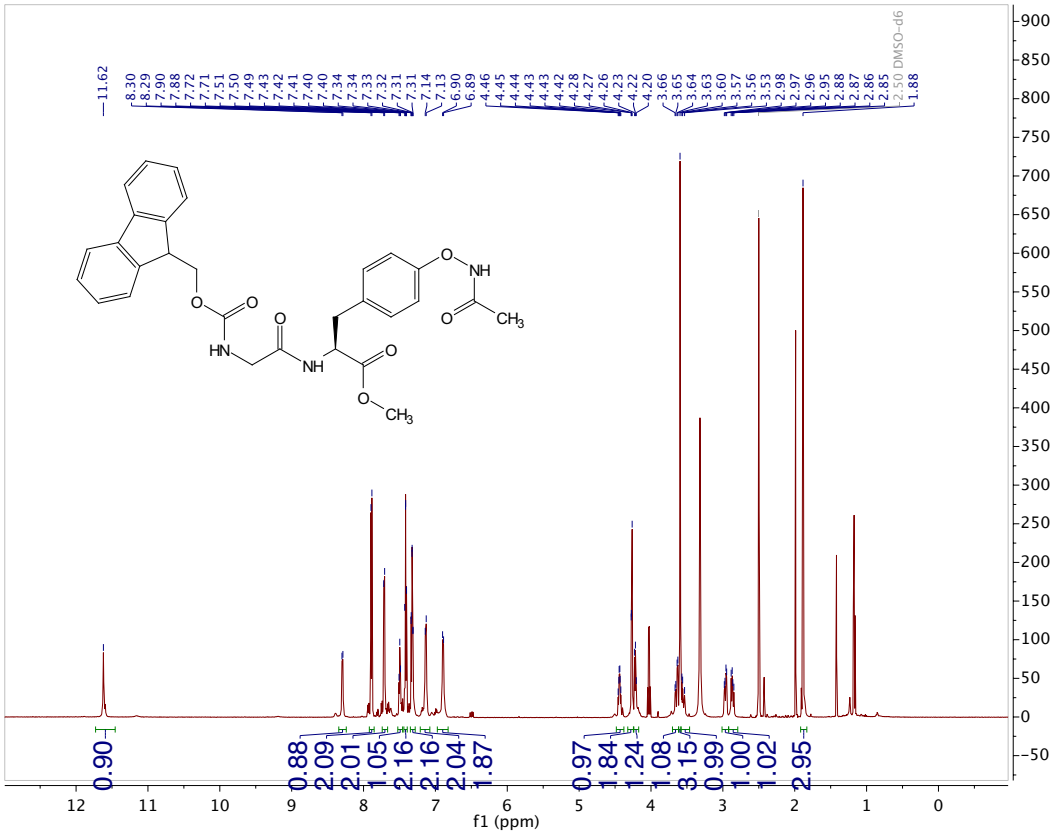

Methyl (S)-3-(4-(acetamidooxy)phenyl)-2-((S)-1-(acryloyl-L-phenylalanylglycyl)pyrrolidine-2-carboxamido)propanoate **(5.55)**